Characterisation of carotid atherosclerotic plaque composition *in vivo* using 3D B-mode ultrasound

by

Declan Paul Coleman

Cardiff University

Ph.D. Thesis

2007

ProQuest LLC
789 East Eisenhower Parkway
P.O. Box 1346
Ann Arbor, MI 48106-1346

Candidate's ID number	**100024844**
Candidate's Surname	**Coleman**
Candidate's Forenames	**Declan Paul**

Declaration

This work presented in this thesis has not already been accepted in substance for any degree and is not being concurrently submitted in candidature for any degree.

Signed ..... (candidate) Date...18/6/07

Statement 1

This thesis is being submitted in partial fulfilment of the requirements for the degree of Ph.D.

Signed ..... (candidate) Date...18/6/07...

Statement 2

The thesis is the result of my own independent work/investigations, except where otherwise stated. Other sources are acknowledged where appropriate. A full bibliography is appended.

Signed ..... (candidate) Date...18/6/07...

Statement 3

I hereby give my consent for my thesis, if accepted, to be available for photocopying and for inter-library loan, and for the title and summary to be made available to outside organisations.

Signed ..... (candidate) Date...18/6/07...

Acknowledgements

I would like to thank all my friends and colleagues in the Medical Physics department for their friendship, support and help over the past 16 years. I would, however, like to thank certain people individually for their contribution to this project.

Firstly, I would like to thank my supervisor, Dr Neil Pugh and head of department, Professor Woodcock for their advice and support and also for giving me the opportunity in the ultrasound section.

I would also like to thank the other members of the ultrasound section, Rhys Morris, Kate Wells, Paul Williams, Gill Sullivan and Barbara Wiltshire for their help and support.

Special thanks must go to Dr Frank Rakebrandt for his work on the MATLAB programs. I would like to also thank Dilwyn Havard for his work on the plaque histology, Brian Western and Darryl Dobbin for their work on the mechanical device, and the staff in the Medical and Surgical teams for their help in recruiting patients.

I would like to thank my wife Sharon, children Andrew, Niamh and Rhys for their love and patience over the past few years. Finally I would like to thank my parents for their love, support and hard work to give my brothers and me opportunities that they never had.

Summary

Embolisation from carotid atherosclerotic plaque is a major cause of ischaemic stroke. Studies have shown that it is not only the degree of narrowing of the carotid artery but also the constituents of the plaques which are important factors in determining whether a plaque ruptures and embolises.

A reliable and repeatable method has been developed to acquire *in vivo* data of carotid plaques using 3D B-mode ultrasound. An artificial neural network was enabled using MATLAB software programs to characterise each of the plaque constituents into one of five classes based on statistical and textural parameters of the B-mode images. Comparison of the method with histology processing post surgery found that characterisation of plaque constituents *in vivo* is not readily achievable. The method, however, was found to be repeatable in serial scans and was used to monitor the effect of two different lipid lowering drug treatments over a 12 week period.

Two patients who underwent LDL apheresis treatment showed reduction in softer class types and increases in the harder class types along with reductions in the overall plaque volumes. Nine patients underwent statin treatment with changes found in 4 of the 9 patients over the period of the study. There are several possible reasons why changes were seen in the apheresis group and only in some of the statin group. The apheresis treatment is more aggressive than the statin treatment, the time period of the study was relatively short and changes in the tissue types are dependant on the initial constituents of the plaque.

CONTENTS

Chapter 1: Introduction

Chapter 2: Methods

Chapter 5: Comparison of serial scans

Abbreviations

2D	2 Dimensional
3D	3 Dimensional
AF	Atrial fibrillation
ANN	Artificial neural network
CAD	Coronary artery disease
CCA	Common carotid artery
CEA	Carotid endarterectomy
CT	Computerised tomography
ECA	External carotid artery
EVG	Elastic von Gieson
FOV	Field of view
FH	Familial hypercholesterolaemia
GSM	Grey scale median
HDL	High density lipoprotein
H&E	Haematoxylin and Eosin
IBS	Integrated backscatter
ICA	Internal carotid artery
IMT	Intima media thickness
LDL	Low density lipoprotein
MI	Myocardial infarction
MF	Multi-resolution Fractal
MGV	Mean grey value
MRI	Magnetic resonance imaging
MSB	Martius scarlet blue

PC	Personal computer
Q-Q	Quantile-Quantile
RF	Radiofrequency
RIND	Reversible ischaemic neurological deficit
ROI	Region of interest
SNR	Signal to noise ratio
SPLDM	Spatial grey level dependency matrices
SPSS	Statistical package for social sciences
TIA	Transient ischaemic attack
UTC	Ultrasound tissue characterisation
UTCI	Ultrasound texture classification images

Chapter 1: Introduction

1.1 General Introduction

The role of carotid atherosclerotic plaque in ischaemic strokes is well documented. There is growing evidence which shows that it is not only the degree of narrowing of the carotid artery, but also the composition of the plaque which play important roles in whether the patient develops further events (ECPSG 1995). Two large multi-centre trials have shown that the risk of a subsequent neurological event in symptomatic patients with a >70% stenosis of the internal carotid artery (ICA), is significantly reduced if the lesion is removed by endarterectomy (NASCET 1991; ECST 1998). However in the medically treated groups in the NASCET trial, only 26% of patients with high-grade stenosis had suffered an ipsilateral hemispheric stroke at 2 years during follow-up (only 9% in the surgically treated group). The other 74% remained stroke free, with differences in plaque composition cited as a probable reason (NASCET 1991). Other studies have also identified that differences in plaque composition are an important factor in the development of symptoms (Fuster et al. 1990; Falk 1992). Factors such as plaque surface features, (e.g. thinning of the fibrous cap) are also important determinants in plaque instability (Golledge et al. 2000).

B-mode ultrasound has been used subjectively to comment on plaque composition and appearance, based on an evaluation of the gray scale appearance of the plaque. It has been shown that plaques that appear heterogeneous and echolucent on ultrasound may be associated with a greater risk of stroke as compared to homogenous echogenic plaques (Gray-Weale et al. 1988; Eliasziw et al. 1994). Various classification criteria have been published, and are still in use, which group plaques into several types

depending on the echogenicity or heterogeneity. See section 1.6 for a more comprehensive review of these subjective methods.

Quantitative methods (section 1.7) of assessing plaque composition have been reported, with some groups using the ability of ultrasonic tissue characterisation (UTC), based on spectral analysis of backscattered radiofrequency (RF) signals, to distinguish among the components of carotid plaques (Noritomi et al. 1997; Lee et al. 1998; Waki et al. 2003). Other objective methods include the use of first order statistics based on measurements of the median grey-scale levels of plaque images, which correlated well with histology sections that were examined by computer morphometric analysis (El-Barghouty et al. 1996). Previous studies from our group used *in vitro* images of excised carotid plaques and multi-discriminant analysis to combine the output of 157 first and second order statistical and textural algorithms into five different classes, and displayed them as ultrasound texture classification images (UTCI). The UTCI were then visually compared to histology. The UTCI and histology demonstrated five texture classes which matched the location of fibrous tissue, elastic tissue, calcium, lipid or haemorrhage (Rakebrandt et al. 2000). A later study by another group used a similar approach, but only used a combination of 32 first and second order statistical parameters computed from the *in vitro* image data and compared the data with histology of the excised plaques (Arnold et al. 2001).

In this project, the aim is to use statistical methods to try to develop and validate a method of characterising carotid atherosclerotic plaque *in vivo* and to apply these methods to serial measurements to try to monitor changes in the plaques in patients undergoing some form of drug treatment. The previous studies mentioned above (Rakebrandt et al. 2000; Arnold et al. 2001) used *in vitro* data from excised carotid plaques. To develop this objective method, 3-dimensional (3D) ultrasound is used to

acquire *in vivo* data of carotid plaques and also use *in vitro* data from the same excised plaques for comparison with histology.

1.2 Atherosclerosis

Atherosclerosis comes from the Greek words athero (meaning gruel) and sclerosis (meaning hardness). It is a progressive disease which involves the laying down of fatty deposits within the inner lining of mainly large and medium sized arteries. The atheromatous plaque is characterised by sub-endothelial deposits of lipid derived from plasma which is accompanied by smooth muscle proliferation, an influx of T-lymphocytes and monocyte derived macrophages and collagen deposition (Falk 1992).

There are several theories on how atherosclerosis begins, with the response to injury theory the most widely accepted (Spector 1999). This theory suggests that the endothelial lining of the lumen is damaged by some mechanism. These mechanisms include the force of the blood in hypertension, certain toxins inhaled in cigarette smoke, antibodies that build up in response to cigarette smoke, other foreign substances or even by high blood levels of cholesterol. Once the endothelium is damaged, platelets aggregate and release a substance that stimulates smooth muscle cell proliferation. Smooth muscle cells from the media migrate to the area of injury. While this is happening, cholesterol and other substances from the blood may enter via the damaged endothelium. Once plaques begin to form they progress over a long period of time. The affected arteries lose their ability to stretch during systole and become increasingly occluded. Other theories include the monoclonal hypothesis which suggests that there is a multiplication of individual muscle cells due to the stimulation of single cells by mitogens. Another hypothesis is the lyposomal theory,

where it is thought that the deposition of cholesterol esters arises from a deficiency in the activity of lyposomal cholesterol hydrolase which may then cause degradation of cellular components (Spector 1999).

1.3 Stroke

The work in this thesis looks at carotid plaque atheroma and the major consequence of this atheroma build up is that it may lead to embolisation causing cerebral ischaemia. The term used to describe this cerebral ischaemia is stroke. Stroke is one of the major complications of atherosclerotic disease. It is also one of the commonest causes of severe disability and the third biggest killer in the United states (American-Heart-Association 2005) and causes 11% of all deaths in the UK (DOH 2005). Stroke is a disease that affects the vessels that supply blood to the brain. It can occur when a blood vessel that brings oxygen and nutrients to the brain either ruptures (haemorrhagic) or is occluded by a blood clot or other embolus (ischaemic). Ischemic stroke is the most common type and is often the result of embolisation from carotid atheroma. Studies have shown that 83-85% of all strokes are ischaemic in cause however only 7-8% of ischaemic strokes result in death within 30 days compared with 37-38% from haemorrhagic strokes (Woo et al. 1999; DOH 2005). There are various degrees of stroke which are classified by their symptoms and neurological effects. In strict terms, stroke should only be applied to patients with an irreversible neurological deficit. Patients who have transient neurological symptoms that resolve with time leaving no permanent deficit are often referred to as having had a 'mini-stroke'. There are three main forms of transient symptoms. Transient ischaemic attack (TIA) is a transient, motor, sensory or speech related symptom that appears suddenly and resolves within 24 hours leaving no residual deficit. The reversible ischaemic

neurological deficit (RIND) is identical to the TIA except it resolves more slowly. Most cases resolve in 48 to 72 hours but some symptoms can last several weeks. The third form is amaurosis fugax which is temporary monocular blindness resulting from temporary embolic occlusion of the retinal artery and is in effect a TIA affecting the eye. Most TIAs and RINDs are a result of embolisation; there are multiple sources from which emboli can originate, including the carotid arteries.

1.4 Stroke Risk factors

Extensive clinical and statistical studies have identified several factors that increase the risk of stroke. Some or most of them can be modified, treated or controlled.

1.4.1 Hyperlipidemia

High levels of serum lipids have traditionally been regarded as a major risk factor for heart disease, but not for cerebrovascular disease.(Goldstein et al. 2001). A meta analysis of 45 different studies comprising 450,000 subjects in which 13,000 strokes occurred found no significant association between total serum cholesterol and total incidence of stroke (PSC 1995). However, serum lipid levels have been directly related to extracranial carotid artery atherosclerosis, including increased carotid wall thickness. It was shown that High Density Lipoprotein (HDL), provides a protective influence (Johnsen et al. 2005) whereas Low Density Lipoprotein (LDL) and total serum cholesterol increase the intima media thickness (IMT) of the carotid wall and help promote atheroma (Heiss et al. 1991). Some more recent clinical trials using serial ultrasound measurements showed that reductions of elevated LDL levels with statins (β-hydroxy-β-methylglutaryl-CoA reductase inhibitors), can modestly retard the progression of asymptomatic carotid atherosclerosis (Furberg et al. 1994; Crouse

et al. 1995). A more detailed review of the effects of cholesterol and lipid lowering drug treatments is discussed in chapter 5.

1.4.2 Atrial Fibrillation (AF)

In atrial fibrillation, instead of beating effectively the heart's atria beat rapidly and irregularly, which can lead to the blood pooling and clotting. If a clot breaks off, enters the bloodstream and lodges in an artery leading to the brain, a stroke results. Chronic AF without valvular disease has been associated with a five fold increase in stroke incidence (Wolf et al. 1991). It has been reported that AF is responsible for 15-20% of all strokes (Go et al. 2001). AF is also an independent risk factor for stroke recurrence and stroke severity (Penado et al. 2003).

1.4.3 Tobacco use

Cigarette smoking is a major, preventable risk factor for stroke. The nicotine and carbon monoxide in tobacco smoke reduce the amount of oxygen in the blood. They also damage the walls of blood vessels, making clots more likely to form. In a meta-analysis of 32 different studies, cigarette smoking was a significant independent contributor to stroke incidence in both sexes and at all ages and was associated with an approximately 50% increased risk overall compared to non-smokers. The risk of stroke in both men and women increases as the number of cigarettes smoked per day increases (Shinton and Beevers 1989). Other studies have shown that stroke risk in cigarette smokers is reduced significantly after two years following smoking cessation (Wolf et al. 1988; Kawachi et al. 1993). One study determined that stroke risk was the same as non-smokers, five years after smoking cessation (Wolf et al. 1988).

1.4.4 Diabetes mellitus

While diabetes is treatable, it still increases a person's risk of stroke. Many people with diabetes also have high blood pressure, high blood cholesterol and are overweight. This increases their risk even more. There is evidence of increased stroke risk in diabetics of 1.8 in men and 2.2 in women after the adjustment for the effect of other factors (Barrett-Connor and Khaw 1988). Other studies have also shown that diabetes increases the risk of stroke with the relative risk ranging from 1.8 to almost 6.0 (Goldstein et al. 2001). Studies have also shown that the impact of diabetes on stroke risk is greater in women than in men (Lukovits et al. 1999; Goldstein et al. 2001).

1.4.5 Other heart disease

People with coronary heart disease or heart failure have a higher risk of stroke than those with hearts that work normally. Dilated cardiomyopathy (an enlarged heart), heart valve disease and some types of congenital heart defects, also raise the risk of stroke. Coronary heart disease pre disposes to stroke by a variety of methods: as a source of embolisation from the heart, by virtue of shared risk factors, as a result of effects of medical and surgical treatments of coronary atherosclerotic disease or as a consequence of pump failure. In the 2 week period following acute myocardial infarction (MI) stroke occurs more frequently at an increased rate between 0.7% and 4.7% (Loh et al. 1997). This study also showed that older age and ventricular dysfunction following MI increased stroke risk. Treatment with aspirin or warfarin decreased the risk in a large group of MI survivors (Miller et al. 1993; Loh et al. 1997).

1.4.6 High blood pressure

High blood pressure (140/90 mmHg or higher) is a principal risk factor for ischaemic stroke as well as for intracerebral haemorrhage. The Framingham study reported an increased risk of stroke in the presence of hypertension of 3.1 in men and 2.9 in women when compared to normotensives (Wolf and D'Agostino 1998).

1.4.7 Physical inactivity and obesity

Being inactive, obese or both can increase the risk of high blood pressure, high blood cholesterol, diabetes, heart disease and stroke. Obese individuals have elevated levels of blood pressure, blood glucose and serum lipids which on that account alone could be expected to have increased stroke risk. Abdominal obesity has been shown to be an independent risk factor for ischaemic stroke (Suk et al. 2003).

1.4.8 Family history, sex and race

Several studies have indicated increased risk of stroke if there is a history of either paternal or maternal stroke (Welin et al. 1987; Kiely et al. 1993). Stroke is more prevalent in men than in women. Also overall, men have higher age specific stroke incidence rates than women (Sacco et al. 1998) . It has been shown that Blacks and Hispanics have higher stroke incidence and mortality rates, compared with Whites (Sacco et al. 1998; Rosamond et al. 1999).

1.5 Carotid Artery Atheroma.

Carotid artery disease is the underlying cause of 10 - 20% of strokes (Bamford et al. 1991). It is well documented that it is not only the degree of narrowing of the carotid artery but also plaque morphology, which are important risk factors for embolisation. The extracranial anatomy of the carotid bifurcation makes it amenable to ultrasound imaging and to surgical removal of atherosclerotic plaque (Fig 1.1).

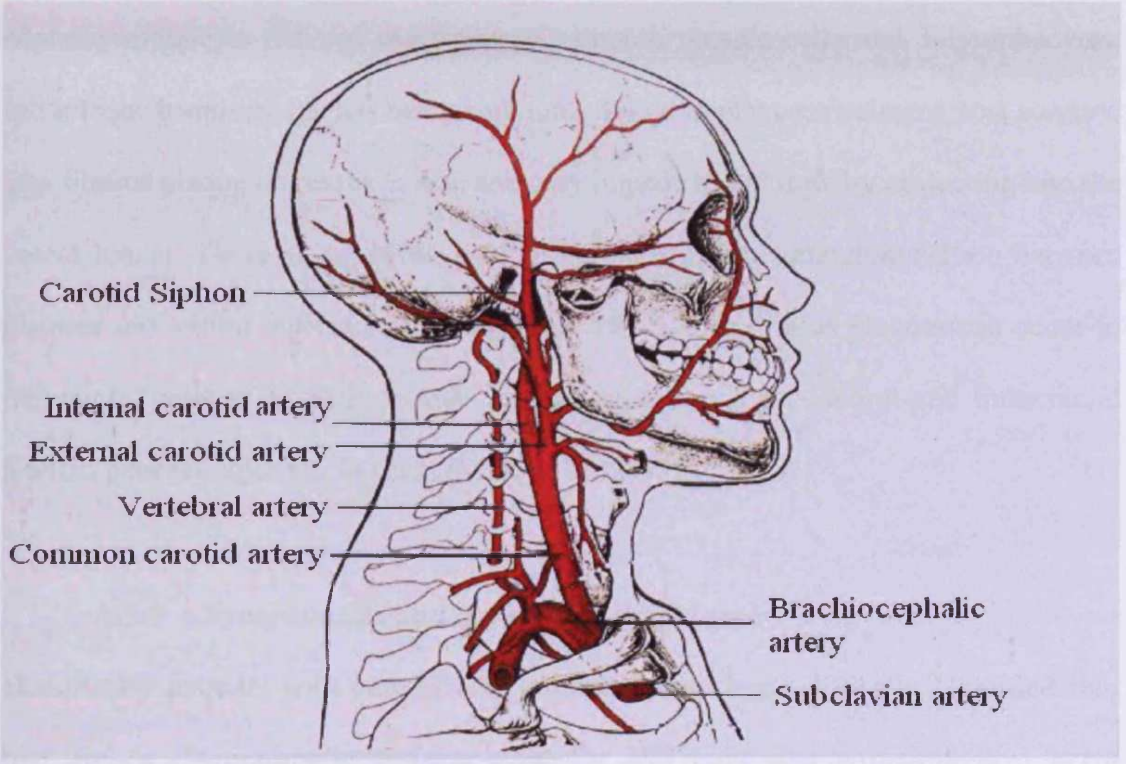

Figure 1.1 Arterial anatomy of the neck (Seeley et al. 2000).

1.5.1 Distribution of lesions in carotid arteries.

Disease of the carotid arteries usually occurs as a single or multi-focal lesion in the artery and not diffusely throughout the artery. The lesions occur most frequently at the bifurcations and curves, and most are found in the first two centimetres distal to the bifurcation. Fewer lesions occur in the intracranial portion in the siphon and

intracranially at the stems of the anterior and middle cerebral arteries (Mohr et al. 1998).

1.5.2 Carotid plaque morphology

The atherosclerotic plaque at the carotid bifurcation is an example of an advanced fibrous plaque. It is composed of a dense cap of connective tissue embedded with smooth muscle cells overlying a core of lipid and necrotic debris (Ross 1993). It contains monocyte derived macrophages, smooth muscle cells and T-lymphocytes. Intraplaque haemorrhage has been commonly found in plaque specimens post surgery. The fibrous plaque increases in size and may impede blood flow by projecting into the vessel lumen. There is, however, a large variability in plaque composition between plaques and within individual plaques (Falk 1992). The fibrous plaques can occur in the carotid arteries as early as age 25, but appear in the vertebral and intracranial arteries between ages 40-50 years (Mohr et al. 1998).

1.5.3 Symptomatic and asymptomatic plaques

Historically patients with carotid artery disease have been clinically classified into two groups. Symptomatic patients typically will have had a neurological event (stroke, TIA, RIND or amaurosis fugax) secondary to cerebral ischaemia, as a result of embolisation from carotid atherosclerotic disease. The asymptomatic group will not have had a neurological event but will have significant carotid disease.

1.5.4 Degree of stenosis

Doppler ultrasound is used in the diagnosis of stenotic lesions of the extracranial carotid arteries and has increasingly become the only examination performed before

surgical intervention (Grant et al. 2003). The criteria for intervention are based on several large multi-centre trials which have shown that symptomatic patients with a high grade stenosis of the internal carotid artery (ICA) would benefit from surgical removal of the lesion if the degree of stenosis is >70% (NASCET 1991; ECST 1998). The degree of stenosis is recognised as an important risk factor for stroke; however some patients with high grade stenosis remain stable and never develop cerebrovascular symptoms. It is well documented that the morphology of the plaque has an important role in whether the plaque remains stable or not. The presence of certain features in the plaque, in particular, intraplaque haemorrhage and ulceration are major factors in the onset of symptoms (Lusby et al. 1982; Imparato et al. 1983; Falk 1992).

1.5.5 Plaque echogenicity / heterogeneity

As described earlier, the use of ultrasound in the evaluation of the degree of stenosis is widely established. There is also a lot of research which has looked at the B-mode ultrasound appearance of the atherosclerotic plaque along with evaluating the degree of stenosis. The work has focussed on describing the plaque on the basis of its echogenicity, heterogeneity and surface characteristics (Reilly et al. 1983; Johnson et al. 1985; Bluth et al. 1986; Gray-Weale et al. 1988; Steffen et al. 1989; Widder et al. 1990; Cave et al. 1995; ECPSG 1995; Geroulakos et al. 1996; de Bray et al. 1998; Montauban van Swijndregt et al. 1998; Arnold et al. 1999; Schulte-Altedorneburg et al. 2000; Mathiesen et al. 2001).

It is important to define what is meant by echogenicity and heterogeneity as these terms are often interchanged in the literature. The echogenicity refers to the brightness level of the echoes in the image. An echolucent image would have no echoes and

appear black on the image, similar to blood. Echolucent plaques are often difficult to detect in the B-scan image and their detection is enhanced by use of colour flow duplex imaging. Echogenic plaques have strong bright reflections and are associated with an increasing amount of calcification and fibrous tissue. The heterogeneity of a plaque refers to the echo texture (Zwiebel and Knighton 1990). Carotid plaques can be homogenous (all the same texture) or heterogeneous (mixture of textures). In the literature some studies grade the plaques in terms of echogenicity (Johnson et al. 1985; Steffen et al. 1989; Cave et al. 1995; Geroulakos et al. 1996; de Bray et al. 1998; Mathiesen et al. 2001), some use heterogeneity only (Reilly et al. 1983; Bluth et al. 1986) and some use both (Gray-Weale et al. 1988; Widder et al. 1990; ECPSG 1995; Montauban van Swijndregt et al. 1998; Arnold et al. 1999; Schulte-Altedorneburg et al. 2000). In practice, echolucent and echogenic plaques can be either heterogeneous or homogenous in texture which is reflected in the varying number of subjective classification grading schemes that has been proposed (see section 1.6).

1.5.6 Plaque rupture

One of the most important questions posed when dealing with atherosclerotic plaques is why some plaques rupture? The risk of plaque rupture is dependent on the composition of the plaque rather than the size of the plaque, because only plaques rich in soft extracellular lipids are vulnerable (Falk 1992). The rupture usually happens at the periphery of the fibrous cap that covers the lipid rich core. This point is where the cap is usually the thinnest and most heavily infiltrated by macrophage foam cells (Fuster et al. 1990; Falk 1992). There are also other factors influencing when rupture happens such as increased shear stress forces in the area of a stenosis and the quantity

of macrophages and T lymphocytes present in the plaque (Fuster et al. 1990; Golledge et al. 2000).

1.6. Subjective ultrasound assessment of carotid plaques

1.6.1 Subjective Grading methods

The subjective grading of carotid plaques was first reported in 1983. Two different types of plaque were described; homogenous plaques were described as plaques with uniformly high or medium level echoes, whereas heterogeneous plaques were defined as plaque with a mixture of high, medium or low level echoes (Reilly et al. 1983). Histologically the homogenous plaques were mainly fibrous whereas the heterogeneous plaques contained variable amounts of intraplaque haemorrhage, lipids and cholesterol crystals. Another *in vitro* study looked at the histology of aorta, iliacs and CEA specimens and compared them to ultrasound echogenicity. They found that with large fibro-fatty lesions, lipid appeared echolucent whereas fibrous tissue was more echogenic, and that calcification appeared the most echogenic (Wolverson et al. 1983). Bluth and colleagues used a similar 2 category method and found it could successfully detect intraplaque haemorrhage (Bluth et al. 1986), this was also the finding of another group who reported high sensitivity and specificity for the detection of intraplaque haemorrhage by B-mode ultrasound (O'Donnell et al. 1985). However Ratliff's group used a five category method and concluded that only calcification could be reliably detected from the B-scan image (Ratliff et al. 1985).

Johnson in 1985 described 3 different types of plaque, calcified, dense (high level echoes) and soft (low level echoes) and found a greater tendency for soft plaques to contain haemorrhage and ulceration (Johnson et al. 1985). A refinement of the above

classification into 4 categories was introduced by Grey –Weale in 1988. This classification criterion has been used in multi-centre trials and is still used in some vascular laboratories today (Gray-Weale et al. 1988).

The 4 categories are

Type 1: Dominantly echolucent plaques with a thin echogenic cap. (Fig. 1.2)

Type 2: Substantially echolucent lesions with small areas of echogenicity. (Fig. 1.3)

Type 3: Dominantly echogenic lesions with small areas of echolucency. (Fig. 1.4)

Type 4: Uniformly echogenic lesions. (Fig. 1.5)

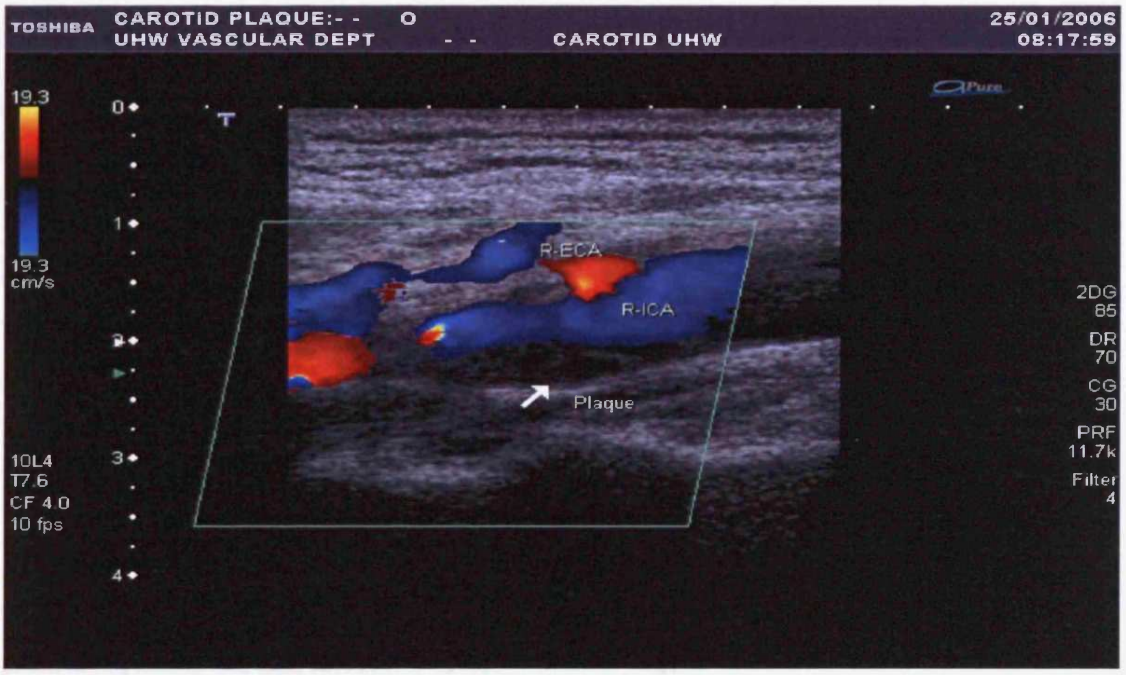

Figure 1.2 Echolucent Grey-Weale type 1 plaque. The colour flow is required to delineate the plaque from the vessel.

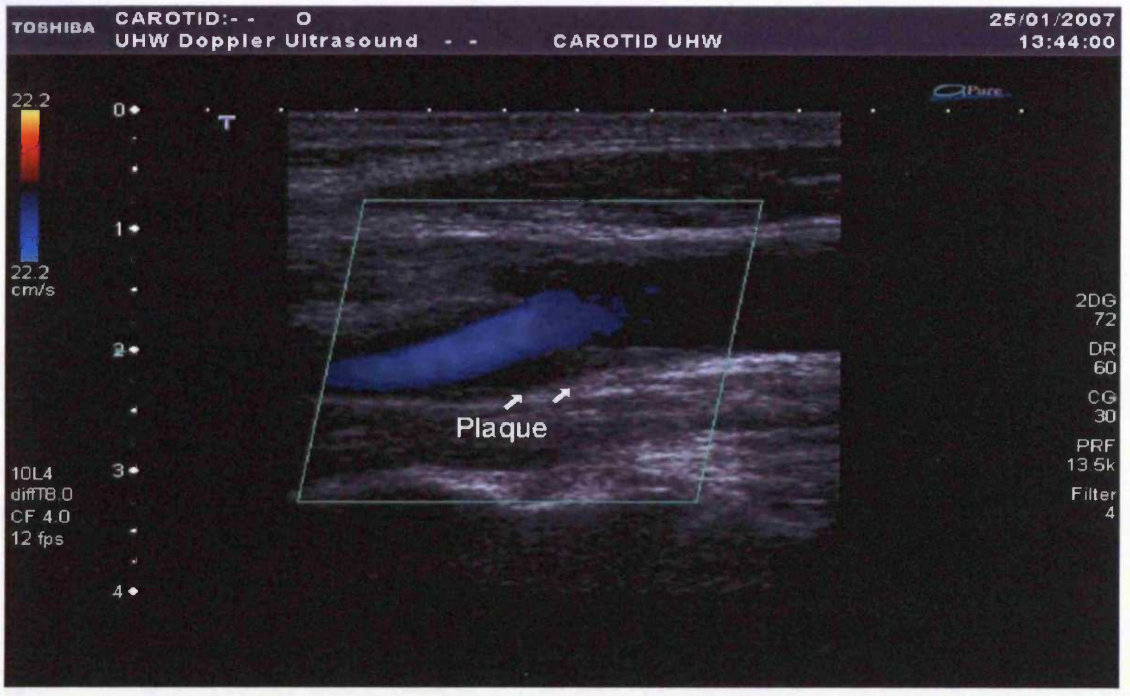

Figure 1.3 Mainly echolucent Grey-Weale type 2 plaque with small areas of echogenic material.

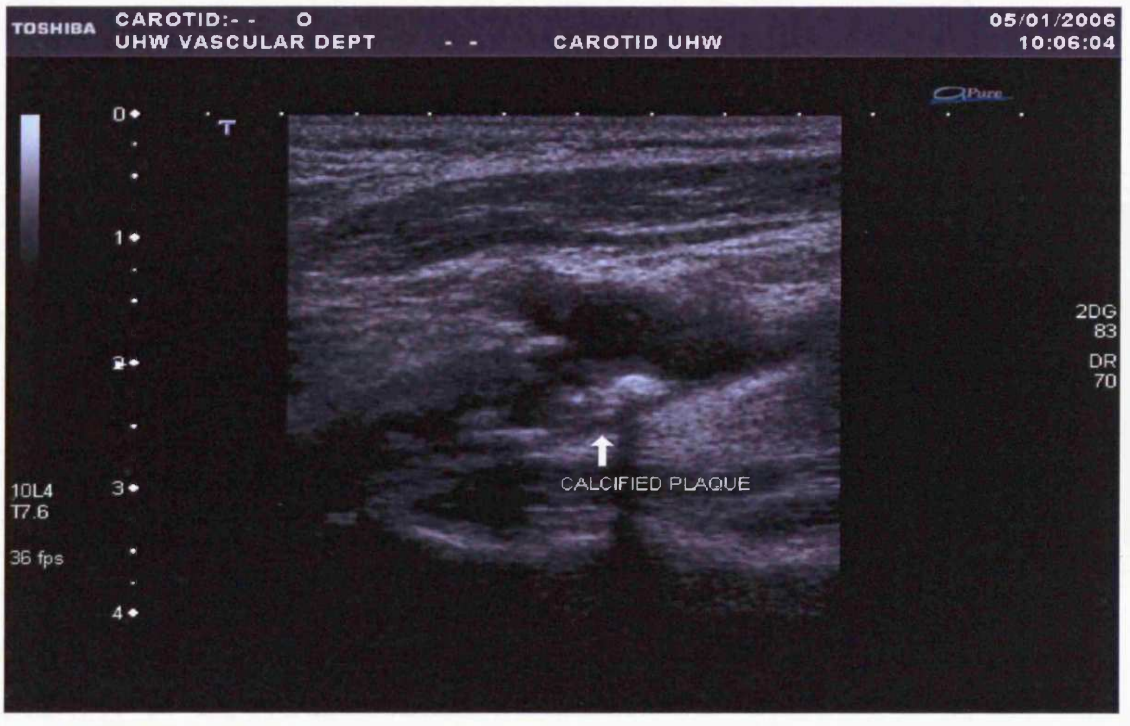

Figure 1.4 Mainly echogenic Grey-Weale type 3 plaque with small areas of echolucent material.

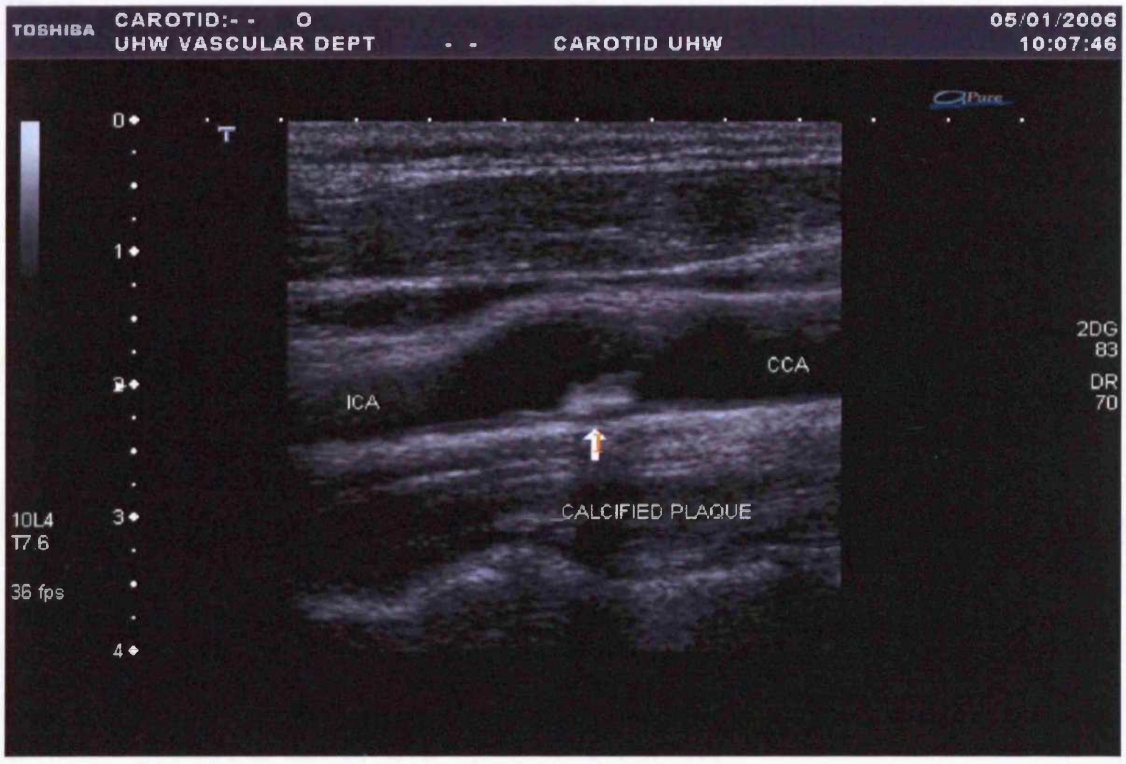

Figure 1.5 Echogenic Grey Weale type 4 plaque.

Later classification methods described a fifth category for calcified plaques that cannot be classified due to acoustic shadowing (Geroulakos et al. 1993). Many other studies which used ultrasound echogenicity, either alone or with heterogeneity concluded that echolucent plaques are related to the unstable plaque. These plaques were found to contain lipid, intraplaque haemorrhage and ulceration (Gray-Weale et al. 1988; Widder et al. 1990; Cave et al. 1995; Geroulakos et al. 1996; ECST 1998; Arnold et al. 1999; Schulte-Altedorneburg et al. 2000). These studies also concluded that the echogenic plaque mainly contained fibrous tissue with or without some calcification.

There is a trend of finding unstable plaque morphology in carotid endarterectomy (CEA) specimens of symptomatic patients, and also of mainly having an echolucent ultrasound appearance (Steffen et al. 1989; Cave et al. 1995; ECST 1998; Mathiesen et al. 2001). In asymptomatic patients there is a tendency to find more echogenic

(Grey-Weale type 3 and 4) plaques. The main histological content of these echogenic plaques was fibrous tissue with some calcification (Reilly et al. 1983; Gray-Weale et al. 1988; Steffen et al. 1989; Geroulakos et al. 1993; Cave et al. 1995; Schulte-Altedorneburg et al. 2000).

The histological appearance of ulceration in the plaques prompted some researchers not only to look at the ultrasound echogenicity/heterogeneity, but to also comment on ultrasound plaque structure (O'Donnell et al. 1985; Widder et al. 1990; Feeley et al. 1991; Eliasziw et al. 1994; ECST 1998). They described the plaque structure by looking at the plaque surface and describing it as regular, irregular, ulcerated or not possible to evaluate.

1.6.2 Variations in subjective grading

There is a considerable variation in the results reported on subjective grading of plaques. This variation can be attributed to several factors. Firstly there appears to be no consensus in methodology or protocol used in most of the studies. For example there is a range from 2 subjective categories (Bluth et al. 1986; Arnold et al. 1999) to 6 categories (Schulte-Altedorneburg et al. 2000) used for grading the plaques. There is also variation in how the ultrasound appearance is described with some groups using heterogeneity, some using echogenicity and some a combination of the two. Some studies are compared to histology and some look at plaque structure. Table 1.1 summarises the methods used and emphasises the lack of standardisation in methodology.

Reference	No of categories	Type	Histology	Plaque structure examined	Repro. studies done	Conclusion
(Reilly et al. 1983)	4	H	Yes	No	No	Ultrasound can be used to detect haemorrhage and ulceration.
(Wolverson et al. 1983)	2	E	Yes	No	No	Lipid echolucent, fibrous more echogenic. Calcification highly echogenic
(O'Donnell et al. 1985)	2	B	Yes	Yes	No	High specificity and sensitivity for detection of ulceration and intraplaque haemorrhage.
(Johnson et al. 1985)	3	E	Yes	No	No	Soft plaques have tendency to contain haemorrhage/ulceration.
(Ratliff et al. 1985)	5	H	Yes	Yes	No	Only calcification can be detected reliably by ultrasound.
(Bluth et al. 1986)	2	H	Yes	Yes	No	Can accurately detect haemorrhage on ultrasound.
(Gray-Weale et al. 1988)	4	E	Yes	Yes	No	Echolucent plaques more unstable and associated with symptoms.
(Steffen et al. 1989)	4	E	Yes	Yes	No	Echolucent heterogeneous plaques associated with haemorrhage and echogenic plaques with fibrous ± calcification.
(Widder et al. 1990)	4	E	Yes	Yes	No	Ulceration cannot be reliably detected by ultrasound and intraplaque haemorrhage cannot be differentiated from atheromatous debris.
(Geroulakos et al. 1993)	5	E	No	No	No	Echolucent plaques correlated with symptoms.
(ECST 1998)	3	B	Yes	Yes	No	Echogenicity related to amount of soft tissue. Symptomatic patients have more soft tissue.
(Cave et al. 1995)	4	E	Yes	No	No	Plaque echolucency related to symptoms.
(White et al. 1997)	4	E	Yes	Yes	Yes	*In vitro* study found poor agreement except for calcification.
(de Bray et al. 1998)	5	E	No	Yes	Yes	Subjective classification could be improved by standardisation of methods used.
(Montauban van Swijndregt et al. 1998)	3	B	Yes	No	Yes	B mode ultrasound cannot accurately determine the volume of fibrosis/lipid and intraplaque haemorrhage.
(Arnold et al. 1999)	2 and 4	B	Yes	No	Yes	Reproducibility grading of ultrasound images not achievable.
(Schulte-Altedorneburg et al. 2000)	6	B	Yes	Yes	No	B-mode ultrasonography is able to predict histology components and texture of carotid plaques.

Key: H = Homogeneity, E = Echogenicity, B = both heterogeneity and echogenicity.

Table 1.1 Subjective methods of classifying carotid atherosclerotic plaques

Secondly when the subjective grading is compared with histology, a wide range of agreements has been reported. Montuaban et al (1998) concluded that the assumption that homogenous and echolucent plaques are related to unstable lipid rich plaques and the heterogeneous echogenic plaques to the stable fibrotic plaques has not been supported by evidence of a connection between the echo pattern and volume of plaque constituents (fibrous, lipid or haemorrhage). Also some investigators (Reilly et al. 1983; O'Donnell et al. 1985; Bluth et al. 1986) considered the echolucent areas within plaques to represent intraplaque haemorrhage, but other investigators have questioned the ability of B-mode ultrasound to identify tissue as being haemorrhage (Ratliff et al. 1985; Widder et al. 1990; Hatsukami et al. 1994). There are also conflicting results published regarding ulceration; some found that it could be accurately detected by ultrasound (Hennerici et al. 1984; O'Donnell et al. 1985) while others found poor correlation (Ratliff et al. 1985; Bluth et al. 1986; O'Leary et al. 1987; Widder et al. 1990). A major factor in the discrepancy arises from the fact there is a lack of a standardised criteria for both ultrasound and histological classification (ECST 1998; Lovett et al. 2005), and in the case of ulceration a lack of a standardised definition of what ulceration appears like on ultrasound (ECPSG 1995).

Finally, there is a problem with reproducibility. There are limited studies on subjective grading reproducibility, and comparison with histology (White et al. 1997; Arnold et al. 1999). Arnold et al. (1999) looked at both inter and intra observer variability using both 2 and 4 category classification systems using 4 different observers. They found only moderate intra and inter-observer agreement for the 2 category and poor to fair agreement for the 4 category when using B-mode hard copy images, with slight improvement in agreement with the addition of colour flow and when using digital images. The range of agreements improved with increasing

observer experience. They found only poor to fair correlation between histology and plaque grading with almost no correlation in some cases. White et al (1997) compared 148 ultrasound and histology images and found only reasonable intra observer agreement for calcification only when one observer examined the images on two separate occasions. They reported very poor inter observer agreement, made by two observers and a pathologist, between the observers or with actual histology identified by a histologist.

In conclusion there is considerable bias associated with these subjective methods of grading plaques which is not helped by the lack of standardisation of protocols and the way in which they are compared to histology. Objective methods have superseded these subjective methods in trials, but the latter are still used in vascular labs.

1.7 Objective assessment using ultrasound

Objective ultrasound methods for characterising tissue usually involve some computer assisted way of looking at the echolucency, heterogeneity, or surface features of the tissue. The main objective methods usually involve either statistical analysis of the grey tones of the video output, or radiofrequency (RF) backscatter analysis. The work in this thesis uses statistical analysis which looks at the tone, texture and speckle patterns that make up an image. The flow diagram in figure 1.6 shows the different objective methods and their relationships.

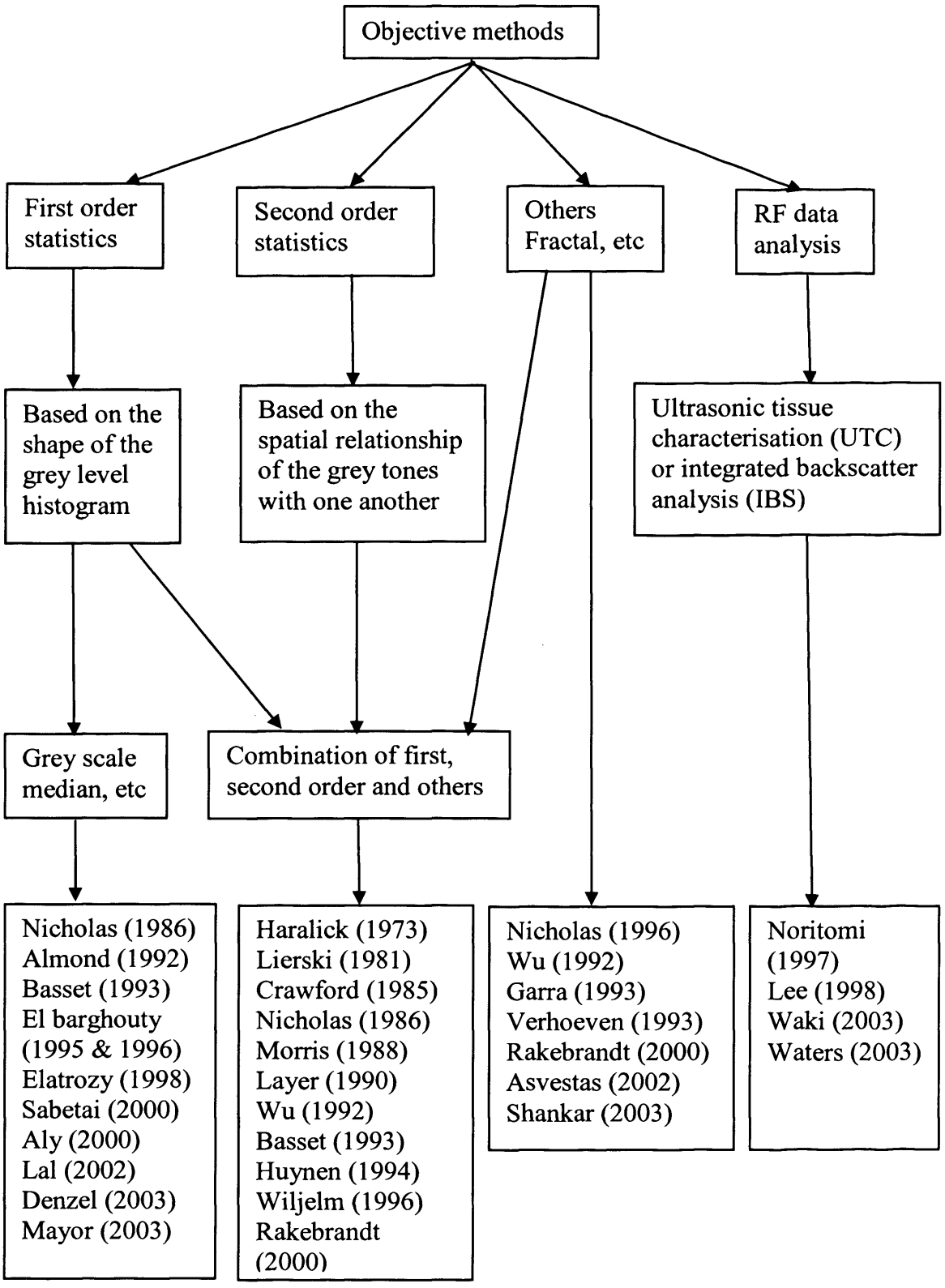

Figure 1.6 Flow chart showing main objective methods of tissue characterisation.

1.7.1 Tone and Texture

It is important initially to define what is meant by the terms, tone, texture, and speckle with respect to ultrasound images. Tone is concerned with the varying shades of grey within a monochromatic image. The spectral features of an image describe the average tonal variations in various bands of the visible portion of the electromagnetic spectrum.

Texture is a property of all surfaces and contains information regarding the structural arrangement of surfaces and their relationship to their environments. In the case of images, texture is concerned with the spatial (statistical) distribution of the grey tones. Textural features contain information about the spatial distribution of tonal variations within a band (Haralick et al. 1973). There are also contextual features which contain information about the area surrounding the area being analysed.

Tone and texture are not independent of one another but are inextricably linked. The features of tone, texture and context are always present in an image, but one feature can dominate the others. The main features of interest are tone and texture, as context contains information derived from regions surrounding the main area of interest (Nicholas et al. 1986). When there is little variation of features of discrete grey tone (i.e. the more black and white an image) then the dominant property of that area is tone and if there is a wide variation of features (i.e. the more shades of grey) then the dominant property is texture (Haralick et al. 1973).

It is easy for observers to define structure in empirical terms, but it is difficult to define precisely and analyse using digital computers.

1.7.2 Speckle

Speckle is the result of the interaction of the ultrasonic field with tissue components. Because tissue consists of structures small compared with the wavelength of sound, the ultrasound wave is scattered. The speckle pattern arises from the locally coherent ultrasound wave fronts scattered from these small structures (Morris 1988a). The speckle pattern is a property of the volume generating it, the transducer generating it, the frequency of the ultrasound pulse, direction of the ultrasound beam into the volume, overlying tissue and signal processing. Therefore the speckle pattern is both tissue dependant and machine dependant, and hence any tissue characterising process will provide information regarding the ultrasound scanning machine and the ultrasound scattering process.

The various features affecting the scattering such as reflector density, size or distribution are specific to each kind of tissue or even to its pathological state (Basset et al. 1993). Although speckle generally is a source of image degradation and is viewed as a source of acoustic noise, speckle also contains information relative to the tissue structure investigated and thereby constitutes a tissue signature.

1.7.3 First order Statistics

These are the simplest and most basic forms of statistics used to characterise images. They are based on the fact that a discrete image array can be represented by a first order probability distribution of image amplitude (Nicholas et al. 1986). It is these features that are used to generate a class of image features. The shape of the histogram characterises the image. Simple measures which describe the shape of the first order histogram are arithmetic mean, median, standard deviation, variance, skewness and kurtosis (appendix 1.1). The mean divided by the standard deviation is the speckle

signal to noise ratio (SNR) (Basset et al. 1993). It has been shown that the speckle caused by a high number of scatterers in the resolution cell is fully developed which corresponds to a SNR = 1.91. The number of scatterers in the resolution cell required for speckle to be fully developed is $>10^4$ cm^{-3} (Oosterveld et al. 1985). Skewness is a measure of the lack of symmetry of the grey scale histogram. A data set is symmetric if it looks the same to the right and left of the centre point.

Kurtosis is a measure of whether the data are peaked or flat relative to a normal distribution. That is data sets with a high kurtosis tend to have a distinct peak near the mean, decline rather rapidly and have long tails which extend further from the mean than those with a normal distribution. Data sets with low kurtosis tend to have a flat top near the mean rather than a sharp peak. First order statistics are highly dependant on the machine settings (Nicholas et al. 1986; Basset et al. 1993).

1.7.4 First order statistics in tissue characterisation

Almond and Pryce (1982) characterised the placenta using the echo peak amplitude distribution to describe two first order parameters, namely coefficient of variation and skew. Their results indicated that the texture value reflected the degree of calcification and fibrin within the tissue (Almond and Pryce 1982). It has also been reported that first order statistics, using mean grey level, may be useful for discriminating features especially for liver tissues (Layer et al. 1990). Measurements of the grey level histogram width value were found to be useful in clinical practice and reproducible when looking at grading the placenta (Maeda et al. 1998).

A lot of work recently has focussed on the use of first order statistics involving measurements of the grey-scale median (GSM) of carotid plaque images. The technique involves capturing the ultrasound image, then digitising the image on a

personal computer (PC). The plaque is outlined and the grey scale content analysed (255- white, 0- black) for mean, standard deviation, median and total pixel count. A histogram is produced and the GSM is used as a measure of the overall plaque echogenicity. Initial studies compared the GSM of carotid plaques with brain CT scans of symptomatic patients and found that high GSM (echogenic plaque) were associated with a low incidence (11%) of CT brain infarct whereas low GSM (echolucent plaques) were associated with a higher incidence (55%) (El-Barghouty et al. 1995). Further studies from the same group showed that GSM correlated well with histology sections that were examined by computer morphometric analysis (El-Barghouty et al. 1996). They found that plaques with a high lipid and haemorrhage content as established histologically, had a low GSM and those with a high fibrous content had a high GSM. These findings were confirmed in a later study (Lal et al. 2002) which concluded that pixel distribution analysis can accurately quantify intraplaque haemorrhage, fibromuscular tissue, calcium and lipid.

El-Barghouty's group improved their approach by developing a standardised method for classification among different ultrasound scanner settings and recording media. They also assessed the relationship between GSM value of carotid plaque and the clinical symptoms of unstable plaque morphology, and found that patients with symptomatic lesions were associated with low GSM values (i.e. echolucent plaques). Asymptomatic lesions tended to have high GSM values (i.e. echogenic plaques) (Elatrozy et al. 1998). A recent publication showed good concordance between visual (subjective) analysis and GSM regarding plaque heterogeneity (Mayor et al. 2003) while another found that the composition of the plaque cannot be visualised with sufficient accuracy by sonographic GSM analysis (Denzel et al. 2003).

Aly and Bishop (2000) used the mean pixel value (MPV) as an index of echogenicity and assessed its value as a measure to characterise carotid atherosclerotic plaque. They found that the MPV of the carotid specimens correlated significantly with the histological findings and that the technique may be used to identify unstable atherosclerotic plaques reliably. Their study showed that as the soft content of the plaque increased, the MPV decreased, and as the fibro-calcific content increased the MPV increased (Aly and Bishop 2000).

In practice two difficulties arise when parameters derived from first order statistics are used. Firstly the mean grey level depends on the gain, and secondly it has been said that tissues affected with the same pathology may have different acoustical properties (Basset et al. 1993). This has been shown with prostate cancers, which in most cases are hypoechoic but may also be iso- or hyperechoic.

The dependence of first order statistics on the equipment settings is crucial and detailed calibration and standardisation of the scanning equipment is vital (Nicholas et al. 1986).

1.7.5 Second order statistics

Early image texture studies employed auto-correlation functions, power spectra, restricted first and second order Markov meshes and relative frequencies of various grey levels of un-normalised images. These methods had limited success but they didn't try specifically to define or model texture.

Haralick proposed that the texture in an image is contained in the overall or average spatial relationship which the grey tones have with one another (Haralick et al. 1973). This assumption more specifically assumes that this texture information is adequately specified by a set of grey tone spatial dependence matrices which are computed from

various angular relationships and distances between neighbouring resolution cell pairs on the image (appendix 1.2). From these grey tone spatial dependence matrices, textural features can be extracted. A set of 14 textural features can be defined (appendix 1.3). Some of these features are related to specific textural characteristics such as homogeneity, contrast and the presence of organised structure within an image. Other measures characterise the complexity and nature of grey tone transitions within an image.

The angular dependencies can create a problem within an image and Haralick suggests that two functions of mean and range, which are invariant of angle, could be used as an input to a classifier. Thus mean and range, for each of the 14 features, comprise a set of 28 features which can be used as a classifier. A feature selection procedure may be applied to select a subset or linear combinations of the 28 features.

The use of second order statistics is computationally more demanding than first order statistics, but that is not such a problem with the advent of high speed personal computers and specialised software.

1.7.6 Second order statistics in tissue characterisation

Initially Haralick et al (1973) used the textural features to look at three sets of data. They looked at photomicrographs of sandstones, an aerial photographic data set and a data set derived from satellite imagery. They used various subsets of the 28 features on each of their three sets of data and achieved 89%, 82.3% and 83.5% classification success for the three sets.

Lerski et al (1981) used RF signals from liver data and discriminant analysis to classify liver disease. They used 8 out of 22 co-occurrence textural features in the multivariate analysis with a classification accuracy of 70-90% for 8 parameters. They

also reduced the number of features from 8 to 4 and down to even one with no significant reduction in the classification rate. Of the 22 features investigated, 13 were found useful in distinguishing textures (Lerski et al. 1981).

Nicholas et al (1986) used five different methods (first order statistics, spatial echo density, spatial derivative, Fourier domain series and second order statistics) which comprised 93 individual features of which 12 were second order statistics. They then used multivariate analysis of variance to discriminate the B scan textures of spleen and livers. The data were separated into two groups, a training set and a test set which were used for calculating and testing of the discriminant function. They achieved an overall probability success of 82% on a single image and 94% on a subject yielding multiple images.

Morris (1988a) described a means of correcting for depth dependence of the co-occurrence matrices (Morris 1988a). He used corrected features to characterise the texture of the images and found the corrected co-occurrence derived features to be correlated with a subjective assessment of the texture. He also demonstrated significant differences in the texture of the placentae of smokers and non-smokers whereas Crawford et al (1985) did not. Morris also showed differences in normotensive and hypertensive patients (Morris 1988a).

Further work from the same author (Morris) used co-occurrence matrices to devise a simple algorithm for deriving a correction factor for depth dependence using a foam phantom and demonstrated its efficacy on placental data. The method used is not restricted to co-occurrence matrices or any particular scanner as the correction curves can be derived for any particular algorithm or scanner (Morris 1988b).

Layer et al (1990) used a combination of first and second order statistics to look at fatty liver disease of rats using B-scan texture analysis. They found over 90%

classification accuracy but also reported that the most useful parameter for classification was the first order statistic of mean grey level (Layer et al. 1990).

Wu (1992) used a combination of spatial grey level dependence matrices (SPLDM), Fourier power spectrum , grey level dependence matrices and Laws texture energy measures and proposed a new texture set called multi-resolution fractal (MF) features to classify 3 sets of different liver texture. They compared the various techniques individually, and also combined the various texture methods and found that a combination of SPLDM and MF had a classification rate of about 90% whereas SPLDM alone was about 83% for the 3 different sets. They also found that SPLDM was very slow and time consuming in calculation (Wu and Chen 1992).

Basset (1993) used second order statistics to discriminate between various prostate tissues (normal, benign prostatic hypertrophy and cancer) and achieved a 78% classification success rate. The success rate decreased when using a smaller region of interest sample size (Basset et al. 1993).

Huynen et al (1994) used 5 second order parameters derived from co-occurrence matrices for the detection of prostatic carcinoma from ultrasound images and compared them to biopsy. They achieved over 77% sensitivity and specificity for both retrospective and prospective studies and determined a positive predictive value for cancer detection of 85.7% which was almost twice as high as the values normally found for prostate examination (Huynen et al. 1994).

1.7.7 Second order statistics in carotid plaque characterisation

Wilhjelm et al. (1996) compared a combination of first and second order statistical textures with histology of carotid plaques. They used a combination of 27 parameters and found that 3 second order parameters (diagonal moment, standard deviation and

autocorrelation) gave the best correlation with both soft tissue materials and fibrous materials (p=0.04). They did conclude, however, that the correlation was not good enough to be used clinically to predict plaque constituents (Wilhjelm et al. 1996). Further work from the same group looked at a quantitative comparison between three types of information, namely subjective visual grading, analysis using first and second order statistics and histology. They concluded that the plaque structure and echogenicity could subjectively be predicted from static ultrasound images with a reasonable degree of accuracy. They also concluded that prediction of plaque volume using the statistical methods showed significant results but were not strong enough to be useful for clinical prediction (Wilhjelm et al. 1998).

Arnold et al (2001) used a combination of first and second order statistical methods to derive discriminant analysis functions for B-scans of 50 carotid atherosclerotic plaques and compared the results retrospectively with histology. They then prospectively applied the discriminant functions to a further 50 carotid plaques for classification.

They achieved 65% grading success of the ROIs into one of 4 groups representing calcium, fibrous tissue, lipid and haemorrhage which shows improved correlation when compared with previous studies of Arnold et al (1999). Their technique also had an increased ability in the detection of intraplaque haemorrhage achieving 81% sensitivity and 83% specificity (Arnold et al. 1999; Arnold et al. 2001).

1.7.8 Spectral backscatter analysis of RF signals

All of the studies mentioned and the techniques used in this thesis have used methods that look at the B-mode images as the raw data, an alternative data source is to use spectral analysis of the backscattered radiofrequency signals. The method is based on

looking at the raw RF signal and using spectral analysis to calculate three parameters of the calibrated power spectrum, namely slope, intercept and total power. This technique has been used in several studies looking at carotid plaque characterisation (Noritomi et al. 1997; Lee et al. 1998; Waki et al. 2003; Waters et al. 2003). All these studies compared their RF data with histology but used two different analysis techniques to display their results. Noritomi et al (1997) and Lee et al (1998) used ultrasonic tissue characterisation (UTC) based on the RF data to classify fibrous, lipid and thrombus constituents of carotid plaques. The classification was derived using discriminant function analysis and both groups reported high overall classification rates of ~88% for the three types of tissue. The approach of Waki et al (2003) and Waters et al (2003) was to compare integrated backscatter (IBS) with histology to derive IBS values for each of the component tissues of the carotid plaque. Waki reported significant differences in the IBS values of lipid from that of fibrous, calcified or haemorrhagic tissue but no significant difference between lipid and thrombus. They also found that the IBS value was lower in the thin fibrous cap than in the main lesion, which may be useful in identifying unstable plaques. Waters constructed parametric images from the IBS values and the slope, intercept and midband values of a straight line fit to a backscatter transfer function. Their results showed good agreement with histology for some parameters but poor for others. They concluded that their investigation identified several improvements in experimental techniques that would benefit future studies. The use of RF data requires specialised equipment to obtain the signals from the scanner which is not readily available in most ultrasound centres.

1.7.9 Other tissue characterisation methods

Several other methods have been used to characterise ultrasound images, often in conjunction with the techniques mentioned previously. Fractal analysis is a measure of the roughness of the intensity surface of an image, the properties of which can be quantified by use of the fractal dimension. The fractal dimension is highly correlated with the human perception of image roughness. The higher the fractal dimension the rougher the texture surface. It has been used to characterise B-mode breast images (Garra et al. 1993), liver images (Verhoeven and Thijssen 1993) and carotid plaque images (Rakebrandt et al. 2000; Asvestas et al. 2002). Other methods include spatial echo density, spatial derivative, Fourier domain series (Nicholas et al. 1986) and Laws texture energy measures (Wu and Chen 1992).

An alternative statistical approach was undertaken by Shankar et al (2003). They conducted a feasibility study to model atherosclerotic plaque in carotid B-mode images. They used a bimodal gamma distribution with five parameters to model the statistics of the pixels in the grey level images and found the bimodal distribution to be a reasonable fit to the statistics of the pixels (Shankar et al. 2003).

1.7.10 Limitations of objective ultrasound assessment

The need to overcome the subjectivity of visual grading of atherosclerotic plaques is obvious (see section 1.6.2). To this end several objective methodologies have been examined, however, these are not without their limitations. The lack of standardisation within methods and between methods is apparent and only one study has addressed the issue by proposing a method to standardise GSM analysis (Elatrozy et al. 1998). Another major source of discrepancy is the comparison of the various imaging methods with histology. Studies comparing histology with imaging have

shown highly variable results even for similar imaging methods, this is more likely due to variable histological techniques rather than imaging methods (Lovett et al. 2005). The goal of objective carotid plaque characterisation of most studies is to elucidate the constituents of the plaque in order to identify the unstable ones. There is a lot of variation reported on what plaque constituents need to be identified to determine what makes up an unstable plaque. Some studies look at objective methods of identifying soft from calcified plaques, others look at identifying fibrous and calcified tissues from lipid and haemorrhage, while others look at the fibrous cap thickness. Another problem with both the imaging methods and the histological techniques is the lack of reproducibility studies. Lovett et al (2005) in his review of 73 studies that compared carotid imaging and histology showed that only17 (23%) of the studies reported reproducibility studies of the imaging technique. Their review of the histology showed that only 9 (12%) of the studies reported reproducibility of the histological assessments. A further 3 (4%) studies reported inter-observer variability and 2 studies reported κ values for the agreement between histological assessment (Lovett et al. 2005). A more comprehensive review of carotid plaque histology assessment is discussed in chapter 4.

1.8 Previous work from our group

One of the aims of this thesis was to use methods previously developed by our group and to build on these methods for use in predicting carotid plaque constituents *in vivo* and to see if these methods could be used to monitor plaque changes over a period of time. The previous work looked at characterising carotid plaques *in vitro* by comparing them with histology post carotid endarterectomy (CEA). The method is based on producing parametric images of B-scan texture using statistical and textural algorithms and using them to predict plaque morphology (Rakebrandt et al. 2000). The following is a summary of the work.

1.8.1 *In vitro* B-scan image acquisition

The technique used intact carotid plaque specimens post CEA which were embedded, at a fixed depth, in a 1% agar solution inside a specially designed block mould. A series of 2D B-scan images was recorded at 0.5mm spacing with the machine settings kept constant for all the plaques. The positional reproducibility was maintained by adapting a positional jig of a BECA beam calibrator system (gammex-RMI, Nottingham, UK.). The BECA system used was regularly tested by NPL, but the positional reproducibility was not tested by Rakebrandt in his study. He used the scale on the jig for probe positioning and recorded a sequence of transverse images. The resulting images were digitally stored and transferred to a PC (Rakebrandt 2001).

1.8.2 Image analysis

For each sequential US image a region of interest (ROI) was drawn around the plaque. The ROI was then segmented into non-overlapping analysis kernels. For the series of 2D images, each kernal represented a 9 x 9 pixel region representing a tissue volume

of 0.85mm (horizontally) x 0.87 (vertically) x 3.9mm (thick). In this study 10 excised plaques were used which yielded a total of 7508 kernals suitable for texture analysis. Using MATLAB (The Math Works inc, Natick MA), 157 textural and structural algorithms were applied to each analysis kernal (Rakebrandt 2001). The idea of applying the algorithms to the kernals was to see which of the algorithms would be useful in separating the data into different types. Initially multivariate discriminant analysis was implemented in SPSS software to determine the discrete number of textures which could be identified in the carotid plaques. The results of the 157 algorithms were normalised, to prevent bias, using Z-score. When a sequence of K-mean cluster analysis was constrained to separate the data into 2 to 12 groups, the classification rate gradually diminished as the number of selected classes increased. A local maxima was observed for 5 classes indicating a preference for the data to be separated into 5 different groups, which concurred with the 5 texture classes indicated by histology. Using the output data constrained to 5 texture groups a sequence of parametric texture images was constructed for each sequential B-scan image for each excised plaque.

1.8.3 Histological comparison with parametric image

Following the *in vitro* imaging, and maintaining the plaque orientation, the plaques were decalcified, embedded in paraffin wax, and histology slices were taken at 1mm intervals throughout the plaque. The slices were mounted on glass slides, stained and examined by a histologist. The five tissue types of elastic, fibrous, lipid, calcium and haemorrhage were identified from the plaques. The histology slices were then visually matched to the parametric images. One plaque, in particular, had deposits of all 5 tissue types and this was used to train the ultrasound texture classification image

(UTCI). This UTCI was then used to test the ability of the system to predict the histology of the other plaques.

1.8.4 Reported results

The proportion of calcium identified by histology was 55% of that predicted by the UTCI which is explained by the histological decalcification process. The plaques were decalcified, using formic acid, to protect the blade when the plaque was sliced. Fibrous and elastic tissue were the dominant tissues found in the plaques and appeared to be predicted accurately by UTCI. Lipid was found to be correctly predicted in 7 of the 10 plaques but over predicted by the UTCI by 25% in the others which was explained by the fact that lipid is dissolved during the histological process especially if found adjacent to calcium. The amount of haemorrhage was under-predicted consistently by UTCI compared with histology; this was explained by the size of the blood clots which were smaller than the kernal size.

1.8.5 Study conclusion

The main problem highlighted was the effect of the histology processing on the plaque. The conclusion was that the UTCI can predict the spatial relationship of plaque constituents from differences in US B-scan texture and can provide sufficient information to classify different tissue types within carotid plaques (Rakebrandt et al. 2000; Rakebrandt 2001).

1.9 3D Ultrasound

In this project 3D ultrasound is used to acquire images of the carotid plaques both *in vivo* and *in vitro* post endarterectomy. 3D ultrasound is an emerging technology with many clinical applications including carotid artery imaging. It has many advantages over 2D ultrasound, most notably allowing direct visualisation of the 3D anatomy. It also allows volume data to be displayed using 2D slice views of coronal, sagittal and axial planes that are difficult or impossible to attain using standard 2D ultrasound. 3D ultrasound also allows measurements of organ volume and irregularly shaped structures to be obtained more accurately (Nelson and Pretorius 1998). The process of forming and using a 3D ultrasound data set follows a three step process. Firstly the 3D US set has to be acquired, then the volume has to be reconstructed and finally the set has to be visualised. Each step in the process is complex with several methods available for each of the steps. The following is a brief overview of the methods involved in the three step process.

1.9.1 3D Ultrasound acquisition techniques

3D ultrasound systems make use of conventional 2D probes to acquire a series of 2D images and differ only in the technique to determine the position and orientation of the 2D image within the 3D volume (Nelson and Pretorius 1998; Fenster et al. 2001; Mercier et al. 2005). There are several factors that need to be optimised to produce distortion-free 3D images. Firstly either a rapid or gated scanning technique is required, also the locations and orientations of the 2D images must be accurately known and finally the scanning apparatus must be easy to use in a patient environment (Fenster et al. 2001). There are four main techniques that can be used to acquire the 3D volume.

1.9.1.1 Mechanical scanners

The constrained sweeping technique is achieved by attaching a motor to the probe and doing a spatially pre-defined sweep of the 2D volume of interest. Because the scanning protocol is pre-defined and precisely controlled, the relative position and orientation of each image is measured accurately. Slices are usually acquired in a wedge pattern, in a series of parallel lines or with rotation around a central axis. The image and position data are stored in a computer for subsequent formation of the 3D volume set. The position data may be obtained from stepping motors within the scan head, a translation or rotational device or a position sensor that may be electromagnetic, acoustic or optical.

1.9.1.2 Freehand with position sensoring devices

This technique uses a freehand image acquisition system where a tracking device is externally attached to the probe which allows image acquisition with unconstrained movement. The externally attached sensor is tracked by a device that calculates the sensor position and orientation at any point in time. This information is used to compare the 3D coordinates of each pixel of the ultrasound image and form the 3D volume. There are several types of sensor used; optical sensing, acoustic sensing, articulated arms, accelerometers and electromagnetic sensing. Position tracking can also be done by analysing the speckle pattern in the ultrasound images using speckle decorrelation (Tuthill et al. 1998).

1.9.1.3 Freehand with no position sensoring devices

A third technique used is where there is no sensor attached to the probes. The 2D images are acquired and the 3D volume reconstructed assuming a predefined scanning

geometry. With this technique the operator must try to move the probe at a constant linear and angular orientation because no geometrical information is acquired during the scan process. With uniform motion and a knowledge of scan distance or total angle good 3D images have been obtained (Downey and Fenster 1995).

1.9.1.4 2D array probes

Another method is to use specifically made 3D probes. These probes usually consist of 2D arrays that allow explicit imaging in 3D and can be either mechanically or electronically steered within the probe housing. A diverging broad beam of ultrasound is transmitted from the 2D phased array transducer and forms a pyramid shaped 3D volume. The returned echoes are processed to display multiple planes from this volume in real time. These planes can be manipulated to visualise the 3D volume in any orientation. These 2D array probes have been used mainly in 3D echocardiology but are not in widespread use as they are very expensive to manufacture.

1.9.2 3D Volume reconstruction

To generate a 3D volume the 2D ultrasound data must be reconstructed by placing each pixel of each image at the proper location within the volume. This location is determined by the position data that was acquired from the position sensing device. How difficult this is depends on the image acquisition system used. The least complicated systems are ones where the position sensing device is integrated within the transducer. These systems have the required scaling and calibration data all present and give a very high quality volume reconstruction, often very quickly. These systems have a field of view (FOV) determined by the scan parameters but the FOV is limited to what the transducer can image from a fixed location. Systems with

externally located position sensing devices are more complicated as they often need calibration at the initial set up to determine scaling and some post processing after image acquisition to determine limits of the volume scanned. These freehand systems can cover a large FOV because the volume is based on images acquired during a sweep of the transducer. 2D array transducer systems have a small FOV, limited by the size of the transducer. Because scaling data is incorporated in nearly all systems, measurements of distance, area and volume are possible. Gated data is also possible if required by synchronising the system with an ECG trigger.

There are two main reconstruction methods used. The first is feature based reconstruction in which features or surfaces of structures are first determined and then reconstructed into a 3D image. This approach has been used mainly in echocardiology to image the ventricles in conjunction with ECG gating and the cine loop function which allows the motion of the heart to be visualised. The second method of reconstruction is to build a voxel based image using the 2D data set. A voxel is short for volume pixel and is defined as the smallest distinguishable box shape of a 3D image. This is the most common method of reconstruction and involves placing each image pixel at its correct 3D coordinates (x, y, and z) based on the 2D coordinates of that pixel in its 2D image, and the position and orientation of that image with respect to the 3D coordinate axis. Then for each image point, the voxel value is calculated by interpolation as the weighted average of the pixel values of its nearest neighbours among the 2D image pixels. This reconstruction preserves all the original information in the acquired 2D images and so by taking suitable cross sections of the 3D volume, the original 2D images can be displayed.

1.9.3 3D Volume visualisation

For 3D ultrasound to be useful in a clinical setting the patient anatomy and function needs to be presented in a manner that shows the areas of interest and allows interactive review of the data. There are three main methods of displaying the 3D images.

1.9.3.1 Surface Rendering

This is a common 3D display technique and is based on visualising the surfaces of organs. The process is very complex involving surface fitting algorithms which firstly define the surface, classify and segment the 3D image data. Then each voxel is classified to which structure it belongs. The organ boundaries are then classified and segmented and the boundary surfaces are each represented by a mesh. The final step is texture mapping with a colour and texture which appropriately represents the corresponding anatomical structure.

1.9.3.2 Multiplanar Reformatting (MPR)

This technique allows views of planar cross-sectional images extracted from the 3D image. This approach requires either a voxel based 3D image to be reconstructed, or an algorithm to be used that can extract an arbitrarily oriented plane from the original 2D images. Some interpolation is required as the extracted plane will not coincide with original planes. The interpolation becomes necessary to fill any gaps in the volume between acquired images especially in the Z plane. Generally the 2D slices are closely spaced to each other, but the gaps may appear due to under sampling which can have an effect on the reconstructed slices (Nelson and Pretorius 1998). The

extracted plane resembles a conventional 2D image which can be easily positioned and oriented to find the optimal display for examination.

As the dimensions of the plaques used in this study are estimated from successive 2D views there may be effects due to interpolation on the spatial resolution in the Z(C) plane on the plaques used in this study. A possible error is introduced in the estimate because the successive frames are separated by 0.045cm (see chapter 4) and the ends of the plaque may not lay in one of the image cross sections. It is, therefore, possible to underestimate the length of the plaque by 0.045cm at each end, giving a total possible underestimate of 0.09cm. A typical plaque extent in this study is in the region of 2cm in length, thus the worst case error in the measurement of the plaque length due to interpolation in 0.09cm in 2.0cm i.e. approximately 0.5%.

There are two main MPR techniques used to view ultrasound images. The first is the orthogonal planes view where three perpendicular planes are displayed on the screen simultaneously with graphical cues showing their relative orientations. The operator can select any plane from any of the three orientations and move it within the 3D volume to provide cross sectional views of any part of the volume (Pretorius et al. 1992). The second MPR technique used is the cube view in which the 3D image is presented as a cube which represents the boundaries of a reconstructed volume. Each face of the cube is rendered with the appropriate image using a texture mapping technique. With the appropriate computer interface any face of the cube can be selected and movement in and out and parallel to this face can be viewed. The whole of the cube can be also be arbitrarily rotated to obtain the desired orientation of the 3D image (Picot et al. 1993)

1.9.3.3 Volume Rendering

Volume rendering presents the display of the entire 3D image on to a 2D plane. It uses ray casting techniques to project the image. The main volume rendering algorithms used are maximum intensity projection and translucency rendering. Volume rendered 3D images are often difficult to interpret and are best suited for simple anatomical structures.

1.9.4 3D Clinical applications

3D ultrasound has many clinical applications and has been used in areas such as obstetrics, gynaecology, cardiology, musculoskeletal, dermatology, ophthalmology, surgery, breast, vascular, urology, and gastroenterology. The earliest work was in the area of cardiology mainly looking at the anatomy and function of the heart. It has also been used to take functional measurements of blood flow and ejection fractions (Ariet et al. 1984), provide visualisation of the atria and septa (Belohlavek et al. 1993), overall cardiac anatomy (Binder et al. 1996), congenital heart disease (Seward et al. 1995) and septal defects (Marx et al. 1995). There has been expansion recently in the use of 3D ultrasound in most clinical fields, due in large part to the huge improvement in 3D systems, and the more routine availability of these systems on ultrasound machines. The clinical areas of obstetrics and gynaecology have been the major areas of development in recent years. In obstetrics, the early work focused on looking at foetal anatomy which is made difficult due to the size and movement of the foetus. Studies also looked at the foetal surface (Pretorius et al. 1992) and the foetal spine (Johnson et al. 1997). The most impressive results have come in the area of visualising the normal foetal face and foetal face anomalies, for example cleft palates, which cannot be easily visualised with 2D ultrasound (Devonald et al. 1995; Merz et

al. 1997). More recently much research has focused on foetal heart anatomy and foetal heart anomalies (Dyson et al. 2000). 3D applications in gynaecology have focused on imaging of uterine anomalies, uterine fibroids, polyps, adhesions (Balen et al. 1993; Weinraub et al. 1996), ovarian masses (Bonilla-Musoles et al. 1995; Hata et al. 1999) and in assisted reproduction (Yaman et al. 1999).

1.9.5 3D Carotid imaging applications

The use of 3D US in carotid imaging has focussed mainly on plaque volume measurements with some research looking at plaque ulceration. The work on plaque volume measurements has looked at either the reproducibility of these measurements or changes in plaque volume over time in patients undergoing some form of drug treatment. 3D ultrasound has advantages over 2D ultrasound in the measurement of plaque volume as a 3D data set can be freely rotated and examined along multiple planes and tomographic views. As plaques are often irregular complex shapes, which often progress asymmetrically, plaque severity and luminal narrowing can be either over or under estimated using 2D ultrasound. The efficacy of using 3D ultrasound to measure plaque volume has been demonstrated both *in vivo* and *in vitro* (Delcker and Diener 1994; Griewing et al. 1997; Palombo et al. 1998; Landry et al. 2005). In these studies good accuracy and reproducibility of plaque volume measurements were found, suggesting that the technique offers a quantitative method of studying carotid atherosclerotic plaque progression. The technique has been used to monitor the effects of lipid lowering drug treatments by measuring atherosclerotic carotid plaque progression. The effect of extracorporeal low density lipoprotein elimination on precipitation from plasma was studied using serial 3D ultrasound plaque volume measurements (Hennerici et al. 1991). They studied 21 plaques in 7 patients with

hypercholesterolemia and found significant plaque volume reduction in all of the subjects.

The atheroma retarding properties of beta-hydroxy-beta-methylglutaryl coenzyme A reductase inhibitors (statins) in both coronary and carotid arteries has been well documented. Clinical trials have shown that statins reduce the incidence of ischaemic stroke and coronary heart disease (Blauw et al. 1997).The radiological monitoring of the effects of statins on plaques has been mainly done by monitoring serial carotid artery intima media thickness (IMT) measurements using 2D ultrasound (Salonen et al. 1995). Their results showed that statins reduced or halted plaque progression, however, because reproducibility of IMT measurements reduces in more advanced lesions, the trials were limited to mild atherosclerotic disease. The approach of using 3D ultrasound volume measurements to monitor the effects of statins has been recently reported (Schminke et al. 2002; Ainsworth et al. 2005). Schminke et al (2002) assessed the feasibility of 3D ultrasound to assess statins in a group of 23 hypercholesterimic patients (31 carotid plaques) using serial plaque volume measurements. 17 patients were treated with statins and low calorie diet, the other 6 on diet alone. The 31 plaques were classified according to their echogenicity and monitored over a period of 15 ± 4.5 months. The results showed that 43% of the plaques progressed in the statin group compared to 61% in non-statin group. There was regression in three of the statin group but none in the non-statin group. The study lacked sufficient statistical numbers to draw valid and generalisable conclusions, but did reveal statistically significant differences in progression rates between the statin and non-statin groups. Ainsworth et al (2005) designed a study to determine sample sizes that would be needed to detect the effects of statin treatment on plaque volume using 3D ultrasound. They studied 38 patients over a 3 month period. 17 were on

statins and 21 on placebo. Their results showed plaque progression in patients taking the placebo, but plaque regression in the patients on statins. They concluded that 3D ultrasound technology promises to be very useful in the evaluation of new therapies. 3D ultrasound volume measurements have also been used to assess the natural course of carotid plaque ulceration with time (Schminke et al. 2000). The group studied 17 ulcerated plaques over a mean period of 17.6 ± 6.3 months and found 3 had regressed over the period while one had progressed. No change was detected in the other plaques.

There have been no reports of the use of 3D ultrasound in carotid plaque characterisation but it has been used to characterise breast tumours (Chen et al. 2005). They acquired 3D data sets of 54 malignant and 107 benign breast tumours and using run difference matrix statistics and neural networks, they correctly identified 48 malignant and 100 benign tumours with a diagnostic accuracy of 91.95%, sensitivity of 88.8% and specificity of 93.5%. This study, however, just looked at characterising malignant from benign tumours; it did not look at detecting tumours from normal breast tissue.

1.9.6 Future uses of 3D ultrasound

Currently the role of 3D ultrasound in routine diagnostic use is limited mainly to some procedures in the areas of obstetrics and gynaecology. This may change in the future with the advent of high speed computer technology on which most modern ultrasound machines are based. 3D software packages are available as standard on most modern machines, however, these are often difficult to use and interpret. Future developments to improve freehand acquisition, volume visualisation and software to improve image

interpretation will ensure that 3D ultrasound will have a more routine role in all areas of diagnostic ultrasound.

1.10 Artificial Neural Network (ANN)

The method used to classify the carotid plaques in this thesis involves using an ANN. This section gives a brief description of ANNs and their uses in the field of tissue characterisation involving ultrasound.

1.10.1 Introduction to ANNs

An artificial neural network (ANN) is a computational technique composed of simple elements operating in parallel. It consists of simple processing elements called neurons which are inspired by the human nervous system. Each neuron is connected to other neurons in the network and the function of the network is determined by the strength or weight of the connection. In practice neural networks are trained so that a specific input will lead to a specific output.

The network is organized into different layers where each neuron receives an input from the input neuron or from the previous hidden layer. In practice there can be several hidden layers. The neuron calculates a weighted sum and passes it through a transfer function which limits the output of the neuron to the next layer. The connections can either feed from input to output layers, a feed forward network (Figure 1.7) or can feedback from a hidden layer to an input called a feedback network.

One of the most important features of ANN training is the way that it learns by example. The simplest method is the feed forward network but several more complicated training algorithms have been developed. One of the most popular is the

back propagation algorithm (Rumelhart et al. 1986). This method uses a log sigmoid transfer function rather than a simple linear transfer function. The log sigmoid transfer function is used because it is continuous and differentiable and allows the gradient of the error to update the weights. That is, the error signal is sent back through the network altering the weighted connections to minimize the error on the next pass. By presenting the network with different examples and changing the weights, the network is trained to produce a desired output for a given input. The training is stopped either when the error has reached a specified level or a given number of training cycles has been run. This system is an example of supervised learning where a specific output is required for a particular input. Unsupervised learning systems require no specific output but simply consist of input and hidden neurons and the network learns by associating specific input patterns with different hidden clusters and nodes.

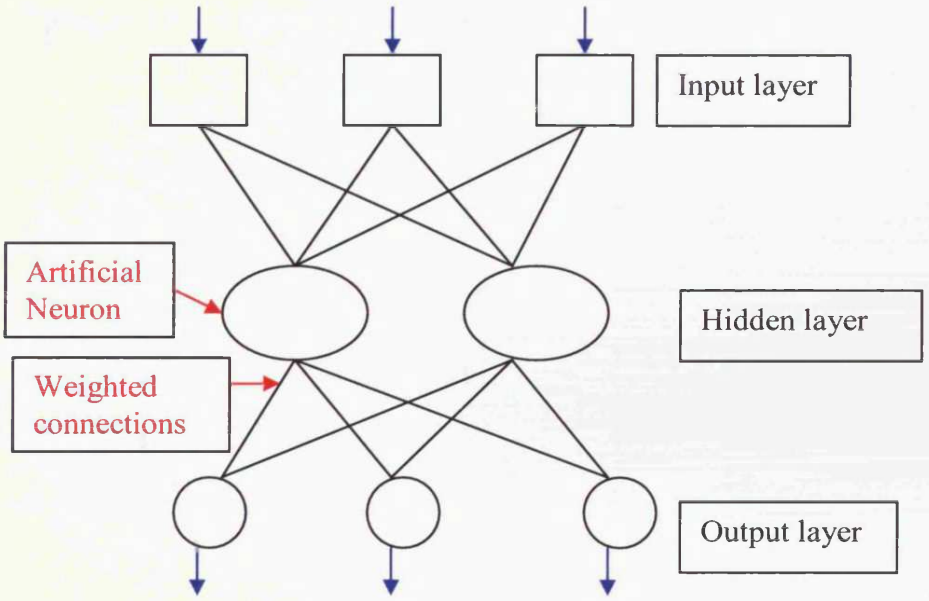

Figure 1.7 Example of a feed forward ANN.

1.10.2 Uses of ANNs in Medicine.

ANNs are extensively used in medicine. They are used in diagnostic systems to detect cancer and heart disease. They have been used in a variety of biochemical analysis systems to analyse blood and urine samples and monitor glucose and iron levels in body fluids. They have also been used to design and develop drugs and in the modelling of biological molecules. They have also been used extensively in the area of medical image analysis with many applications using x-rays, MRI and CT. The uses of ANNs in medicine are summarised in the following review papers (Miller et al. 1992; Baxt 1995).

There also has been extensive use of the classification of ultrasound images with applications including Doppler waveform analysis of common femoral artery for detecting proximal arterial disease (Wright et al. 1997), classification of liver parenchyma from normal liver tissue (Daponte and Sherman 1991) and the diagnosis of prostate cancer (Ronco and Fernandez 1999).

Chapter 2: Methods

2. General Introduction

The experimental methods used can be split into the following main areas.

- The 3D acquisition system.
- The design and construction of the mechanical device that drives the transducer. These methods are used in the plaque data collection.
- The MATLAB programs that analyse the raw data. These programs are the main analysis method and are fundamental to the thesis.
- The measurement of the plaque volume which is used in chapter 4 to assess the effects of histological processing, and in chapter 5 to monitor any plaque volume changes in the serial scans. The histology methods are detailed in chapter 4.

2.1 3D Acquisition System

The 3D system used in this project is a software package that is commercially available on the Toshiba Powervision 6000 ultrasound scanner (Toshiba Medical Systems). The system can create a 3D volume using both linear and curvilinear array transducers. The system allows creation of 3D volumes of desired height, width and depth. The selection of the height and width of the 3D volume is done by selecting a box on an initial 2D image where the depth selection is controlled by selecting a set distance. The selection of the frame rate and scan duration determines the number of 2D images in the 3D volume. The major limiting factor of this software is that there is no position sensor attached to the transducer, which means that the scan is done freehand. Freehand scanning is reliant on the operator moving the transducer through

the selected distance in the set time. It has been reported that good quality images have been obtained using this method (Downey and Fenster 1995), however, this technique is very difficult to do even for experienced operators and could lead to poor accuracy and reproducibility especially when serial scans are involved. To overcome this limitation a device was designed and built to drive the transducer a fixed distance in a set time.

2.2 Mechanical Device

There were several people involved in the design and construction of this device. Staff from ultrasound, mechanical workshop and the Nucleonics section all had input at various stages into the design and construction of the device.

2.2.1 Design

In designing the device several questions needed to be answered.

- What is the device required to do?
- What parameters are required for the scan?
- What scan distances are required and at what speed?
- How is the device to be tested?

To answer these questions the group decided the following criteria would have to be met.

- The device needed to house the transducer.
- It needed to drive the transducer a set distance at a set speed in a repeatable and reproducible fashion.
- It needed to be electrically and mechanically safe for the patient.
- It also needed to be flexible for positioning purposes

Using these criteria it was decided that the device should be wall mounted, suspended on a frame connected to a ball and socket type device for flexibility in positioning. The transducer would be bolted to a Perspex™ frame that would be driven up and down by an electric motor.

The dimensions of the Perspex™ frame were dependant on the translational distance required for the scan. A preliminary investigation in the vascular clinic revealed that, in most patients examined, a total translational distance of 70mm was required adequately to scan from just under the jaw, imaging the internal and external carotid arteries, to the clavicle, imaging the common carotid artery. In addition this investigation also revealed that a 3D image acquisition time of 12 seconds would be the best compromise between patient's compliance with breath holding and good B-mode image quality. This determined that the translational speed of the motor needed to be 6.7 mm/s (i.e. 70 mm in 12 sec).

2.2.2 Construction

The device was constructed in the Medical Physics mechanical workshop by Mr Brian Western. The device was wall mounted using a 90 cm metal bar to which the metal frame containing the ball and socket joint was attached. The ball and socket joint allowed flexibility in positioning, so when the desired position could be found it could be locked in position. The motor was a Premotec BL58 50 watt DC motor (Precision motor technology b.v. Dordrecht, The Netherlands). The motor had an adjustable speed loop which was set to 6.7mm/sec and included speed sensing with no quoted errors or tolerances. The motor and ball and socket joint were attached to a Perspex™ frame. The rigid part of the Perspex™ frame consisted of 2 Perspex™ blocks, connected by 4 metal rods, 20 cm apart. The motor was housed on top of one of the

blocks, and was connected to the other block by a drive screw. In between and parallel to the two fixed Perspex™ blocks was another block which was driven up and down by the motor and screw. The positioning of this block determined the translational distance of the scan. Connected to this moveable block at 90 degrees was another Perspex™ block that housed the transducer. This block had a removable section where the transducer was placed. Connected to the ends of the fixed blocks were electric switches which automatically turned the motor off (Figure 2.1). The device was tested to ensure it was electrically safe for patient use.

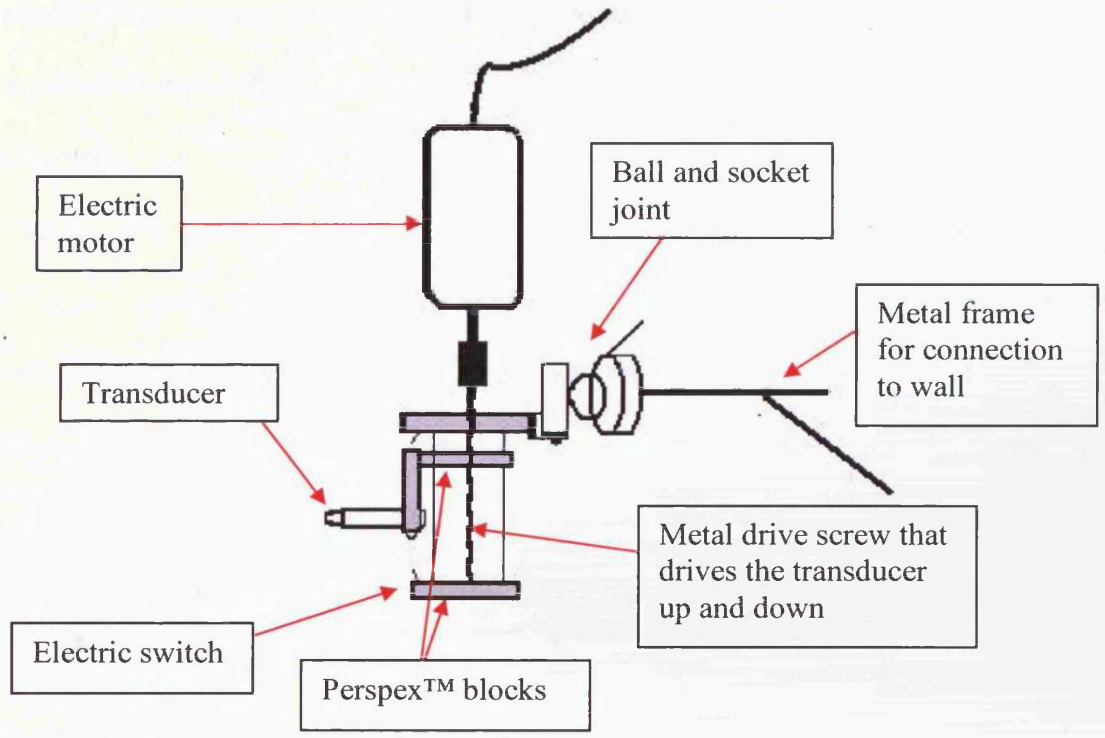

Figure 2.1 Schematic Diagram of Mechanical Device.

2.2.3 Testing

The device was tested at various stages throughout the construction process. During this process modifications were made to the device which included increasing the length of the wall mounted metal bar and changes to the supporting frame which allowed more flexibility in positioning.

The wall mounted arm was attached to the wall via a metal plate with four large bolts. Once the arm was extended, it was locked into position, and the reproducibility of the whole system was tested by performing duplicate scans (section 3.3). This was found to be within an acceptable limit of 3.64%. Therefore it was not thought necessary to test the spatial rigidity of the wall mounted arm on a phantom. Once the transducer was placed in the starting position under the jaw, the device was fixed in position by locking the ball and socket joint so the only movement allowed was the transducer down the neck.

The translational speed of the device was tested by timing the device to travel the fixed 70mm distance. This was found to be approximately 12 seconds which was the desired acquisition time. This was confirmed by the fact that the number of transverse 2D slices through the 3D Volume was 155. The 3D frame rate was set to 13 frames per second, so the time taken to acquire 155 images would be 11.9 seconds. The number of transverse 2D images acquired throughout this project remained constant at 155.

At this stage positioning of the device on volunteers was tested and it was found that scanning from the jaw downwards (i.e. from ICA to CCA) was best. It was found that scanning the opposite way (i.e. from CCA to ICA) occasionally caused the skin in the volunteer's neck to fold, so the transducer would not run smoothly. The translational movement of the scan was checked immediately by reviewing the completed 3D scan

to ensure it was uniform and that there was no significant movement artefact. Various patient positions were tested and the most repeatable and easy to position was selected and incorporated into a scan acquisition protocol. (See appendix 2.1). No testing of the system on ultrasound phantoms was performed.

The machine settings were kept constant between each scan and are summarised in table 2.1. The machine settings were selected to minimise the effects of the scanner's preset image processing settings on the data. The persistence, echo enhance, post processing and image smooth values were all turned off. A high dynamic range was selected to have more shades of grey between the various tissues. By having a high dynamic range, more echoes from smaller scatterers will be displayed making it easier to display differences in tissue texture. Multiple foci were chosen to improve image resolution. The 2D frame rate was chosen to match that of the 3D system. A depth of 40mm was deemed sufficient to ensure that the carotid arteries could be visualised in all the length of the scan.

B-mode scanner setting	Image acquisition value
Gain setting	80
Depth (max.)	40 mm
Focus	Multiple at 10mm, 20mm, 30mm
Persistence value	0
Echo enhance value	0
Post process value	0
Image smooth	Off
Dynamic range	75dB
Frame rate	13Hz

Table 2.1 B-mode scanner settings.

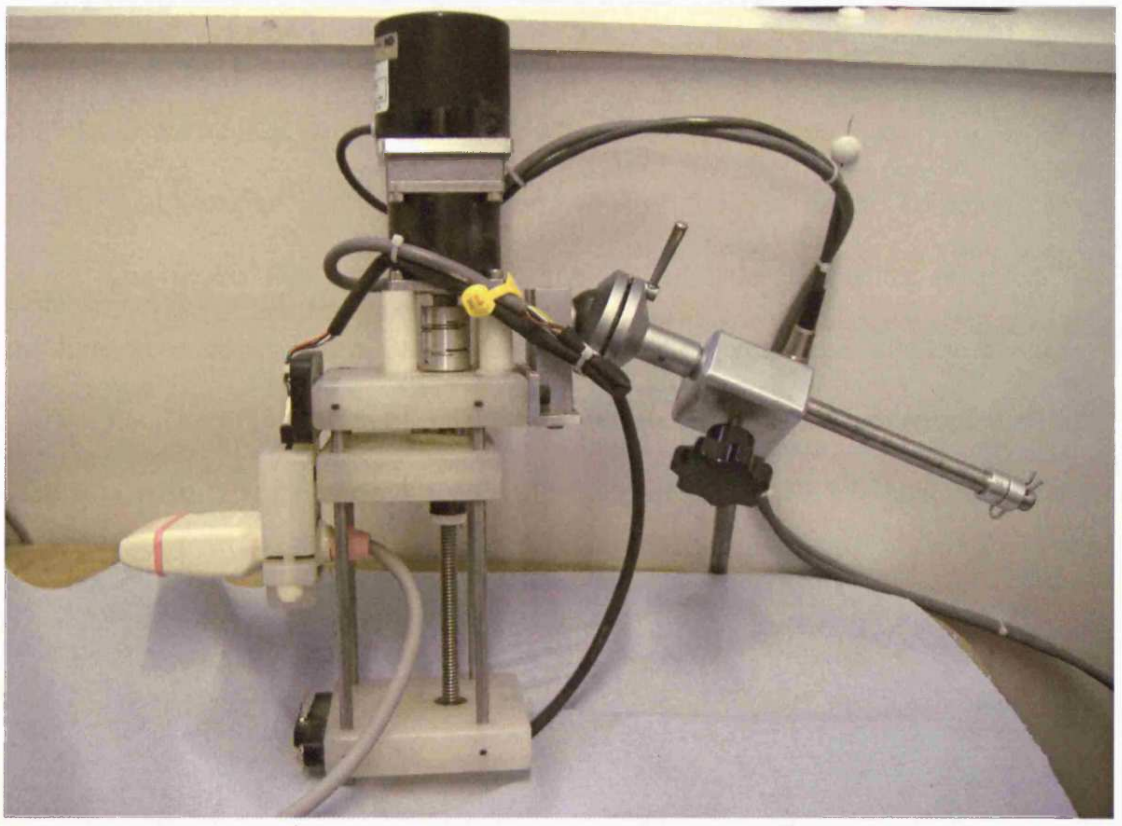

Figure 2.2 Mechanical Device components

2.2.4 Patient Acquisition Protocol

The patient was placed supine on a bed with the head extending back and tilting slightly to the contra lateral side (Fig. 2.3). Each scan commenced visualising the internal and external carotid arteries and always finished in the common carotid artery. The probe was replaced under the jaw and the procedure repeated. The machine recorded a series of 2D images throughout the volume. Using the specialised software a 3D representation of the captured ultrasound data was constructed. The 3D scan data were then transferred, using a DICOM network, to a personal computer for further analysis.

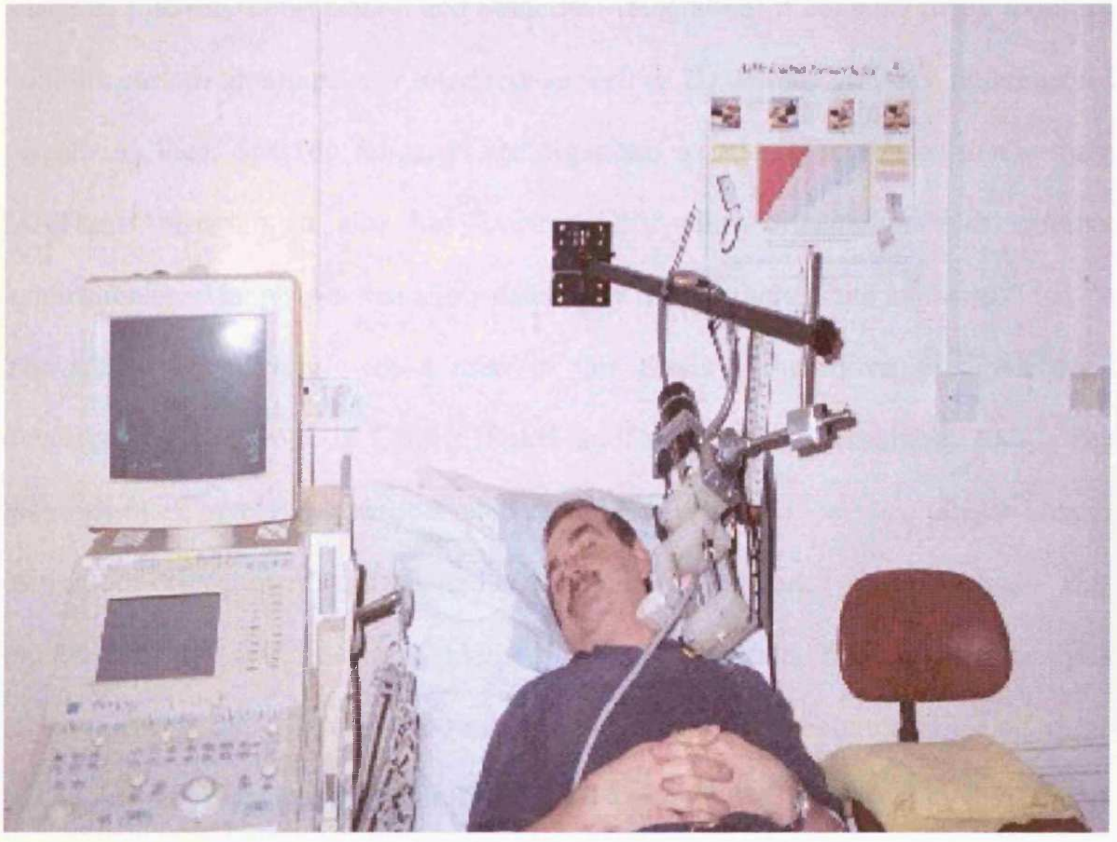

Figure 2.3 Mechanical device in operation.

2.3 MATLAB Analysis

2.3.1 Introduction to MATLAB

MATLAB (the Math Works Inc, Natick, MA, USA) is a high level technical programming language with an interactive environment for algorithm development, data visualization, data analysis and numeric computation. It has a vast range of applications including image processing, communications, control design, signal processing, test and measurement, financial analysis and computational modeling. Its key features include interactive tools for iterative exploration, design and problem solving. It also contains mathematical functions for linear algebra, statistics, Fourier analysis, filtering, optimization and numerical integration. It contains many tools for building custom graphical user interfaces as well as 2D and 3D graphics functions for visualizing data. Specific functions are organized as add-on toolboxes to the main MATLAB program. It also has functions that allow integration with external applications and languages that allow data easily to be imported and exported.

The statistical analysis method used in this thesis is based on previous work developed by our group in Cardiff (Rakebrandt et al. 2000; Rakebrandt 2001). The previous work involved statistical and textural analysis of 2D *in vitro* plaque images using both discriminant analysis and artificial neural network (ANN) methods. This project aims to expand the ANN method to 3D *in vivo* data. The statistical analysis techniques and the ANN used are similar to the previous work but modification of the MATLAB programs by Dr. Frank Rakebrandt was required to incorporate the 3D data into the classification analysis program. Dr Rakebrandt's contribution involved converting the 3D data set into MATLAB format, he wrote MATLAB programs to display the 3D data and adapted the previous ANN to analyse the 3D data sets.

The MATLAB analysis procedure can be split into 3 distinct sections. The first section involves taking the raw data in order to visualise the 3D volume. This 3D visualisation program allows the volume to be displayed in any of the 2D planes and regions of interest selected. The next section is the setting up and analysis of a training set whose output is used to set up an ANN classification program. The final section is to analyse carotid plaques using the classification program. A flow diagram of the MATLAB programming procedure is shown in figure 2.4

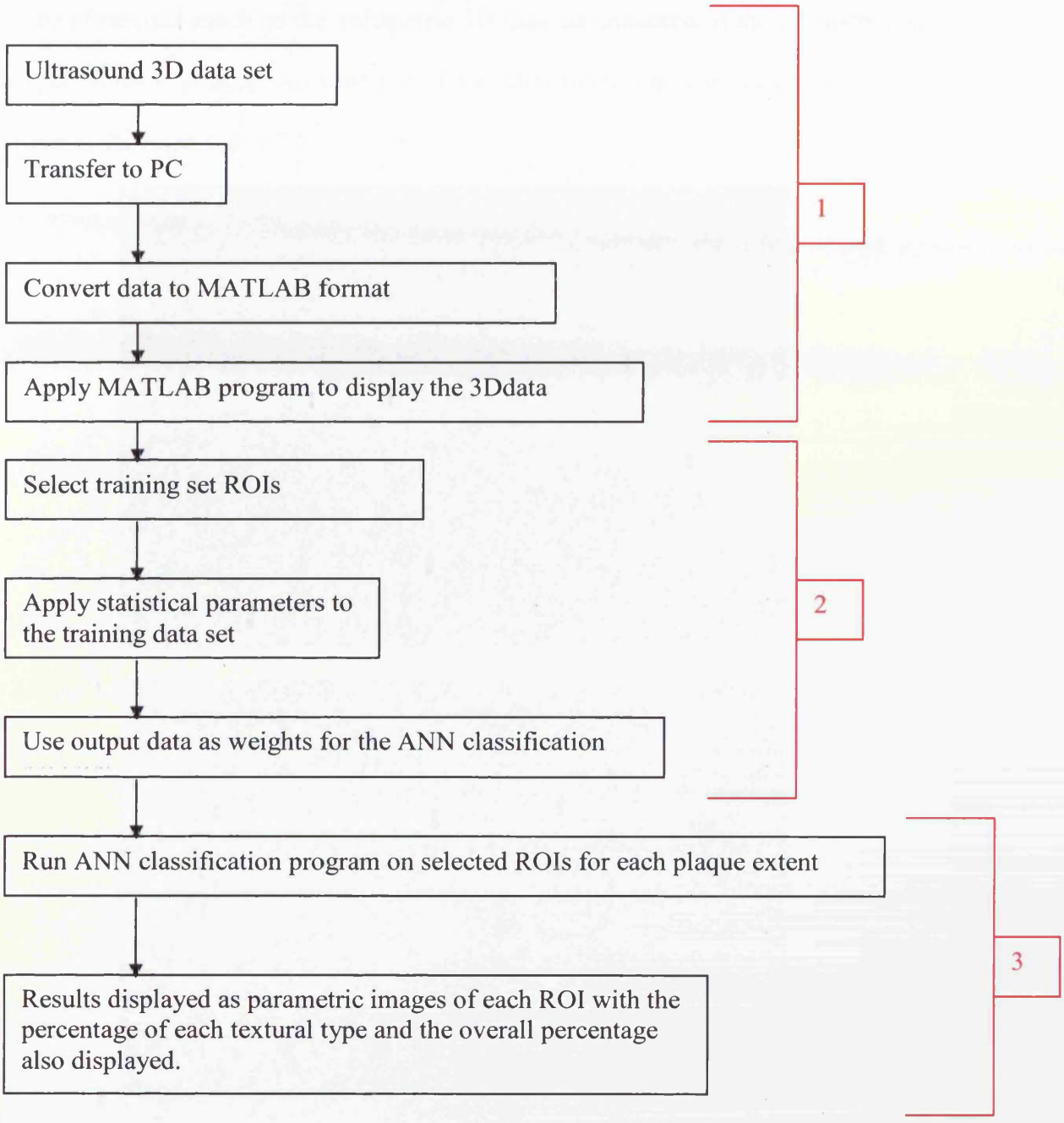

Figure 2.4 MATLAB analysis flow chart with brackets showing the 3 distinct sections.

2.3.2 3D Volume Visualisation

On the ultrasound machine the volumetric 3D data set consisted of the reconstructed parallel B-mode images. An example of the ultrasound machine reconstructed 3D volume is shown in figure 2.5.

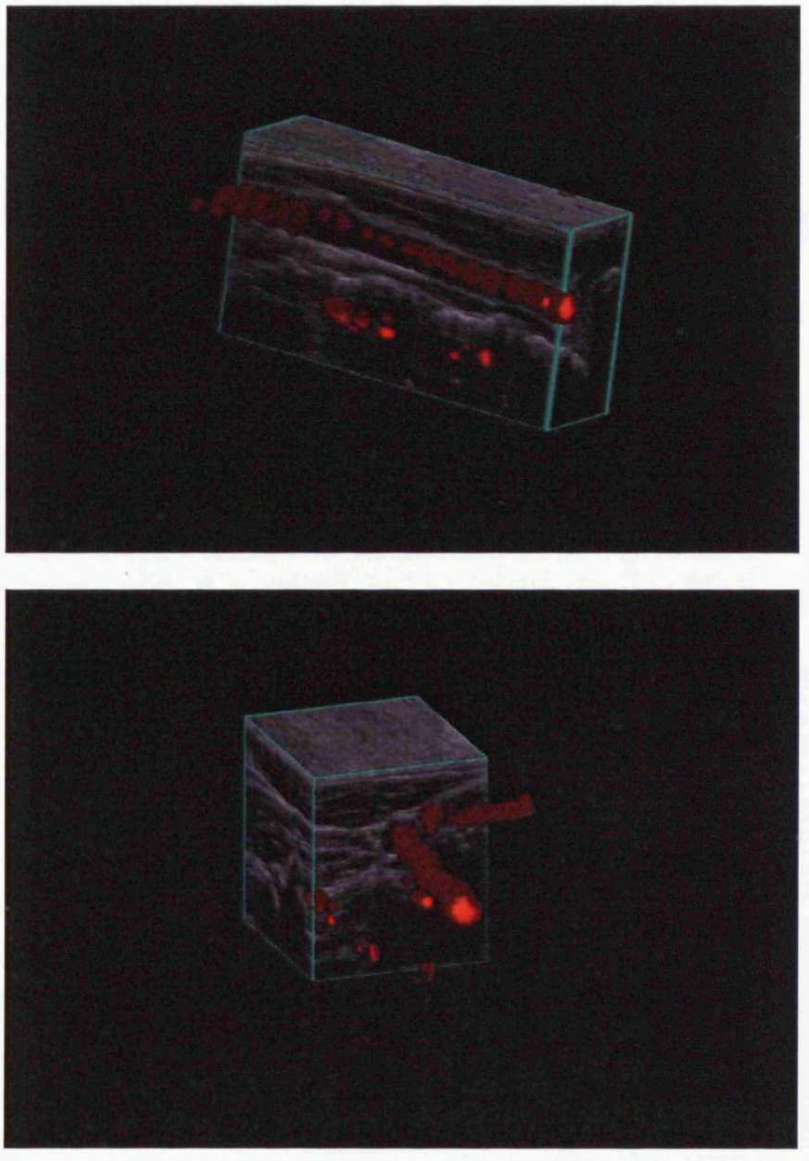

Figure 2.5 Examples of the ultrasound machine reconstructed 3D volume showing different cut planes through the volume.

A free cut plane orientation around the 3 axes allowed any desired plane or section through the 3D volume to be visualised. The blood flow through the volume can also

be visualised. However, to visualise the data on a PC, the raw data had to be converted into a MATLAB file type. The converted raw data was the input to a MATLAB software program which allowed the data to be displayed in all 3D orthogonal planes (fig. 2.6). In the example in figure 2.6, the front view image is to scale but the side and top view images have been compressed so as to fit all three images into one page. It was decided, using the ultrasound machine reconstructed 3D volume, that the front view which gave a cross sectional cut through the carotid arteries would be the easiest plane to visualise the plaque in the artery. The MATLAB programs were written such that the front view is to scale and the side and top views compressed in the MATLAB image. The MATLAB programs could have been adapted, to display the longitudinal or top views if required.

The program displays a single 2D image and displays all 3D views. The front view image is a cross sectional cut through the 3D volume. The blue line through the image gives the position of the side view, while the green line gives the position of the top cut through the image. Similarly in the side and top view images the red, green and blue lines give the position of the other cuts through that image. The 3 large sliders on the bottom right hand side allow scrolling through the entire 3D set in any of the 3 views. The smaller double sliders beneath each image control the white diagonal lines in the image above. These sliders can be moved in or out and are used in the selection of the plaque ROI.

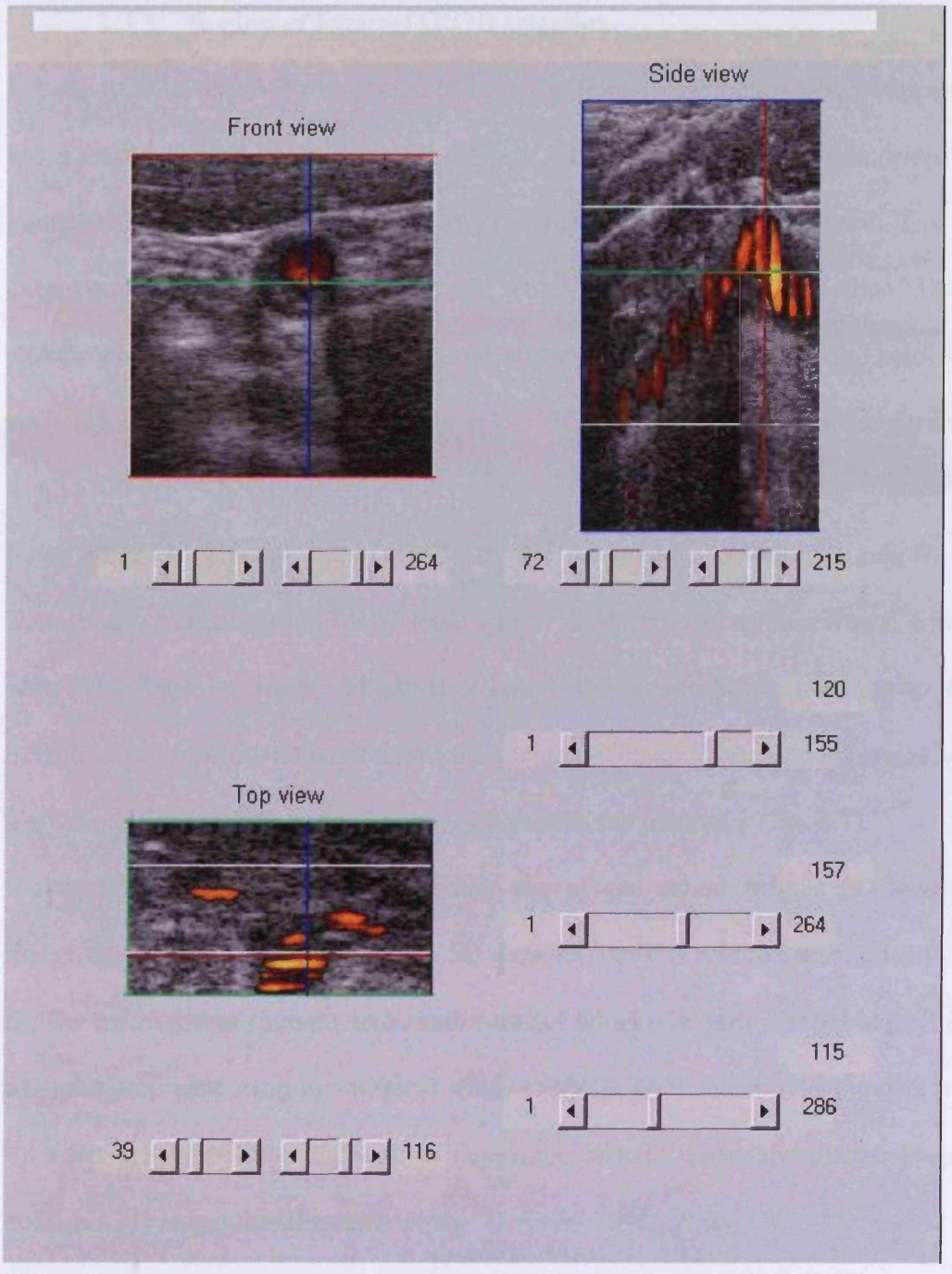

Figure 2.6 Example of a single 2D image displaying all 3D views (front, side and top). This is a MATLAB image and only the front view image is to scale; the other orthogonal views are compressed and are only used for positional information. The sliders allow scrolling through the entire 3D data set in any of the three views.

2.3.3 Region of Interest (ROI) selection.

For the ROI selection it was decided to use the front view images which represented a cross sectional cut through the carotid artery. The front plane 3D set comprised of 155 parallel 2D B-mode images from which a plaque extent was selected. The plaque extent was the number of 2D images in which the plaque was contained. The white sliders were moved to the maximum to ensure that all ROIs could be selected. For each 2D image within the plaque extent, a ROI was drawn around the plaque. The MATLAB program required the outer lumen of the plaque to be drawn manually. The inner lumen is selected automatically by the presence of coloured pixels (in power flow mode) indicating the blood flow within the artery. In certain views, coinciding with late diastole, where blood flow was absent, the ROI information from a neighbouring image was copied into the image and used. If the copied image was not a good match the inner lumen boundary was selected manually (fig. 2.7).

It may have been possible to determine the plaque extent from a 2D longitudinal image taken at the same time as the 3D data set, but this method was not used as the former method was thought to be more useful when comparing serial scans (chapter 5) and when comparing histological slices to the *in vivo* and *in vitro* images (chapter 4). Also it is sometimes difficult to determine exactly where the plaque begins and ends in a 2D longitudinal image.

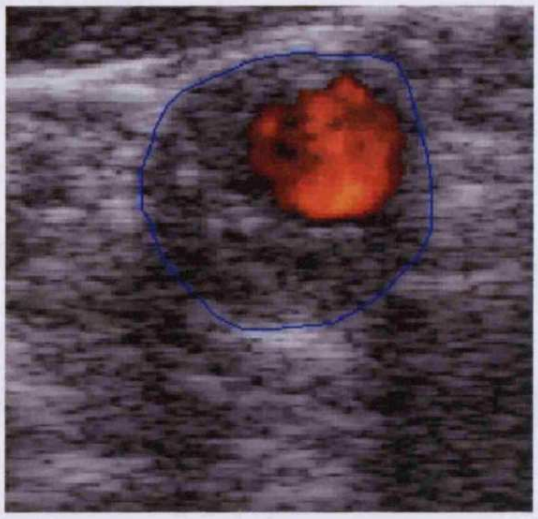

Figure 2.7 Image showing ROI selection.

2.3.4 Analysis of training set texture characteristics

To identify a training set, 15 carotid plaques were selected from 10 pre-endarterectomy, 3 statin and 2 apheresis subjects with the assumption that all 5 tissue types identified in previous work were present in these plaques. Initially the plaque extent, which is the number of 2D images in which the plaque is contained, was determined for each of the 15 plaques. For each 2D image the ROIs were drawn around the plaque from which a total of 132840 overlapping analysis kernels (9 x 9 pixel areas) were identified from the 15 plaques. The six different statistical and textural analysis methods previously identified (Rakebrandt et al. 2000) were applied to the analysis kernals in SPSS (statistical package for the social sciences: SPSS inc. SPSS UK Ltd. Woking, Surrey, UK). The methods were variance of grey scale values, maximum grey scale values, information measures of correlation, intercept for sum of variance, slope of correlation and mean grey level. In order to prevent bias the results of the six statistical analyses were normalised using the z-score technique by

setting each mean value to zero and the standard deviation to unity (Norusis 1985). The following formula was used.

$$Y(i) = \frac{X(i) - \text{mean}(X(i))}{SD(X(i))}$$

Where Y(i) = normalised value for kernal(i)

X (i) = individual value of kernal (i)

Mean X(i) = mean value of all 132840 kernals for that parameter

SD X(i) = standard deviation of all 132840 kernals for that parameter.

The normalised z-score value gives an indication of how far and in what direction each individual value deviates from its distribution's mean expressed in terms of its standard deviation. K-mean cluster analysis was then used to separate the normalised data into 5 classes. The normalised output values (see appendix 2.2) from the training set were used as the ANN weighted connections to train a supervised ANN with a back propagation algorithm. The ANN architecture is the same as the one used in previous work (Rakebrandt 2001).

2.3.5 Training set output

In order to classify a ROI, the six statistical values would be computed for each kernel in the ROI, the values normalised and classified into one of 5 classes by the ANN. An indication of how the program discriminates between the five classes using the six statistical methods can be seen in figure 2.8. This graph plots the mean normalised value against statistical method for each of the five classes. However, there may be considerable overlap between the values of each statistic, which is not easily shown in

this graph, so a more detailed analysis of the six statistics is necessary to show why a complex classification method is required to separate the data into the five classes. The normalised mean and standard deviation value is plotted against class type for each of the 6 different statistical methods. This shows the considerable overlap that can occur between the five classes (figures 2.9 to 2.14).

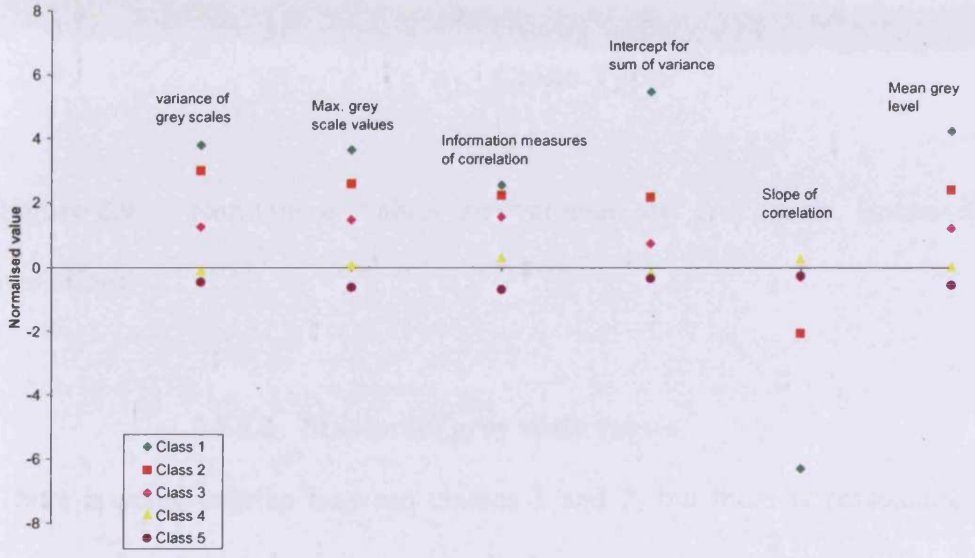

Figure 2.8 Graph of normalised data for the 6 methods used to separate the data into 5 classes for the training ANN.

2.3.5.1 Variance of grey scales

It can be seen from figure 2.9 that there is considerable overlap between classes 1 and 2 and between 2 and 3. By using just this statistic the classifier could not distinguish between classes 1, 2 and 3. The values of classes 4 and 5 are small and close together in value but do not overlap with the other three classes.

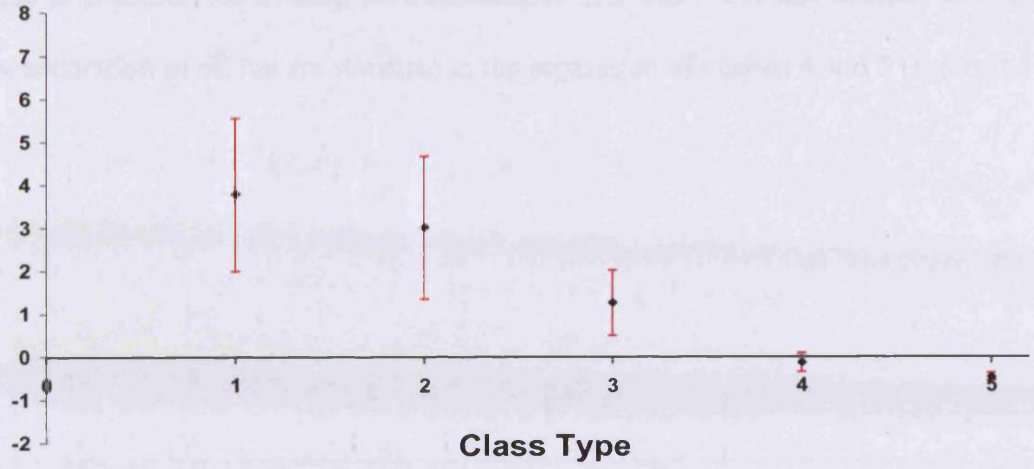

Figure 2.9 Normalised values of variance of grey scale (mean ± standard deviation).

2.3.5.2 Maximum grey scale values

There is some overlap between classes 1 and 2, but there is reasonable separation between the other classes (figure 2.10).

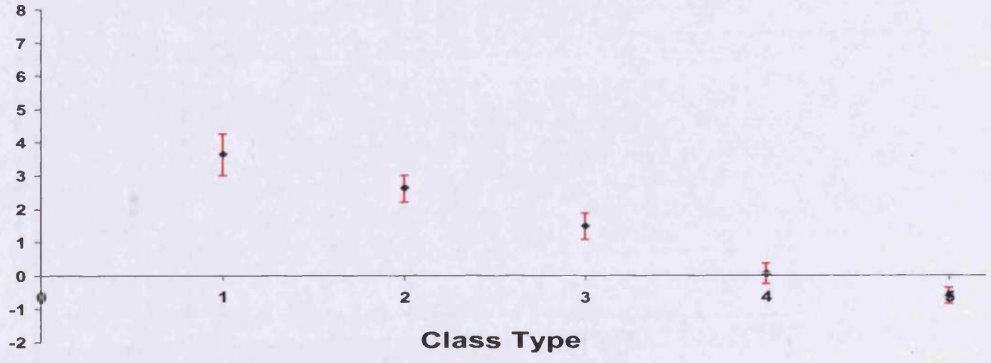

Figure 2.10 Normalised values of maximum grey scale values (mean ± standard deviation).

2.3.5.3 Information measures of correlation

There is considerable overlap between classes 1, 2 and 3 but this statistic shows the best separation of all the six statistics in the separation of classes 4 and 5 (figure 2.11).

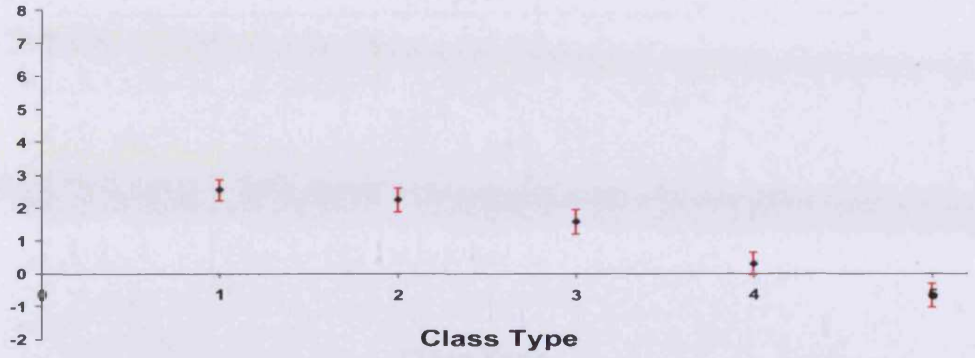

Figure 2.11 Normalised values of information measures of correlation (mean ± standard deviation).

2.3.5.4 Intercept for sum of variance

This statistic shows separation between class 1 and 2 but there is considerable overlap between classes 2 and 3 and also between 4 and 5 (figure 2.12).

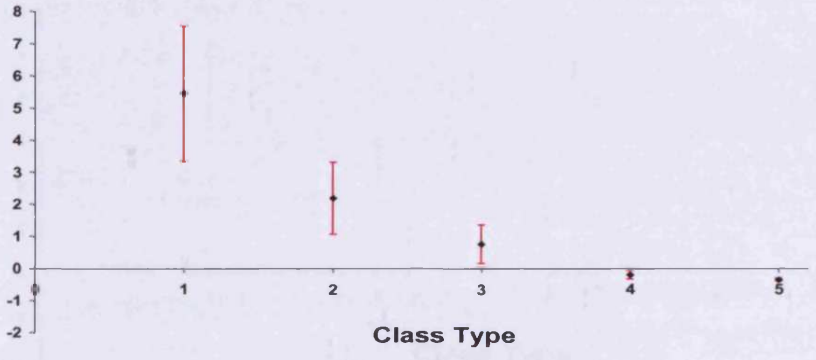

Figure 2.12 Normalised values intercept for sum of variance (mean ± standard deviation).

2.3.5.5 Slope of correlation

This statistical method displays good separation between classes 1 and 2 but shows considerable overlap between classes 3, 4 and 5 (figure 2.13).

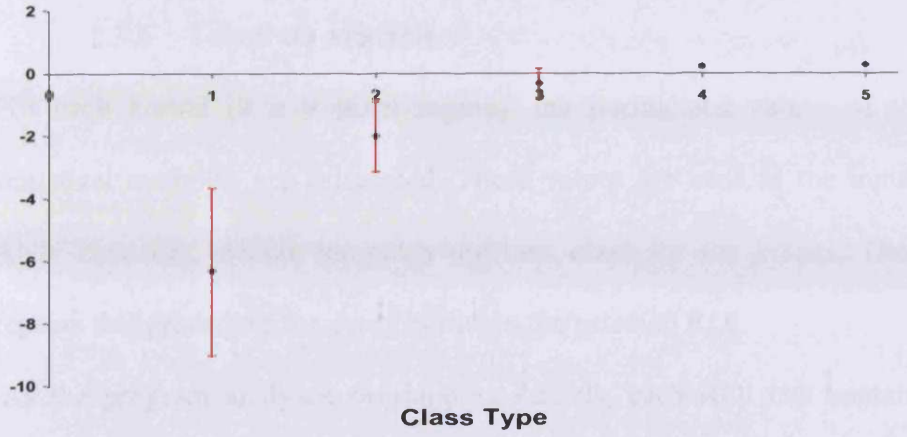

Figure 2.13 Normalised values of slope of correlation (mean ± standard deviation).

2.3.5.6 Mean grey level

This has a similarity to the intercept for sum of variance statistic with good separation between classes 1 and 2 but there is overlap between classes 2 and 3 and also between 4 and 5 (Figure 2.14).

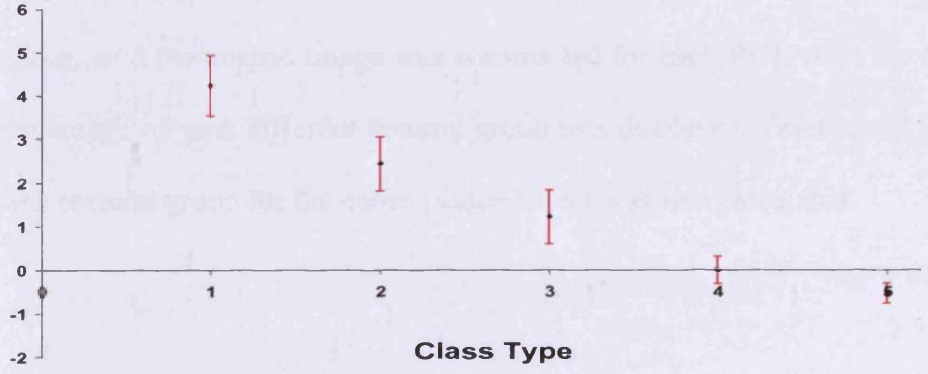

Figure 2.14 Normalised values of mean grey level (mean ± standard deviation).

In summary, no single statistic could distinguish the five classes, so a complex ANN is required to classify the data.

2.3.6 Test Data analysis

For each kernel (9 x 9 pixel region), the normalised values of the six selected statistical methods, are calculated. These values are used as the input to the trained ANN classifier, which computes the best class for the kernel. The program then repeats this procedure for every kernel in the selected ROI.

As the program analyses overlapping kernels, each ROI can contain thousands of analysis regions and is very demanding on computing power and time. For example a typical time to analyse a plaque with 10 ROIs would be 4-5 hours during which time the computer could not be used for any other purpose. The PC used in the MATLAB analysis was a Research Machines workstation with a 751 MHz Intel Pentium III processor and 256 MB of RAM.

The program then used the output data from each kernal to construct a series of parametric images, of each ROI in the plaque extent (fig. 2.15). That is, the program assigned each kernal to its appropriate class and each class was assigned an arbitrary colour, so a parametric image was constructed for each ROI. Also for each ROI, the percentage of each different textural group was displayed. The overall percentage for each textural group for the entire plaque extent was also calculated.

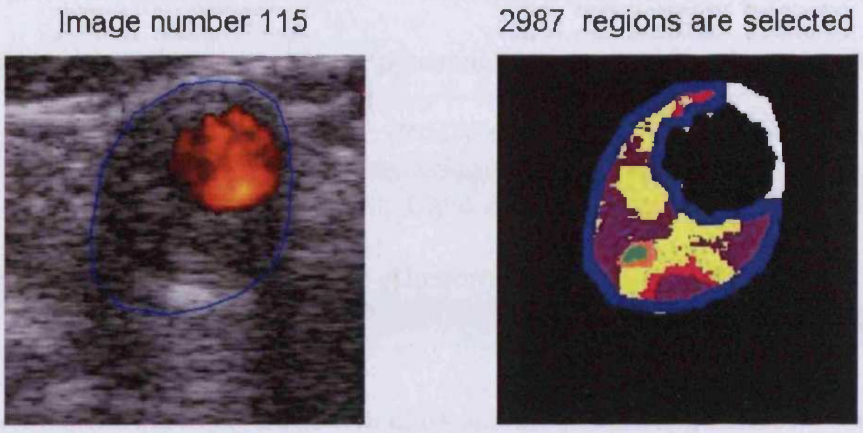

Class 1 Green :	80 ==	2.6783 %
Class 2 Orange :	101 ==	3.3813 %
Class 3 Pink :	245 ==	8.2022 %
Class 4 Yellow :	1238 ==	41.4463 %
Class 5 Purple :	1323 ==	44.2919 %

Figure 2.15 Example of parametric output display showing % of each of the five classes.

2.3.7 Comparison of *in vivo* MABLAB classifier with *in vitro* classifier.

In chapter 1 the literature has widely supported the theory that an echolucent plaque appearance on ultrasound is associated with the softer tissue types of lipid and haemorrhage and an echogenic plaque appearance is associated with the harder tissue types of fibrous tissue and calcification (Reilly et al. 1983; Gray-Weale et al. 1988; Steffen et al. 1989; Widder et al. 1990; Cave et al. 1995; Geroulakos et al. 1996; ECST 1998; Arnold et al. 1999; Schulte-Altedorneburg et al. 2000).

In this project there is a similarity in the way that the MATLAB classifier works that shows an association between the *in vivo* class and the plaque appearance.

There are two sources of evidence to support this association. The first is a comparison of the graphs of normalised data for the six different statistics *in vivo* with the corresponding *in vitro* graph used by Rakebrandt (2001). By comparing the *in vivo* and *in vitro* graphs (figure 2.16), similar patterns can be seen in the way the classification has occurred both *in vivo* and *in vitro*. A similar pattern can be seen *in vivo* for class 1, 2, and 3 to the data for haemorrhage and lipid from the *in vitro* graph. Also there is a similar trend for the *in vivo* classes 4 and 5 with that of calcification, elastic and fibrous tissues *in vitro*. The normalised values for *in vivo* classes 1, 2 & 3 have values <1.5 for five of the six statistics and large negative values for the sixth. A similar trend is seen with the *in vitro* statistical data for haemorrhage and lipid. The normalised data for *in vivo* classes 4 & 5 have values between 0 and -1 which is similar to the values of calcification, elastic and fibrous tissue *in vitro*.

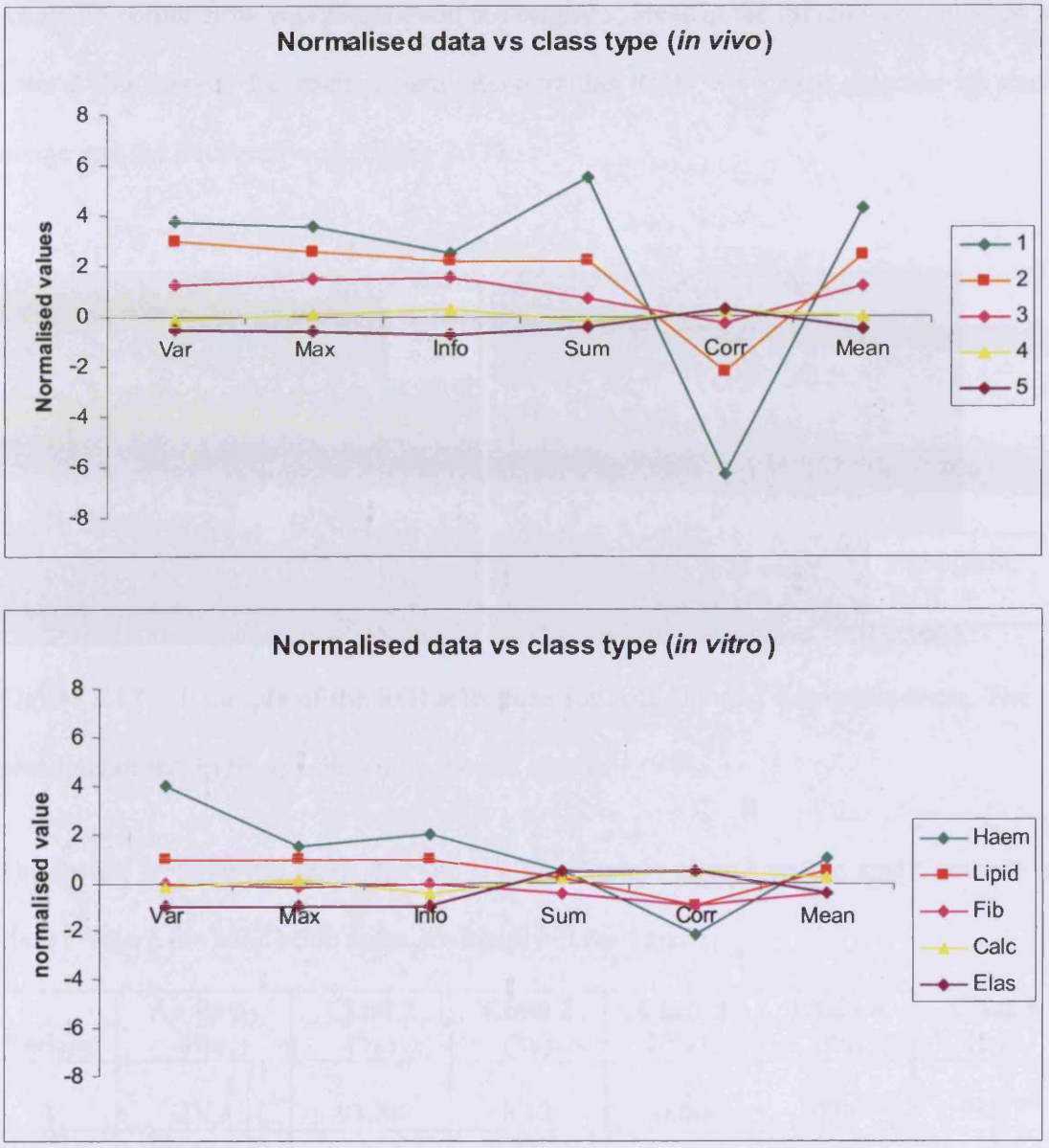

Figure 2.16 Normalised data versus class type for the six statistical parameters for *in vivo* and *in vitro* (data for *in vitro* graph from Rakebrandt 2001).

Echoes from blood within the internal jugular vein (IJV) and the brightest and most echogenic areas of the transverse scans of the carotid artery in three patients were chosen and analysed using the MATLAB classifier. The reasoning is similar to that used in GSM analysis where the blood has very low GSM and the most echogenic areas have a high GSM (El-Barghouty et al. 1995; Elatrozy et al. 1998). The IJV

where no colour flow was present and the brightest areas in the image were selected in several 2D images for each patient. Rectangular ROIs were then selected on each image and the data analysed (figure 2.17).

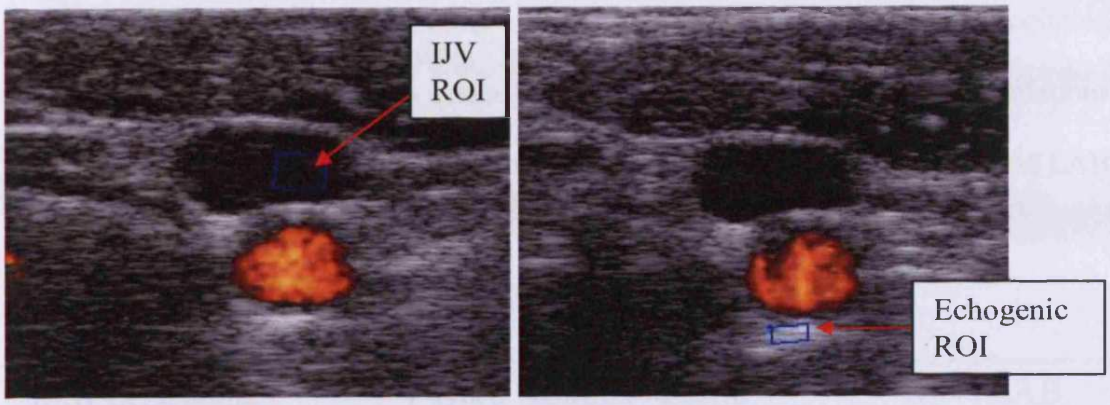

Figure 2.17 Example of the ROI selections for both IJV and echogenic areas. The positions of the ROIs are shown by the red arrows

The results in table 2.2 show that the IJV was mainly class 1 with a small amount in class 2 where the echogenic areas are mainly class 4 and 5.

Patient	Analysis site	Class 1 (%)	Class 2 (%)	Class 3 (%)	Class 4 (%)	Class 5 (%)
1	IJV 1	91.88	8.12	0.00	0.00	0.00
1	Echogenic 1	0.00	0.00	0.00	21.86	78.14
2	IJV 2	100.00	0.00	0.00	0.00	0.00
2	Echogenic 2	0.00	0.00	0.00	60.57	39.43
3	IJV 3	98.89	1.11	0.00	0.00	0.00
3	Echogenic 3	0.00	0.00	0.00	27.04	72.96

Table 2.2 MATLAB results for IJV and echogenic areas.

In conclusion there is a link between the MATLAB classifier, tissue type and the echogenicity reported for GSM analysis. The link suggests the more echogenic the tissue kernal, the more likely it is to be classified higher, however the MATLAB classifier does not classify the tissue by echogenicity alone but also takes into account the spatial arrangement of the kernals to their neighbours. Also there is an association between tissue type and class. A schematic diagram showing the possible associations between the kernal GSM echogenicity, tissue types and the *in vivo* MATLAB classification is shown in figure 2.18.

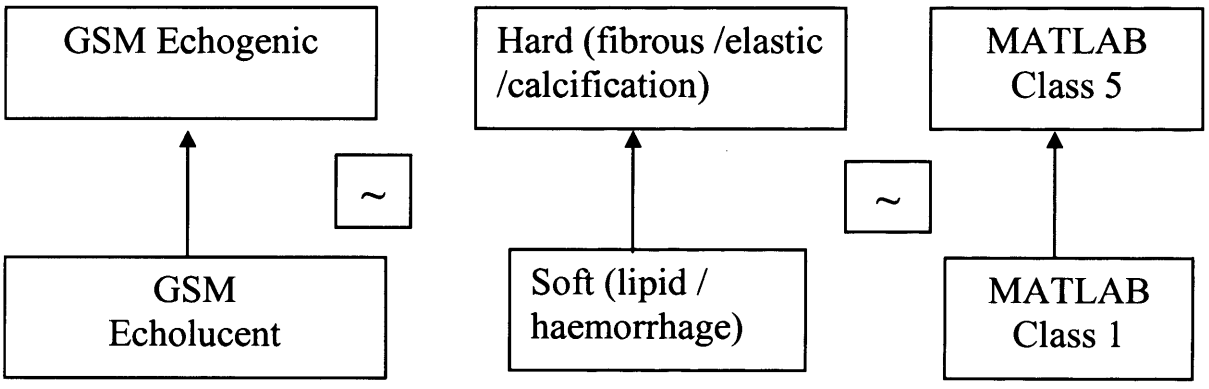

Figure 2.18 Possible associations between kernal echogenicity, tissue types and MATLAB classification.

In conclusion, it is possible for the classifier to distinguish *in vivo* between harder and softer tissue types. The ability of the classifier to distinguish specific tissue types is discussed in chapter 4.

2.4 Plaque Volume Measurements

The use of serial carotid plaque volume measurements in the monitoring of the effects of drug treatments has previously been reported. These studies have reported good accuracy and reproducibility of the volume measurements and have suggested that this technique offers a quantitative method of studying carotid plaque progression. (Hennerici et al. 1991; Delcker and Diener 1994; Griewing et al. 1997; Palombo et al. 1998; Schminke et al. 2002; Ainsworth et al. 2005; Landry et al. 2005).

2.4.1 Manual planimetry method

The method used is based on the manual planimetry method. This method can be used for parallel transverse images of known spatial interval and known transducer angle between slices. In this work the spatial interval is known and the angle between slices is zero. The volume of a sliced solid can be measured by the summation of the cross sectional areas of each 2D slice, k, where $0 < k \leq m$, and m is the total number of slices within the 3D volume and multiplying by the interslice distance, Δp (Landry and Fenster 2002)

The volume of the slice is given by

$V = A(k)\ \Delta p$ where A(k) is the area of the kth slice

The total volume is given by

$$\sum V = \sum A(k)\ \Delta p$$

This method has been used by several groups to measure 3D volume.

(Palombo et al. 1998; Landry and Fenster 2002; Landry et al. 2004; Ainsworth et al. 2005)

2.4.2 ImageJ software

The software used to measure the plaque volumes is a public domain Java image processing software program. It is freely available on the Internet as a downloadable application for any Windows based computer. It can display, edit, analyse, process and save almost all images and can handle many image formats like JPEG, GIF and TIFF for example. It can measure distance and angles, calculate area and pixel value statistics of user defined selections. It can create pixel density histograms and line profile plots as well as supporting standard image processing functions used for image manipulation. Image J allows scaling, magnification and zooming and also allows spatial calibration to provide measurements in units like millimetres etc.

2.4.2.1 Set Scale

The initial step was to define the scale of the active image so measurement results can be displayed in calibrated units, in this case millimetres. This was done by taking measurements of an ultrasound image with known calibrations. The ultrasound image was that of the ATS multipurpose test phantom (model 539, ATS laboratories inc. Bridgeport, Connecticut, USA) which has wires set at known distances, it was also calibrated against the top and side calibration on the image and also against the machine calibration (figure 2.19). The straight line selection tool on the imageJ software was used to make a line selection that corresponds to a known distance. The calipers were placed on the leading edge of the wires in all measurements. This was done five times for each of the four calibration methods and it was found that 9.4 pixels corresponded to 1mm.

There are errors associated with caliper measurement; firstly because the ultrasound image is made up of pixels, then the smallest distance that can be represented in an

image is one pixel, therefore all distance measurement have an inherent uncertainty of ± 1 pixel. Another possible error is that caliper systems have a limited caliper increment which may be larger than the pixel size. Another possible source of error is the image resolution, because ultrasound has a finite spatial resolution the edges of the image may appear blurred or enlarged. This could lead to an error depending on where the cursor was placed on the on wire. To estimate the error two lines were measured; one from the top on the first wire to the top of the second wire (red line in figure 2.19), the other from the top of the first wire to the bottom of the second (blue line). To estimate the possible error this would introduce into a volume measurement, the formula for combining errors in products or ratios was used.

If V = volume = (L_1 x L_2 x L_3). Assuming L= L_1 = L_2 = L_3 =1cm, the distance between the wires in figure 2.19. The differences between the top and bottom wires were measured at 1.0 ± 0.04 cm.

The formula for combining errors in products is

$$\frac{dv}{V} = \sqrt{\left(\frac{dl}{L}\right)^2 \times \left(\frac{dl}{L}\right)^2 \times \left(\frac{dl}{L}\right)^2} \text{ cm}^3$$

$$\frac{dv}{V} = \sqrt{3\left(\frac{dl}{L}\right)^2} \text{ cm}^3$$

$$dv = V\sqrt{3\left(\frac{dl}{L}\right)^2} \text{ cm}^3$$

Where dv is the error in volume and dl is the difference in length. = 0.04cm

This gives, $dv = 1\sqrt{3(0.04)^2}$ cm^3

$dv = 0.07$ cm^3

Therefore an estimation of the largest possible error in a volume calculation by measuring at different caliper placements is in the order of approximately 7%

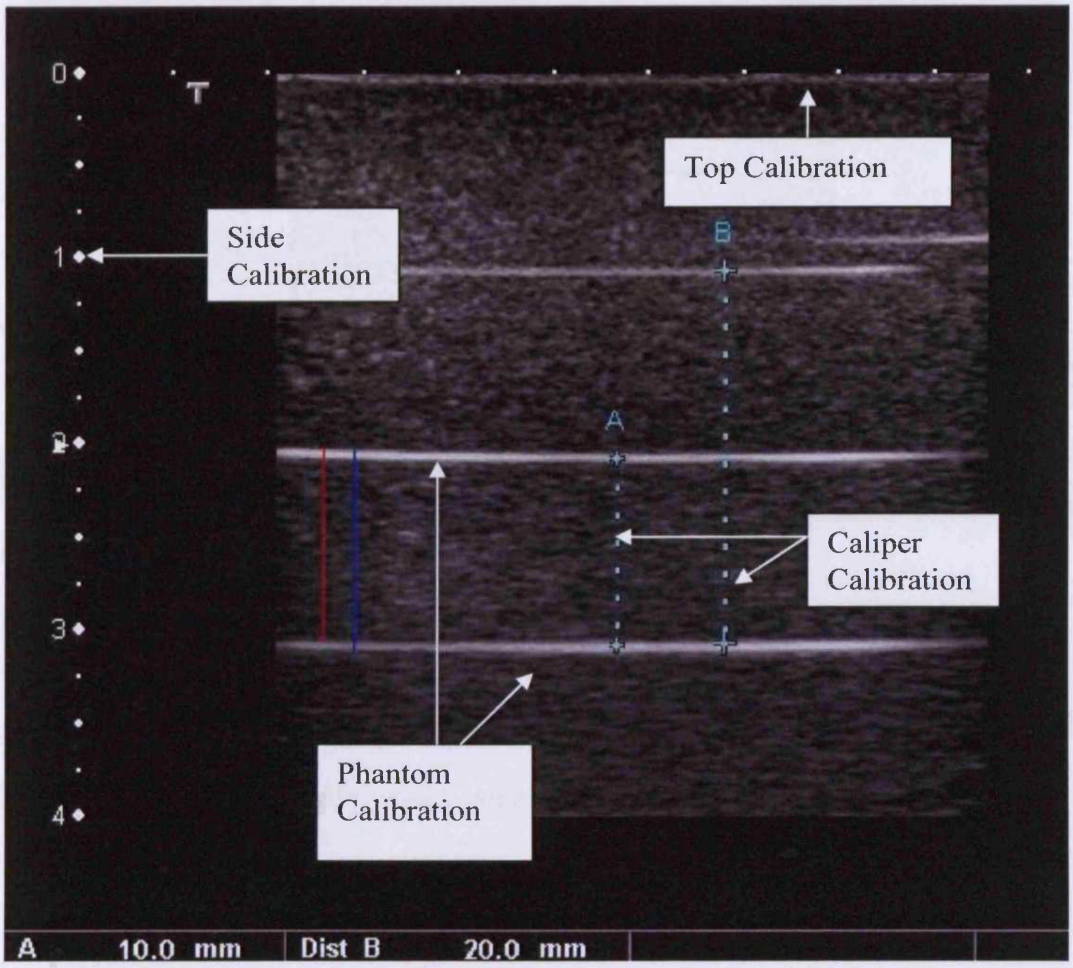

Figure 2.19 Calipers used in imageJ calibration.

The set scale dialog box (figure 2.20) was selected and the known distance and unit of measurement entered. The imageJ software automatically enters the distance in pixels field and calculates the scale. By selecting the global field the software will apply this scale to all images instead of just the active image. To test that the scale was accurate a series of measurements was performed on four different images of the test phantom using the four different types of calibration. The results showed that measurements of the scale were accurate with a mean % error of 0.28% (See appendix 2.3).

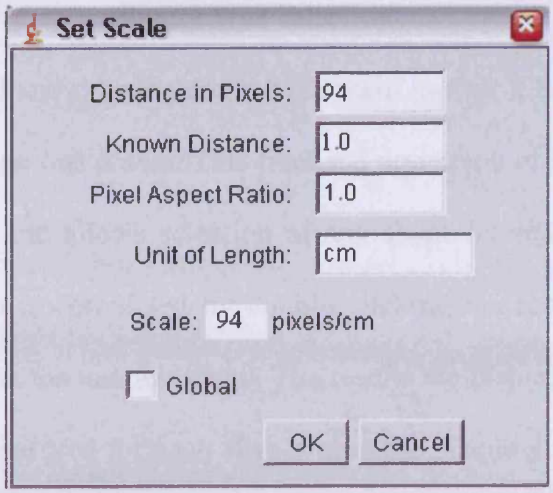

Figure 2.20 Example of set scale dialog box.

2.4.2.2 Set Measurements

Once the scale was set, the set measurements dialog box was selected. This box allows the user to specify which measurements are recorded when analysing the selected regions. Only the area measurement was required for this project.

2.4.2.3 Image selection for analysis

The images used for analysis were the same as those used for analysis by the MATLAB program. This was to ensure that the plaque extent analysed was the same for the MATLAB programs and volume measurements.

2.4.2.4 Image cropping and magnification.

In order to aid in the drawing of the ROIs, all the plaque images were initially cropped and then magnified by 200%. There was no loss of scale after cropping and magnification. Using the rectangular selection tool in the main imageJ toolbar a 15 x 15mm box was drawn around the plaque extent. This was the area which was cropped and magnified by 200%. The same procedure was applied to all images.

2.4.2.5 Plaque area selection

By selecting the freehand drawing tool on the main toolbar a ROI around the plaque on the magnified image was drawn. This freehand drawing tool is easily controlled by the computer mouse and allows selection of any shape by small movements of the mouse. The selection is completed by double clicking the mouse and analysed by selecting "measure" on the analyse menu. The results are displayed in a results dialog box. The area was measured for each slice within the plaque volume. The procedure was repeated five times for each plaque to check the reproducibility of the area selections. The results were then saved into an Excel spreadsheet (see section 2.4.3) which calculated the plaque volume. This method is used to calculate the plaque volumes in chapters 4 and 5.

2.4.3 Volume calculation in Microsoft Excel

A Microsoft Excel (Microsoft Corporation, Thames Valley Park, Reading, Berkshire, UK) template was written to analyse the data and calculate the plaque volume. The template calculated the plaque volume for all five measurements by multiplying the total plaque area by the distance between the images (0.903 mm). The mean plaque volume and standard deviation of the five measurements were then calculated. An example of the spreadsheet is shown in figure 2.21.

Imagej	MATLAB no.	Area 1 (mm^2)	Area 2 (mm^2)	Area 3 (mm^2)	Area 4 (mm^2)	Area 5 (mm^2)		Mean (mm^2)
1	59	5.307	4.648	5.041	5.492	5.099		5.117
2	61	5.353	4.914	5.053	6.024	5.457		5.360
3	63	6.59	5.793	5.839	5.457	5.203		5.776
4	65	6.671	6.879	8.174	8.602	7.411		7.547
5	67	9.146	7.504	7.804	7.908	8.66		8.204
6	69	9.539	9.77	10.325	9.909	10.279		9.964
7	71	10.071	10.487	10.163	11.238	9.805		10.353
8	73	9.088	8.498	8.498	9.122	8.359		8.713
	Total area (mm^2)	61.765	58.493	60.897	63.752	60.274		61.037
	Volume (mm^3)	55.774	52.819	54.990	57.568	54.427		55.116
	Mean Volume (mm^3)	55.116						
	St Dev (mm^3)	1.747						

Figure 2.21 Example of Excel spreadsheet volume calculation.

2.4.4 Verification of imageJ area measurements

In order to test the imageJ area calculation, a series of imageJ measurements carried out on a phantom were compared to measurements calculated by two different ultrasound machines. The -15dB anechoic target of the ATS multipurpose phantom was imaged at a depth of 4cm on both Toshiba Powervision and Toshiba Xario ultrasound machines. The ROI was drawn around the target and the area calculated by the ultrasound machine (figure 2.22). A series of five images were recorded on each machine and the overall mean area and standard deviation (SD) calculated (table 2.3)

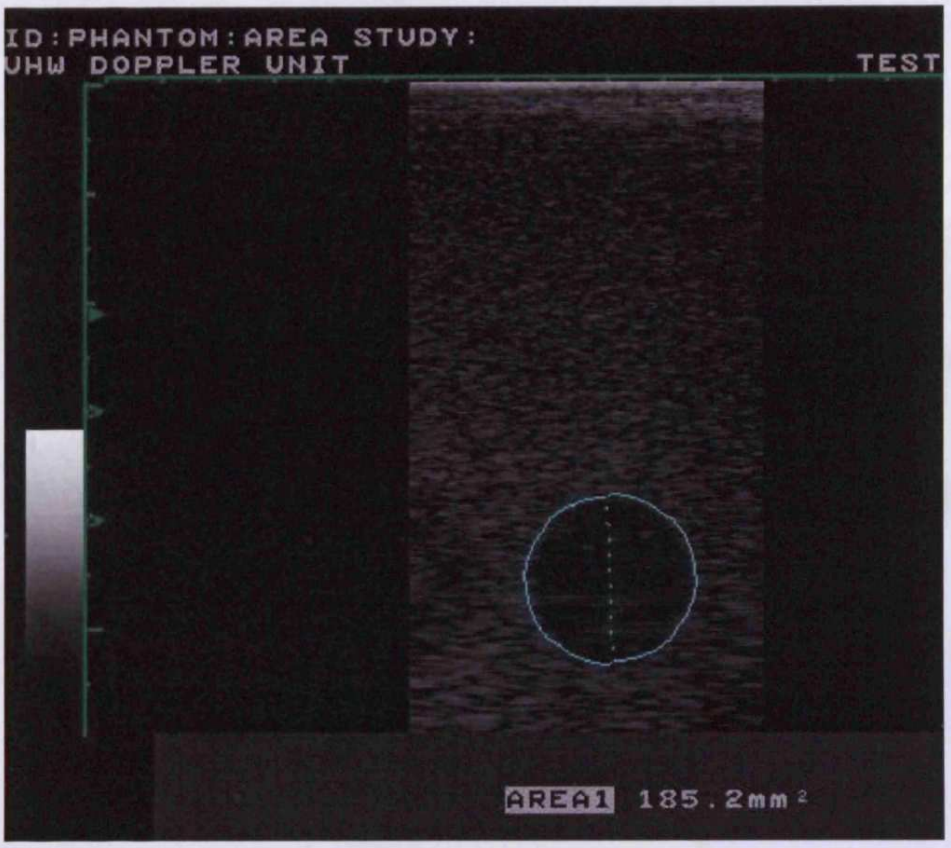

Figure 2.22 Phantom area measurement carried out on Toshiba Powervision scanner.

	Aplio	Powervision
Area 1 (mm^2)	181.0	180.0
Area 2 (mm^2)	177.0	185.2
Area 3 (mm^2)	177.0	185.0
Area 4 (mm^2)	181.0	186.0
Area 5 (mm^2)	181.0	176.0
Overall mean (mm^2)	180.9	
Overall SD (mm^2)	3.6	

Table 2.3 Area measurements from Toshiba ultrasound scanners.

For the imageJ area calculations five different images of the phantom were recorded. The ROI was drawn around the target and the area calculated by the imageJ software

(figure 2.23). This was repeated five times for each of the five images. The overall mean area and standard deviation was calculated (table 2.4).

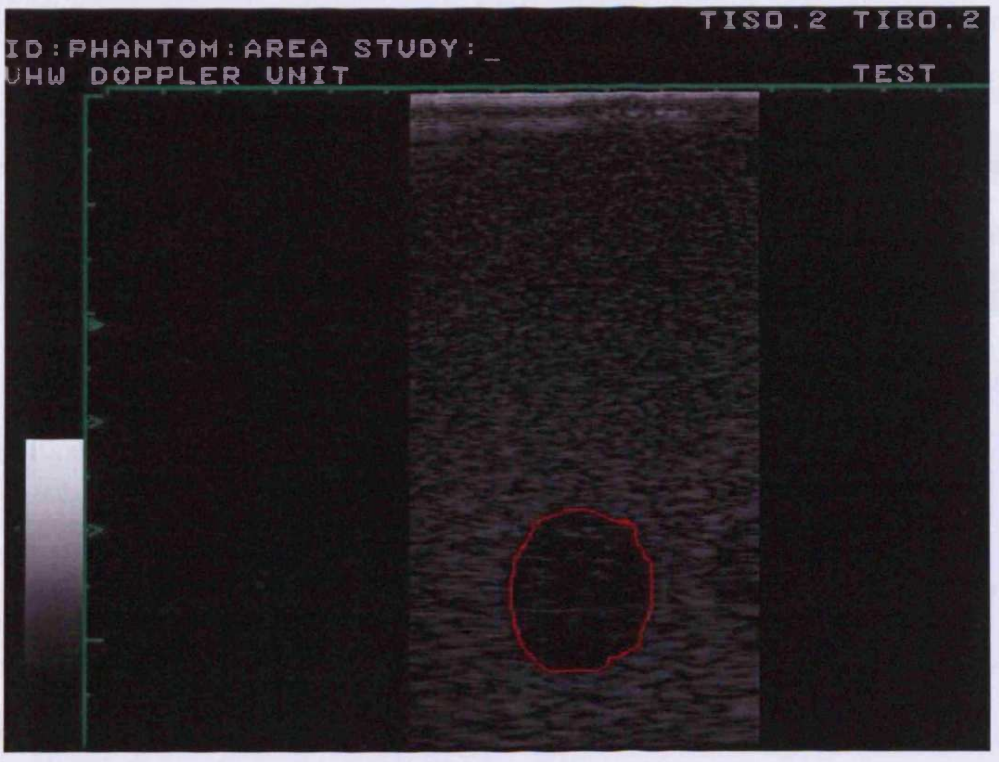

Figure 2.22 Phantom image with ROI drawn around target.

	Image 1	Image 2	Image 3	Image 4	Image 5
Area 1 (mm^2)	181.3	180.8	183.3	176.9	176.1
Area 2 (mm^2)	183.2	174.1	184.7	177.9	181.7
Area 3 (mm^2)	175.8	180.4	180.2	183.2	177.2
Area 4 (mm^2)	179.5	177.7	173.2	178.4	177.2
Area 5 (mm^2)	177.9	178.9	179.6	180.3	183.3
Overall mean (mm^2)	179.3				
Overall SD (mm^2)	3.0				

Table 2.4 Area measurements on phantom target using imageJ.

The mean imageJ area calculation of 179.3 ± 3 mm^2 is within the standard deviation of the mean ultrasound machine calculations (180.9 ± 3.6 mm^2).

Chapter 3: Variability studies

3.1 Aims

In this chapter the aim is to test the system that has been developed. The system is based on previous work from our laboratory and has been expanded into a reliable system for 3D *in vivo* data acquisition of carotid plaques. The previous work was an *in vitro* system which looked at carotid plaque specimens embedded in agar. This has been expanded into a 3D mechanical system for *in vivo* acquisition which mimics the *in vitro* system used in the laboratory. This chapter aimed to see if the 3D B-mode acquisition system that was developed would be useful in comparing serial scans and able to identify changes in tissue type.

In this chapter, 4 different studies were carried out to estimate the variability of the process. The first was an intra (within) observer study which was conducted to estimate the repeatability of the ROI selection process. A single observer selected the ROIs of 10 plaques on 10 different occasions and the degree of repeatability between the measurements calculated. The second was another intra observer study conducted to estimate the variability of a duplicate scan on the same plaque. The same observer analysed duplicated scans on 10 plaques and compared the results with the original scans to estimate the effects of repositioning. Another intra observer study was also carried out to further estimate the effects of repeat measurements and repositioning. Two patients with carotid plaques were imaged 5 times over a short period of time with a break between scans. The grey scale values of the plaques were measured and compared. The fourth was an inter (between) observer study conducted to see if different observers would select similar ROIs and estimate the variability between

them. Three different observers selected the ROIs of the same 10 plaques and an estimation of the agreement between them was calculated.

Three different observers with considerable experience in vascular ultrasound imaging conducted the studies. The observers were Dr N Pugh (NP), Consultant Medical Physicist (observer 1), who has over 15 years experience in routine vascular ultrasound imaging. The second was Mr D Coleman (DC), Principal Medical Physicist (observer 2), with over 8 years experience in routine vascular ultrasound imaging and the third was Dr F Rakebrandt (FR), a post doctoral research fellow (observer 3), with over 5 years experience in the field of ultrasound tissue characterisation but no experience in routine vascular imaging.

3.2 ROI intra observer variability study

3.2.1 Methods

Initially the three observers agreed the criteria for plaque selection (See table 3.1). One observer (DC) selected 10 *in vivo* plaques for inclusion into the study. The same 10 plaques were used in this intra study and the inter study (see section 3.5). The ten plaques selected were from both symptomatic and asymptomatic patients and the plaques stenoses ranged from non significant (<40%) to highly significant (>95%). The plaque extent, which is the number of 2D images in which the plaque was contained, was selected as a group by all three observers for each of the ten plaques. This was done to ensure that the same 2D images were selected by all three observers. This intra observer variability study was conducted by one observer (DC) who analysed the 10 plaques on 10 separate occasions, separated by at least a day, using the agreed criteria with the aim to estimate the repeatability of selecting the ROIs.

- Initially select image which give the best impression of the plaque borders
- Include intima/media in ROI.
- Do not include reverberation/artefact error.
- Exclude areas where the blood flow is absent by comparing with previous and subsequent images.
- Overlay ROI from previous image on top of new image for an indication of outline – then select new ROI.
- Check parametric image after ROI selection. If not acceptable then reselect ROI.
- Save the data when all ROIs for plaque extent are selected.

Table 3.1 Criteria for ROI Selection.

3.2.2 Statistical analysis techniques

For the intra observer variability study we needed to assess how repeatable the process was. The within observer variation assumes that the true underlying value is constant and that the variations are due only to the observer. There is no relative bias in the measurements but it is a measure of the accuracy of the observer in making the measurement. The variation within an observer is assumed to be random.

The population of differences between replicated measurements can safely be assumed to have an approximately normal distribution. From the properties of normal distribution 95% of the differences between replicated measurements should lie between ±1.96 standard deviations of the average difference where the population of differences is assumed to have a zero mean and the standard deviation is taken as an estimate of the standard deviation in the population. Thus, since the sign of the difference is irrelevant when repeated measures are in question, 95% of the differences should be less than 1.96SD (d). This quantity is called the 95% coefficient of repeatability.

3.2.3 Results

The data were checked that it had a normal distribution using quantile-quantile (Q-Q) plots in SPSS. Initially the mean value of the 10 measurement for each class for the 10 plaques was calculated. Then for each of the 10 plaques, the mean differences and the standard deviation of the differences, between the 10 measurements were calculated. From which the mean 95% coefficient of repeatability was then calculated for each of the five classes. Then the overall mean coefficients were calculated for each of the five classes (table 3.2).

A plot (fig. 3.1) of absolute difference for each class and for each plaque against mean of readings is drawn with a line indicating the maximum limit of repeatability (class 5). This plot shows that there is no relationship between the size of the difference and the magnitude of the readings.

	Class 1	Class 2	Class 3	Class 4	Class 5
Plaque 1	1.02	0.85	1.45	1.46	2.85
Plaque 2	0	0.24	0.93	2.17	2.21
Plaque 3	0	0.11	1.17	2.34	2.28
Plaque 4	0.01	0.3	1.19	0.66	0.35
Plaque 5	0	0.15	0.13	1.27	1.31
Plaque 6	0	0.05	0.39	1.08	1.31
Plaque 7	0	0.03	0.84	1.51	1.94
Plaque 8	0.89	0.66	1.8	0.97	1.04
Plaque 9	0.28	1.16	0.89	1.18	0.85
Plaque 10	0.01	0.24	0.49	0.4	0.52
Mean	0.22	0.38	0.93	1.30	1.47

Table 3.2 95% coefficient of repeatability values for the 10 plaques and the overall mean 95% coefficient of repeatability for each of the 5 classes.

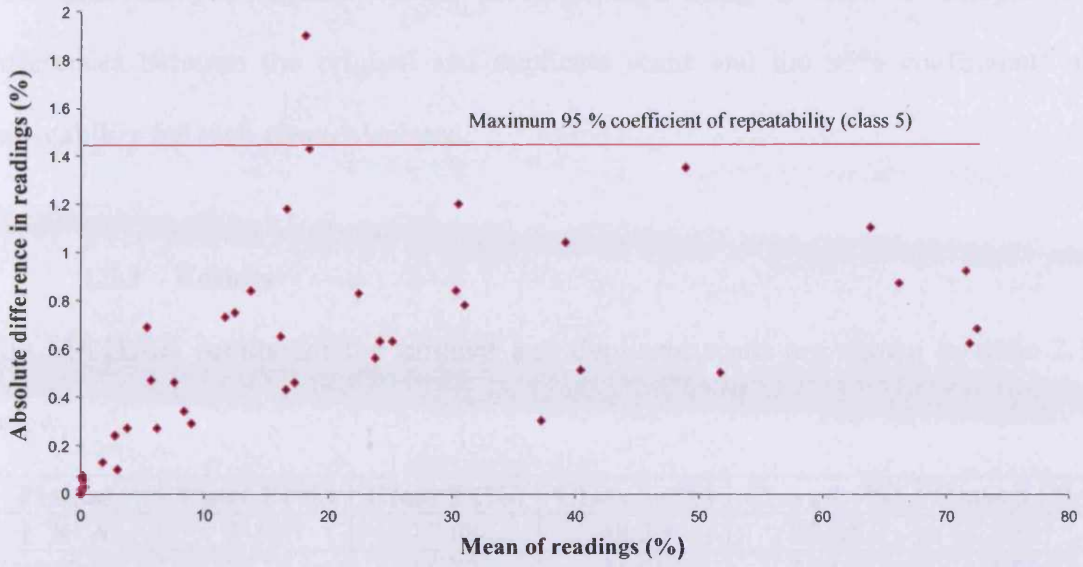

Figure 3.1 ROI intra observer study plot of absolute difference in readings versus the mean of readings with a line indicating the maximum 95% coefficient of repeatability (class 5).

3.3 Duplicate intra observer variability study

3.3.1 Methods

This study aimed to measure the variability of duplicate scans to estimate the effects of patient repositioning and scan orientation. The ten plaques used in this study were the 4 apheresis plaques and 6 of the statin plaques that were used in the serial scan study in chapter 5. The images were from the patients initial visits on the study and were compared to the duplicate scans that was recorded at that initial visit. The duplicate scan was acquired using the same protocol as the original scan (see section 2.2.4). The plaques are identified using the labelling system described in section 5.3.1.

3.3.2 Statistical analysis techniques

The same analysis method as the previous intra study is used to analyse the differences between the original and duplicate scans and the 95% coefficients of repeatability for each class calculated.

3.3.3 Results

The MATLAB results for the original and duplicate scans are shown in table 3.3 below.

Plaque	Class 1 (%)	Class 2 (%)	Class 3 (%)	Class 4 (%)	Class 5 (%)
1_R_A	9.19	17.08	48.23	22.24	3.25
Duplicate	10.15	18.33	46.89	21.19	3.07
1_L_A	10.86	28.87	43.02	16.59	0.66
Duplicate	12.97	32.14	38.29	15.88	0.72
2_R_A	11.11	15.42	34.17	30.27	9.03
Duplicate	11.20	16.83	31.43	31.79	8.75
2_L_A	19.46	19.26	30.62	22.32	8.34
Duplicate	13.15	18.86	30.89	23.07	14.03
3_R_S	16.52	34.33	39.20	9.09	0.85
Duplicate	17.55	34.58	37.98	9.10	0.78
4_L_S	0.00	0.01	13.25	63.44	23.31
Duplicate	0.00	0.54	12.27	61.44	25.75
5_R_S	19.22	46.58	30.78	3.42	0.00
Duplicate	20.12	46.36	28.27	5.21	0.04
6_R_S	0.00	0.00	27.12	58.46	14.38
Duplicate	0.00	0.00	27.73	56.20	16.07
7_R_S	5.58	38.16	39.33	16.85	0.08
Duplicate	6.30	36.37	38.55	17.50	1.28
8_R_S	0.64	20.27	48.03	28.16	2.89
Duplicate	1.36	19.90	47.80	27.74	3.84

Table 3.3 MATLAB results for duplicate and original scans for the ten plaques.

The data were checked that it had a normal distribution using quantile-quantile (Q-Q) plots in SPSS. The differences between the original and duplicate scan were calculated for each class for the 10 plaques. The mean differences (d), standard

deviations of the differences and 95% coefficients of repeatability were also calculated and the results displayed in table 3.4.

Plaque	Class 1 (%)	Class 2 (%)	Class 3 (%)	Class 4 (%)	Class 5 (%)
1_R_A	0.96	1.25	1.34	1.05	0.18
1_L_A	2.11	3.27	4.73	0.71	0.06
2_R_A	0.09	1.41	2.74	1.52	0.28
2_L_A	6.31	0.40	0.27	0.75	5.69
3_R_S	1.03	0.25	1.22	0.01	0.07
4_L_S	0.00	0.53	0.98	2.00	2.44
5_R_S	0.90	0.22	2.51	1.79	0.04
6_R_S	0.00	0.00	0.61	2.26	1.69
7_R_S	0.72	1.79	0.78	0.65	1.20
8_R_S	0.72	0.37	0.23	0.42	0.95
Mean diff. (d)	1.28	0.95	1.54	1.12	1.26
SD (d)	1.87	1.01	1.41	0.74	1.76
95% Coeff.	3.64	1.95	2.73	1.43	3.41

Table 3.4 Differences between original and duplicate scans showing the calculated 95% coefficient of repeatability for each class for the 10 plaques.

From these results it can be seen that 95% of the duplicate values lie within ± 2 standard deviations of the original value. In plaque 2_L_A, there is a twofold increase with 6.31 and 5.69% differences between classes 1 and 5 respectively. There is also a 12 fold increase in class 5 of plaque 7_R_S, but the absolute difference is very small at 1.26%. The reasons for these differences may be due in part to repositioning but also may be due to ROI selection. The data in table 3.4 is used to calculate the 95% coefficient of repeatability of the duplicate scans which is used to estimate the total variation in section 3.6.

A plot (figure 3.2) of absolute difference against the mean reading of original and duplicate scans is drawn with a line indicating the maximum 95% coefficient of repeatability (class 1). This plot shows that there is no relationship between the size of the difference and the magnitude of the readings.

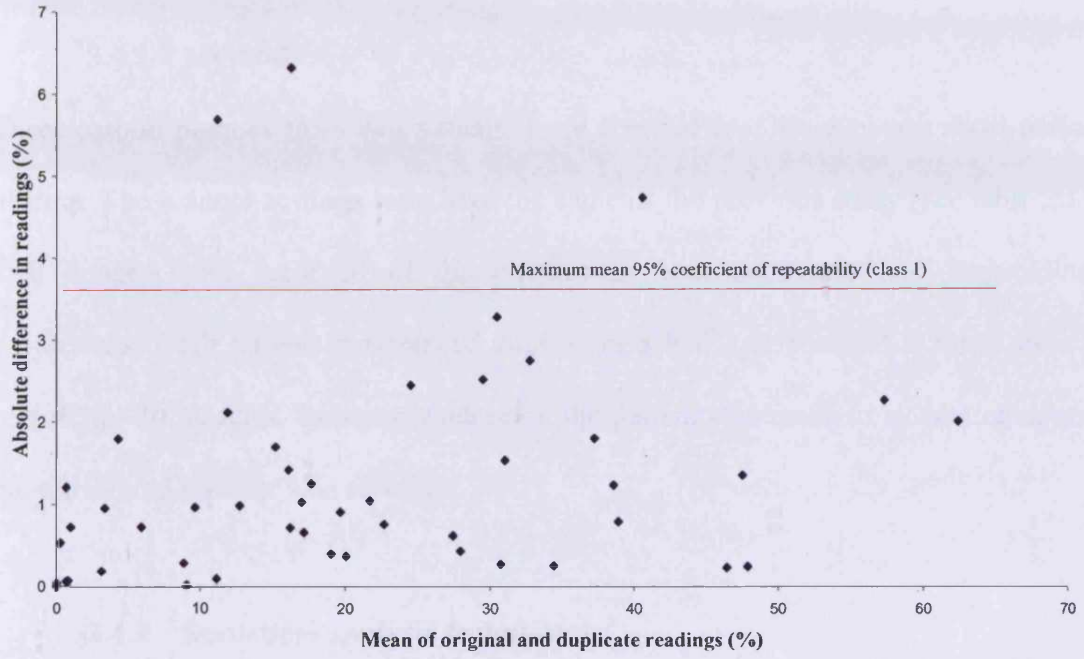

Figure 3.2 Duplicate intra observer study plot of absolute difference in readings versus the mean of the original and duplicate readings with a line indicating the maximum 95% coefficient of repeatability (class 1).

3.4 Effects of repositioning on grey scale values

The aim of this study was to look at the effects of repositioning of the transducer on the neck region and to study any changes in the mean grey level values of a defined region of interest. This study was done in retrospect to the other variability studies and it was not possible to use the MATLAB system, as the same Toshiba Powervision scanner used in the rest of this project is no longer in routine use. It was not possible to acquire a 3D volume data set. The reason is that the large 3D data sets were

transferred to a PC via a DICOM network. This network no longer exists so it is not possible to extract the 3D data set from the scanner. Also renovations to the ultrasound scanning room mean that the mechanical device is no longer attached to the wall.

3.4.1 Methods

Three carotid plaques from two patients were scanned five times over a short period of time. The scanner settings were kept the same as the previous study (see table 2.1). Still images were recorded of the plaques in both transverse and longitudinal projections. Each patient was placed supine on a bed and scanned 5 times over a period of ~30 minutes. Between each scan, the patient was made to sit in a chair and the ultrasound scanner was rebooted.

3.4.2 Statistical analysis techniques

The results were analysed using the same statistical analysis technique as the previous intra observer studies.

3.4.3 Results

A region of interest was drawn around the plaque using imageJ software on two different transverse images and two different longitudinal images (one image taken antero-laterally, the other postero-laterally) and the mean grey value of the plaque was calculated. The data were checked that it had a normal distribution using quantile-quantile (Q-Q) plots in SPSS. An example of one of the images is shown in figure 3.3

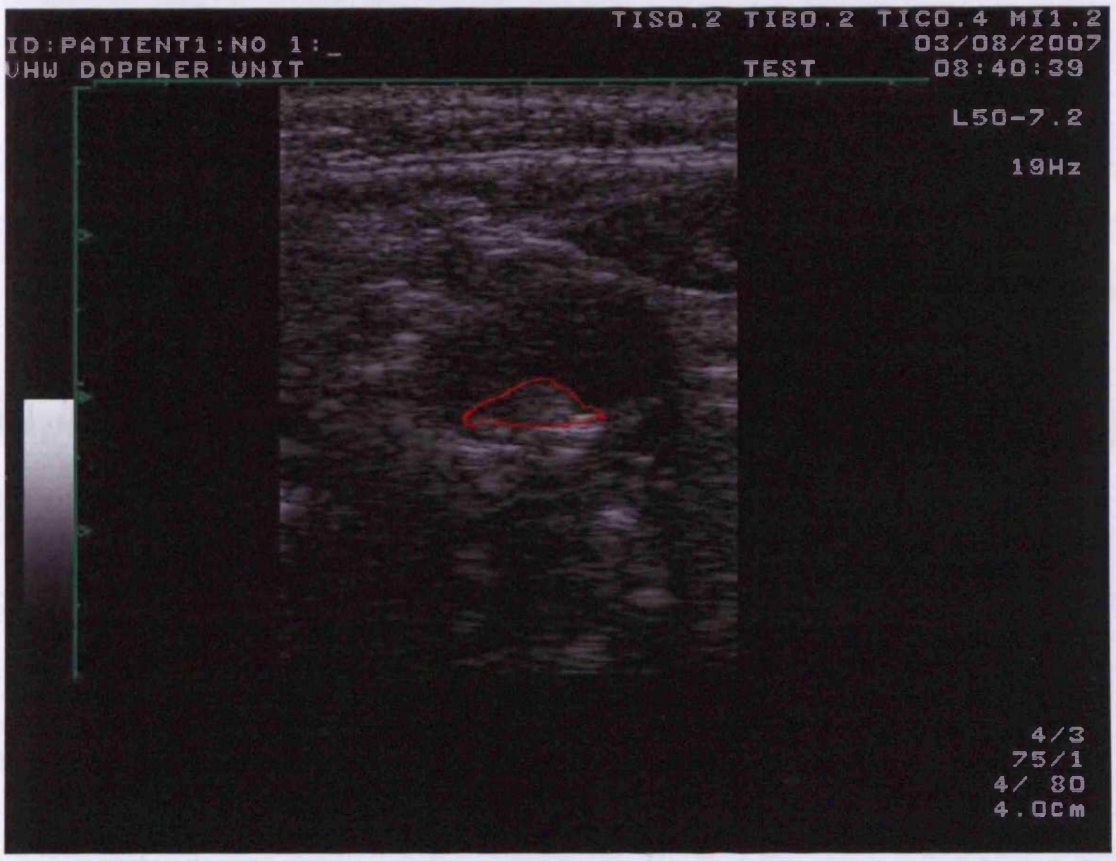

Figure 3.3 Transverse image of plaque 1 showing the ROI drawn around the plaque.

The results for plaque 1 are summarized in table 3.5 below.. The mean grey scale measurement values (MGV) were recorded for the five repeated measurements, from which an overall mean grey scale value was calculated. The absolute difference in the means (overall – measurement) for each of the five measurements was then calculated. As the other intra and inter studies are expressed as percentages, the difference in means was expressed as a percentage of the overall mean. From which a mean % difference of the five measurements and a 95% coefficient of repeatability were calculated. An overall 95% coefficient of repeatability of 4.53% was calculated. The appearance of this plaque was echogenic and the overall MGV of this plaque was

42.2 which is consistent with reported values of GSM for echogenic plaques (Elatrozy et al. 1998).

	Measurement 1 (MGV)	Measurement 2 (MGV)	Measurement 3 (MGV)	Measurement 4 (MGV)	Measurement 5 (MGV)
Image 1-transverse	41.9	45.0	38.3	45.3	46.6
Image 2-transverse	41.5	43.2	44.8	39.4	41.5
Image 3-longitudinal	35.8	39.9	46.6	42.3	37.9
Image 4-longitudinal	42.5	41.0	47.1	41.3	42.3
Measurement mean	40.4	42.3	44.2	42.1	42.1
Overall mean (MGV)	42.2				
Difference in means (overall-measurement) (MGV)	1.79	0.07	1.99	0.13	0.13
% Difference in means (%)	4.23	0.15	4.71	0.32	0.32
Mean% difference	1.95				
St dev (difference) (%)	2.31				
95% coefficient (%)	4.53				

Table 3.5 95% coefficient of repeatability for plaque 1 in the repositioning study.

The second patient had bilateral non significant carotid plaques. The plaque on the right hand side (plaque 2) was a large echogenic plaque. The plaque on the left hand side (plaque 3) was a smaller plaque which had an echolucent appearance on ultrasound. Both plaques were analysed in the same way as plaque 1 above. The results for the two plaques are displayed in tables 3.6 and 3.7.

	Measurement 1 (MGV)	Measurement 2 (MGV)	Measurement 3 (MGV)	Measurement 4 (MGV)	Measurement 5 (MGV)
Image 1-transverse	47.6	43.6	39.8	39.2	46.2
Image 2-transverse	39.9	41.3	48.2	42.8	42.7
Image 3-longitudinal	45	48	46.7	47.9	46.1
Image 4-longitudinal	40.9	44.2	46.6	40.4	46.2
Measurement mean	43.4	44.3	45.3	42.6	45.3
Overall mean (MGV)	44.2				
Difference in means (overall-measurement) (MGV)	0.81	0.11	1.16	1.59	1.14
% Difference in means (%)	1.85	0.25	2.63	3.60	2.57
Mean% difference	2.18				
St dev (difference) (%)	1.25				
95% coefficient (%)	2.44				

Table 3.6 95% coefficient of repeatability for plaque 2 in the repositioning study.

	Measurement 1 (MGV)	Measurement 2 (MGV)	Measurement 3 (MGV)	Measurement 4 (MGV)	Measurement 5 (MGV)
Image 1-transverse	23.9	21.3	22.8	26.7	24.4
Image 2-transverse	21.8	26.9	26.9	26.4	25.6
Image 3-longitudinal	25.1	23.6	26.4	24.5	22.3
Image 4-longitudinal	24.5	26.7	24.5	22.8	21.2
Measurement mean	23.8	24.6	25.2	25.1	23.4
Overall mean (MGV)	24.4				
Difference in means (overall-measurement) (MGV)	0.59	0.21	0.73	0.68	1.04
% Difference in means (%)	2.42	0.86	3.01	2.81	4.26
Mean% difference	2.67				
St dev (difference) (%)	1.22				
95% coefficient (%)	2.40				

Table 3.7 95% coefficient of repeatability for plaque 3 in the repositioning study.

It is well documented that the lower the GSM value, the more echolucent the plaque. El Barghouty (1995) reported that a carotid plaques with GSM value of <32 was associated with a higher risk of CT brain infarction and could be considered a high risk unstable plaque. A plaque with a GSM of >32 had a lower incidence of CT brain infarction and could be considered as low risk stable plaque (El-Barghouty et al. 1995). The same author also reported that the lower the GSM the more haemorrhage and lipid content was found in the plaque histology and the higher the GSM the more fibrous content was found (El-Barghouty et al. 1996). Elatrosy (1998) also reported a high GSM was associated with asymptomatic stable plaques and a low GSM

associated with symptomatic, high risk unstable plaques (Elatrozy et al. 1998). In this study MPV was measured which is comparable to GSM values. The results for the three plaques indicate that plaques 1 and 2, with MPVs of <40 are more echogenic and likely to be considered as low risk stable plaques. Plaque 3, which has a MPV of 25, is a more echolucent plaque and is likely to be considered as a higher risk unstable plaque.

The results show that measurements of serial grey scale values of these 3 carotid plaques had 95% coefficients of variability of 4.53%, 2.44% and 2.4% respectively. There appears to be no significant difference in repeatability between the echogenic (plaques 1 & 2) and the echolucent plaque (plaque 3) found in patient 2 of this study. The 95% coefficient of repeatability is larger for the echogenic plaque of patient 1.

3.5 ROI inter observer variability study

The aim of this study was to estimate the variability of different observers in the selection of the ROIs.

3.5.1 Methods

The same 10 plaques from the ROI intra observer study were utilized in this study. The three observers independently selected the ROIs for each of the 10 plaques using the agreed criteria. When each observer had selected the ROIs for all 10 plaques the data were subsequently analysed using the MATLAB classification program.

3.5.2 Statistical analysis techniques

For the inter observer study we needed to know the level of agreement between the three observers. In theory when two or more observers make measurements on the

same data there may be relative bias between the measurements. This between observer variations can be caused by having different criteria for making a measurement or by having different measurement techniques. This variation can be reduced substantially by standardizing both the measurement criteria and the training of the observers in the technique. Between observer variation of measurements has an effect of biasing results and the problem is not which of the observers is right but whether the measurements agree or not. The observers will have to have a high level of precision in making the measurements otherwise this will contribute to a lack of agreement. The approach of using correlation to measure agreement cannot be used (Bland and Altman 1986). The concepts of correlation and agreement are different, correlation will show whether the measured values are related to each other, but does not necessarily tell you that there is a high level of agreement between the measurements.

The use of kappa statistics to measure agreement in this case, was not suitable as it only gives a simple binary response – the presence or absence of some factor. To estimate the level of agreement the differences between observer's readings were examined directly. The differences are scattered on either side of the average difference and there is no tendency for the differences to increase as the magnitude increases. The average difference (d) shows the relative bias and since the distribution of the differences should approximately be normal you can expect 95% of the differences in readings to lie between ±1.96 standard deviations (SD) of the average difference. These are called the 95% limits of agreement.

3.5.3 Results

The data were checked that it had a normal distribution using quantile-quantile (Q-Q) plots in SPSS. The 10 plaques were analysed by the three observers from which a mean value for each class was calculated. The difference between the three observers was examined in pairs (i.e.: observer 1-observer 2 etc) from which a mean difference was calculated for each of the five classes. Then for each plaque the standard deviation (SD) and the limit of agreement (±1.96SD) of all the differences for each of the 5 classes were calculated. This yields a limit of agreement for each plaque for that class, from which an overall mean limit of agreement for each class was calculated (Table 3.8).

	Class 1	Class 2	Class 3	Class 4	Class 5
Mean value (%)	2.76	5.75	18.33	41.19	32.26
Mean difference obs1-obs3 (%)	0.18	0.52	0.27	-1.23	0.28
Mean difference obs3-obs2 (%)	-0.46	-0.93	1.17	1.15	-0.94
Mean difference obs2-obs1 (%)	0.27	0.42	-1.32	0.10	0.93
St. Dev. of differences	0.60	1.54	3.70	6.60	6.25
Mean 95% coefficient of agreement	1.18	3.02	7.25	12.93	12.24

Table 3.8 Inter observer study showing the mean differences between the three observers and the mean 95% coefficient of agreement for all the five classes.

A graph (fig 3.4) of the difference between observers against mean reading for that plaque is plotted with lines showing the mean and maximum (class 4) 95% limit of agreements derived in table 3.8. The limits of agreement lines are derived from the overall mean difference ± coefficient of agreement. The graph also shows that the difference between the observers does not increase with the magnitude of the readings so there is no necessity for a transformation of the data (Bland and Altman 1986).

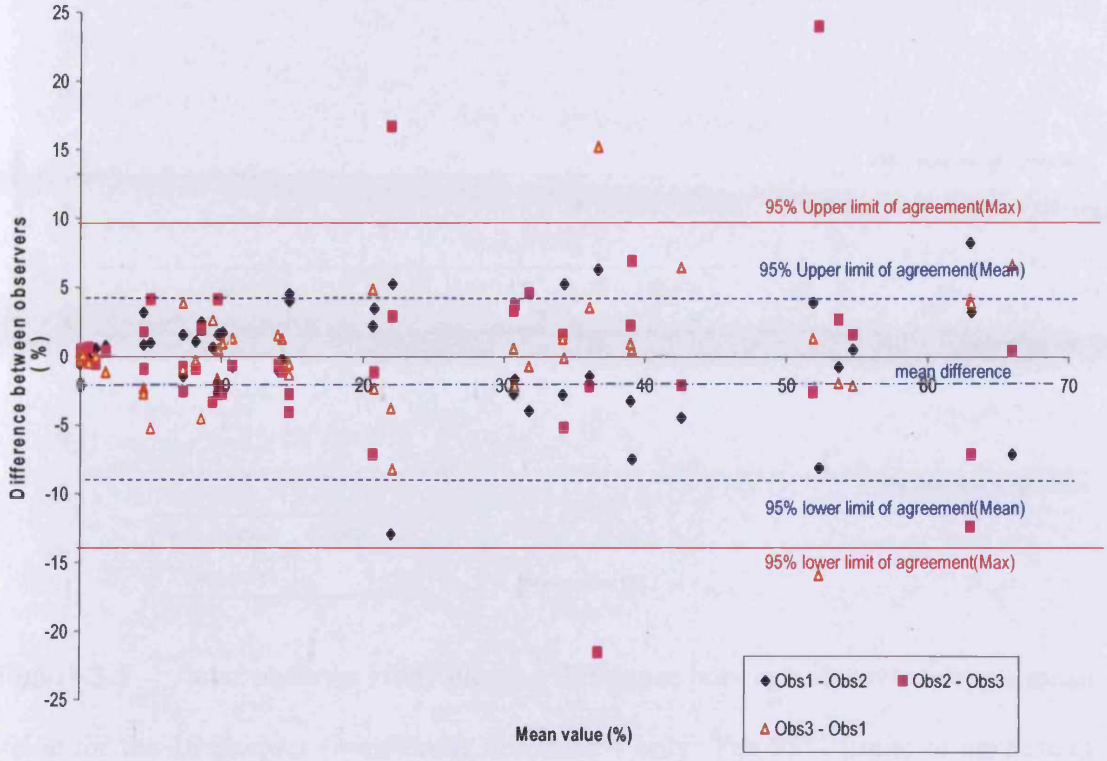

Figure 3.4 Inter observer study showing the 95% coefficients of agreements for all 10 plaques and all 5 classes.

This graph shows that most of the differences lie within the maximum 95% limits of agreement, which occurs for class 4. The largest coefficients of agreements are for class 4 and 5, as these two classes are the dominant classes in the 10 different plaques analysed (see mean value column in table 3.8).

The differences that lie outside the agreement limits, can be examined more in depth by studying the differences for class 4 (figure 3.5) and class 5 (figure 3.6) separately.

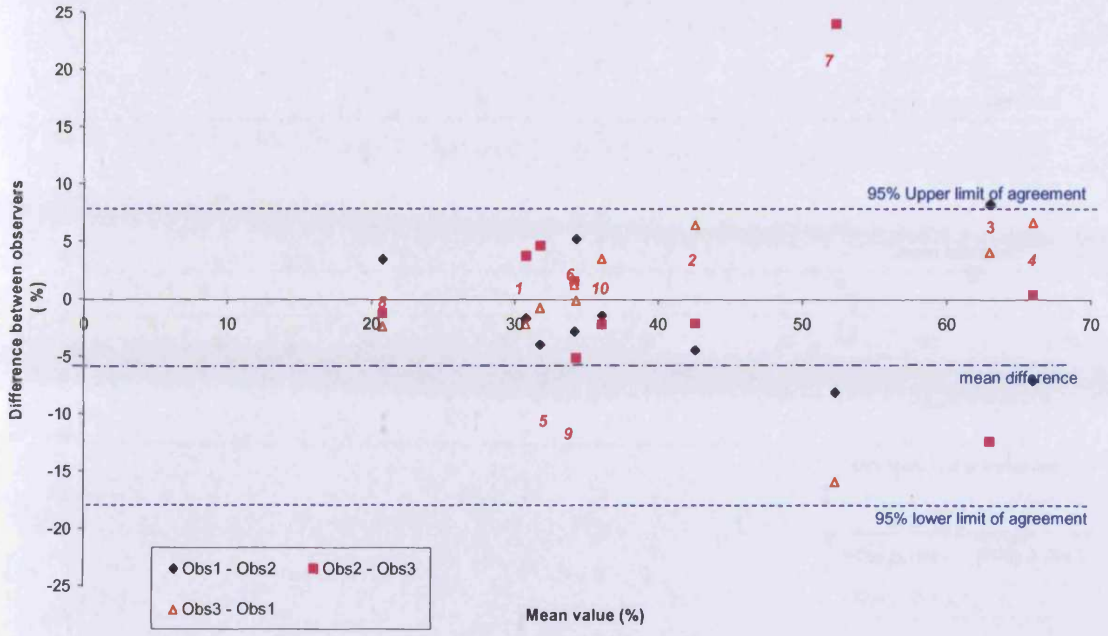

Figure 3.5 Inter observer study plotting difference between observers versus mean value for the 10 plaques (numbered), for class 4 only. The 95% limits of agreement are also plotted.

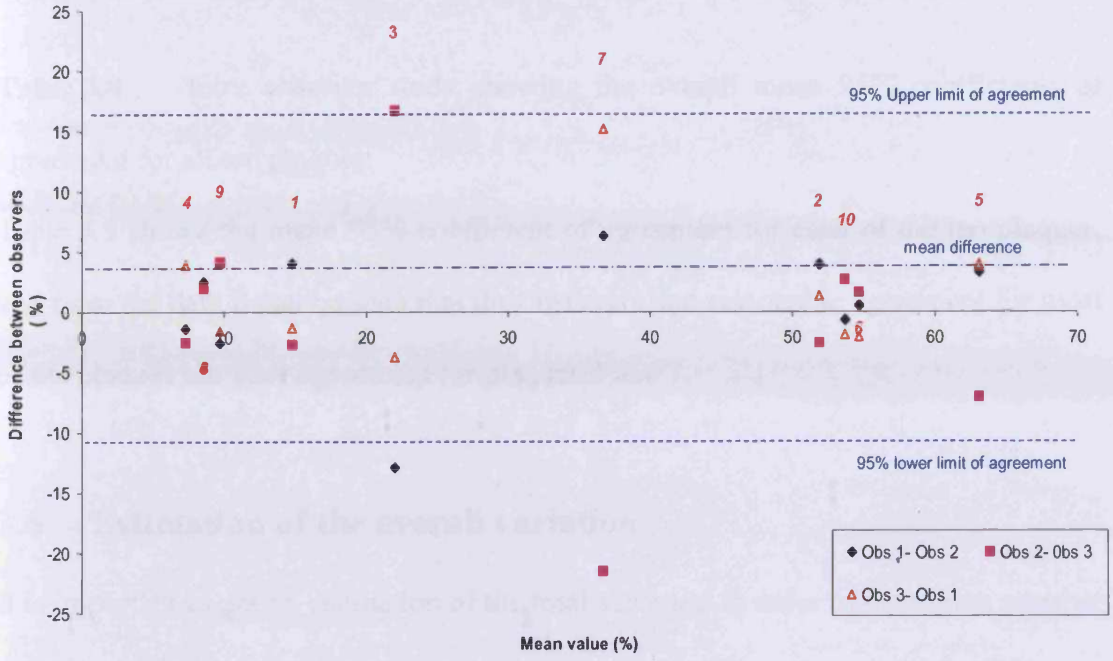

Figure 3.6 Inter observer study plotting the difference between observers versus mean value for the 10 plaques (numbered) for class 5 only. The 95% limits of agreement are also plotted.

What can be seen from both figures 3.5 and 3.6 and table 3.8 is that the three observers had reasonable agreement in the selection of the ROIs for most of the 10 plaques but the results were significantly biased by the differences from plaques numbered 3 and 7. It can also be noted from the graphs that the largest differences involved observer 3, who had the least experience of routine vascular ultrasound imaging.

Plaque no.	1	2	3	4	5	6	7	8	9	10
Mean 95% Coefficient (%)	2.4	4.48	10.84	5.31	4.21	1.89	16.72	4.74	3.23	1.98

Table 3.9 Inter observer study showing the overall mean 95% coefficients of agreement for all ten plaques.

Table 3.9 shows the mean 95% coefficient of agreement for each of the ten plaques, and from the data it can be seen that the observers had reasonable agreement for most of the plaques but poor agreement for plaques 3 and 7.

3.6 Estimation of the overall variation

It is important to get an estimation of the total variation in order to determine whether differences in the serial measurements (chapter 5) are due to changes in the plaque or due to experimental variation. In this chapter, four different variability studies have been carried out to try to evaluate the possible sources of variation. From the studies two main sources of variation were identified. Both the duplicate intra observer and effects of repositioning studies assessed variation due to changes in repositioning of the patient for repeat scans. The ROI intra and inter observer variability studies assessed the variation in the ROI selection. To assess the combined effect of both sources of variation, the sum of errors equation was used.

$$\text{Sum of errors} = \sqrt{\{(\text{error } 1)^2 + (\text{error } 2)^2\}}$$

It would not be correct to include the variability of all four studies into this equation as they are only estimating two variations. The maximum 95% coefficients of the two types of coefficient were used as inputs to this formula; 12.93% from ROI inter study and 4.53% from plaque 1 in the grey scale repositioning study.

$$\text{Sum of errors} = \sqrt{\{(12.93)^2 + (4.53)^2\}}$$

$$\text{Sum of errors} = 13.70\%$$

3.7 Discussion

In chapter 5, the MATLAB system is used to compare serial scans in patients undergoing lipid lowering treatments. In order to compare the serial scans it is necessary to have an estimation of what constitutes a real change and whether any differences between serial measurements are due to variations in the measurement system.

Several sources of variation were identified and this chapter attempts to quantify this variation in terms of a 95% coefficient value above which the percentage change is likely to be due to changes in the plaque and not attributed to variations in the system.

Two main sources of variation were identified; the selection of the ROIs and variation due to repositioning in repeat measurements. For each of these variations two different studies were conducted to try quantify the variation. Inter and intra observer studies were conducted using the criteria of 95% coefficients of agreements and repeatability rather than weighted κ analysis which was not suitable due to the way the results are displayed.

The ROI variation studies were conducted to estimate the test precision by measuring the repeatability of the selection process, and secondly, to assess the level of agreement in the selection of the ROIs. The ROI intra observer variability study gave a range of 95% coefficients of repeatability up to 2.85% with a mean maximum value of 1.47% (Class 5) indicating that the selection of the ROIs is repeatable when a single trained observer is used. The results of the inter observer variability study show that the selection of the ROI can be subjective. A maximum mean 95% limit of agreement for all the plaques of ±12.9% (Class 4) was determined. Looking at the results for the plaques individually (table 3.8), there was poor agreement between the three observers for plaques 3 and 7 with 95% limits of agreements of ±10.84% and

±16.72% respectively. These poor agreements can be attributed to poor delineation of the plaque border from the surrounding tissue. The poor agreement may be affected by operator experience especially when there are difficulties in delineating the borders. Examples of the difficulties in the selection of the ROI can be seen in figures 3.7 and 3.8.

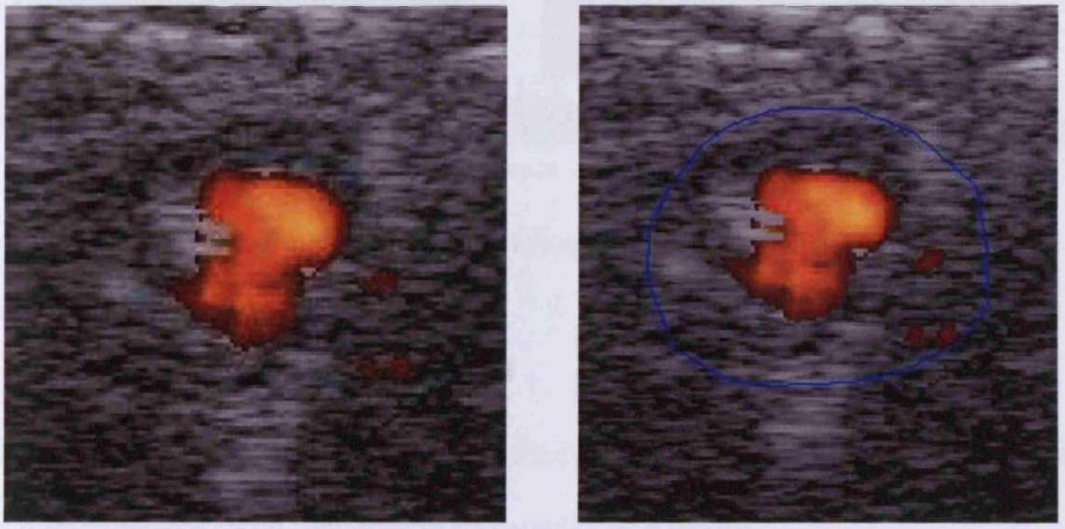

Figure 3.7 Images of a ROI from plaque 3 where the borders are difficult to delineate from the surrounding tissue. The second image has the ROI drawn around the plaque.

In figure 3.7 there is colour filling of the inner lumen but the outer lumen is difficult to delineate. The drawn ROI would have been selected with reference to its neighbouring images.

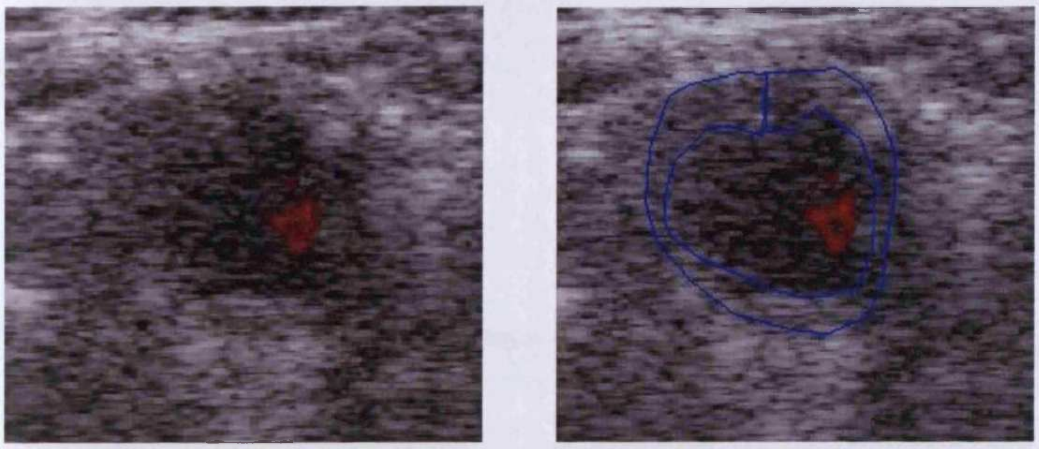

Figure 3.8 Images of a ROI from plaque 7 where both the inner and outer borders are difficult to delineate from the surrounding tissue. The second image has the ROI drawn around the plaque.

Figure 3.8 is an example of the most difficult ROI to select. The drawn ROI would have been selected with reference to its neighbouring images.

There was closer agreement between the more experienced observers 1 and 2 than there was with observer 3. There was closer agreement seen in plaques 1, 6 and 10 with 95% limits of agreement of ±2.4, ±1.89 and ±1.98% respectively. Example of a plaque where the plaque borders can be delineated more readily from the surrounding tissue is shown in figure 3.9.

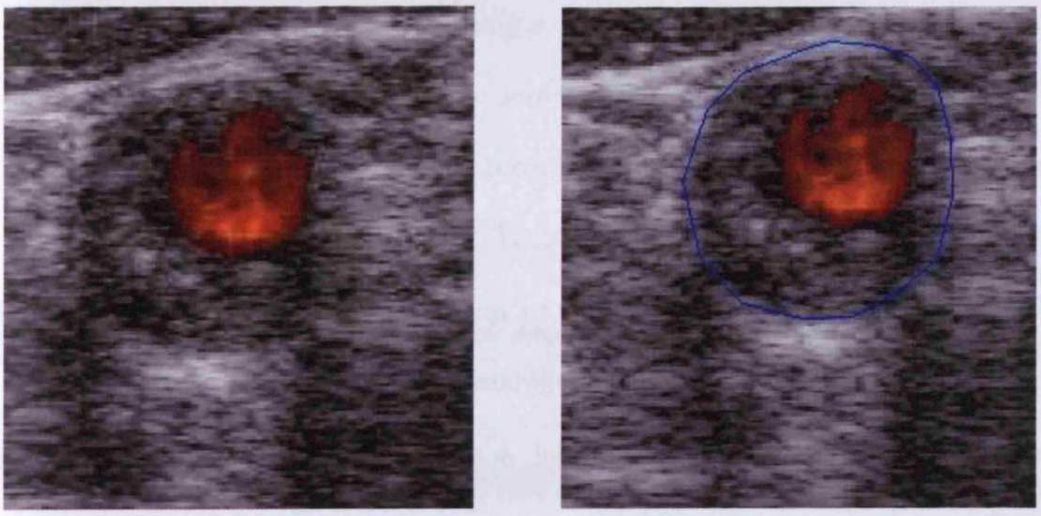

Figure 3.9 Images of a ROI from plaque 10 where the borders can be readily delineated from the surrounding tissue. The second image has the ROI drawn around the plaque.

All three observers agreed, in retrospect, that certain plaques were more difficult to select than others due to poor border delineation and incomplete colour filling. The incomplete colour filling is a limitation of the system. This is due to the fact that no ECG gating was enabled on our system. In general ECG gating requires some method of synchronisation with the 3D system and is demanding from a data storage, analysis and display point of view, and is not widely available on most commercial systems (Nelson and Pretorius 1998). This was apparent in our system in the absence of blood flow in some image slices, which made region of interest selection more difficult.

The second possible source of variation is due to effects of repositioning in repeat scans and what effects that will have on the statistical values of the image pixels, and also to assess whether changes in scan orientation have affected the image speckle pattern. Ideally to do this a patient with a plaque who was not on any treatment would be scanned repeatedly using the MATLAB system to assess for changes due to repositioning. However, it was not possible to carry out this type of study. To get an

estimation of the effect of repositioning a duplicate scan carried out at the same time as the original was analysed for the initial visits on ten plaques of the serial scan studies. After the original scan was recorded the transducer was replaced under the patient's neck, and the scan repeated. These duplicate scans were compared with their originals and a mean 95% coefficient of repeatability for each class calculated. A maximum 95% coefficient of repeatability of 3.64% for class 1 was calculated. Another study was carried out, at a later date, to assess further the effect of repositioning on the mean grey scale values with three carotid plaques from two patients, each imaged five times. It was not possible to use the MATLAB system for reasons described previously, so a 95% coefficient of repeatability was calculated from the mean grey values. 95% coefficients of repeatability of 4.53%, 2.44% and 2.4% respectively were calculated for the three plaques.

One reason why these repositioning studies were carried out was to estimate the effect repositioning had on the plaques ultrasound speckle pattern. The speckle pattern is dependant, along with other factors, on the direction of the ultrasound beam into the volume and also the tissue overlying it. Changes in the speckle pattern may effect the texture classification of the plaques, but by calculating the texture parameters from several directions on the same plaque (as done in section 3.4) and ensuring that the scans are conducted in a repeatable manner, the effects of repositioning and any slight differences in the speckle pattern will be minimised and accounted for within the total error.

There will be some overlap of the two types of variation, for example in the duplicate study the ROIs had to be re-selected, so this study will have variation from both ROI selection and repositioning variations. In order to quantify the variation to estimate what is likely to represent a possible change in the plaque, the maximum values

obtained from the studies done on the two possible sources of variations were combined using the sum of errors formula to give a total variation of 13.7%.

In conclusion, this chapter has estimated the variation associated with the system in order to try to identify what constitutes a real change when comparing the serial plaques.

Chapter 4: Comparison with Histology

4.1 General introduction

4.1.1 Aim

This chapter describes the attempt to compare the *in vivo* B mode images of carotid plaque with histology, using the 3D system. This study was a pilot study to assess the potential of the MATLAB programs for predicting the plaque morphology from the *in vivo* images of the plaques taken prior to carotid endarterectomy (CEA). In this introduction the processes involved in getting the plaque specimen and how it is handled histologically are described. Also a brief review of the reported literature of histology and ultrasound imaging of carotid plaques is included. These processes have a bearing on the final comparison and are discussed at the end of the chapter.

4.1.2 CEA surgery

CEA is the surgical removal of atherosclerotic plaque from the extracranial carotid arteries. The operation is usually done using a local anaesthetic but can be done under a general anaesthetic. The operating technique involves making an incision along the anterior Sterno-mastoid muscle of the neck to expose the carotid arteries. When exposing the arteries, several layers of muscle and tissues have to be exposed and retracted out of the way. The carotid sinus and carotid body nerves are then either ligated or blocked by an injection of lignocaine. The ICA is mobilised distally at a point well above the atheromatous lesion where it appears soft and not diseased. The plaque may be friable so extra care needs to be taken when manipulating the artery to ensure none of the atheroma dislodges and embolises before the ICA is clamped off

distally. The artery is then clamped distally and the surgeon can either put in a shunt to maintain cerebral blood flow or can temporarily occlude the carotid arteries to see if the patient has an adequate compensating cerebral circulation. With the latter technique the surgeon monitors any effects on the patient's ability to move their hands or feet and also their speech. This latter technique can only be done under local anaesthetic and adequate cerebral circulation is found in 85-90% of patients (Krupski and Moore 2005). Once this technique has been decided the CCA, distal ECA and distal ICA can be clamped. The artery is then dissected with the optimal plane for dissection lying between the diseased intima and the circular fibres of the arterial media. The dissection is started in the internal carotid artery and continued with a dissector circumferential about the artery. It is continued proximally into the ECA to remove any plaque and then proceeds into the common carotid artery. The plaque will suddenly become free at point where the intima is essentially normal leaving a smooth tapering end. The remaining surface is then irrigated to remove any loose bits of debris and to make sure there are no intimal flaps. To close the artery sutures are usually used, but it may also be closed using a vein patch. The clamps are removed and flow is restored to the vessels. Figure 4.1 shows a photograph of a CEA specimen (which corresponds to plaque 1 in the results section).

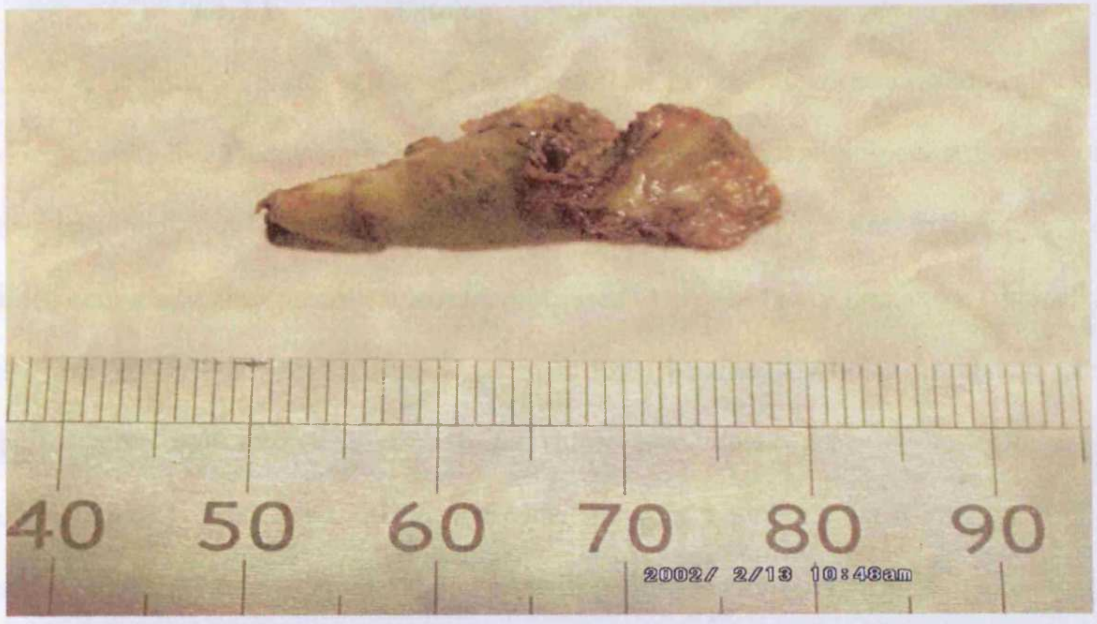

Figure 4.1: CEA specimen (plaque 1).

4.1.3 Histology

Histology is the study of the structure of biological material and the way in which the components of the material structurally and functionally interact. Cells are the building blocks of most biological tissues, but cells are highly variable, sophisticated and complex units. The cell develops attributes to suit its function and can be grouped together because of these common functional attributes. Cells are mostly classified according to their main function. Most tissues are a collection of cells organised in a specific way. The tissues can be simple structures comprising cells of the same structure or can be complex tissue comprising many different types of cells. Most tissues are complex in structure. Histology is the study of these cells and plays a key role in biological and medical science and in the understanding of disease processes and its effects.

4.1.3.1 Histology specimen processing

Once a sample of tissue is taken, the tissue can be examined macroscopically or microscopically. Macroscopic analysis looks at the gross morphological structures of the specimen, and no processing is required. To examine the finer structure microscopically, the specimen must be processed to produce very fine slices (typically 5-8 μm thick). Once a specimen is taken, it must be fixed by being immersed in a preservative solution (e.g. formalin), which precipitates proteins and prevents degradation. It then needs to be embedded in a firm medium so it can be easily sectioned. The standard method for preparing thin sections is paraffin embedding, which is low cost, simple to perform, and can be easily automated. Before embedding the specimen, all water must be removed, which is done by passage through a series of alcohol solutions. The specimen is then immersed in paraffin wax at a temperature just above the melting point of the wax and then allowed to cool so the wax solidifies. The wax acts as a firm support to the specimen allowing thin sections to be cut. If the specimen contains calcification, it is often decalcified by placing it in a solution of formic acid. This is done to protect the fine microtome blade during sectioning. Other methods of embedding specimens are to use acrylic resin or epoxy resin. Frozen sectioning can also be used when urgent diagnosis is required.

4.1.3.2 Histology stains

For tissues to be seen in detail they need to be stained. Cells are almost colourless and cannot be differentiated unless stained. There are four main types of staining but the most common type and the one described in this thesis is called empirical staining. A stain is essentially a dye which colours the different constituents of the tissue. The exact mechanism of how the dyes colour the tissue constituents is not fully understood

but may be related to the size of the dye molecules, or sometimes to the ionic charge on the dye molecules. It may also be due to a chemical reaction between a specific tissue component and the dye (Stevens and Lowe 2005).

There are many different types of stains, some are very specific to a given cell or tissue. One of the most commonly used stains is Hematoxylin and Eosin (H&E), which is a combination of two dyes and is the most useful stain for the examination of biological tissue. H&E stains cell nuclei purple/black while components of the cell cytoplasm stain red. Another common stain is Elastic von Gieson (EVG) stain which stains collagen pinkish/red, elastic fibres black and muscle yellow. This stain is often used to distinguish between support cell fibres like elastic tissue and collagen. Other common stains are based on the trichrome method, and are a combination of three different dyes which stain different components in different colours. Examples of trichrome stains are Martius scarlet blue (MSB), Gomari trichrome and Masson trichrome. MSB highlights erythrocytes yellow and fibrin red showing old haemorrhage.

4.1.3.3 Examination of histology sections

The examination of wax embedded sections by light microscopy is the main routine technique used in histology. The resolution seen in the thin sections is of the order of 0.5μm for wax embedded sections. The degree of magnification and the resolution of light microscopy are limited by the wavelength of light. To examine smaller structures, as small as 1nm, electron microscopy can be used. Instead of light, it uses parallel beams of electrons allowing the study of subcellular structures (Stevens and Lowe 2005). The resolution of the ultrasound images is relatively poor compared to light microscopy by a factor of approximately 10^{-3}. The ultrasound axial resolution is

typically 0.5mm and the lateral resolution typically 1mm.for the 7MHz linear transducer. Therefore the detail that can be seen in the microscopic histology sections is much greater than in the ultrasound images. Comparison of the ultrasound images with gross histology where the resolutions would be of similar magnitude may be more appropriate but may only be useful in the detection of intraplaque haemorrhage and ulceration. However, in this chapter, the relative amounts of five different tissue types are required so light microscopic analysis of the histological sections is used.

4.1.4 Previous histological work

The previous work from our group was a comparison of *in vitro* B mode images of carotid plaques post CEA with histology (Rakebrandt et al. 2000; Rakebrandt 2001). The five tissue types of elastic, fibrous, lipid, haemorrhage and calcium were identified by histology. A full description of the previous work is given in section 1.8. In this study, the same 5 histological features previously identified will be used. The ultimate aim is to compare the *in vivo* image to the histology. To assist with this, an *in vitro* comparison will be done to see if a link between the *in vivo* and CEA specimen exists. The problem lies in trying to orientate the *in vivo* scan with the CEA specimen. There will be several effects that will affect this orientation process including the effect of overlying vessels, the effect the CEA operation has on the plaque, whether the plaque specimen come out en bloc, or has any of the artery also been removed. These effects are not as significant when comparing *in vitro* scans to histology.

4.1.5 Review of published histology procedures

There have been many reported studies comparing imaging methods to histological analysis of carotid plaques. This section is a chronological review of the histology methods used when comparing with ultrasound images of carotid plaques. This review shows how the histological methods have changed with time, and how variable the methodology has been. A summary of the reported studies is shown in table 4.1.

Some of the earlier studies looked at gross histology mainly (i.e. macroscopic analysis) (Imparato et al. 1983; O'Donnell et al. 1985; Bluth et al. 1986; Gray-Weale et al. 1988; Widder et al. 1990). In most of these studies the main identifiable features were intraplaque haemorrhage and ulceration (Imparato et al. 1983; Bluth et al. 1986; Gray-Weale et al. 1988; Widder et al. 1990). Some of the early studies (Reilly et al. 1983; Wolverson et al. 1983; Ratliff et al. 1985) used microscopic histological techniques, several of which also compared the gross histology features (Reilly et al. 1983; Wolverson et al. 1983). These studies were able to distinguish other tissue types associated with the plaques, such as calcification, lipid and fibrous tissue. All of these studies compared the histology with echogenicity and heterogeneity, with conflicting results. Some reported that ultrasound can reliably detect intraplaque haemorrhage and ulceration (Imparato et al. 1983; Reilly et al. 1983; O'Donnell et al. 1985; Bluth et al. 1986; Gray-Weale et al. 1988) whereas others disagreed (Ratliff et al. 1985; Widder et al. 1990).

From 1990 there was shift away from macroscopic to microscopic analysis, this led to more features being described. Combinations of the following features calcification, intraplaque haemorrhage, ulceration, lipid and fibrous tissue are central to most studies, although no one single study reported all five tissue types. Other tissue types were also reported, these include thrombus, cholesterol, elastic tissue, necrotic core

and foam cells. The wide selection of histological stains used reflects the variety of tissue types that were reported. About one third of the reported studies which used microscopic analysis, decalcified the plaque during the processing stage. No mention of decalcification was reported in the other studies.

There was also a significant change, from1990 on, in the imaging method to which the histology was compared, from subjective methods to objective methods. Some studies still did comparisons with subjective methods (Hatsukami et al. 1994; Gaunt et al. 1996; Montauban van Swijndregt et al. 1998; Schulte-Altedorneburg et al. 2000), others compared the histology with symptoms (Avril et al. 1991; Van Damme et al. 1992; Kardoulas et al. 1996).The objective methods included were GSM analysis (El-Barghouty et al. 1996; Tegos et al. 2000; Denzel et al. 2003; Denzel et al. 2003), statistical analysis (Wilhjelm et al. 1996; Wilhjelm et al. 1998; Rakebrandt et al. 2000; Arnold et al. 2001), pixel distribution analysis (Lal et al. 2002) and specific ultrasound features (White et al. 1997; Lammie et al. 2000).

From this review it can be seen that there is a lack of standardisation in the histological techniques used for analysing carotid plaques and a wide variety of imaging techniques to which they are compared.

Author (Year)	No. of CEAs	Decalcified	Histology stains	Tissue types	Imaging method
Wolverson (83)	6	?	Gross & microscopic histology	Calc, lipid, fibrous	E
Reilly (83)	45	?	H&E	Calc, lipid, fibrous, IPH, ulceration	B
Imperato (83)	376	?	Gross histology	IPH, ulceration	E
Ratliff (85)	42	Yes	H&E, Gomari trichrome	Calc, fibrous, IPH, necrosis	B
O'Donnell (85)	79	?	Gross histology mainly	IPH, ulceration	B
Bluth (86)	50	Yes	Gross histology	IPH, ulceration	B
Grey Weale (88)	244	?	Gross histology mainly	IPH, ulceration, fibrous	B
Widder (90)	180	?	Gross histology	IPH, ulceration, atheromatous debris	B
Avril (90)	187	?	Wiegert, Dahl, Masson trichrome,	Calc, IPH, ulceration, , thrombosis	Symptoms
Van Damme (92)	134	?	Masson trichrome, H&E, Prussian Blue	IPH, ulceration, thrombus	Symptoms
Hatsukami (94)	24	Yes	H&E	Calc, fibrous, necrotic core, foam cells, cholesterol	E
El Barghouty (96)	52	?	H&E, EVG, Perls, MSB	Calc, fibrous, IPH, cholesterol	GSM
Kardoulas (96)	36	?	H&E, EVG, Masson trichrome, Alazarin red	Calc fibrous, lipid, IPH, ulceration	E + Symptoms
Gaunt (96)	50	?	H&E	IPH, ulceration, thrombus	B
Wiljhelm (96)	44	?	?	Calc, lipid, IPH, thrombus, fat,	Statistical
White (97)	148	?	H&E, EVG	Calc, fibrous, IPH, elastic tissue, cholesterol	US features
Wiljhelm (98)	53	?	H&E,Verhoeff	Calc, thrombus, lipid, fat, IPH,	Statistical
Montuaban (98)	46	Yes	H&E, EVG, Masson trichrome	Calc, fibrous, IPH, thrombus	E
Lammie (00)	42	Yes	H&E, Perls, MSB	Fibrous cap size, IPH, ulceration, necrotic core	US features
Tegos (00)	71	Yes	H&E, MSB	Necrotic core, fibrous, lipid	GSM
Schulte (00)	44	Yes	H&E	Calc, fibrous, cholesterol thrombus, IPH	B
Rakebrandt (00)	10	Yes	H&E. EGV. MSB	Calc, IPH, elastic tissue, fibrous, Lipid	Statistical
Arnold (01)	100	?	H&E	Calc, fibrous, IPH, Lipid	Statistical
Lal (02)	20	?	H&E. Gomari trichrome	Calc, fibrous, IPH, Lipid	Pixel distribution
Denzel (03)	15	Yes	H&E, EVG	Calcium rich hard ,combined ,lipid rich soft	GSM
Denzel (03)	107	?	H&E, EVG	Calcium rich hard ,combined ,lipid rich soft	GSM

EGV= Elastic Van Geison, H&E= Haematoxylin and Eosin, MSB = Martius Scarlett Blue, ? = not stated in literature
Calc = Calcification, IPH = Intraplaque haemorrhage E=echogenicity, B= both echogenicity and homogeneity. GSM=Grey Scale Median

Table 4.1 Chronological review of histology method

4.2 Methods

4.2.1 Patients

Four carotid plaque specimens were obtained en bloc from patients undergoing carotid endarterectomy. The four patients were symptomatic with >70% stenosis documented by Doppler ultrasound. The day prior to the CEA a 3D *in vivo* scan was taken of the plaque, a 2D longitudinal image of the plaque was also taken that may be used as an aide in the subjective analysis. The 3D scan was taken using the standard protocol described in section 2.2.4.

4.2.2 *In vitro* scans

A direct comparison between the histology and the *in vitro* scans is the basis for the previous work (Rakebrandt et al. 2000), however this was not the aim of this study. This 3D system has been set up using *in vivo* statistical and textural data as the training set. The training set data will be different *in vivo* from *in vitro*, due mainly to absorption and attenuating effects of the overlying tissues.

There are, however, several reasons why an indirect comparison of the histology to the 3D *in vitro* scan may be useful. Firstly it will give an indication of the length of the plaque. By knowing how many *in vitro* images contained plaque, the number of images that need to be analysed in the 3D *in vivo* data set can be calculated. This distance between the histology sections can also be calculated by knowing the number of *in vitro* images that contain the plaque. Secondly a volume measurement carried out on the *in vitro* scan data, compared with the *in vivo* and histology volume measurements, will give an estimation of the effect that both the CEA surgery and

histological processing has on the plaques. And thirdly to see if the *in vitro* scans could be used as a link between the *in vivo* scans and histology.

The method used to obtain the 3D *in vitro* data set is as follows. The excised plaques were immersed in formalin solution to preserve the structure and stabilise the plaque. A 3D *in vitro* scan of each of the four plaques was obtained prior to histological processing. Each plaque was placed in a 1% agar solution in a Perspex block mould similar to that used in previous work (Rakebrandt et al. 2000; Rakebrandt 2001). The plaques were embedded in the agar at a depth of 20 mm, and were oriented longitudinally with the position of the ICA noted by placing a paperclip in the agar mould edge. A 3D scan was recorded starting from the ICA edge using the standard protocol.

4.2.3 Histology processing

The plaque was removed from the agar solution and was then placed in 8% formic acid solution to remove the calcium present. The plaques were dehydrated by passing through alcohol and embedded in paraffin wax to preserve the orientation. Three transverse sections, each 5μm thick, were taken at regular spaced intervals throughout the length of the plaque. Each section was floated onto glass slides and each transverse section was stained with either, H&E, EVG or MSB. The three stains were used to detect the five tissue types identified in previous work. H&E was used to identify calcium, lipid and fibrous tissue. In the previous work, even though the plaque has been decalcified, the histologist was able to estimate where the calcium had been deposited using morphological and tinctorial examination (Rakebrandt et al. 2000; Rakebrandt 2001). MSB was used to detect the presence of haemorrhage and EVG was used to detect the presence of elastic tissue. The EGV triplet of each section

was scanned to acquire a digital image using a flatbed scanner (SNAPSCAN 1212 AGFA). The digital image was enlarged (X10) and printed onto clear acetates and also a black and white paper image.

The histologist examined each triplet section under a microscope to look for the presence of the five tissue types. Each of the five tissue types was arbitrarily assigned a colour and when a tissue was detected in a section the histologist would colour the same area in the black and white image. This was done for every section of all four plaques. An example is shown in figure 4.2.

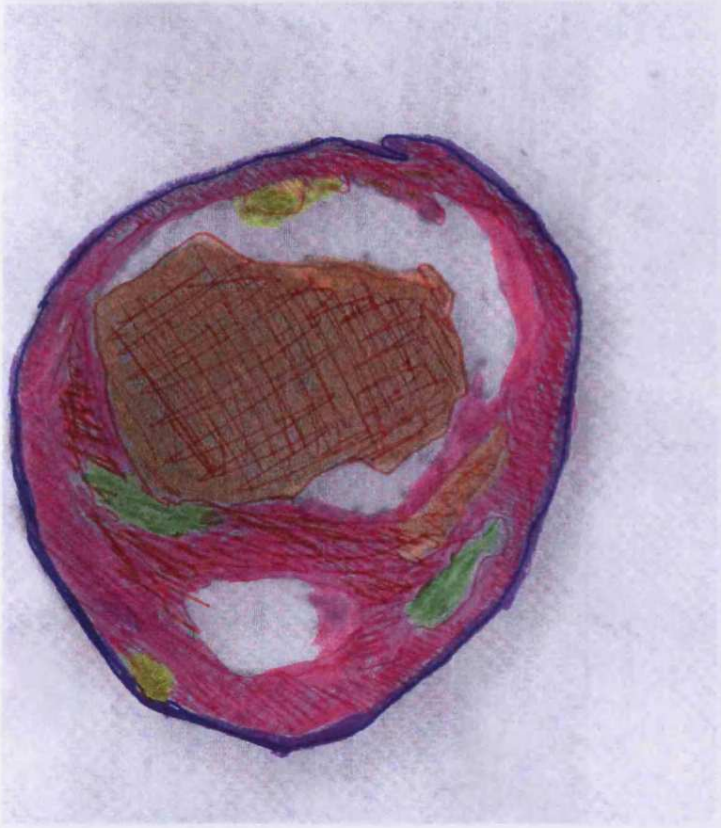

Figure 4.2 Example of a histology section, the different colours represent different tissues.

4.2.4 Estimation of % tissue types from histology

Two methods were used to estimate the percentage of each of the five tissue types from histology. The first method was a manual method, where a grid of 0.5 x 0.5 cm squares on a sheet of acetate was placed over the magnified coloured histology image (Figure 4.3). The number of squares, and part squares of each of the tissue types was recorded. This was done for all sections of the plaque. When all sections were analysed the percentage of each tissue type was calculated.

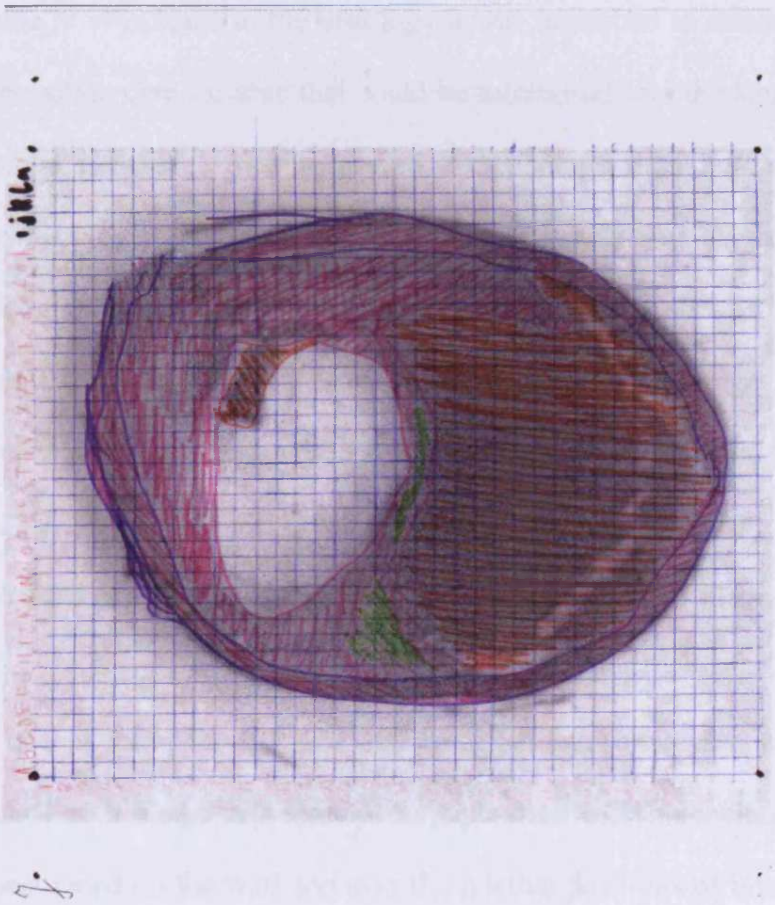

Figure 4.3: Example of coloured histology slice with acetate grid on top.

The second method is similar to that used to calculate the *in vivo* plaque volumes. It uses the imageJ software to measure the area of each of the tissue types in each

section. By measuring the original size of one of the sections on the histology glass slide, the scale can be set on the imageJ software. The distance between each histology section can be calculated from the *in vitro* plaque data. This means that as well as estimating the percentage of each tissue type, an estimation of the histological plaque volume can also be made.

4.2.5 *In vivo* scan comparison

To compare the *in vivo* scans to the histology it was important to minimise as many variables as possible. One variable that could be minimised was the length of plaque analysed. Plaque number 1 was measured and photographed before processing, however, the histologist failed to measure or photograph any of the other three plaques. Hence the plaque length was determined using the number of images which contained plaque in the *in vitro* data set. Since the number of 2D images that make up the 3D volume is always the same (155 images over 7cm). The plaque length can be calculated. A 2D longitudinal image taken of the plaque was not used to measure the plaque length as it was difficult to decide, precisely where the plaque started and ended.

For each of the plaques, the 3D data set was examined image by image and the characteristics of each image that contained plaque detailed. This included where the plaque was positioned on the wall and also the relative positions of bifurcation, ICA and ECA in the data set. An estimation of the cross sectional area that the plaque occupied in each image was also noted. The plaque extent was then selected (i.e. the number of 2D images in which the plaque was contained) to match the number of corresponding *in vitro* images. The regions of interest were selected (section 2.3.3)

and subsequently analysed. The plaque volume was then calculated from the 3D data set using the imageJ software (section 2.4.2).

4.2.6 Comparison of histology to *in vivo* and *in vitro* images.

The comparison of the histology sections to the images of the plaques was looked at in two ways. Firstly the individual sections and their corresponding images were matched. This was done by using a subjective analysis. This subjective analysis was based on the shape, size and orientation of the corresponding images and section. The match was graded a match, partial match or not matched. A match was when the shape, size and orientation all agreed. The orientation was checked by rotating the histology sections that had been scanned onto the acetate sheets. The scaling of the images was kept the same when the three different types of images were matched. A partial match was where some but not all the features agreed. No match was where none of the features agreed. For the orientation to match, the neighbouring images were checked to see if they also matched. (see discussion at the end of the chapter). As each histology section corresponded to several *in vivo* and *in vitro* images, the matching process compared the section with all the images in the range for a match. Examples of the different types of matching can be found in figures 4.4 to 4.8 in the results section.

The second comparison looked at the total amounts of the different tissue types predicted by histology and how they compared with the *in vivo* MATLAB analysis results.

4.3 Results

Four plaques were analysed for this chapter, each will be described individually below with conclusions drawn at the end. The analysis of each plaque will look at the *in vitro*, histology, and *in vivo* data separately.

4.3.1 Plaque 1

4.3.1.1 *In vitro*

The number of 2D *in vitro* images which contained the plaque was 60. This corresponds to a calculated plaque length of 27mm (i.e. number of images times the distance between images). This is corroborated by figure 4.1, which is a picture of plaque 1 prior to histology processing. The picture shows the length of plaque 1 to be approximately 27mm. Photographs of the other three plaques were not taken.

The number of histology sections was 20, therefore the distance between sections is approximately 1.35mm.

A total plaque volume of 704.6 ± 9.6 mm^3 was measured from the *in vitro* images using the imageJ method described previously. The full result is found in appendix 4.1.1.

4.3.1.2 Histology

The % totals of the five different tissues types estimated from histology using the manual method and the imageJ method are shown in table 4.2. The mean value of the two methods is also shown in the table. The area that each tissue type covered per section, the overall area of each type and the estimated total plaque volume (assuming 1.35mm between sections) using the imageJ method are also shown in table 4.2 (full

results in appendix 4.1.2). The total plaque volume is calculated by multiplying the total area of all tissue types by distance between sections.

	Haemorrhage	Lipid	Fibrous	Calcium	Elastic
Total tissue type imageJ (%)	28.57	3.55	53.62	2.10	12.16
Total tissue type manual (%)	31.12	3.58	54.81	1.95	8.53
Mean tissue type (%)	29.85	3.56	54.21	2.03	10.35
Total tissue type area (mm^2)	106.1	13.2	199.1	7.8	45.2

Total plaque volume (mm^3)	501.2

Table 4.2: Histology estimations of the five tissue types for plaque 1 using manual and imageJ method.

4.3.1.3 *In vivo*

A plaque extent, similar in size to the *in vitro* data set was determined by examining the 2D *in vivo* plaque characteristics. Using this plaque extent, a MATLAB analysis was done to separate the plaque into 5 different classes. A summary of the results is shown in table 4.3 with the full results shown in appendix 4.1.3.

	Class 1 (%)	Class 2 (%)	Class 3 (%)	Class 4 (%)	Class 5 (%)
All	0.14	3.93	12.01	25.40	58.52

Table 4.3: MATLAB analysis summary of plaque 1.

An *in vivo* plaque volume of 751.6 ± 4.8 mm^3 was calculated by the imageJ method using the same plaque extent as used in the MATLAB analysis. The full results are found in appendix 4.1.4.

4.3.1.4 Plaque 1 conclusion

The effect that histological processing has on plaque 1 can be readily seen by comparing the three estimated plaque volumes (histology, *in vitro* and *in vivo*). There is ~33% reduction in volume between the *in vivo* and histology volumes, ~29% reduction between the *in vitro* and histology volumes and ~6% reduction in the estimated *in vivo* and *in vitro* volumes. These 33% and 29% volume reductions are possibly due to the decalcification and dehydration processes in the preparation of the sections.

The comparison of the histology sections with the *in vivo* images found no matches (see appendix 4.1.5). The subjective comparison of *in vitro* images with histology found that 5 images matched for shape, size and orientation, 9 had partial matches for some of the features, with the other 6 not matching. Figure 4.3 is an example of a match between *in vitro* and histology, and no match between *in vivo* and histology. The images shown are from plaque 1, *in vitro* image 89, using histology section h, and *in vivo* image 113.

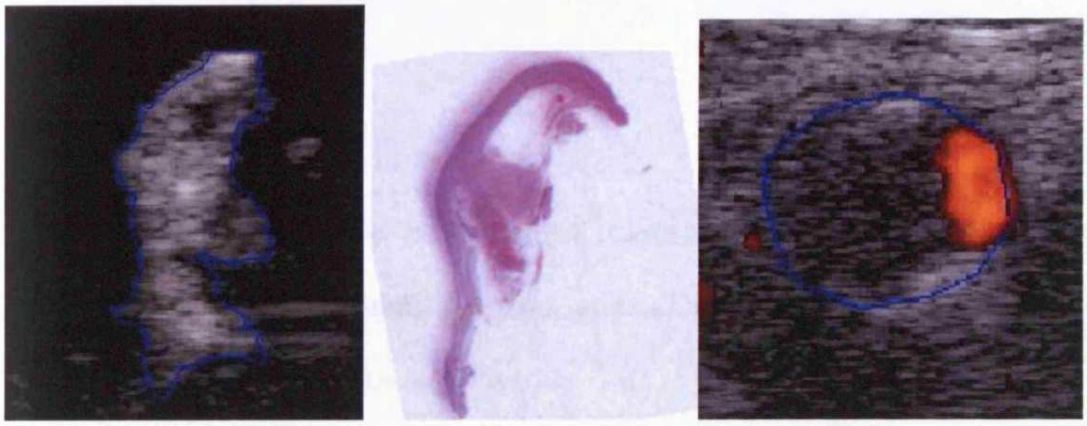

In vitro Histology *In vivo*

Figure 4.3 Examples of corresponding images in plaque 1.

The second comparison was to see if there is any agreement between the amounts of the five different tissue types estimated from histology and the amounts of the five classes predicted by the MATLAB *in vivo* data for the whole plaque. The combined MATLAB predicted value for classes 4 and 5, which is associated with the harder tissue types of fibrous, elastic and calcium, was 83.92%. Histologically these three tissue types comprised only 66.59% of the plaque volume. The other 33.41% is made up of 29.85% haemorrhage and 3.56% lipid. These tissue types are associated with MATLAB classes 1-3 which predicted only a total of 16.08% for this plaque. Possible reasons for the differences are discussed in section 4.4.

.

4.3.2 Plaque 2

4.3.2.1 *In vitro*

The number of 2D *in vivo* images which contained the plaque was 58, which corresponds to a plaque length of ~26.2 mm. There were 20 histology sections, therefore the distance between sections was ~ 1.31 mm.

An *in vitro* plaque volume of 541.2 ± 8.9mm^3 was calculated. The full result can be found in appendix 4.2.1.

4.3.2.2 Histology

The % totals of the five different tissue types estimated using the manual method and the imageJ method are shown in table 4.4. The mean value of the two methods is also shown in the table.

The area that each tissue type covered per section, the overall area of each type and the estimated plaque volume (assuming 1.31mm between sections) using the imageJ method are also shown in table 4.4 (full results in appendix 4.2.2).

	Haemorrhage	Lipid	Fibrous	Calcium	Elastic
Total tissue type imageJ (%)	18.35	6.67	50.65	0.06	24.27
Total tissue type manual (%)	20.53	7.16	48.69	0.06	23.57
Mean tissue type (%)	19.44	6.91	49.67	0.06	23.92
Total tissue type area (mm^2)	69.5	25.4	191.9	0.2	92.0

Total plaque volume (mm^3)	496.3

Table 4.4: Histology estimations of the five tissue types for plaque 2 using imageJ method and manual methods.

4.3.2.3 *In vivo*

A plaque extent, similar in size to the *in vitro* data set, for the 3D *in vivo* images was determined. Using this plaque extent, a MATLAB analysis was done to separate the plaque into 5 different classes. A summary of the results is shown in table 4.5 with the full results shown in appendix 4.2.3.

	Class 1 (%)	Class 2 (%)	Class 3 (%)	Class 4 (%)	Class 5 (%)
All	0.28	7.35	23.09	59.68	9.6

Table 4.5: MATLAB analysis summary of plaque 2.

An *in vivo* plaque volume of 573.3 ± 6.9 mm^3 was calculated by the imageJ method using the same plaque extent as used in the MATLAB analysis. The full results are found in appendix 4.2.4.

4.3.2.4 Plaque 2 conclusion

As seen in plaque 1 there is a reduction in the estimated volume for histology when compared with both calculated *in vivo* and *in vitro* volumes. This reduction is less than seen in the previous plaque, with ~15 % reduction between *in vivo* and histology and ~9% between *in vitro* and histology. The reduction between *in vivo* and *in vitro* is similar to plaque 1 at ~6%.

There was no match between the *in vivo* and histology sections. The comparison of the histological slices with the *in vitro* scans showed that of the 20 histology sections there were six that had no match with the corresponding 2D *in vitro* images. 7 sections had a partial match and 7 matched (appendix 4.2.5).

Figure 4.5 is an example of a partially matched comparison between *in vitro* and histology, and no match between *in vivo* and histology. The *in vitro* image has matching size and orientation but appears different in shape. The images shown are from plaque 2, using histology section g, *in vitro* image 61, and *in vivo* image 49.

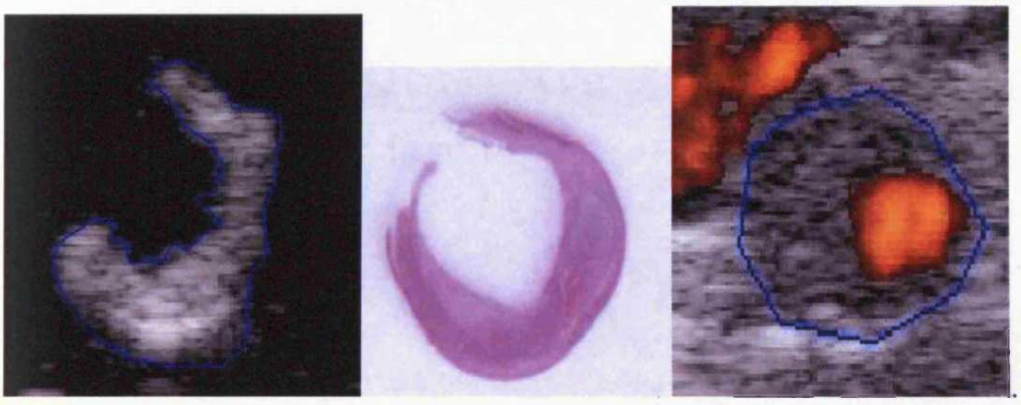

In vitro Histology *In vivo*

Figure 4.5 Example of a comparison from plaque 2.

The second comparison was to see if there is any correlation between the amounts of the five different tissue types estimated from histology and the amounts of the five classes predicted by the MATLAB *in vivo* data for the whole plaque. The comprised MATLAB predicted value for class 4 and 5 was 69.28% of the plaque, which is associated with the harder tissue types of fibrous, elastic and calcium. These three comprised 73.65% of the plaque volume measured by histology. The other 26.35% is made up of 19.44% haemorrhage and 6.91% lipid. These are compared to the more echolucent MATLAB Classes 1-3 which predicted 30.72% for this plaque. This was the only one of the four plaques where the amounts measured by histology were greater than that predicted by the MATLAB classifier for the more echogenic tissue types. Possible reasons for the differences are discussed in section 4.4.

4.3.3 Plaque 3

4.3.3.1 *In vitro*

The number of 2D *in vivo* images which contained the plaque was 15, which leads to a plaque length of ~13.5 mm. There were 10 histology sections, therefore the distance between sections was ~ 1.35 mm.

An *in vitro* plaque volume of 190.9 ± 3.0 mm^3 was calculated. The full result can be found in appendix 4.3.1.

4.3.3.2 Histology

The % totals of the five different tissue types estimated using the manual method and the imageJ method are shown in table 4.6. The mean value of the two methods is also shown in the table.

The area that each tissue type covered per section, the overall area of each type and the estimated plaque volume (assuming 1.35mm between sections) using the imageJ method are also shown in table 4.6 (full results in appendix 4.3.2).

	Haemorrhage	Lipid	Fibrous	Calcium	Elastic
Total tissue type imageJ (%)	9.07	2.31	63.84	0.00	24.79
Total tissue type manual (%)	7.98	2.29	67.52	0.00	22.21
Mean tissue type (%)	8.52	2.30	65.68	0.00	23.50
Total tissue type area (mm^2)	11.7	3.0	82.1	0.0	31.9

Total plaque volume (mm^3)	173.6

Table 4.6: Histology estimations of the five tissue types for plaque 3 using imageJ method.

4.3.3.3 *In vivo*

A plaque extent, similar in size to the *in vitro* data set was determined by examining the 2D *in vivo* plaque characteristics. Using this plaque extent, a MATLAB analysis was done to separate the plaque into 5 different classes. A summary of the results is shown in table 4.7 with the full results shown in appendix 4.3.3

	Class 1 (%)	Class 2 (%)	Class 3 (%)	Class 4 (%)	Class 5 (%)
All	0.00	0.00	0.23	47.59	52.18

Table 4.7: MATLAB analysis summary of plaque 3.

An *in vivo* plaque volume of 200.8 ± 2.5 mm^3 was calculated by the imageJ method using the same plaque extent as used in the MATLAB analysis. The full results are found in appendix 4.3.4.

4.3.3.4 Plaque 3 conclusion

The volume reductions in plaque 3 are very similar to plaque 2. There is an ~14.5% reduction between *in vivo* and histology and an ~9% reduction between histology and *in vitro* volumes. There is an ~5% reduction between *in vitro* and *in vivo* volumes.

There were only two matches in the comparison of histology with *in vitro* images. There were three partial matches but there was no match for five out of the ten comparisons (appendix 4.3.5). As in the previous plaques there was no match found between any of the corresponding *in vivo* images and histology sections. Figure 4.6 is an example of corresponding images and section showing no match between *in vitro* and histology, and also no match between *in vivo* and histology. The images shown are from plaque 3, using histology section e, *in vitro* image 89, and *in vivo* image 55

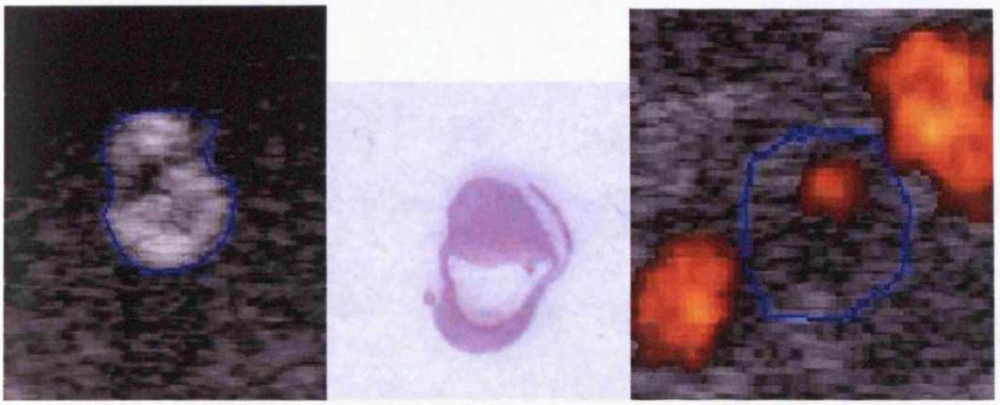

In vitro Histology *In vivo*

Figure 4.6 Example of a comparison from plaque 3.

The second comparison was to see if there is any agreement between the amounts of the five different tissue types estimated from histology and the amounts of the five classes predicted by the MATLAB *in vivo* data for the whole plaque. The combined MATLAB predicted value for class 4 and 5 is 99.77% of the plaque. This was compared to the amounts of the three tissue types of fibrous, elastic and calcium which comprised only 89.18% of the plaque volume measured by histology. The other 10.82% is made up of 8.52% haemorrhage and 2.3% lipid. These are compared to the more echolucent MATLAB Classes 1-3 which predicted only 0.23% for this plaque. Possible reasons for the differences are discussed in section 4.4.

4.3.4 Plaque 4

4.3.4.1 *In vitro*

The number of 2D *in vivo* images which contained the plaque was 50, which leads to a plaque length of ~22.54 mm. There were 20 histology sections, therefore the distance between sections was ~ 1.13 mm.

An *in vitro* plaque volume of 721.0 ± 4.8 mm^3 was calculated. The full result can be found in appendix 4.4.1

4.3.4.2 Histology

The % totals of the five different tissues types estimated using the manual method and the imageJ method are shown in table 4.8. The mean value of the two methods is also shown in the table.

The area that each tissue type covered per section, the overall area of each type and the estimated plaque volume (assuming 1.13mm between sections) using the imageJ method are also shown in table 4.8 (full results in appendix 4.4.2).

	Haemorrhage	Lipid	Fibrous	Calcium	Elastic
Total tissue type imageJ (%)	37.94	3.80	44.60	0.75	12.92
Total tissue type manual (%)	39.13	4.92	45.91	0.75	9.29
Mean tissue type (%)	38.53	4.36	45.25	0.75	11.11
Total tissue type area (mm^2)	189.3	19.0	222.5	3.7	64.5

Total plaque volume (mm3)	563.8

Table 4.8: Histology estimations of the five tissue types for plaque 4.

4.3.4.3 *In vivo*

A plaque extent, similar in size to the *in vitro* data set, for the 3D *in vivo* images was determined. Using this plaque extent, a MATLAB analysis was done to separate the plaque into 5 different classes. A summary of the results is shown in table 4.9 with the full results shown in appendix 4.4.3.

Image no.	Class 1 (%)	Class 2 (%)	Class 3 (%)	Class 4 (%)	Class 5 (%)
All	0.00	0.67	7.16	39.54	52.63

Table 4.9: MATLAB analysis summary of plaque 4.

An *in vivo* plaque volume of 752.9 ± 8.6 mm^3 was calculated by the imageJ method using the same plaque extent as used in the MATLAB analysis. The full results are found in appendix 4.4.4.

4.3.4.4 Plaque 4 conclusion

There is a 25% and 23% reduction in histology volumes compared with *in vivo* and *in vitro* volumes respectively. There is a 4% reduction between the *in vitro* and *in vivo* volumes.

There was again no match between any of the corresponding histology sections and *in vivo* images. The histology and *in vitro* match was not very good, with not one of the corresponding section or images matching for all features. Six of the corresponding sections and images had a partial match with the other 14 not matching (appendix 4.4.5). Figure 4.7 is an example of a corresponding section and images showing no match between *in vitro* and histology, and no match between *in vivo* and histology. There is a partial match for shape and size between the *in vivo* and *in vitro* images.

The images shown are from plaque 4, using histology section p, *in vitro* image 57, and *in vivo* image 87.

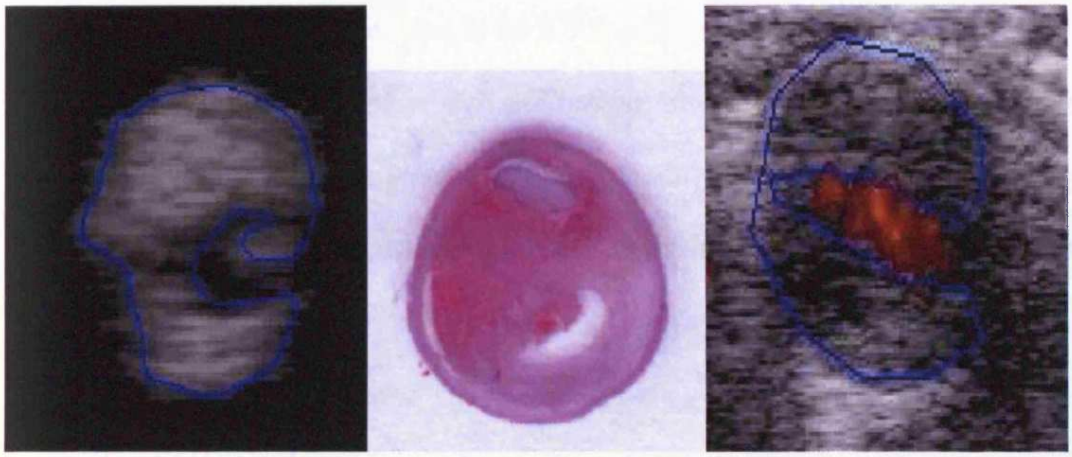

In vitro Histology *In vivo*

Figure 4.7 Example of a comparison from plaque 4.

The second comparison was to see if there is any agreement between the amounts of the five different tissue types estimated from histology and the amounts of the five classes predicted by the MATLAB *in vivo* data for the whole plaque. The combined MATLAB predicted value for class 4 and 5 was 92.17% of the plaque, which is associated with the harder tissue types of fibrous, elastic and calcium predicted by histology. These three comprised only 57.11% of the plaque volume measured by histology. The other 42.89% is made up of 38.53% haemorrhage and 4.36% lipid. These are compared to the more echolucent MATLAB Classes 1-3 which predicted only 7.83% for this plaque. Possible reasons for the differences are discussed in section 4.4.

4.4 Discussion

One of the principal aims of the thesis was to compare *in vivo* texture measurements with the gold standard of histology. It was found that the agreement was poor, and as Rakebrandt (2001) had shown that *in vitro* comparison with histology was good, there was no reason to compare the *in vivo* and *in vitro* ultrasound scans. The evidence has shown that with these techniques it is not possible to derive detailed histological information from *in vivo* ultrasound texture measurements, which was one of the main aims of this thesis. The reasons for inclusion of the *in vitro* data are detailed in section 4.2.2. One possible reason why the *in vivo* comparison is poor is that the step from comparing *in vitro* to histology and comparing *in vivo* to histology is very complex. It introduces a lot more variables that are not an issue when the *in vitro* images were compared to histology in the previous study (Rakebrandt 2001).

The first possible variable is one of orientation of the plaque. When a plaque is removed, some form of marking like a suture can be placed on the plaque specimen by the surgeon to mark a particular landmark (e.g. the bifurcation and plane in which the plaque lies) (Kardoulas et al. 1996). This landmark can be used as a precise reference when taking the *in vitro* images for comparison with histology. This reference landmark may also be useful in comparing the *in vivo* data but will not be as precise as the *in vitro* orientation especially in orienting the plane. The orientation of the four plaques in this study was not marked at the time of removal.

A second major difference will be the effect of overlying tissues on the *in vivo* data when compared to *in vitro* (Montauban van Swijndregt et al. 1998; Wilhjelm et al. 1998; Arnold et al. 2001). There will be attenuation of the backscattered ultrasound by the overlying tissues. The level of the attenuation will vary with depth and also because the tissue layers from patient to patient will be different, so the ultrasound

path will be different from patient to patient. Therefore the level of attenuation will have an inter patient variation (Wilhjelm et al. 1998). The *in vitro* scans were done with the plaque embedded in agar at a fixed depth so the attenuating effects are minimal or non existent compared to the *in vivo* scans.

Another possible variable with *in vivo* compared with *in vitro* is that it can be very difficult to distinguish the outline of the plaque from the surrounding tissue *in vivo*, whereas *in vitro* there is no surrounding tissue.

Another possible difference may be the effect the CEA operation had on the plaque. The *in vitro* scan will be of the plaque as it was removed, but some of the plaque may not come out en bloc, or some of the artery may have been removed during the operation. This would change the size of *in vivo* plaque compared with the histological plaque. The four plaques used in this study all came out en bloc and the estimated % reduction between in vivo and in vitro remains constant between 4-6%, suggesting that the surgical procedure had a constant effect on the plaques (table 4.10 below).

Estimations of the histological, *in vitro* and *in vivo* plaque volume were calculated for the four plaques. This was done to see the effect that both histological processing and decalcification has on the plaques. The percentage reductions between the three are shown in table 4.10.

Plaque no.	**% Reduction between *in vivo* and histology**	**% Reduction between *in vitro* and histology**	**% Reduction between *in vivo* and *in vitro***
1	33	29	6
2	15	9	6
3	14.5	9	5
4	25	23	4

Table 4.10: Estimated % reductions in calculated plaque volumes for the four plaques.

The % reduction between the *in vivo* and *in vitro* is consistent across the four plaques. A possible reason for the reduction is that the carotid vessel pre-CEA will not be totally occluded and will still have some blood flowing through it. This reduction may be due to a slight collapse of the vessel post CEA due to lack of blood flow.

The larger reductions seen between *in vivo* / *in vitro* and histology are most likely due to the effects of histological processing. This reduction due to histological processing is corroborated by a study which looked at the effects on cross sectional area of arterial rings after histological processing (Dobrin 1996). The study looked at the effects of different fixatives and embedding techniques on rings of canine femoral and carotid arteries. The study reported between 19-25% reduction in cross sectional area from fresh tissue for three different fixatives that were embedded with paraffin. The study found a 4-13% increase in area for the same three fixatives that were embedded in glycol methacrylate. It was assumed that the changes in cross sectional area were reflected throughout the length of the ring and reflect a similar change in the tissue volume.

The carotid plaques in this study were fixed in formalin and embedded in paraffin, Dobrin's study reported a 19% reduction in cross sectional area for this combination. Because living tissues are 60-65% water, the reason for the reduction is mainly due to the fact that the tissue has to be dehydrated using alcohol solutions prior to paraffin embedding. Embedding with glycol methacrylate does not require dehydration of the tissues (Dobrin 1996). This reduction in plaque volume will have an effect on the comparison of histology and *in vivo* images.

The subjective comparison of the corresponding *in vivo* images and histology sections found no matches for any of the four plaques. This subjective method tried to match the corresponding images and sections on the basis of similar shape, size and

orientation. The subjective comparison of *in vitro* images with histology was poor with only 5/20, 7/20, 2/10 and 0/20 sections matching for shape, size and orientation for the 4 plaques respectively. It is not surprising that given the relatively poor results of the *in vitro* matching data that no matches were found with the *in vivo* data. This subjective method has several limitations: firstly the correct orientation of the three different sections in relation to one another is not known, secondly the reduction of the size of the histology selection and thirdly there may be some selection bias that is associated with subjective analysis. When analysing the sets of images for orientation, the in vivo images were kept constant and the corresponding in vitro and histology images rotated to see if any match could be made. For example in figure 4.5, no match can be seen in the case of orientation between in vivo and histology. The images shown are from plaque 2, using histology section g, *in vitro* image 61, and *in vivo* image 49.

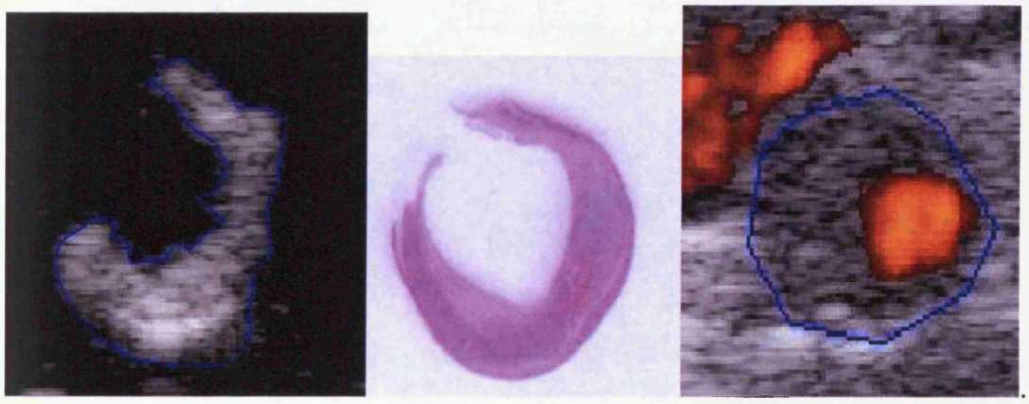

In vitro Histology *In vivo*

Figure 4.5 Example of a comparison from plaque 2.

However if the in vivo image is rotated by 225°, there may be a similarity in the orientation of both in vivo and the histology slices. This rotation is shown in figure 4.8 along with its neighbouring images also rotated by 225°.

In vitro image 57, histology image f, *in vivo* image 45

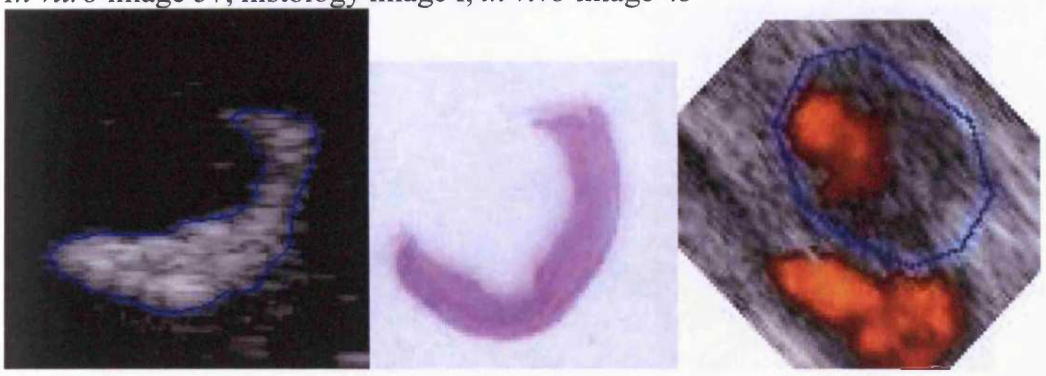

In vitro image 61, histology image g, *in vivo* image 49

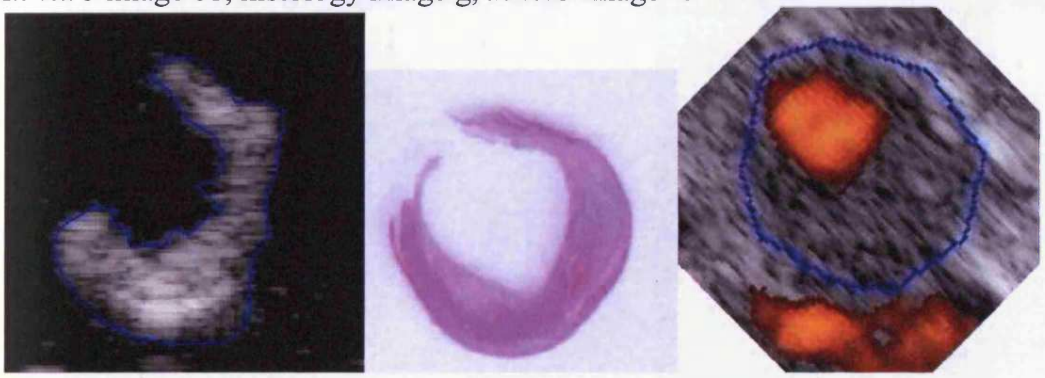

In vitro image 65, histology image h, *in vivo* image 53

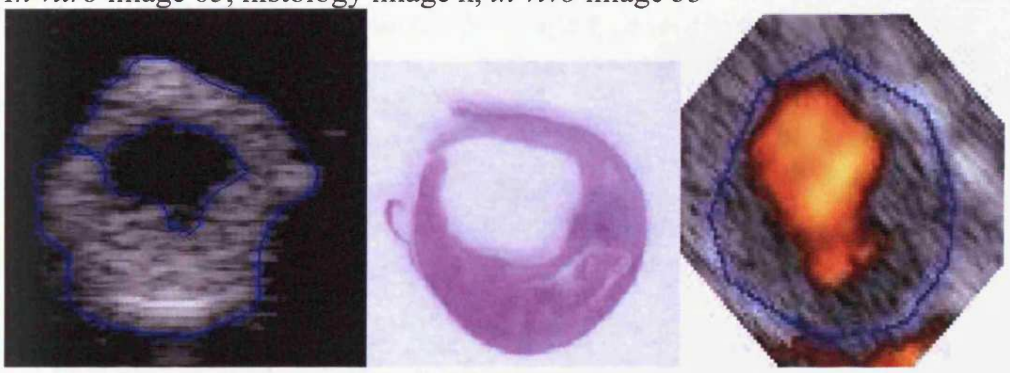

Figure 4.8 Plaque 3 images with in vivo image rotated 225°.

Another example is in plaque 3, figure 4.6, by rotating the in vivo image by 180°, there may be a match between in vivo and histology. Figure 4.9 shows the neighbouring images.

Plaque 3, *in vitro* image 91, histology image d, *in vivo* image 51.

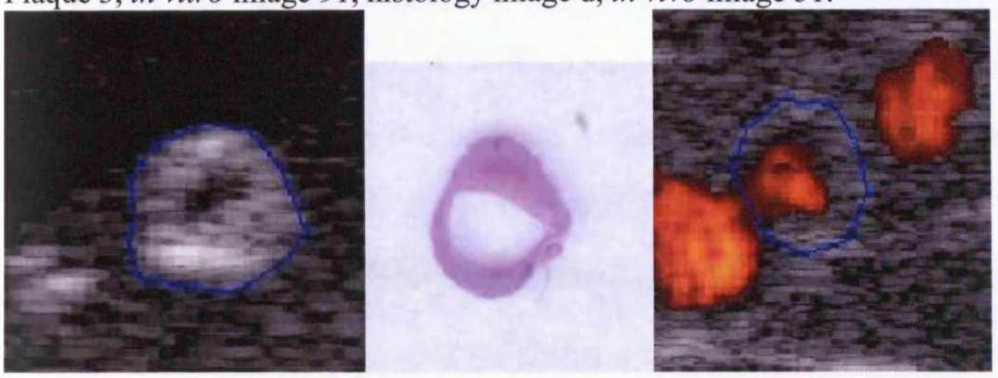

Plaque 3, *in vitro* image 89, histology image e, *in vivo* image 55.

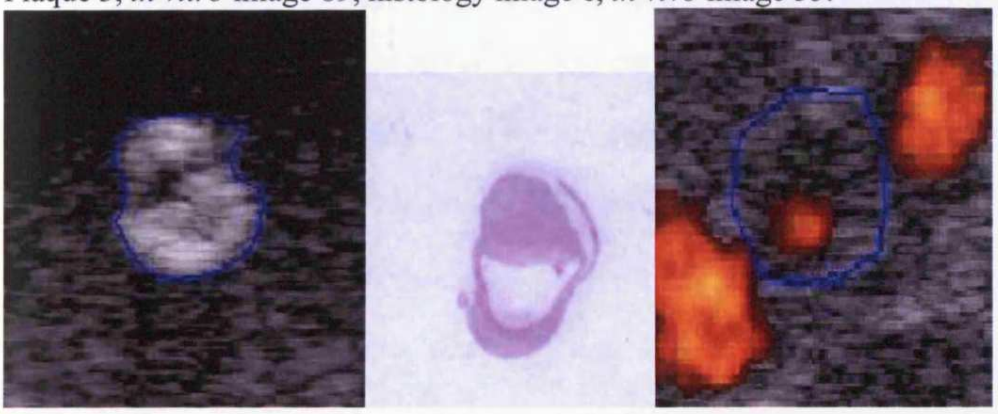

Plaque 3, *in vitro* image 87, histology image f, *in vivo* image 57.

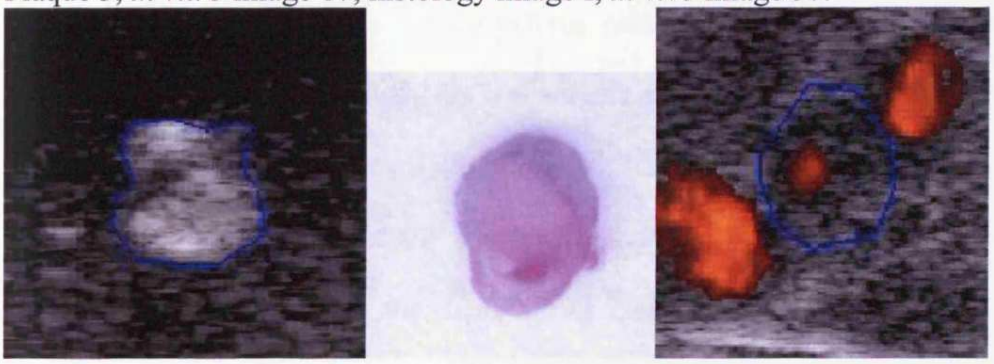

Figure 4.9 Plaque 3 images with *in vivo* image rotated 180°.

From these it can be seen that the neighbouring images orientation do not fully match. The correct orientation is not known, that is why, in this subjective analysis, for the orientation to match, the neighbouring images had also to match. Another limitation is the fact that the histological processing affected the size of the plaque specimen; this was not taken into account when the images were matched. By not adjusting for the

reduction in size of the histology section, a true reflection of the effect of processing would be seen in the comparisons. In hindsight it may have been more realistic to try find better agreement with shape, which is also be affected by the histological processing but not to the same degree as the size.

The comparison of the total plaque content measured by histology and that predicted by the MATLAB classifier yielded no comparable results for any of the four plaques. There are several possible reasons for this involving both histology and the MATLAB methods. One possible reason has to do with the amount of haemorrhage present in the plaques. The main ultrasound appearance of lipid and haemorrhage is that of an echolucent area within a plaque (Reilly et al. 1983; O'Donnell et al. 1985; Bluth et al. 1986; Gray-Weale et al. 1988; Schulte-Altedorneburg et al. 2000), this suggests that both these tissues should be in class 1 to 3 in the MATLAB classifier (see section 2.3.7). However the combined predicted amounts of classes 1-3 in three of the four plaques are lower than the corresponding amount of haemorrhage measured by histology. In the previous study by Rakebrandt (2001), the amount of haemorrhage detected by the classifier was underestimated due to the size of the analysis kernel. This has been overcome by using overlapping kernels where the previous study used non overlapping kernels so the detection of haemorrhage has been improved. The large amounts of haemorrhage, 29.85%, 19.44%, 8.52%, 38.53%, measured by histology far exceeded the amounts found in the 10 plaques in the previous work (Rakebrandt 2001). It found a mean proportion of 8% of the plaques were haemorrhage with only 2 of the 10 plaques having >10% haemorrhage. Another study reported levels of haemorrhage of ~10% and ~13% for echogenic and echolucent plaque respectively (Kardoulas et al. 1996). Lal et al. reported 11% haemorrhage for symptomatic plaques and 2% for asymptomatic plaques (Lal et al. 2002). The large

amount of haemorrhage measured was not expected and one possible reason may have been some bleeding into the plaque during the CEA surgery. Some studies did not include haemorrhage caused by operative manipulation when looking at intraplaque haemorrhage (Hatsukami et al. 1994; Tegos et al. 2000). Another possible reason is that the patient may have had a recent ischaemic event prior to the CEA, which has caused a haemorrhage at the site of a plaque rupture (Golledge et al. 2000). The histology report in this study did not differentiate what type of haemorrhage was present in the four plaques. Some studies have reported several types of haemorrhage including intraplaque haemorrhage as a blood diffusion into the plaque, fresh acute haemorrhage arising from ulcerated plaque and organised thrombus from an old haemorrhagic event that has endothelialised and become incorporated into the vessel wall (Van Damme et al. 1992). Others have differentiated intraplaque haemorrhage from thrombus as different components of the plaque (Avril et al. 1991; Gaunt et al. 1996; Montauban van Swijndregt et al. 1998; Wilhjelm et al. 1998; Schulte-Altedorneburg et al. 2000).

In the 4 plaques, the amount of calcium measured by histology was minimal. Plaque one had 2% calcium, the other plaques contained less than 1 % by volume. These amounts are smaller than was detected by Rakebrandt (2000) in his study. He predicted a mean of 11% of the plaques were calcium using his classifier and a mean of 6% measured by histology for ten plaques.

The decalcification process may be one of the reasons for the small amounts. The decalcification process involves placing the plaque in a solution of 8% formic acid until it is deemed soft enough for sectioning. The amount of time needed for decalcification will depend on the relative amount of calcium present, but normally the plaques are left in the solution for an arbitrary time. It is possible to test

biochemically for the calcium in solution to assess the endpoint of decalcification but this is not done routinely.

The histological method used to measure the amount of calcium was by morphological and tinctorial examination. This involves examining the H&E section in which any remaining calcium will appear purple or appear as gaps in the tissue section where calcium has been (Rakebrandt et al. 2000; Rakebrandt 2001; de Weert et al. 2005). This method appears subjective and is possibly dependant on the experience of the histologist. In conclusion the amount of calcium in the four plaques is not accurately known due mainly to decalcification and the histological method in which it is detected. A recent review report found that few studies reported on the effect of decalcification and other processing methods when these could have a bearing on the histology – imaging correlations (Lovett et al. 2005).

Fibrous and elastic tissues are connective tissues which give tissue strength and elasticity. Elastic tissue is found in the walls of arteries and hence the elastic tissue identified in the histological sections of all the four plaques was found at the edges of the sections. As a consequence the amount of elastic tissue may not be fully identified by the MATLAB classifier, this is because the kernels at the edge of the selected ROI were not included in the analysis.

The lack of standardisation in both histology and imaging methods has already been mentioned (section 4.1.5). As a result of this lack of standardisation, one group has suggested that consensus guidelines are required on the performance and reporting of studies. They have suggested a series of recommendations for the performance and reporting of studies of carotid plaque imaging versus histology (Lovett et al. 2005) and suggest that these recommendations act as a basis for the consensus guidelines. They put forward 8 recommendations which included doing reproducibility studies on

histology and imaging methods, ensuring that all details of symptoms, time of recent events, details of histological processing methods, positions of the relevant sections are reported. They also suggested that certain plaque features should be described to avoid subjective publication: these features were haemorrhage, lipid core to fibrous tissue ratio, rupture, minimum cap thickness and thrombus.

Histology in this thesis is used as the gold standard for the identification of the individual plaque tissue types, but as been shown in this study the effect of processing on the plaques is significant. If histology is to remain the gold standard for plaque composition in future studies the proposed guidelines of Lovett (2005) should be followed. Alternative methods of processing should also be used, for example, using glycol methacrylate instead of paraffin as a fixative which would eliminate the need for dehydration of the plaque. Also the plaques should not be decalcified during processing, as the calcium is an integral part of carotid atherosclerotic plaque and its presence is indicative of the more stable plaque type. In conclusion, however, one of the aims of the work in this thesis is to describe the natural history of atherosclerotic plaque in a given individual, over time. This necessarily involves a description of the plaque constituent components because it is the variation over time which may contribute both to the risk assessment for the patient and optimal management of the condition. Hence there is a necessity for histology to remain an integral part of any tissue classification process.

In conclusion the characterisation of individual plaque components from *in vivo* ultrasound imaging was not readily achievable using the MATLAB classifier. This is consistent with other studies which found that *in vivo* ultrasonic characterisation of carotid plaques yielded unreliable results for the prediction or quantification of different tissue types (Ratliff et al. 1985; Widder et al. 1990; Gaunt et al. 1996; White

et al. 1997; Montauban van Swijndregt et al. 1998; Lammie et al. 2000; Denzel et al. 2003). The study was stopped after four specimens were analysed as it was apparent from the analysed specimens that no comparison would be possible. The earlier discussion has shown that however, whilst it is not possible to identify the individual plaque components, i.e. it is not possible to link a specific class to a specific tissue type. It is possible, however, to use the classifier to objectively identify hard versus soft tissue and therefore is of use in investigating changes in plaque composition over time. The association between hard and soft tissue types and the MATLAB classifier has been discussed in section 2.3.7. The association showed that MATLAB classes 1, 2 and 3 were associated with the soft tissue types of haemorrhage and lipid, while classes 4 and 5 are associated with the harder tissue types of calcium, elastic and fibrous tissue.

Chapter 5: Comparison of serial scans

5.1 Aim

The aim of this chapter is to use the MATLAB classifier to compare a set of serial scans on patients undergoing lipid lowering drug treatments. The goal is to try record any change in the ultrasound appearance of the carotid plaque while the patient is on the treatment. The plaque volumes will also be measured to see if any significant reduction or increase occurs. As seen from the last chapter it will not be possible to determine the exact histological tissue type present in the plaques, only to assess whether a change has occurred or not.

5.2 Introduction

Two different lipid lowering drug treatments were tested in this study: statins and low density lipoprotein (LDL) apheresis.

5.2.1 Statins

The transportation of cholesterol around the body is done by two different types of lipoprotein, high density lipoprotein (HDL) and low density lipoprotein. HDL lipoprotein is classified as good whereas the LDL lipoprotein promotes atherosclerosis (Heiss et al. 1991; Johnsen et al. 2005). In many cases the high levels of LDL cholesterol can be reduced by diet, medication, increased physical activity and by stopping smoking. Statins (5-hydroxy-3-methylglutaryl-co-enzyme A reductase inhibitors) are a class of hypolidipemic agents that act to reduce the levels of LDL cholesterol in the blood. They work by inhibiting the enzyme HMG-CoA reductase, which controls the speed of cholesterol synthesis. The inhibition of this

enzyme in the liver stimulates the LDL-receptors, which results in an increased clearance of LDL from the bloodstream and a decrease in blood cholesterol levels. Statins have other effects as well as lowering LDL cholesterol, It is believed that statins have an effect on atherosclerosis by regulating inflammatory response, improving endothelial function, maintaining plaque stability and preventing thrombus formation (Furberg 1999; Maron et al. 2000).

There are several classes of statins on the market, including, simvastatin, lovastatin, pravastatin which are naturally derived from fungal fermentation. There are other statins that are synthetically derived including fluvastatin, cerivastatin and atorvastatin (which is the statin used in this project). They are well tolerated by patients and have an excellent safety record, but there are some adverse effects involving the liver and also muscle toxicity (Maron et al. 2000).

5.2.2 Effects of statins on atherosclerotic plaques

The effects of different types and doses of statins on reducing blood cholesterol levels have been documented (Maron et al. 2000).

One of the other effects of lowering LDL cholesterol is that of plaque stabilization. The reason for this plaque stabilization has been attributed to changes in the plaque composition (Crisby et al. 2001). Crisby et al (2001) used histological methods to investigate the effects of 3 months of pravastatin treatment on carotid plaques, of CEA patients prior to the surgery and compared them to CEA patients on no lipid lowering therapy. They reported increased collagen content and decreased lipid content, inflammation and metalloproteinases in the statin group.

There have been reported studies which have examined the effects of different types of statins on the intima media thickness (IMT) of the carotid artery (Salonen et al.

1995; de Groot et al. 1998; Taylor et al. 2002). A report from the regression growth evaluation statin study (REGRESS), a multi-centre trial found that 2 years pravastatin treatment had highly significant effects, with reduction in the IMT of carotid and femoral arteries of a treated group with no change in a placebo group. They concluded that B-mode ultrasound IMT measurements were a suitable way to monitor the effects of antiatherogenic treatments (de Groot et al. 1998). Similar results were reported by Salonen in 1995. A different trial compared the effects of 2 different types of statins, pravastatin a naturally derived product and atorvastatin which is a synthetic product. They found that the atorvastatin group showed regression of carotid IMT over 12 months whereas the IMT of the pravastatin group was stable (Taylor et al. 2002). A similar effect was found in another trial between atorvastatin and simvastatin (Smilde et al. 2001). In these studies atorvastatin reduced the levels of LDL cholesterol more than the natural statins as well as regressing the IMT levels where pravastatin and simvastatin did not, which supports the theory that aggressive lipid treatment has an effect on progression of atherosclerotic disease (Smilde et al. 2001; Taylor et al. 2002).

Other imaging modalities than B-mode ultrasound have been used to monitor the effects of statins on atherosclerotic plaques. A recent study used 3D integrated backscatter intravascular ultrasound to monitor the effects of pravastatin and atorvastatin on the tissue characteristics of coronary plaques (Kawasaki et al. 2005). They reported significant increases in the volumes of fibrous and mixed volume tissue and a decrease in lipid volume for both types of statins after 6 months of treatment. They did, however, report no change in the degree of stenosis caused by the plaque.

There have also been several studies involving magnetic resonance imaging (MRI).

One study using MRI examined the long term effects of lipid lowering therapies on coronary artery disease (CAD) patients. The patients were receiving intensive lipid lowering treatments for an average of 10 years. The treatments included lovastatin, niacin and colestipol and were compared to a group of patients with CAD but who had never been on lipid lowering drugs. The study measured carotid artery luminal and plaque extents by planimetry, and also estimated the plaque composition as a fraction of total planimetry area. The study found that the treated group had significantly less plaque lipid content and lipid composition compared to the untreated group. There was also more calcium in the treated group when compared to the untreated group. There was no difference in plaque content for fibrous tissue but the overall composition of fibrous tissue tended to be greater in the treated group (Zhao et al. 2001). Another study examined the effects of simvastatin on carotid and aortic plaques using high resolution MRI on 18 hypercholesterimic patients (Corti et al. 2001). They monitored changes in lumen area, vessel wall thickness and vessel wall area as markers of atherosclerotic disease. They found there was no significant change after 6 months treatment, but there was a significant reduction in vessel area and wall thickness but no change in lumen area of both aortic and carotid arteries after 12 months of treatment. A more recent study used MRI to construct 3D volumes of aortic plaques and found a significant reduction in plaque volume after 6 months of treatment with simvastatin. They also found that plaque regression was significantly related to serum LDL cholesterol reduction (Lima et al. 2004).

In conclusion all these studies have shown that statins lower LDL cholesterol levels and also have an effect of changing the tissue characteristics of the plaques. The changes in characteristics involve mainly reducing lipid content, increasing fibrous content sometimes with and sometimes without a change in the plaque size/volume.

This has an overall effect of stabilizing the plaque. The type of statin, dose and treatment period has a bearing on the amount of reduction with the synthetic statins having a larger effect than the natural statins.

5.2.3 LDL apheresis

There are some medical conditions where the levels of LDL cholesterol cannot be reduced to target levels by drug therapy or other methods. Patients with familial hypercholesterolaemia (FH) have an inherited faulty gene that affects the way that cholesterol is produced by their bodies. The condition can be severe where drug treatments and lifestyle changes have no effect on the cholesterol levels. In these cases the only way to reduce the level is by plasma apheresis.

LDL apheresis is a procedure that filters out and removes the LDL cholesterol from the blood without removing HDL cholesterol. The process works in a similar way to kidney dialysis where blood is taken from a patient's vein and run through a machine that separates out the plasma. The blood is returned to the patient through a different vein while the plasma is diverted through another part of the machine that removes the LDL cholesterol. The plasma is then returned to the patient.

The most common machine used in the apheresis process is called a liposorber system, which is an extracorporeal circulation system. The blood is passed through a single use adsorption column containing porous cellulose beads with immobilized dextran sulphate as the adsorbant. The dextran sulphate has an affinity for LDL cholesterol but will not remove any of the good HDL from the blood (Yamamoto and Yamashita 1998). There are other types of apheresis systems including a reusable immunoadsorption column coated with polyclonal sheep antibodies and a novel device which directly adsorbs the lipoproteins. All three systems are effective in

reducing LDL cholesterol, total cholesterol and triglycerides (Schmaldienst et al. 2000).

LDL apheresis is safe and has been established in patients with FH, but it is costly and time consuming and only available at specialist centres. LDL apheresis is not a cure and on going treatment is required. Apheresis is often used in combination with statins to maximize the effect of the treatment, as blood LDL cholesterol levels often rebound quickly after apheresis.

5.2.4 Effect of LDL apheresis on atherosclerotic plaques

There have been several reports of the effects of LDL apheresis on changing atherosclerotic lesions. In 1991 a study by Hennerici looked at the effects of LDL apheresis on 7 patients with heterozygous FH using 3D B-mode ultrasound. They examined 4 flat and 17 soft plaques and reported significant plaque volume reduction after an average follow up period of 17 months. The LDL apheresis was combined with simvastatin drug treatment. They reported that the volume reduction was only seen in soft or flat plaques and that they did not observe any regression of large calcified plaques (Hennerici et al. 1991).

A study by Koga in 1999 looked at the long term effects of LDL apheresis combined with statin treatment. They used B-mode ultrasound to monitor carotid IMT over 7.8 years for a group on the two treatments against a group on statins only who were on the medication for 5.5 years. The LDL apheresis group comprised 2 homozygous FH patients and 9 heterozygous FH patients. The results found a small annual IMT progression in the homozygous group (0.0002 mm/year) and an IMT regression in the heterozygous group (-0.0023 mm/ year). This is significant when compared to IMT progression in the medication group (0.0252 mm/ year). They concluded that LDL

apheresis delays the progression of atherosclerotic disease in FH patients (Koga et al. 1999).

An intravascular ultrasound study that looked at the effects of LDL apheresis on coronary plaque extent for a period of 12 months found significant regression in plaque extent in a group of FH patients on statin plus apheresis treatment, compared with a group just on statins (Matsuzaki et al. 2002).

Another study looked at the effects of LDL apheresis combined with aggressive statin treatment, using the maximum allowed dose of atorvastatin, on coronary calcified plaques using computed tomography over a 29 month period. They found a decrease in the volume of the calcified plaques of 23 ± 15% and also reported a significant increase in the mean density of the calcified plaque (Hoffmann et al. 2003).

In conclusion LDL apheresis in combination with statins has an effect of reducing atherosclerotic plaque in FH patients.

5.3 Methods

5.3.1 Patient groups

There were two different patient groups used in this study. The first group consisted of two patients with severe FH who were undergoing regular LDL apheresis. This was a pilot study to see if the apheresis had any effect on carotid plaques over the course of the treatments.

The second group was the statin group which consisted of 9 patients. These were patients recruited onto a drug trial to look at the effects and benefits to patients of atorvastatin. One of the criteria for entry onto the trial was that the patient had a non-significant carotid plaque. There were other strict criteria for entry including that the

patients were not on statins before the trial. The trial intended to recruit 30 patients, however due to the strict criteria only 9 patients were recruited. The results of the other part of the trial were not available, so this chapter will only look at the effects of the statins on the carotid plaques with time. One major limitation of this trial was the time period. The time period was determined by the drug trial, of which the ultrasound study was just a small part. The study was approved by the Trusts Ethical Committee and therefore the time period of the ultrasound study was limited to 3 months.

Some of the patients had bilateral carotid plaques; some had unilateral plaques so the following labelling system was used to distinguish between the different groups and which side the plaque was on. Patient number followed by which side, R for right, L for left, followed by either S for statin group or A for apheresis group. E.g. Patient 1_R_A. denotes the right carotid plaque for patient number 1 of the apheresis group

5.3.2 Frequency of visits

Both groups of patients were scanned initially before commencing treatment and then every four weeks for a total of twelve weeks. There were some minor discrepancies in the timings with some patients going 5 weeks between scans. The 2 apheresis patients were scanned the day after the LDL treatment had taken place. The 3D *in vivo* scans were acquired using the standard protocol (see section 2.2.4). A series of four scans for each patient was acquired.

5.3.3 Selection of plaque extent for the serial scans.

To compare the serial scans the number of ROIs in all 4 scans has to be the same. Also the selection of the individual ROIs has to be as similar as possible in the serial

scans. A limitation of the MATLAB software is that only one set of images can be displayed at any one time, so all four serial scans cannot be displayed simultaneously. The software takes a long time to load so to change from one serial scan to another takes a long time. To overcome this, the ROI of each serial scan was selected using the following protocol.

The plaque extent of visit 1 was defined using the standard protocol (see section 2.3.3). Each region of interest was selected and a sketched record of the ROI was recorded (see Figure 5.1). This was used as a template to select the other ROIs.

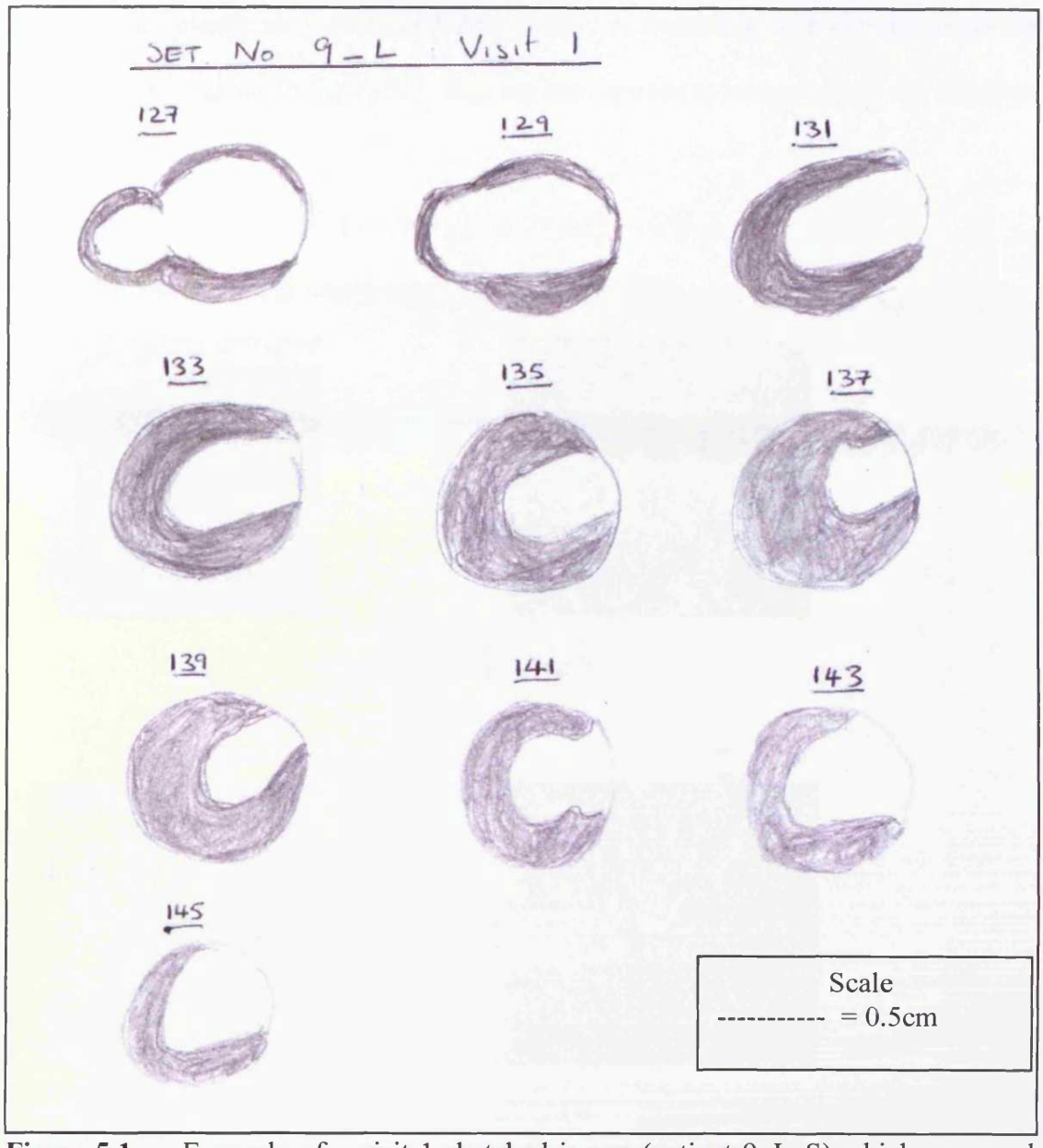

Figure 5.1 Example of a visit 1 sketched image (patient 9_L_S) which was used as a template for the selection of the ROIs for the other serial scans.

Specific landmarks in the scan, like the position of the ICA and bifurcation were also recorded. This was done for every single ROI in the plaque extent. The subsequent visits plaque extents and ROIs were selected using a comparison with visit 1, ensuring a similar number of ROIs are selected. Corresponding 2D images from the serial scans were not compared individually using the MATLAB classifier, as only changes

in the overall plaque were examined. An example of a set of corresponding images for a serial scan is shown in figure 5.2. This set corresponds to image 135 in the sketched figure 5.1.

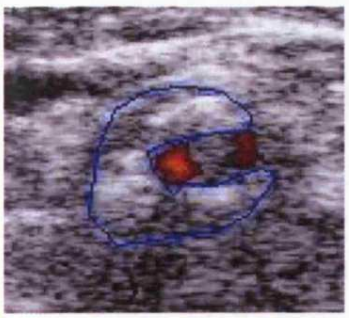

Visit 1

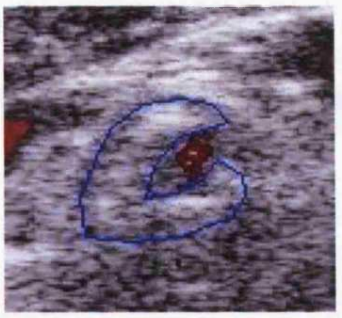

Visit 2

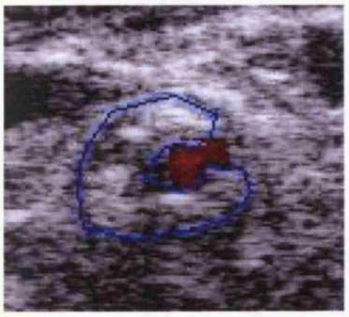

Visit 3

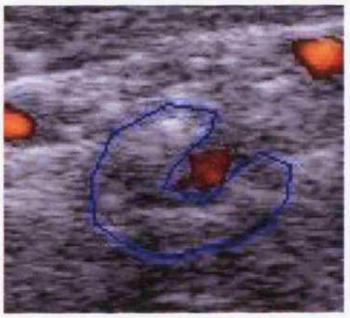

Visit 4

Figure 5.2 Example of four corresponding images from patient 1_L_A serial scans.

5.3.4 Volume measurements of the serial scans

The plaque volume of each serial visit was measured 5 times using the method described in section 2.4. The volumes measured were compared using SPSS to see if there was any significant difference between the visits. The statistical method used was a one way analysis of the variance of the means of each visit. The statistics were used to see if there was a significant change in the plaque volumes between the visits. The statistical analysis results for all the volume measurements patients in both groups can be found in appendices 5.1 and 5.2.

5.3.5 MATLAB Statistical analysis

The analysis of the serial MATLAB classification was very difficult, due to the way that the data is presented, i.e. percentages. The aim was to see if there was a statistical difference between the visits i.e. is there a real change in the tissue type that is not due to experimental error?

In chapter 3, four different reproducibility studies were conducted to try and estimate the possible sources of variation in the system. Two major sources were identified: variation due to the selection of the plaque ROI and variation due to patient repositioning for repeat (serial) scans. The 95% coefficients of repeatability or agreement were calculated for the four studies and the maximum 95% coefficients for the two major sources were used to estimate the total variation of the system. A total 95% coefficient of 13.7% was calculated (section 3.6). This variation value suggests that any change above 13.7% has a <5% probability of being due to variation in the system and is more likely to reflect a change in the plaque tissue constituents.

The differences between the baseline visit (V1) and the final visit (V4) are examined to see if changes in class type have occurred. The data are also examined to look at

whether changes from classes 1, 2 & 3, which are associated with soft tissue types, to classes 4 & 5 which are associated to the harder tissue types, has occurred. A graph showing the percentages of each class for each visit is plotted, showing the trend of what is happening over the period of the trial. Corresponding 2D images from the serial scans were not compared using the MATLAB classifier, as only changes in the overall plaque were examined. All the information for the study was collected from the 3D data set and it was not felt necessary to perform a hand held longitudinal scan.

5.4 Results

5.4.1 Analysis of the apheresis group serial scans

5.4.1.1 Patient 1_R_A

This patient had a plaque that was mainly on the posterior and left side wall that extended to the anterior wall of the distal CCA and just into the ICA. Similar regions of interest for all 4 visits were selected and analysed and the results displayed in table 5.1. The table also shows the percentage change in the class type over the period of the study. The table also shows the mean volume measured for each of the four visits and the percentage change in volume over the period of the study.

	Class 1 (%)	Class 2 (%)	Class 3 (%)	Class 4 (%)	Class 5 (%)	Mean Volume (mm^3)
V1	9.19	17.08	48.23	22.24	3.25	253.0
V2	18.05	20.85	29.87	22.73	8.50	215.7
V3	17.99	24.62	37.91	18.36	1.12	195. 8
V4	1.00	14.17	34.89	25.83	24.11	183.3
Difference V4-V1 (%)	-8.19	-2.91	-13.34	3.59	20.86	-21.4%

Table 5.1 MATLAB and volume results for patient 1_R_A.

A graph of the MATLAB percentage class versus visit is shown in figure 5.3. This graph shows the trend of change over the four visits.

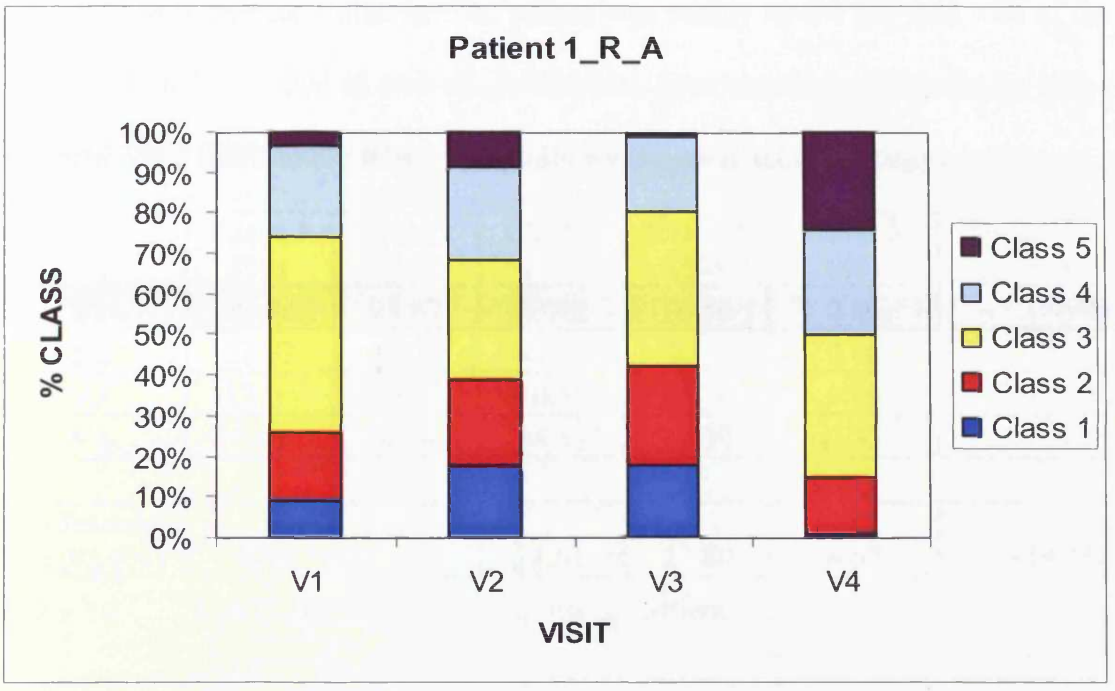

Figure 5.3 MATLAB analysis of % class versus visit for patient 1_R_A

From the table it can be seen that there is an increase in class 5 type tissue of 20.86% which is greater than the 13.7% limit which suggest a possible real change in tissue type. This increase in class 5 is made up mainly of a reduction of class 3 (13.34%) tissue. Looking at the change from classes 1, 2 & 3 (soft) to classes 4 & 5 classes 4, 5 (hard), shows a 24.45% increase in classes 4 & 5. There has been a significant 21.4% reduction in the plaque volume from V1 to V4 ($p<0.001$). There has also been a significant reduction in volume between each visit ($p<0.001$ for each visit) No comparisons could be made with reductions in blood cholesterol levels for any patients in this study as these results were not available.

5.4.1.2 Patient 1_L_A

The contralateral carotid artery of patient 1 also contained a significant plaque which was analysed in the same manner. The plaque was mainly on the left side wall of the distal CCA and extended in size to include both anterior and posterior walls at the bifurcation and just into the ICA. The results are shown in table 5.2 below.

	Class 1 (%)	Class 2 (%)	Class 3 (%)	Class 4 (%)	Class 5 (%)	Mean Volume (mm^3)
V1	10.86	28.87	43.02	16.59	0.66	193.0
V2	22.32	40.20	34.50	2.98	0.00	191.7
V3	12.02	35.71	40.55	10.74	0.99	176.5
V4	1.47	6.30	38.51	44.39	9.33	165.9
Difference V4-V1 (%)	-9.39	-22.57	-4.51	27.80	8.67	-14.1%

Table 5.2 MATLAB and volume results for patient 1_L_A

A graph of the MATLAB percentage class versus visit is shown in figure 5.4. This graph shows the trend of change over the four visits.

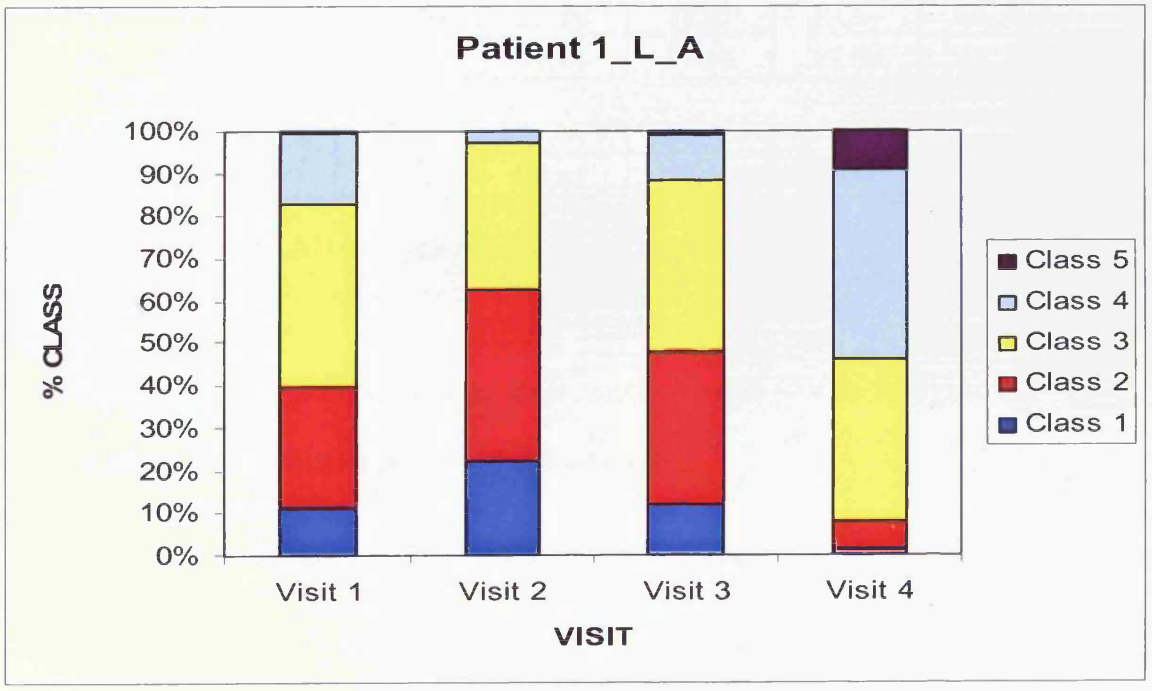

Figure 5.4 MATLAB analysis of % class versus visit for patient 1_L_A

There is a similar trend to the contralateral plaque of this patient with a 36.47% change from the classes 1, 2 & 3 (soft) to the classes 4 & 5 (harder types). There is an increase in class 4 type of 27.8% with a decrease in class 2 type of 22.57%. There was a 14.1% reduction in volume from V1 to V4 ($p<0.001$). There was no significant difference in the plaque volumes between visit 1 and 2 ($p = 0.864$), but there was a significant difference between V2 and V3 and also between V3 and V4 ($p<0.001$).

5.4.1.3 Patient 2_R_A

The second apheresis patient also had bilateral carotid plaques. The plaque was concentric around the distal CCA with the majority of the plaque on the anterior wall. The results of the right carotid plaque MATLAB analysis and measured volumes are shown in table 5.3.

	Class 1 (%)	Class 2 (%)	Class 3 (%)	Class 4 (%)	Class 5 (%)	Mean Volume (mm^3)
V1	11.11	15.42	34.17	30.27	9.03	309.0
V2	3.76	16.62	35.97	32.28	11.37	278. 5
V3	10.66	15.46	33.30	28.01	12.57	275.3
V4	0.12	3.29	26.06	57.44	13.09	271.3
Difference V4-V1 (%)	-10.99	-12.13	-8.11	27.17	4.06	-13.9%

Table 5.3 MATLAB and volume results for patient 2_R_A

A graph of the MATLAB percentage class versus visit is shown in figure 5.5. This graph shows the trend of change over the four visits.

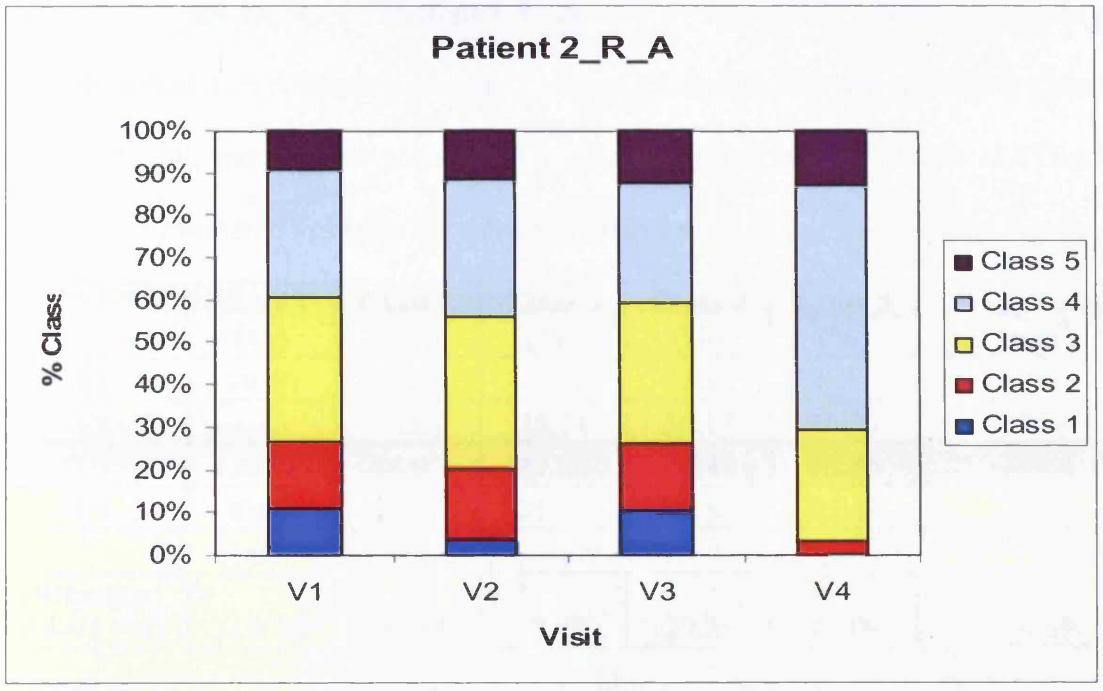

Figure 5.5 MATLAB analysis of % class versus visit for patient 2_R_A

The results show the same trend as the other apheresis patient. There is a 27.16% increase in class 4 which is made up by reduction in classes 1, 2 and 3. There is a 31.23% increase in the classes 4 & 5 (harder type tissues). There is a 13.9 % reduction in the plaque volume from V1 to V4 which is significant ($p<0.001$). There was a significant difference between V1 and V2 ($p<0.001$) but there was no significant difference between V2 and V3 ($p=0.664$) and also V3 and V4 ($p=0.467$).

5.4.1.4 Patient 2_L_A

The plaque was also concentric around the distal CCA with the majority of the plaque on the left side and anterior walls. The results of the left carotid plaque MATLAB analysis and measured volumes are shown in table 5.4.

	Class 1 (%)	Class 2 (%)	Class 3 (%)	Class 4 (%)	Class 5 (%)	Mean Volume (mm^3)
V1	19.46	19.26	30.62	22.32	8.34	282.0
V2	1.43	12.28	25.34	34.17	26.79	269.2
V3	16.12	18.97	29.64	24.41	10.86	268.2
V4	0.00	2.15	21.84	42.57	33.43	254.5
Difference V4-V1 (%)	-19.46	-17.11	-8.78	20.25	25.09	-10.8%

Table 5.4 MATLAB and volume results for patient 2_L_A

A graph of the MATLAB percentage class versus visit is shown in figure 5.6. This graph shows the trend of change over the four visits.

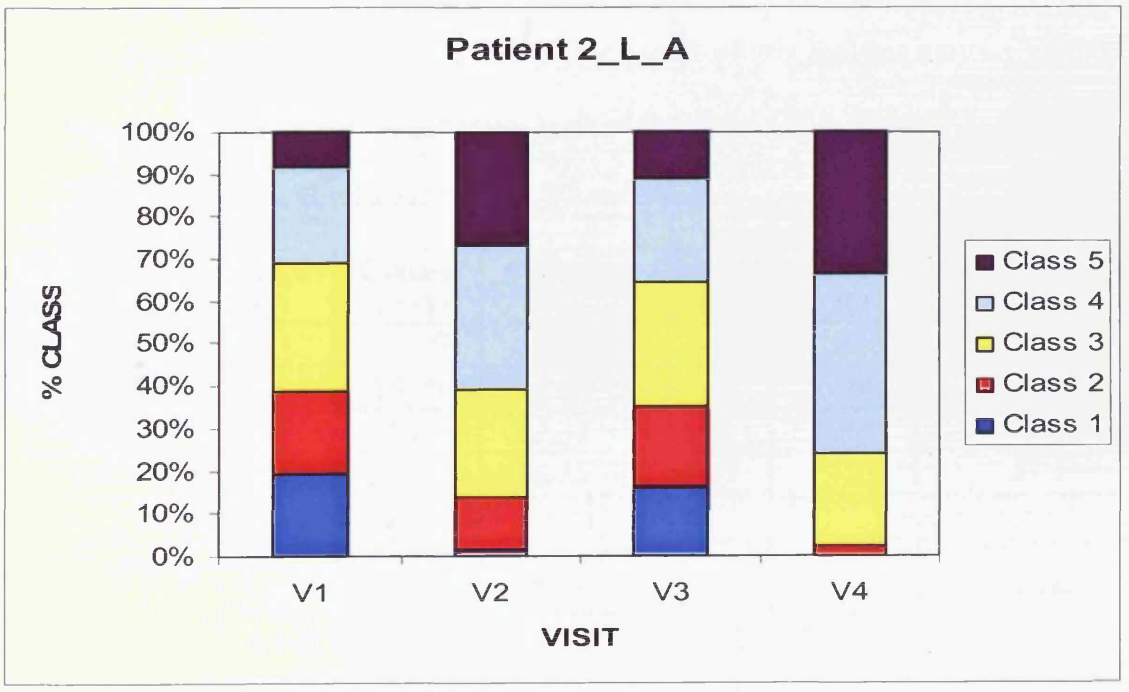

Figure 5.6 MATLAB analysis of % class versus visit for patient 2_L_A

Again the trend is similar to the previous apheresis plaques. There are significant increases in both classes 4 and 5 of 20.25% and 25.09% respectively. This is made up of reductions in both classes 1 and 2. There was a significant 10.8% reduction in volume from V1 to V4 ($p<0.001$). There was a significant difference in the plaque volumes between visit 1 and 2 ($p=0.001$), and also between V3 and V4 ($p=0.001$), but there was no significant difference between V2 and V3 ($p = 0.98$).

5.4.2 Analysis of the statin group serial scans

5.4.2.1 Patient 1_R_S

This was the very first patient that was scanned on the trial and there were problems with the storage of the V1 data set, which was realized only when the data was being transferred from the ultrasound machine to the computer. It was decided at the time to continue to record the data from subsequent visits as the patient did complete the other components of the study, even though the results of this analysis may be flawed. This was a small plaque on the posterior wall of the distal CCA. Table 5.5 shows the MATLAB and volume results for the V2, V3 andV4.

	Class 1 (%)	Class 2 (%)	Class 3 (%)	Class 4 (%)	Class 5 (%)	Mean Volume (mm^3)
V1	-	-	-	-	-	-
V2	2.35	36.79	41.68	18.40	0.78	58.8
V3	0.00	32.45	52.32	14.88	0.35	58.2
V4	0.00	28.97	36.21	20.89	13.93	57.7
Difference V4-V2 (%)	-2.35	-7.82	-5.47	2.49	13.15	-1.1%

Table 5.5 MATLAB and volume results for patient 1_R_S.

A graph of % class versus visit is shown in figure 5.7.

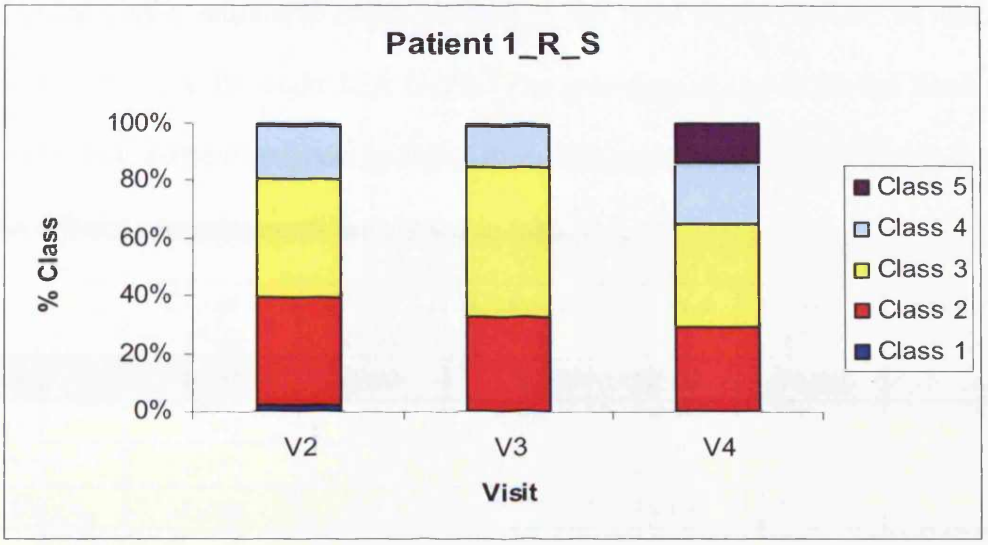

Figure 5.7 MATLAB analysis of % class versus visit for patient 1_R_S

As there is no baseline visit it is not possible to fully analyse this serial set of data. It can be seen that V2 and V3 are very similar but there is an increase in the harder classes 4 and 5 in V4 with a 13.15% increase in class 5 which is below the 13.7% variation and may be due to system variation. The volume measurements are similar with a non significant 1.1% difference between V2 and V4 (p=0.583). There was no significant volume change between V2 and V3 (p=0.866) and also V3 and V4 (p= 0.872).

5.4.2.2 Patient 1_L_S

As happened on the right side, no initial visit data was stored. There was also no final visit data for the left carotid artery of this patient as one of the switches which stops the motor on the mechanical device failed after the left carotid plaque scan was completed. The results are not included for this patient's left carotid artery.

5.4.2.3 Patient 2_R_S

This patient had a unilateral small plaque on the right posterior wall of the CCA which extended into the right ICA origin. The selection of the ROIs for these serial visits was very difficult especially for visit 3. The results of the MATLAB analysis and the volume measurements are shown in table 5.6.

	Class 1 (%)	Class 2 (%)	Class 3 (%)	Class 4 (%)	Class 5 (%)	Mean Volume (mm^3)
V1	0.00	0.00	1.31	22.19	76.50	231.8
V2	0.00	0.00	0.00	57.57	42.43	240.4
V3	0.00	0.00	0.37	16.73	82.91	227.3
V4	0.00	0.00	2.53	78.93	18.54	235.9
Difference V4-V1 (%)	0.00	0.00	1.22	56.74	-57.94	1.7%

Table 5.6 MATLAB and volume results for patient 2_R_S

A graph of % class versus visit is shown in figure 5.8.

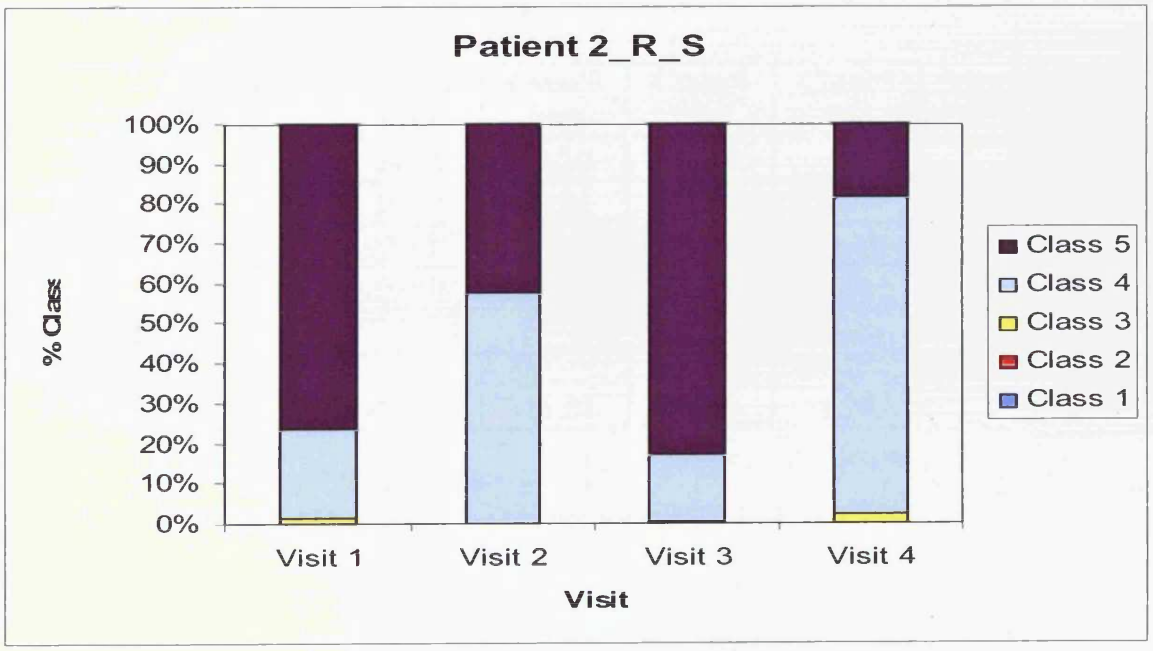

Figure 5.8 MATLAB analysis of % class versus visit for patient 2 _R_S

The results show that this plaque is made up of classes 4 & 5 (the harder tissue types) class 4 and 5, with very little of classes 1, 2 & 3 (the softer tissue types). The visits appear to alternate between classes 4 and 5 suggesting that the MATLAB classifier finds it difficult to distinguish between the two. There is a significant 1.7% increase in plaque volume between V1 and V4 (P=0.009). There are significant changes between V1 and V2 ($p<0.001$), V2 and V3 ($p<0.001$) and also V3 and V4 ($p<0.001$). These results follow a similar pattern to the MATLAB analysis with an increase in volume in V2 followed by a reduction in V3 and another increase in V4. Another possible reason for the up and down variations of MATLAB classes and volume changes may be due to difficulties in the selection of the ROIs.

5.4.2.4 Patient 3_R_S

This patient had bilateral plaques with the right sided plaque mainly on the posterior wall of the distal CCA. The MATLAB analysis and volume measurements are summarized in table 5.7.

	Class 1 (%)	Class 2 (%)	Class 3 (%)	Class 4 (%)	Class 5 (%)	Mean Volume (mm^3)
V1	16.52	34.33	39.20	9.09	0.85	185.4
V2	5.73	19.22	48.94	21.15	4.97	170.5
V3	0.00	2.10	31.43	53.06	13.41	156.2
V4	0.00	10.19	28.19	52.97	8.64	161.2
Difference V4-V1 (%)	-16.52	-24.14	-11.01	43.88	7.79	-15%

Table 5.7 MATLAB and volume results for patient 3_R_S

A graph of % class versus visit is shown in figure 5.9.

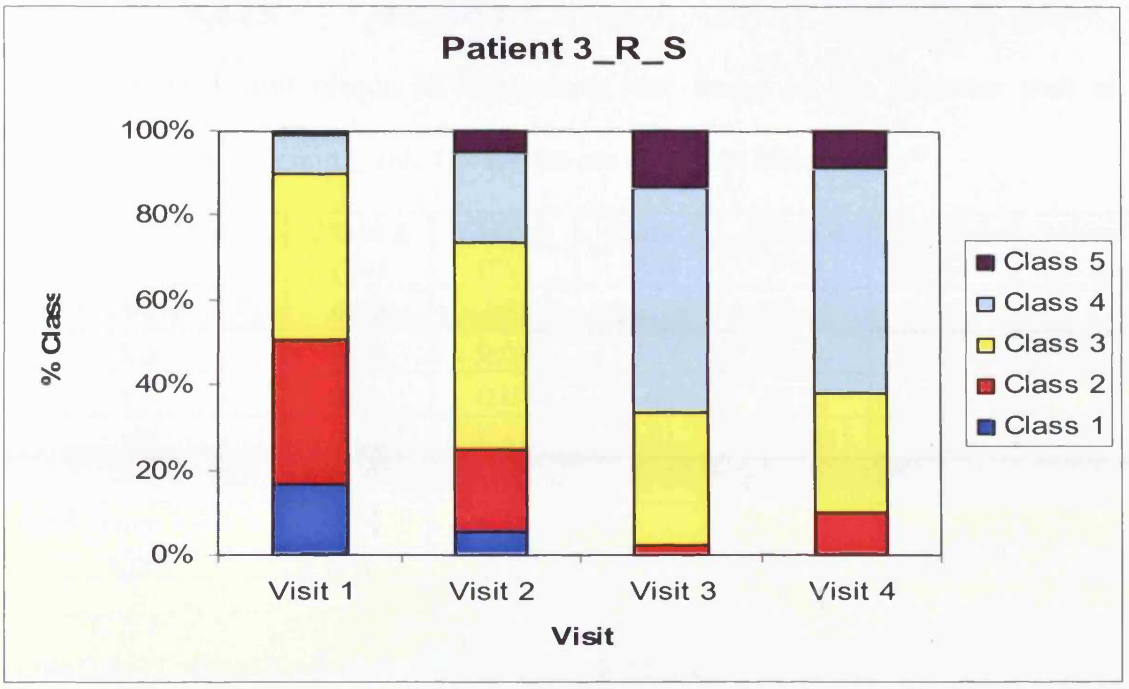

Figure 5.9 MATLAB analysis of % class versus visit for patient 3_R_S

There is a large 43.88% increase in class 4 from V1 to V4 made up of a reduction in class 1 and class 2 mainly. This corresponds to a 51.67% increase in classes 4 & 5 (harder tissue types). There is a significant 15% reduction in plaque volume from V1 to V4 ($p<0.001$). There are significant reductions in volumes fromV1 to V2 ($p<0.001$), V2 toV3 ($p<0.001$) and also V3 to V4 ($p=0.024$).

5.4.2.5 Patient 3_L_S

The left sided carotid plaque of this patient was found on the posterior wall at bifurcation and ICA origin level. The results are shown in table 5.8.

	Class 1 (%)	Class 2 (%)	Class 3 (%)	Class 4 (%)	Class 5 (%)	Mean Volume (mm^3)
V1	0.95	7.87	25.73	29.64	35.81	80.5
V2	0.32	9.04	43.76	17.16	29.71	80.0
V3	0.00	0.00	5.40	47.02	47.58	77.6
V4	0.00	0.42	9.81	43.50	46.27	78.9
Difference V4-V1 (%)	-0.95	-7.45	-15.92	13.86	10.46	-2.1%

Table 5.8 MATLAB and volume results for patient 3_L_S

A graph of % class versus visit is shown in figure 5.10.

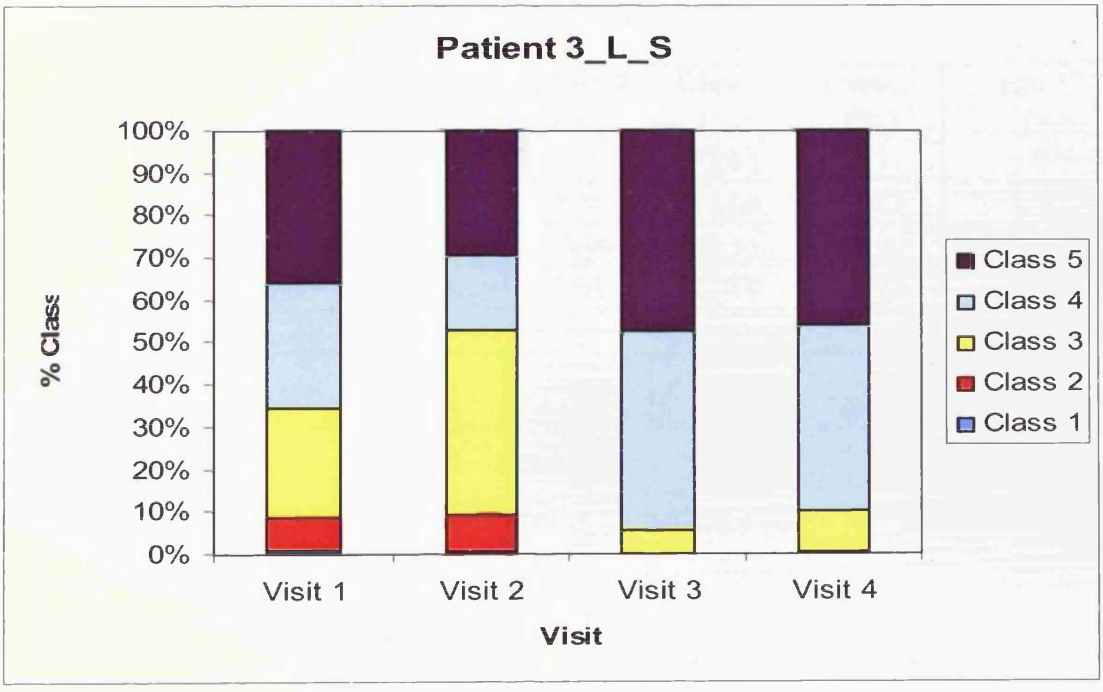

Figure 5.10 MATLAB analysis of % class versus visit for patient 3_L_S

The MATLAB analysis results for this patient show a similar trend to the contralateral plaque with a 24.32% increase in classes 4 & 5 (harder tissue types). This is made up mainly of 13.86% class 4 and 10.46% class 5 increases, and a 15.92% reduction in class 3. There is a non significant 2.1% reduction in plaque volume between V1 and V4 (p=0.071). There are also non significant reductions between V1 and V2 (p=0.858), V3 and V4 (p=0.210), but the reduction between V2 and V3 is significant (p=0.006).

5.4.2.6 Patient 4_L_S

This patient had a unilateral plaque which was found on the posterior and side wall of the distal CCA and the ICA origin. The MATLAB analysis and volume measurements are summarised in table 5.9.

	Class 1 (%)	Class 2 (%)	Class 3 (%)	Class 4 (%)	Class 5 (%)	Mean Volume (mm^3)
V1	0.00	0.01	13.25	63.44	23.31	404.4
V2	0.00	0.02	7.06	73.09	19.83	406.0
V3	0.01	0.70	13.99	66.31	19.00	400.9
V4	0.00	0.06	7.03	77.19	15.72	404.6
Difference V4-V1 (%)	0.00	0.05	-6.22	13.75	-7.59	0.04%

Table 5.9 MATLAB and volume results for patient 4 _L_S

A graph of % class versus visit is shown in figure 5.11.

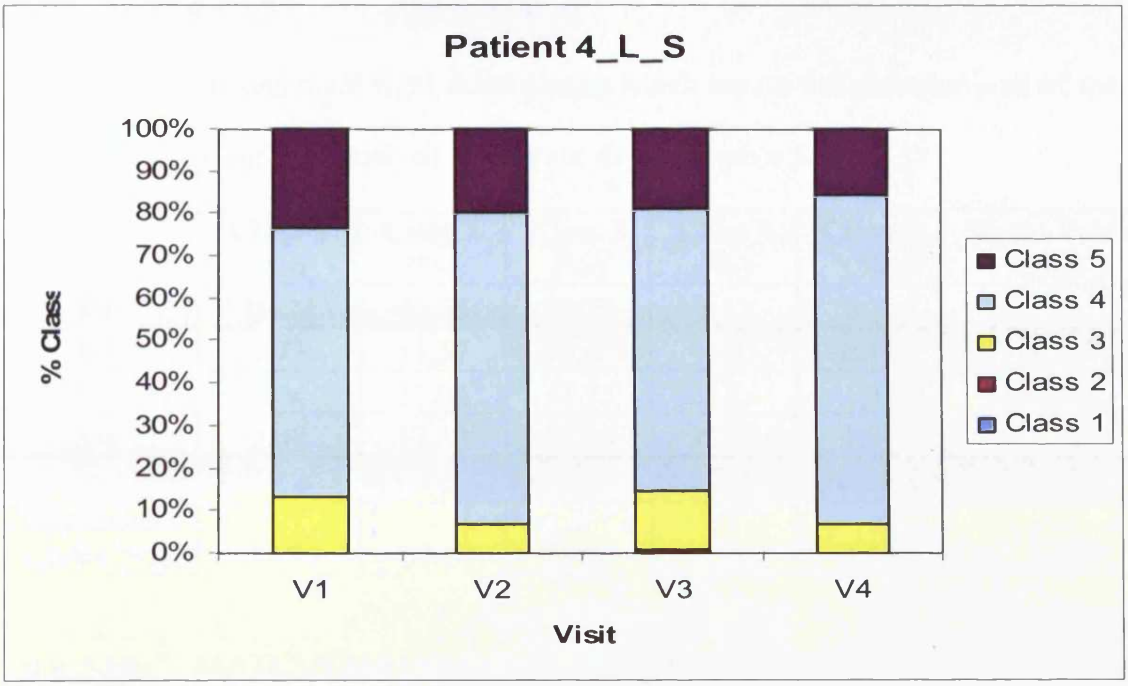

Figure 5.11 MATLAB analysis of % class versus visit for patient 4_L_S

There is a small increase of 13.75% in class 4 which is just above the 13.7% which constitutes a possible real change. This change is made up of reductions in both classes 3 and 5. This corresponds to a small increase of 6.16% in harder tissue types. There is no significant change in plaque volume between V1 and V4 ($p=1.0$). There is also no significant change between each of the visits, V1 & V2, V2 & V3, and V3 & V4 ($p=0.816$, $p=0.185$, $p=0.539$).

5.4.2.7 Patient 5_R_S

This patient had a unilateral right sided plaque which lay on the posterior wall of the CCA and ICA origin. The analysis results are shown in table 5.10.

	Class 1 (%)	Class 2 (%)	Class 3 (%)	Class 4 (%)	Class 5 (%)	Mean Volume (mm^3)
V1	19.22	46.58	30.78	3.42	0.00	114.7
V2	2.72	11.57	36.68	40.85	8.19	109.5
V3	5.64	31.04	38.73	23.24	1.35	118.1
V4	0.49	13.38	53.85	30.97	1.31	121.8
Difference V4-V1 (%)	-18.73	-33.20	23.07	27.55	1.31	5.9%

Table 5.10 MATLAB and volume results for patient 5_R_S

A graph of % class versus visit is shown in figure 5.12.

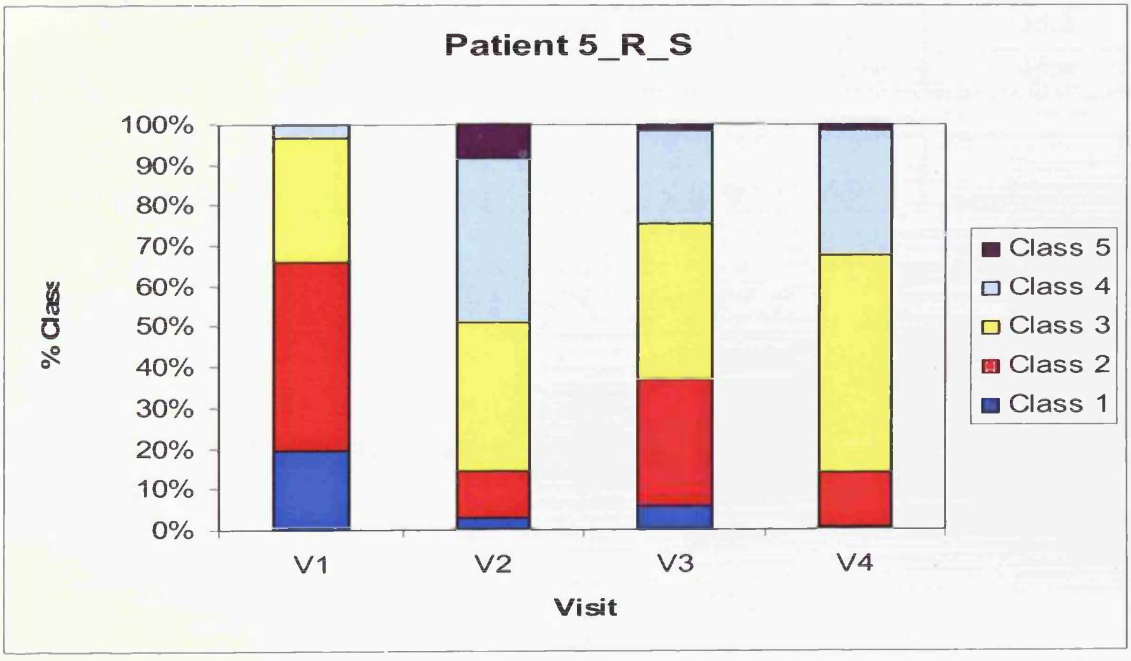

Figure 5.12 MATLAB analysis of % class versus visit for patient 5_R_S

The results show large increases in classes 3 and 4 of 23.07 and 27.55% respectively. This is made up of large reductions in classes 1 and 2 of 18.73 and 33.2% respectively. This gives a 28.86% increase in classes 4 & 5 (harder tissue types). There is a significant 5.9% increase in the plaque volume between V1 and V4 ($p<0.001$). The increases between the subsequent visits V1 & V2, V2 & V3, and V3 & V4 are all significant ($p=0.004$, $p<0.001$, $p=0.041$).

5.4.2.8 Patient 6_R_S

The plaque was found on the posterior wall of the distal CCA. The analysis results are shown in table 5.11.

	Class 1 (%)	**Class 2 (%)**	**Class 3 (%)**	**Class 4 (%)**	**Class 5 (%)**	**Mean Volume (mm^3)**
V1	0.00	0.09	27.12	58.46	14.34	45.0
V2	0.00	0.00	21.89	66.31	11.80	45.0
V3	0.00	0.00	10.06	55.16	34.79	45.8
V4	0.00	0.00	10.34	70.36	19.29	45.4
Difference V4-V1 (%)	0.00	-0.09	-16.78	11.90	4.95	0.8

Table 5.11 MATLAB and volume results for patient 6_R_S

A graph of % class versus visit is shown in figure 5.13.

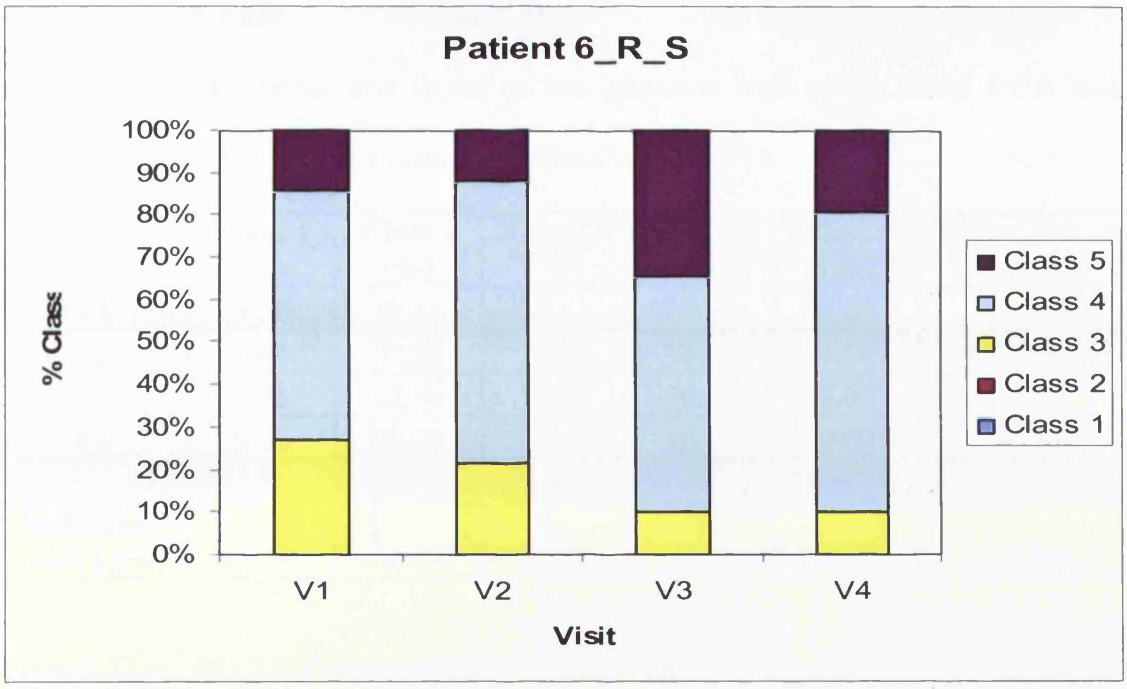

Figure 5.13 MATLAB analysis of % class versus visit for patient 6_R_S

There is a small 16.78% reduction of class 3 which corresponds with slight increases in classes 4 and 5. There is a similar increase in the amount of classes 4 & 5 (hard tissue) of 16.85% from V1 to V4. There is no significant change in plaque volume between V1 and V4 ($p=0.99$), and between all the intermediate visits V1 & V2, V2 & V3, and V3 & V4 ($p=0.956$, $p=0.413$, $p=0.864$).

5.4.2.9 Patient 7_R_S

The right carotid plaque was found on the posterior wall of the distal CCA and bifurcation area. The analysis results are found in table 5.12.

	Class 1 (%)	Class 2 (%)	Class 3 (%)	Class 4 (%)	Class 5 (%)	Mean Volume (mm^3)
V1	5.58	38.16	39.33	16.85	0.08	73.8
V2	4.01	22.88	37.69	33.89	1.54	70.0
V3	4.81	32.86	38.21	20.07	4.06	70.9
V4	0.00	22.25	61.12	16.63	0.00	74.0
Difference V4-V1 (%)	-5.58	-15.91	21.79	-0.22	-0.08	0.2%

Table 5.12 MATLAB and volume results for patient 7_R_S

A graph of % class versus visit is shown in figure 5.14.

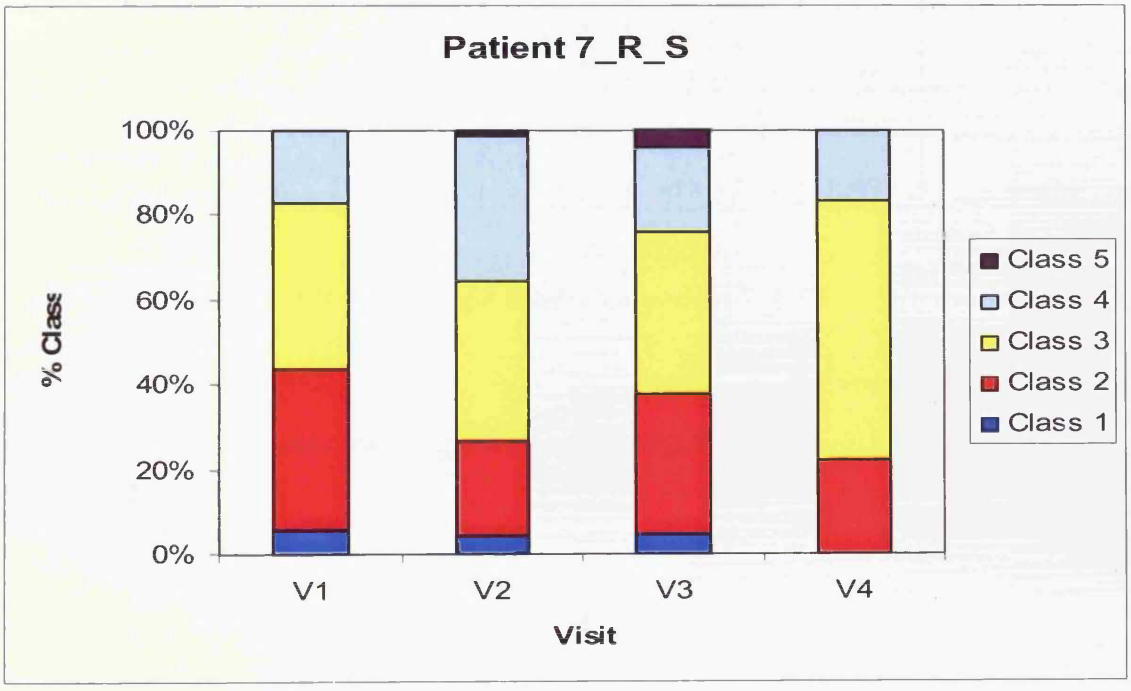

Figure 5.14 MATLAB analysis of % class versus visit for patient 7_R_S

There is a 21.79% increase in class 3 with a reduction in class 2 of 15.91%. There is no change in classes 4 or 5, and almost no change from the classes 1, 2 & 3 (soft) to classes 4 & 5 (harder type tissues). There is no significant change in plaque volume between V1 and V4 (p=0.995). The volume changes between V1 and V2 and also between V3 and V4 are significant (p=0.001, p=0.006), but the volume change between V2 and V3 is not significant (P=0.64).

5.4.2.10 Patient 7_L_S

The left carotid plaque was found on the posterior wall of the distal CCA. The analysis results are found in table 5.13.

	Class 1 (%)	**Class 2 (%)**	**Class 3 (%)**	**Class 4 (%)**	**Class 5 (%)**	**Mean Volume (mm^3)**
V1	0.00	12.86	37.43	37.89	11.83	55.1
V2	0.00	17.59	40.09	33.00	9.32	56.2
V3	0.90	20.62	43.35	27.62	7.51	56.5
V4	2.96	36.15	32.82	24.32	3.76	56.1
Difference V4-V1 (%)	2.96	23.29	-4.61	-13.57	-8.07	1.8%

Table 5.13 MATLAB and volume results for patient 7_L_S

A graph of % class versus visit is shown in figure 5.15.

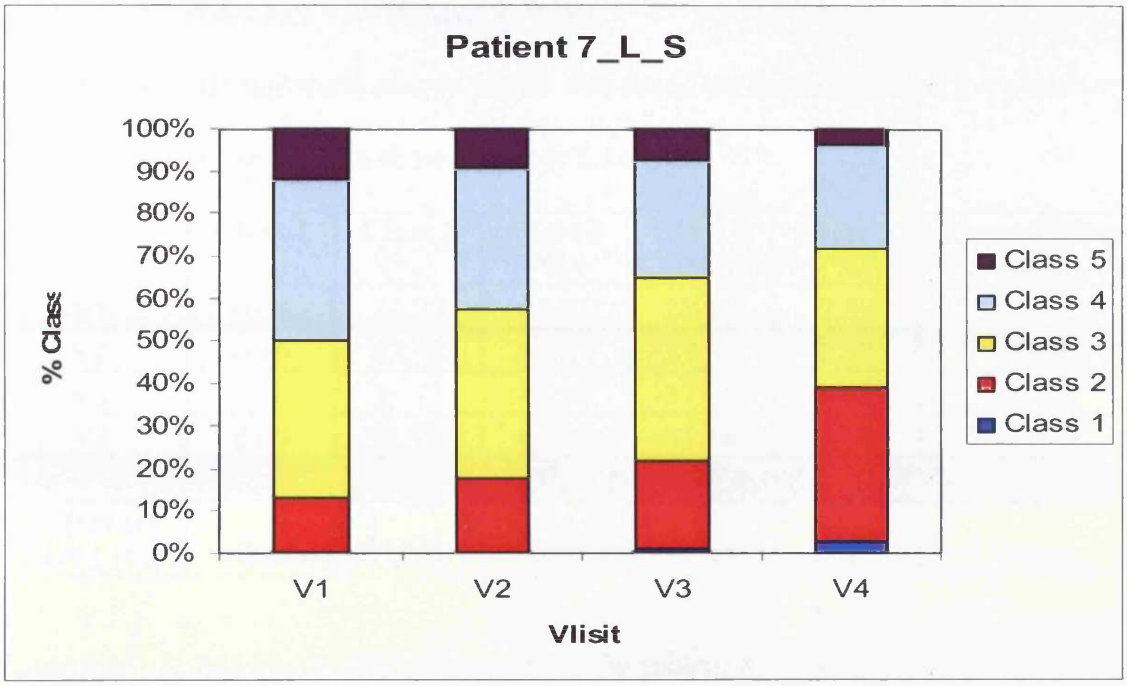

Figure 5.15 MATLAB analysis of % class versus visit for patient 7_L_S

The results of this patient's left carotid plaque show a different trend than all the other statin patients and even this patient's contralateral plaque. There is an increase in class 2 of 23.29% which is made up of reductions in the harder classes 4 and 5 of 13.57% and 8.07% respectively. This results in an increase of 21.64% of the classes 1, 2 & 3 (softer type tissues).

There is a non significant 1.8% increase in plaque volume (p=0.791) between V1 and V4 and between all the intermediate visits V1 & V2, V2 & V3, and V3 & V4 (p=0.753, p=0.996, p=0.991).

5.4.2.11 Patient 8_R_S

This patient had a unilateral plaque which was found on the left side of the posterior wall. The analysis results are shown in table 5.14.

	Class 1 (%)	Class 2 (%)	Class 3 (%)	Class 4 (%)	Class 5 (%)	Mean Volume (mm^3)
V1	0.64	20.27	48.03	28.16	2.89	85.3
V2	0.16	13.58	46.17	37.57	2.52	84.4
V3	0.00	13.77	42.53	37.01	6.69	85.7
V4	0.00	6.57	48.92	41.14	3.36	86.2
Difference V4-V1 (%)	-0.64	-13.70	0.89	12.98	0.47	1.0%

Table 5.14 MATLAB and volume results for patient 8_R_S

A graph of % class versus visit is shown in figure 5.16.

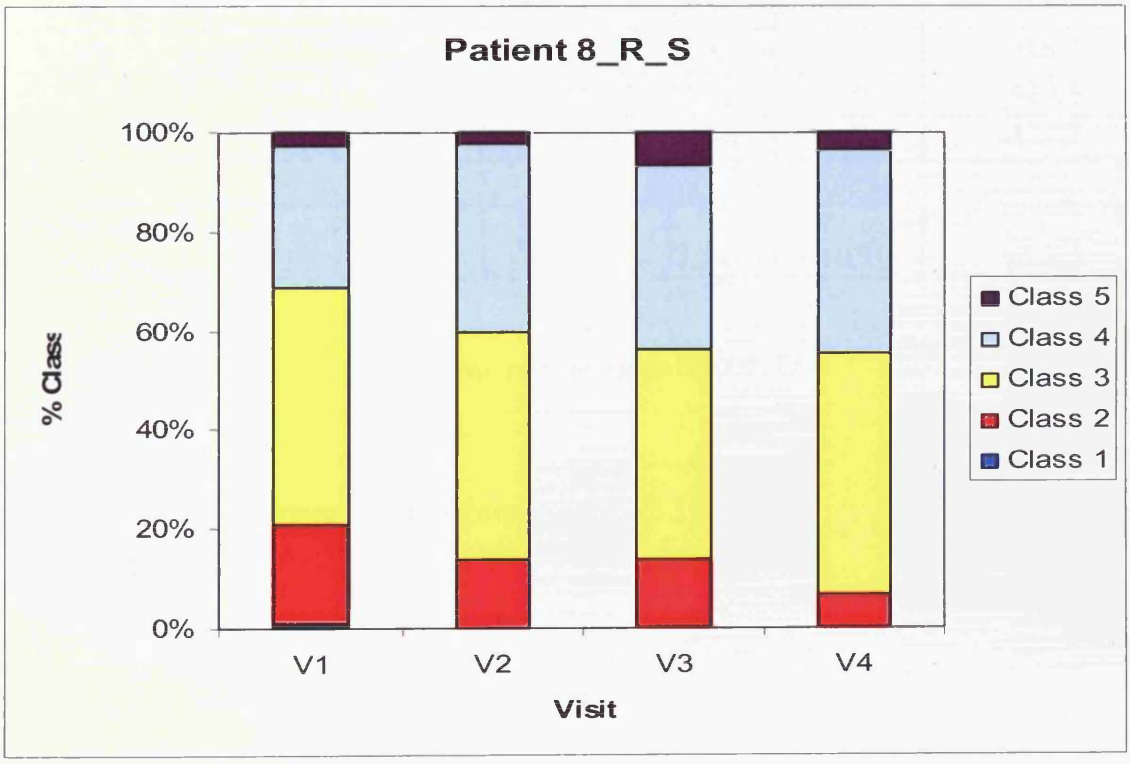

Figure 5.16 MATLAB analysis of % class versus visit for patient 8_R_S

This patient shows a slight increase of 12.98% in class 4 which is within the estimated system variation and is just below the level of what constitutes a real change. There is a reduction in class 2 of 13.7%. The change from classes 1, 2 & 3 (soft types) to classes 4 & 5 (harder types) is 13.45%. There is a non significant 1.0% increase in plaque volume (p=0.743) between V1 and V4 and between all the intermediate visits V1 & V2, V2 & V3, and V3 & V4 (p=0.743, p=0.45, p=0.955).

5.4.2.12 Patient 9_L_S

The plaque was found on the anterior, right side and posterior walls of the distal CCA and extended into the proximal ICA. The results are shown in table 5.15.

	Class 1 (%)	**Class 2 (%)**	**Class 3 (%)**	**Class 4 (%)**	**Class 5 (%)**	**Mean Volume (mm^3)**
V1	2.73	20.38	33.03	27.10	16.76	415.7
V2	0.63	8.90	36.79	44.61	9.07	418.2
V3	1.89	19.61	28.22	35.18	15.09	420.3
V4	2.16	19.95	37.09	34.84	5.96	414.2
Difference V4-V1 (%)	-0.57	-0.43	4.06	7.74	-10.80	-0.3%

Table 5.15 MATLAB and volume results for patient 9_L_S

A graph of % class versus visit is shown in figure 5.17.

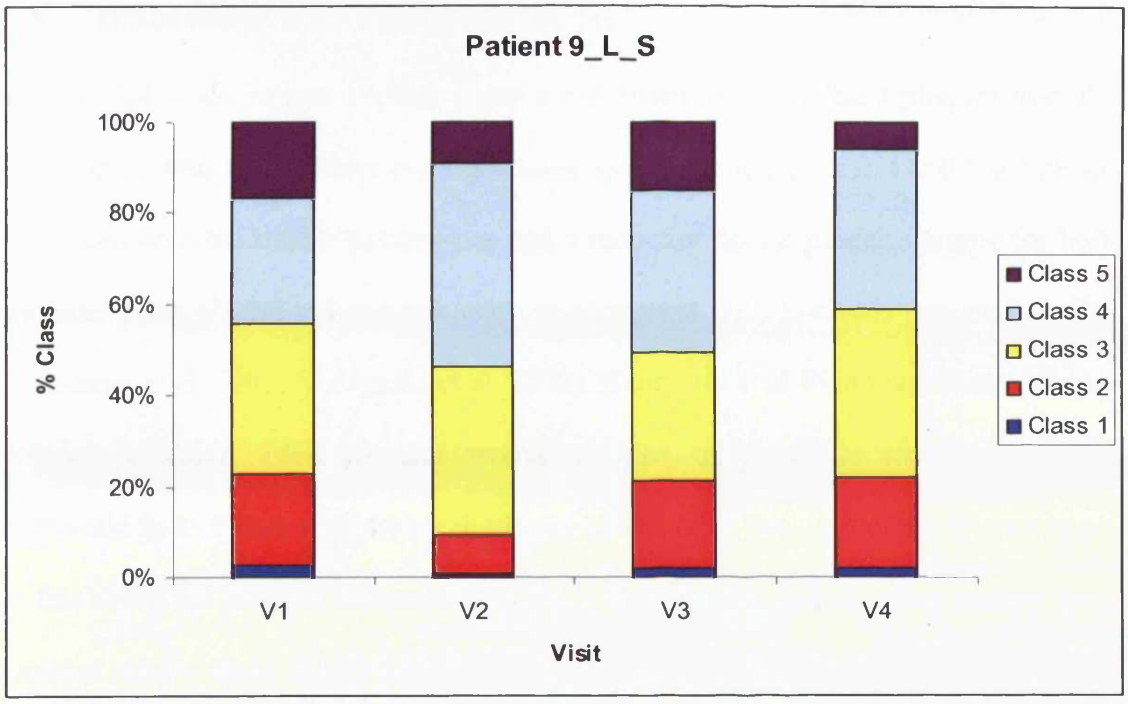

Figure 5.17 MATLAB analysis of % class versus visit for patient 9_L_S

There is no real change in any of the classes over the 4 visits; all changes are below 13.7%. There is no significant change in plaque volume (p=0.975) between V1 and V4 and between all the intermediate visits V1 & V2, V2 & V3, and V3 & V4 (p=0.788, p=0.889, p=0.207).

5.5 Discussion

The two apheresis patient's results show a consistent trend for the 4 plaques over the series of the four visits. There is a significant increase in the classes 4 and 5 which are associated with the harder tissue types and a reduction in the plaque volume for both patients. This plaque volume reduction is consistent with previous reported studies (Hennerici et al. 1991; Matsuzaki et al. 2002). Hennerici et al found significant plaque volume reduction after six and twelve months of apheresis treatment, where Matsuzaki et al found a reduction in plaque extent after twelve months of treatment. In this study the plaques were assessed for a three month period, other studies have reported results from longer periods of treatment from six months to 7.8 years. It is evident that the effects of the apheresis can be seen soon after the treatment has been started with significant plaque volume reductions seen in 3 of the 4 plaques after four weeks. However, the major change in the tissue types is not seen until the final visit where the significant increases in classes 4 and 5 occur for all the four plaques. Future studies would need to assess the treatment effects over longer time periods.

The reported studies (Hennerici et al. 1991; Koga et al. 1999; Matsuzaki et al. 2002) all look at changes in plaque volume, area or IMT and have not reported any changes of the tissue type. The study by Hoffmann et al (2003) showed changes in calcified plaque density and plaque volume reduction and is the only study to report changes in a specific component of the plaque.

In this study it has been shown that LDL apheresis has the effect of reducing plaque volume and changing the plaque constituents to classes 4 & 5 which are associated with the more stable tissue types of calcification, elastic and fibrous tissue.

The results for the statin patients are not as clear or pronounced as the apheresis patients.

Of the nine patients changes in either tissue type or plaque volume can be seen in four (patient #'s 3, 5, 6 & 7). No real change can be seen in another four of the patients (#'s 2, 4, 8 & 9) with one patient (#1) inconclusive due to missing data. There may be several reasons why changes are seen in the apheresis and some statin patients but not in the others.

The reduction in plasma LDL cholesterol levels for a liposorber apheresis system is in the region of 80% after a single 2-3 hour treatment (Schmaldienst et al. 2000). A daily dose of 40mg of atorvastatin has been reported to lower plasma LDL cholesterol by 48% (Roberts 1997). The greater reduction in plasma LDL cholesterol levels in apheresis patients combined with the relatively short period of time of this study may have contributed to why the effects were seen in both apheresis, but only half the statin patients. A comparison of changes in the plaques with reductions in blood cholesterol levels was not possible but may have shown useful trends. As stated earlier the effects of changing tissue type was only seen between V3 and V4 in the apheresis patients and because of the smaller reduction in plasma LDL cholesterol levels from statins it may take a longer period of treatment for the effects to be noticed. One reported study found no change in vessel area and wall thickness after 6 months of treatment but significant reduction after 12 months (Corti et al. 2001). The short period of time involved in this study is unusual, only one study mentioned previously used the same three month period (Crisby et al. 2001). Other studies have monitored the effects over six months (Corti et al. 2001; Lima et al. 2004; Kawasaki et al. 2005), others twelve months or longer (de Groot et al. 1998; Corti et al. 2001; Zhao et al. 2001; Taylor et al. 2002).

Another possible reason why changes are seen in some statin patients and not in the others may be linked to the amount of the classes 4 and 5 (harder types) present in the

plaque at the initial visit. Previous studies have shown that lipid content decreases and collagen, calcium and fibrous tissue increases after statin treatment (Crisby et al. 2001; Zhao et al. 2001; Kawasaki et al. 2005). So if not much lipid is present in the plaque then the changes over the period of the treatment will be minimal. Two of the four patients (#2 & #4) where no significant reduction was seen consisted mainly of classes 4 and 5 in their initial visit. The other two patients (#8 & #9) where no significant reduction occurred consisted of ~30% and 50% classes 4 & 5 respectively at initial visit.

One of the four patients (#6), where a change occurred, consisted of ~70% classes 4 and 5 initially and showed a slight increase in these classes over the visits but with no increase in plaque volume. The largest changes were seen in plaques #3 and #5. Initially plaque #5 consisted almost entirely of classes 1, 2 & 3 but there was ~30% increase in class 4 over the visits, with a slight increase in plaque volume. Patient #3 had bilateral plaques with different plaque components at the initial visit. The plaque on the left consisted of ~66% classes 4 or 5 initially which increased to ~90% over the four visits with no significant plaque volume reduction. The right sided plaque consisted of only 10% classes 4 and 5 initially which increased to over 60% over the visits. This increase was accompanied by a significant plaque volume reduction. All four plaques of the two apheresis patients consisted of less than 40 % of classes 4 & 5 and showed significant increases in these classes with reduction of plaque volumes over the four visits. The results show that change is dependant on the amount of lipid and soft tissue components present in the plaque initially. Only one patient showed a different trend over the period of the study (#7), with the plaque on the left side showing an increase in classes 1, 2 & 3 (softer tissue types) with no significant change in plaque volume.

The effects of apheresis and statin treatment on the plaques is to make the overall plaque composition harder. This may be due to the removal of the softer classes 1, 2 and 3 thus making the overall composition harder, or it may be due to classes 1, 2 and 3 being converted into more fibrotic type material. Either of these processes will increase the hardness of the whole plaque.

In conclusion the results suggest the more aggressive apheresis treatment had the effect of changing the tissue characteristics and volume of carotid atherosclerotic plaques over a period of three months. The effects of statin treatment are not as noticeable over the three month period but may manifest over a longer time period. The results also suggest that change may also be dependant on the amount of soft tissue components present in the plaque at initial presentation.

Chapter 6: Conclusions

The main aim of this project was to see whether the constituents of carotid atherosclerotic plaque could be characterised using B-mode ultrasound. Previous studies from the department (Rakebrandt et al. 2000; Rakebrandt 2001) characterised B-mode ultrasound *in vitro* images of carotid plaques with histology using statistical and textural analysis methods. This study expanded the methods developed in the previous work to *in vivo* images of carotid plaques.

The initial work was to develop a method of acquiring the *in vivo* images. A commercially available 3D ultrasound system was used to acquire the *in vivo* data set. The 3D system had no positioning device so a mechanical gantry device was designed and built to house the ultrasound transducer and drive it down the patient's neck at a set rate and a set distance in a repeatable manner. The 3D data set was transferred to a PC and analysed using MATLAB software programs. The MATLAB software allowed the 3D data to be displayed in the 3 orthogonal orientations. Using a cross sectional cut through the artery, regions of interest around the plaque could be selected for each 2D image in the 3D volume set. An artificial neural network was trained using the statistical and textural parameter data to classify the regions of interest into one of five classes. Inter and intra observer variability studies were calculated to estimate the agreement between different observers in the selection of the ROIs and to estimate the degree of repeatability of the selections and also to estimate the variation that is associated with repositioning in the serial (repeat) scans.

Four carotid plaques were subjected to histological analysis for the five tissue types of fibrous, elastic, calcium, lipid and haemorrhage and compared to the 3D *in vivo* data set acquired pre CEA. The plaques were also scanned *in vitro* to aid in the comparison procedure. No comparison was found between any of the individual

histology sections and corresponding *in vivo* images or for the plaques taken as a whole. After studying the 4 plaques, the conclusion was that characterisation of carotid plaque components from *in vivo* imaging is not achievable using the MATLAB classifier, so no further studies were performed. There are several possible reasons for the lack of correlation including problems with plaque orientation, effects of the overlying tissues, and the effect of the CEA operation on the plaques and the histological processing and analysis. The histology processing appears to have the significant effect on the comparison; plaque volume measurements estimated reductions of between 14.5 and 33% between *in vivo* and histology for the four plaques. The decalcification of the plaques during the processing stage has a bearing on the estimation of the amounts of the different plaque constituents. The amounts of haemorrhage in the 4 plaques that were reported by histology were larger than expected and may be due to a lack of differentiation of the different types of haemorrhage that may be present in a plaque (e.g. haemorrhage caused by surgery). In summary, the conclusion that characterisation of *in vivo* carotid plaque tissue was not readily achievable using the MATLAB classifier is consistent with other reported studies.(Ratliff et al. 1985; Widder et al. 1990; Gaunt et al. 1996; White et al. 1997; Montauban van Swijndregt et al. 1998; Lammie et al. 2000).

Another aim of this project was to see if the system was capable of monitoring the effects of lipid lowering therapies on carotid atherosclerotic plaques. Although the system is not capable of identifying specific tissue types, it may be capable of monitoring changes in the statistical and textural parameters in serial scans which may indicate a change in general tissue type (soft or hard). There were two types of lipid treatments tested over a 12 week period. Two patients on LDL apheresis treatment both showed reductions in classes 1, 2 and 3, which are associated with the softer

tissue types and increases in the classes 4 and 5 which are associated with the harder tissue types. There was also a significant reduction in the plaque volume over the study period.

The second group consisted of 9 patients on statin drug treatment. The results are not as clear as the apheresis group with approximately half the patients showing some effects. There are several possible reasons why changes were seen in some and not in others. The 12 week time period is very short, with only one other reported study of 3 months, so the effects may take longer to manifest in the statin group than in the apheresis group where the treatment is more aggressive. The results also suggest that the relative amounts of class types 1, 2 & 3 (soft tissues) present in the plaque at the start of the study has a bearing on whether changes will occur or not. Patients with mainly classes 4 and 5 (hard tissue types) appear to show no significant change over the period of the study. These results are consistent with reported studies which have shown that lipid content decreases and the harder tissue types of collagen, fibrous and calcium increases (Crisby et al. 2001; Zhao et al. 2001; Kawasaki et al. 2005).

Future work may involve refining the techniques to look at soft versus hard plaque characteristics and try to objectively distinguish the dangerous types of plaques. A refinement of the classifier to 3 classes instead of 5 may be more useful. Classification of carotid plaques into soft, intermediate or hard may be more useful for the surgeon in deciding whether to operate, especially in the case where the degree of carotid stenosis is less than 70%. It may also be useful if future studies of the classifier could be compared with some other method of objective classification, for example GSM analysis. Future studies on the effects of drug treatments should monitor for longer time periods and the techniques could be used to better target

plaques to a specific type of statin (e.g. more aggressive atorvastatin to soft type plaques).

Future work could also benefit from recent advances in ultrasound technology. The work in this thesis began in 2001 and the Toshiba Powervision ultrasound machine has now been replaced by a new generation of ultrasound machines. The new generation of machines are of higher specification and often incorporate new and emerging ultrasound technology including spatial compound imaging, frequency compounding and single crystal transducer technology which improves image quality and allow better delineation of the plaque from the vessel. The new machines also include 3D ultrasound systems as standard, which with the advent of high speed computers allow faster generation of reconstructed 3D images. The new 3D systems allow cardiac gating, 3D real time (4D) scanning is also possible using 2D array transducers, and they also can use an automated segmentation approach or edge tracking technique to select ROI boundaries. In future work, it may be possible to apply the classification system directly to the raw 3D data without the need for MATLAB. It may also be possible to analyse the plaques in any of the three orthogonal planes and calculate the plaque volume directly from the ultrasound 3D scan.

References

Ainsworth, C. D., Blake, C. C., Tamayo, A., Beletsky, V., Fenster, A., et al. (2005). "3D ultrasound measurement of change in carotid plaque volume: a tool for rapid evaluation of new therapies." Stroke **36**(9): 1904-9.

Almond, D. C. and Pryce, W. I. J. (1982). "Characterisation of in vivo placental ultrasonic images using digital techniques - A preliminary report." Ultrasound Med. Biol. **8**(1): 29-39.

Aly, S. and Bishop, C. C. (2000). "An objective characterization of atherosclerotic lesion: an alternative method to identify unstable plaque." Stroke **31**(8): 1921-4.

American-Heart-Association (2005). "Heart disease and stroke statistics - 2005 update" Dallas, Texas: © 2005 American Heart Association.

Ariet, M., Geiser, E. A., Lupkiewicz, S. M., Conetta, D. A. and Conti, C. R. (1984). "Evaluation of a three-dimensional reconstruction to compute left ventricular volume and mass." Am J Cardiol **54**(3): 415-20.

Arnold, A., Taylor, P., Poston, R., Modaresi, K. and Padayachee, S. (2001). "An objective method for grading ultrasound images of carotid artery plaques." Ultrasound Med Biol **27**(8): 1041-7.

Arnold, J. A., Modaresi, K. B., Thomas, N., Taylor, P. R. and Padayachee, T. S. (1999). "Carotid plaque characterization by duplex scanning: observer error may undermine current clinical trials." Stroke **30**(1): 61-5.

Asvestas, P., Golemati, S., Matsopoulos, G. K., Nikita, K. S. and Nicolaides, A. N. (2002). "Fractal dimension estimation of carotid atherosclerotic plaques from B-mode ultrasound: a pilot study." Ultrasound Med Biol **28**(9): 1129-36.

Avril, G., Batt, M., Guidoin, R., Marois, M., Hassen-Khodja, R., et al. (1991). "Carotid endarterectomy plaques: correlations of clinical and anatomic findings." Ann Vasc Surg **5**(1): 50-4.

Balen, F. G., Allen, C. M., Gardener, J. E., Siddle, N. C. and Lees, W. R. (1993). "3-dimensional reconstruction of ultrasound images of the uterine cavity." Br J Radiol **66**(787): 588-91.

Bamford, J., Sandercock, P., Dennis, M., Burn, J. and Warlow, C. (1991). "Classification and natural history of clinically identifiable subtypes of cerebral infarction." Lancet **337**(8756): 1521-6.

Barrett-Connor, E. and Khaw, K. T. (1988). "Diabetes mellitus: an independent risk factor for stroke?" Am J Epidemiol **128**(1): 116-23.

Basset, O., Sun, Z., Mestas, J. L. and Gimenez, G. (1993). "Texture analysis of ultrasonic images of the prostate by means of co-occurrence matrices." Ultrason Imaging **15**(3): 218-37.

Baxt, W. G. (1995). "Application of artificial neural networks to clinical medicine." Lancet **346**(8983): 1135-8.

Belohlavek, M., Foley, D. A., Gerber, T. C., Greenleaf, J. F. and Seward, J. B. (1993). "Three-dimensional ultrasound imaging of the atrial septum: normal and pathologic anatomy." J Am Coll Cardiol **22**(6): 1673-8.

Binder, T., Globits, S., Zangeneh, M., Gabriel, H., Rothy, W., et al. (1996). "Three-dimensional echocardiography using a transoesophageal imaging probe. Potentials and technical considerations." Eur Heart J **17**(4): 619-28.

Bland, J. M. and Altman, D. G. (1986). "Statistical methods for assessing agreement between two methods of clinical measurement." Lancet **1**(8476): 307-10.

Blauw, G. J., Lagaay, A. M., Smelt, A. H. and Westendorp, R. G. (1997). "Stroke, statins, and cholesterol. A meta-analysis of randomized, placebo-controlled, double-blind trials with HMG-CoA reductase inhibitors." Stroke **28**(5): 946-50.

Bluth, E. I., Kay, D., Merritt, C. R., Sullivan, M., Farr, G., et al. (1986). "Sonographic characterization of carotid plaque: detection of hemorrhage." AJR Am J Roentgenol **146**(5): 1061-5.

Bonilla-Musoles, F., Raga, F. and Osborne, N. G. (1995). "Three-dimensional ultrasound evaluation of ovarian masses." Gynecol Oncol **59**(1): 129-35.

Cave, E. M., Pugh, N. D., Wilson, R. J., Sissons, G. R. and Woodcock, J. P. (1995). "Carotid artery duplex scanning: does plaque echogenicity correlate with patient symptoms?" Eur J Vasc Endovasc Surg **10**(1): 77-81.

Chen, W. M., Chang, R. F., Kuo, S. J., Chang, C. S., Moon, W. K., et al. (2005). "3-D ultrasound texture classification using run difference matrix." Ultrasound Med Biol **31**(6): 763-70.

Corti, R., Fayad, Z. A., Fuster, V., Worthley, S. G., Helft, G., et al. (2001). "Effects of lipid-lowering by simvastatin on human atherosclerotic lesions: a longitudinal study by high-resolution, noninvasive magnetic resonance imaging." Circulation **104**(3): 249-52.

Crisby, M., Nordin-Fredriksson, G., Shah, P. K., Yano, J., Zhu, J., et al. (2001). "Pravastatin treatment increases collagen content and decreases lipid content, inflammation, metalloproteinases, and cell death in human carotid plaques: implications for plaque stabilization." Circulation **103**(7): 926-33.

Crouse, J. R., 3rd, Byington, R. P., Bond, M. G., Espeland, M. A., Craven, T. E., et al. (1995). "Pravastatin, Lipids, and Atherosclerosis in the Carotid Arteries (PLAC-II)." Am J Cardiol **75**(7): 455-9.

Daponte, J. S. and Sherman, P. (1991). "Classification of ultrasonic image texture by statistical discrimination analysis of neural networks." Computer Med Imaging Graph **15**(1): 3-9.

de Bray, J. M., Baud, J. M., Delanoy, P., Camuzat, J. P., Dehans, V., et al. (1998). "Reproducibility in ultrasonic characterization of carotid plaques." Cerebrovasc Dis **8**(5): 273-7.

de Groot, E., Jukema, J. W., Montauban van Swijndregt, A. D., Zwinderman, A. H., Ackerstaff, R. G., et al. (1998). "B-mode ultrasound assessment of pravastatin treatment effect on carotid and femoral artery walls and its correlations with coronary arteriographic findings: a report of the Regression Growth Evaluation Statin Study (REGRESS)." J Am Coll Cardiol **31**(7): 1561-7.

de Weert, T. T., Ouhlous, M., Zondervan, P. E., Hendriks, J. M., Dippel, D. W., et al. (2005). "In vitro characterization of atherosclerotic carotid plaque with multidetector computed tomography and histopathological correlation." Eur Radiol **15**(9): 1906-14.

Delcker, A. and Diener, H. C. (1994). "Quantification of atherosclerotic plaques in carotid arteries by three-dimensional ultrasound." Br J Radiol **67**(799): 672-8.

Denzel, C., Balzer, K., Muller, K. M., Fellner, F., Fellner, C., et al. (2003). "Relative value of normalized sonographic in vitro analysis of arteriosclerotic plaques of internal carotid artery." Stroke **34**(8): 1901-6.

Denzel, C., Fellner, F., Wutke, R., Bazler, K., Muller, K. M., et al. (2003). "Ultrasonographic analysis of arteriosclerotic plaques in the internal carotid artery." Eur J Ultrasound **16**(3): 161-7.

Devonald, K. J., Ellwood, D. A., Griffiths, K. A., Kossoff, G., Gill, R. W., et al. (1995). "Volume imaging: three-dimensional appreciation of the fetal head and face." J Ultrasound Med **14**(12): 919-25.

Dobrin, P. B. (1996). "Effect of histologic preparation on the cross-sectional area of arterial rings." J Surg Res **61**(2): 413-5.

DOH (2005). Reducing brain damage: Faster access to better stroke care. Department of Health, National Audit Office. London.

Downey, D. B. and Fenster, A. (1995). "Vascular imaging with a three-dimensional power Doppler system." AJR Am J Roentgenol **165**(3): 665-8.

Dyson, R. L., Pretorius, D. H., Budorick, N. E., Johnson, D. D., Sklansky, M. S., et al. (2000). "Three-dimensional ultrasound in the evaluation of fetal anomalies." Ultrasound Obstet Gynecol **16**(4): 321-8.

ECPSG (1995). "Carotid artery plaque composition--relationship to clinical presentation and ultrasound B-mode imaging. European Carotid Plaque Study Group." Eur J Vasc Endovasc Surg **10**(1): 23-30.

ECST (1998). "Randomised trial of endarterectomy for recently symptomatic carotid stenosis: final results for MRC European Carotid Surgery Trial (ECST)." Lancet **351**: 1379-1387.

El-Barghouty, N., Geroulakos, G., Nicolaides, A., Androulakis, A. and Bahal, V. (1995). "Computer-assisted carotid plaque characterisation." Eur J Vasc Endovasc Surg **9**(4): 389-93.

El-Barghouty, N. M., Levine, T., Ladva, S., Flanagan, A. and Nicolaides, A. (1996). "Histological verification of computerised carotid plaque characterisation." Eur J Vasc Endovasc Surg **11**(4): 414-6.

Elatrozy, T., Nicolaides, A., Tegos, T., Zarka, A. Z., Griffin, M., et al. (1998). "The effect of B-mode ultrasonic image standardisation on the echodensity of symptomatic and asymptomatic carotid bifurcation plaques." Int Angiol **17**(3): 179-86.

Eliasziw, M., Streifler, J. Y., Fox, A. J., Hachinski, V. C., Ferguson, G. G., et al. (1994). "Significance of plaque ulceration in symptomatic patients with high-grade carotid stenosis. North American Symptomatic Carotid Endarterectomy Trial." Stroke **25**(2): 304-8.

Falk, E. (1992). "Why do plaques rupture?" Circulation **86**(6 Suppl): III30-42.

Feeley, T. M., Leen, E. J., Colgan, M. P., Moore, D. J., Hourihane, D. O., et al. (1991). "Histologic characteristics of carotid artery plaque." J Vasc Surg **13**(5): 719-24.

Fenster, A., Downey, D. B. and Cardinal, H. N. (2001). "Three-dimensional ultrasound imaging." Phys Med Biol **46**(5): R67-99.

Furberg, C. D. (1999). "Natural statins and stroke risk." Circulation **99**(2): 185-8.

Furberg, C. D., Adams, H. P., Jr., Applegate, W. B., Byington, R. P., Espeland, M. A., et al. (1994). "Effect of lovastatin on early carotid atherosclerosis and cardiovascular events. Asymptomatic Carotid Artery Progression Study (ACAPS) Research Group." Circulation **90**(4): 1679-87.

Fuster, V., Stein, B., Ambrose, J. A., Badimon, L., Badimon, J. J., et al. (1990). "Atherosclerotic plaque rupture and thrombosis. Evolving concepts." Circulation **82**(3 Suppl): II47-59.

Garra, B. S., Krasner, B. H., Horii, S. C., Ascher, S., Mun, S. K., et al. (1993). "Improving the distinction between benign and malignant breast lesions: the value of sonographic texture analysis." Ultrason Imaging **15**(4): 267-85.

Gaunt, M. E., Brown, L., Hartshorne, T., Bell, P. R. and Naylor, A. R. (1996). "Unstable carotid plaques: preoperative identification and association with intraoperative embolisation detected by transcranial Doppler." Eur J Vasc Endovasc Surg **11**(1): 78-82.

Geroulakos, G., Hobson, R. W. and Nicolaides, A. (1996). "Ultrasonographic carotid plaque morphology in predicting stroke risk." Br J Surg **83**(5): 582-7.

Geroulakos, G., Ramaswami, G., Nicolaides, A., James, K., Labropoulos, N., et al. (1993). "Characterization of symptomatic and asymptomatic carotid plaques using high-resolution real-time ultrasonography." Br J Surg **80**(10): 1274-7.

Go, A. S., Hylek, E. M., Phillips, K. A., Chang, Y., Henault, L. E., et al. (2001). "Prevalence of diagnosed atrial fibrillation in adults: national implications for rhythm management and stroke prevention: the AnTicoagulation and Risk Factors in Atrial Fibrillation (ATRIA) Study." Jama **285**(18): 2370-5.

Goldstein, L. B., Adams, R., Becker, K., Furberg, C. D., Gorelick, P. B., et al. (2001). "Primary prevention of ischemic stroke: A statement for healthcare professionals from the Stroke Council of the American Heart Association." Stroke **32**(1): 280-99.

Golledge, J., Greenhalgh, R. M. and Davies, A. H. (2000). "The symptomatic carotid plaque." Stroke **31**(3): 774-81.

Grant, E. G., Benson, C. B., Moneta, G. L., Alexandrov, A. V., Baker, J. D., et al. (2003). "Carotid artery stenosis: gray-scale and Doppler US diagnosis--

Society of Radiologists in Ultrasound Consensus Conference." Radiology **229**(2): 340-6.

Gray-Weale, A. C., Graham, J. C., Burnett, J. R., Byrne, K. and Lusby, R. J. (1988). "Carotid artery atheroma: comparison of preoperative B-mode ultrasound appearance with carotid endarterectomy specimen pathology." J Cardiovasc Surg (Torino) **29**(6): 676-81.

Griewing, B., Schminke, U., Morgenstern, C., Walker, M. L. and Kessler, C. (1997). "Three-dimensional ultrasound angiography (power mode) for the quantification of carotid artery atherosclerosis." J Neuroimaging **7**(1): 40-5.

Haralick, R. M., Shanmugam, K. and Dinstein, I. (1973). "Textural features for image classification." IEEE Transactions on Systems, Man and Cybernetics **3**(6): 610-621.

Hata, T., Yanagihara, T., Matsumoto, M., Hanaoka, U., Maesato, T., et al. (1999). "Three-dimensional sonographic features of Hydrops fetalis." Gynecol Obstet Invest **48**(3): 172-5.

Hatsukami, T. S., Thackray, B. D., Primozich, J. F., Ferguson, M. S., Burns, D. H., et al. (1994). "Echolucent regions in carotid plaque: preliminary analysis comparing three-dimensional histologic reconstructions to sonographic findings." Ultrasound Med Biol **20**(8): 743-9.

Heiss, G., Sharrett, A. R., Barnes, R., Chambless, L. E., Szklo, M., et al. (1991). "Carotid atherosclerosis measured by B-mode ultrasound in populations: associations with cardiovascular risk factors in the ARIC study." Am J Epidemiol **134**(3): 250-6.

Hennerici, M., Kleophas, W. and Gries, F. A. (1991). "Regression of carotid plaques during low density lipoprotein cholesterol elimination." Stroke **22**(8): 989-92.

Hennerici, M., Reifschneider, G., Trockel, U. and Aulich, A. (1984). "Detection of early atherosclerotic lesions by duplex scanning of the carotid artery." J Clin Ultrasound **12**(8): 455-63.

Hoffmann, U., Derfler, K., Haas, M., Stadler, A., Brady, T. J., et al. (2003). "Effects of combined low-density lipoprotein apheresis and aggressive statin therapy on coronary calcified plaque as measured by computed tomography." Am J Cardiol **91**(4): 461-4.

Huynen, A. L., Giesen, R. J., de la Rosette, J. J., Aarnink, R. G., Debruyne, F. M., et al. (1994). "Analysis of ultrasonographic prostate images for the detection of prostatic carcinoma: the automated urologic diagnostic expert system." Ultrasound Med Biol **20**(1): 1-10.

Imparato, A. M., Riles, T. S., Mintzer, R. and Baumann, F. G. (1983). "The importance of hemorrhage in the relationship between gross morphologic characteristics and cerebral symptoms in 376 carotid artery plaques." Ann Surg **197**(2): 195-203.

Johnsen, S. H., Mathiesen, E. B., Fosse, E., Joakimsen, O., Stensland-Bugge, E., et al. (2005). "Elevated high-density lipoprotein cholesterol levels are protective against plaque progression: a follow-up study of 1952 persons with carotid atherosclerosis the Tromso study." Circulation **112**(4): 498-504.

Johnson, D. D., Pretorius, D. H., Riccabona, M., Budorick, N. E. and Nelson, T. R. (1997). "Three-dimensional ultrasound of the fetal spine." Obstet Gynecol **89**(3): 434-8.

Johnson, J. M., Kennelly, M. M., Decesare, D., Morgan, S. and Sparrow, A. (1985). "Natural history of asymptomatic carotid plaque." Arch Surg **120**(9): 1010-2.

Kardoulas, D. G., Katsamouris, A. N., Gallis, P. T., Philippides, T. P., Anagnostakos, N. K., et al. (1996). "Ultrasonographic and histologic characteristics of symptom-free and symptomatic carotid plaque." Cardiovasc Surg **4**(5): 580-90.

Kawachi, I., Colditz, G. A., Stampfer, M. J., Willett, W. C., Manson, J. E., et al. (1993). "Smoking cessation and decreased risk of stroke in women." Jama **269**(2): 232-6.

Kawasaki, M., Sano, K., Okubo, M., Yokoyama, H., Ito, Y., et al. (2005). "Volumetric quantitative analysis of tissue characteristics of coronary plaques after statin therapy using three-dimensional integrated backscatter intravascular ultrasound." J Am Coll Cardiol **45**(12): 1946-53.

Kiely, D. K., Wolf, P. A., Cupples, L. A., Beiser, A. S. and Myers, R. H. (1993). "Familial aggregation of stroke. The Framingham Study." Stroke **24**(9): 1366-71.

Koga, N., Watanabe, K., Kurashige, Y., Sato, T. and Hiroki, T. (1999). "Long-term effects of LDL apheresis on carotid arterial atherosclerosis in familial hypercholesterolaemic patients." J Intern Med **246**(1): 35-43.

Krupski, W. C. and Moore, W. S. (2005). "Indications, surgical technique, and results of repair of extracranial occlusive lesions." Philadelphia Elsevier Saunders.

Lal, B. K., Hobson, R. W., 2nd, Pappas, P. J., Kubicka, R., Hameed, M., et al. (2002). "Pixel distribution analysis of B-mode ultrasound scan images predicts histologic features of atherosclerotic carotid plaques." J Vasc Surg **35**(6): 1210-7.

Lammie, G. A., Wardlaw, J., Allan, P., Ruckley, C. V., Peek, R., et al. (2000). "What pathological components indicate carotid atheroma activity and can these be identified reliably using ultrasound?" Eur J Ultrasound **11**(2): 77-86.

Landry, A. and Fenster, A. (2002). "Theoretical and experimental quantification of carotid plaque volume measurements made by three-dimensional ultrasound using test phantoms." Med Phys **29**(10): 2319-27.

Landry, A., Spence, J. D. and Fenster, A. (2004). "Measurement of carotid plaque volume by 3-dimensional ultrasound." Stroke **35**(4): 864-9.

Landry, A., Spence, J. D. and Fenster, A. (2005). "Quantification of carotid plaque volume measurements using 3D ultrasound imaging." Ultrasound Med Biol **31**(6): 751-62.

Layer, G., Zuna, I., Lorenz, A., Zerban, H., Haberkorn, U., et al. (1990). "Computerized ultrasound B-scan texture analysis of experimental fatty liver disease: influence of total lipid content and fat deposit distribution." Ultrason Imaging **12**(3): 171-88.

Lee, D. J., Sigel, B., Swami, V. K., Justin, J. R., Gahtan, V., et al. (1998). "Determination of carotid plaque risk by ultrasonic tissue characterization." Ultrasound Med Biol **24**(9): 1291-9.

Lerski, R. A., Smith, M. J., Morley, P., Barnett, E., Mills, P. R., et al. (1981). "Discriminant analysis of ultrasonic texture data in diffuse alcoholic liver disease. 1. Fatty liver and cirrhosis." Ultrason Imaging **3**(2): 164-72.

Lima, J. A., Desai, M. Y., Steen, H., Warren, W. P., Gautam, S., et al. (2004). "Statin-induced cholesterol lowering and plaque regression after 6 months of magnetic resonance imaging-monitored therapy." Circulation **110**(16): 2336-41.

Loh, E., Sutton, M. S., Wun, C. C., Rouleau, J. L., Flaker, G. C., et al. (1997). "Ventricular dysfunction and the risk of stroke after myocardial infarction." N Engl J Med **336**(4): 251-7.

Lovett, J. K., Redgrave, J. N. and Rothwell, P. M. (2005). "A critical appraisal of the performance, reporting, and interpretation of studies comparing carotid plaque imaging with histology." Stroke **36**(5): 1091-7.

Lukovits, T. G., Mazzone, T. M. and Gorelick, T. M. (1999). "Diabetes mellitus and cerebrovascular disease." Neuroepidemiology **18**(1): 1-14.

Lusby, R. J., Ferrell, L. D., Ehrenfeld, W. K., Stoney, R. J. and Wylie, E. J. (1982). "Carotid plaque hemorrhage. Its role in production of cerebral ischemia." Arch Surg **117**(11): 1479-88.

Maeda, K., Utsu, M. and Kihaile, P. E. (1998). "Quantification of sonographic echogenicity with grey-level histogram width: a clinical tissue characterization." Ultrasound Med Biol **24**(2): 225-34.

Maron, D. J., Fazio, S. and Linton, M. F. (2000). "Current perspectives on statins." Circulation **101**(2): 207-13.

Marx, G. R., Fulton, D. R., Pandian, N. G., Vogel, M., Cao, Q. L., et al. (1995). "Delineation of site, relative size and dynamic geometry of atrial septal defects by real-time three-dimensional echocardiography." J Am Coll Cardiol **25**(2): 482-90.

Mathiesen, E. B., Bonaa, K. H. and Joakimsen, O. (2001). "Echolucent plaques are associated with high risk of ischemic cerebrovascular events in carotid stenosis: the tromso study." Circulation **103**(17): 2171-5.

Matsuzaki, M., Hiramori, K., Imaizumi, T., Kitabatake, A., Hishida, H., et al. (2002). "Intravascular ultrasound evaluation of coronary plaque regression by low

density lipoprotein-apheresis in familial hypercholesterolemia: the Low Density Lipoprotein-Apheresis Coronary Morphology and Reserve Trial (LACMART)." J Am Coll Cardiol **40**(2): 220-7.

Mayor, I., Momjian, S., Lalive, P. and Sztajzel, R. (2003). "Carotid plaque: comparison between visual and grey-scale median analysis." Ultrasound Med Biol **29**(7): 961-6.

Mercier, L., Lango, T., Lindseth, F. and Collins, D. L. (2005). "A review of calibration techniques for freehand 3-D ultrasound systems." Ultrasound Med Biol **31**(4): 449-71.

Merz, E., Weber, G., Bahlmann, F. and Miric-Tesanic, D. (1997). "Application of transvaginal and abdominal three-dimensional ultrasound for the detection or exclusion of malformations of the fetal face." Ultrasound Obstet Gynecol **9**(4): 237-43.

Miller, A. S., Blott, B. H. and Hames, T. K. (1992). "Review of neural network applications in medical imaging and signal processing." Med Biol Eng Comput **30**(5): 449-64.

Miller, V. T., Rothrock, J. F., Pearce, L. A., Feinberg, W. M., Hart, R. G., et al. (1993). "Ischemic stroke in patients with atrial fibrillation: effect of aspirin according to stroke mechanism. Stroke Prevention in Atrial Fibrillation Investigators." Neurology **43**(1): 32-6.

Mohr, J. P., Gautier, J.-C. and Pessin, M. S. (1998). "Internal carotid artery disease." Stroke : Pathophysiology, Diagnosis and Management. H. J. Barnett, J. P. Mohr, B. Stein and F. M. Yatsu. Philadelphia, Churchill Livingstone: 355-400.

Montauban van Swijndregt, A. D., Elbers, H. R., Moll, F. L., de Letter, J. and Ackerstaff, R. G. (1998). "Ultrasonographic characterization of carotid plaques." Ultrasound Med Biol **24**(4): 489-93.

Morris, D. T. (1988a). "An evaluation of the use of texture measurements for the tissue characterisation of ultrasonic images of in vivo human placentae." Ultrasound Med Biol **14**(5): 387-95.

Morris, D. T. (1988b). "The correction of ultrasonic image analysis features for their depth dependence." Int J Biomed Comput **22**(2): 143-52.

NASCET (1991). "Beneficial effect of carotid endarterectomy in symptomatic patients with high-grade carotid stenosis. North American Symptomatic Carotid Endarterectomy Trial Collaborators." N Engl J Med **325**(7): 445-53.

Nelson, T. R. and Pretorius, D. H. (1998). "Three-dimensional ultrasound imaging." Ultrasound Med Biol **24**(9): 1243-70.

Nicholas, D., Nassiri, D. K., Garbutt, P. and Hill, C. R. (1986). "Tissue characterization from ultrasound B-scan data." Ultrasound Med Biol **12**(2): 135-43.

Noritomi, T., Sigel, B., Swami, V., Justin, J., Gahtan, V., et al. (1997). "Carotid plaque typing by multiple-parameter ultrasonic tissue characterization." Ultrasound Med Biol **23**(5): 643-50.

Norusis, M. J. (1985). "SPSS-X advanced statistics guide." New York McGraw-Hill.

O'Donnell, T. F., Jr., Erdoes, L., Mackey, W. C., McCullough, J., Shepard, A., et al. (1985). "Correlation of B-mode ultrasound imaging and arteriography with pathologic findings at carotid endarterectomy." Arch Surg **120**(4): 443-9.

O'Leary, D. H., Holen, J., Ricotta, J. J., Roe, S. and Schenk, E. A. (1987). "Carotid bifurcation disease: prediction of ulceration with B-mode US." Radiology **162**(2): 523-5.

Oosterveld, B. J., Thijssen, J. M. and Verhoef, W. A. (1985). "Texture of B-mode echograms: 3-D simulations and experiments of the effects of diffraction and scatterer density." Ultrason Imaging **7**(2): 142-60.

Palombo, C., Kozakova, M., Morizzo, C., Andreuccetti, F., Tondini, A., et al. (1998). "Ultrafast three-dimensional ultrasound: application to carotid artery imaging." Stroke **29**(8): 1631-7.

Penado, S., Cano, M., Acha, O., Hernandez, J. L. and Riancho, J. A. (2003). "Atrial fibrillation as a risk factor for stroke recurrence." Am J Med **114**(3): 206-10.

Picot, P. A., Rickey, D. W., Mitchell, R., Rankin, R. N. and Fenster, A. (1993). "Three-dimensional colour Doppler imaging." Ultrasound Med Biol **19**(2): 95-104.

Pretorius, D. H., Nelson, T. R. and Jaffe, J. S. (1992). "3-dimensional sonographic analysis based on color flow Doppler and gray scale image data: a preliminary report." J Ultrasound Med **11**(5): 225-32.

PSC (1995). "Cholesterol, diastolic blood pressure, and stroke: 13,000 strokes in 450,000 people in 45 prospective cohorts. Prospective studies collaboration." Lancet **346**(8991-8992): 1647-53.

Rakebrandt, F. (2001). "Development of a B-scan texture system for the non-invasive assessment of atherosclerotic plaques." PhD thesis, University of Wales, College of Medicine.

Rakebrandt, F., Crawford, D. C., Havard, D., Coleman, D. and Woodcock, J. P. (2000). "Relationship between ultrasound texture classification images and histology of atherosclerotic plaque." Ultrasound Med Biol **26**(9): 1393-402.

Ratliff, D. A., Gallagher, P. J., Hames, T. K., Humphries, K. N., Webster, J. H., et al. (1985). "Characterisation of carotid artery disease: comparison of duplex scanning with histology." Ultrasound Med Biol **11**(6): 835-40.

Reilly, L. M., Lusby, R. J., Hughes, L., Ferrell, L. D., Stoney, R. J., et al. (1983). "Carotid plaque histology using real-time ultrasonography. Clinical and therapeutic implications." Am J Surg **146**(2): 188-93.

Roberts, W. C. (1997). "The rule of 5 and the rule of 7 in lipid-lowering by statin drugs." Am J Cardiol **80**(1): 106-7.

Ronco, A. L. and Fernandez, R. (1999). "Improving ultrasonographic diagnosis of prostate cancer with neural networks." Ultrasound Med Biol **25**(5): 729-33.

Rosamond, W. D., Folsom, A. R., Chambless, L. E., Wang, C. H., McGovern, P. G., et al. (1999). "Stroke incidence and survival among middle-aged adults: 9-year follow-up of the Atherosclerosis Risk in Communities (ARIC) cohort." Stroke **30**(4): 736-43.

Ross, R. (1993). "The pathogenesis of atherosclerosis: a perspective for the 1990s." Nature **362**(6423): 801-9.

Rumelhart, D. E., Hinton, G. E. and McClelland, J. L. (1986). "A general framework for parallel distributed processing: explorations in the microstructure of cognition volume 1 foundations." Cambridge, Massachusetts. MIT Press.

Sacco, R. L., Boden-Albala, B., Gan, R., Chen, X., Kargman, D. E., et al. (1998). "Stroke incidence among white, black, and Hispanic residents of an urban

community: the Northern Manhattan Stroke Study." Am J Epidemiol **147**(3): 259-68.

Salonen, R., Nyyssonen, K., Porkkala, E., Rummukainen, J., Belder, R., et al. (1995). "Kuopio Atherosclerosis Prevention Study (KAPS). A population-based primary preventive trial of the effect of LDL lowering on atherosclerotic progression in carotid and femoral arteries." Circulation **92**(7): 1758-64.

Schmaldienst, S., Banyai, S., Stulnig, T. M., Heinz, G., Jansen, M., et al. (2000). "Prospective randomised cross-over comparison of three LDL-apheresis systems in statin pretreated patients with familial hypercholesterolaemia." Atherosclerosis **151**(2): 493-9.

Schminke, U., Hilker, L., Motsch, L., Griewing, B. and Kessler, C. (2002). "Volumetric assessment of plaque progression with 3-dimensional ultrasonography under statin therapy." J Neuroimaging **12**(3): 245-51.

Schminke, U., Motsch, L., Griewing, B., Gaull, M. and Kessler, C. (2000). "Three-dimensional power-mode ultrasound for quantification of the progression of carotid artery atherosclerosis." J Neurol **247**(2): 106-11.

Schulte-Altedorneburg, G., Droste, D. W., Haas, N., Kemeny, V., Nabavi, D. G., et al. (2000). "Preoperative B-mode ultrasound plaque appearance compared with carotid endarterectomy specimen histology." Acta Neurol Scand **101**(3): 188-94.

Seeley, R. R., Stephens, T. D. and Tate, P. (2000). "Anatomy & Physiology." London McGraw-Hill.

Seward, J. B., Belohlavek, M., O'Leary, P. W., Foley, D. A. and Greenleaf, J. F. (1995). "Congenital heart disease: wide-field, three-dimensional, and four-dimensional ultrasound imaging." Am J Card Imaging **9**(1): 38-43.

Shankar, P. M., Forsberg, F. and Lown, L. (2003). "Statistical modeling of atherosclerotic plaque in carotid B mode images--a feasibility study." Ultrasound Med Biol **29**(9): 1305-9.

Shinton, R. and Beevers, G. (1989). "Meta-analysis of relation between cigarette smoking and stroke." Bmj **298**(6676): 789-94.

Smilde, T. J., van Wissen, S., Wollersheim, H., Trip, M. D., Kastelein, J. J., et al. (2001). "Effect of aggressive versus conventional lipid lowering on atherosclerosis progression in familial hypercholesterolaemia (ASAP): a prospective, randomised, double-blind trial." Lancet **357**(9256): 577-81.

Spector, T. D. (1999). "An introduction to general pathology" Edinburgh Churchill livingstone.

Steffen, C. M., Gray-Weale, A. C., Byrne, K. E. and Lusby, R. J. (1989). "Carotid artery atheroma: ultrasound appearance in symptomatic and asymptomatic vessels." Aust N Z J Surg **59**(7): 529-34.

Stevens, A. and Lowe, J. (2005). "Human Histology." Philadelphia Elsevier Mosby.

Suk, S. H., Sacco, R. L., Boden-Albala, B., Cheun, J. F., Pittman, J. G., et al. (2003). "Abdominal obesity and risk of ischemic stroke: the Northern Manhattan Stroke Study." Stroke **34**(7): 1586-92.

Taylor, A. J., Kent, S. M., Flaherty, P. J., Coyle, L. C., Markwood, T. T., et al. (2002). "ARBITER: Arterial Biology for the Investigation of the Treatment Effects of Reducing Cholesterol: a randomized trial comparing the effects of atorvastatin and pravastatin on carotid intima medial thickness." Circulation **106**(16): 2055-60.

Tegos, T. J., Kalodiki, E., Sabetai, M. M., Stavropoulos, P. and Nicolaides, A. N. (2000). "New information on the value of plaque characterisation--relation to symptoms." Acta Chir Belg **100**(6): 255-8.

Tuthill, T. A., Krucker, J. F., Fowlkes, J. B. and Carson, P. L. (1998). "Automated three-dimensional US frame positioning computed from elevational speckle decorrelation." Radiology **209**(2): 575-82.

Van Damme, H., Demoulin, J. C., Zicot, M., Creemers, E., Trotteur, G., et al. (1992). "Pathological aspects of carotid plaques. Surgical and clinical significance." J Cardiovasc Surg (Torino) **33**(1): 46-53.

Verhoeven, J. T. and Thijssen, J. M. (1993). "Potential of fractal analysis for lesion detection in echographic images." Ultrason Imaging **15**(4): 304-23.

Waki, H., Masuyama, T., Mori, H., Maeda, T., Kitade, K., et al. (2003). "Ultrasonic tissue characterization of the atherosclerotic carotid artery: histological correlates or carotid integrated backscatter." Circ J **67**(12): 1013-6.

Waters, K. R., Bridal, S. L., Cohen-Bacrie, C., Levrier, C., Fornes, P., et al. (2003). "Parametric analysis of carotid plaque using a clinical ultrasound imaging system." Ultrasound Med Biol **29**(11): 1521-30.

Weinraub, Z., Maymon, R., Shulman, A., Bukovsky, J., Kratochwil, A., et al. (1996). "Three-dimensional saline contrast hysterosonography and surface rendering of uterine cavity pathology." Ultrasound Obstet Gynecol **8**(4): 277-82.

Welin, L., Svardsudd, K., Wilhelmsen, L., Larsson, B. and Tibblin, G. (1987). "Analysis of risk factors for stroke in a cohort of men born in 1913." N Engl J Med **317**(9): 521-6.

White, A. D., Carolan, G. S., Newcombe, R. G., Wilkins, P., Woodcock, J. P., et al. (1997). "Problems in the comparison of ultrasound morphology and histology of carotid artery atheromatous plaques." J Vasc Invest **3**(4): 168-176.

Widder, B., Paulat, K., Hackspacher, J., Hamann, H., Hutschenreiter, S., et al. (1990). "Morphological characterization of carotid artery stenoses by ultrasound duplex scanning." Ultrasound Med Biol **16**(4): 349-54.

Wilhjelm, J. E., Gronholdt, M. L., Wiebe, B., Jespersen, S. K., Hansen, L. K., et al. (1998). "Quantitative analysis of ultrasound B-mode images of carotid atherosclerotic plaque: correlation with visual classification and histological examination." IEEE Trans Med Imaging **17**(6): 910-22.

Wilhjelm, J. E., Rosendal, K., Gronholdt, M. L., Jespersen, S. K., Hansen, L. K., et al. (1996)._Digital Image Analysis of Ultraosund B-mode Images of Carotid Atherosclerotic Plaque: Correlation with Histological Examination.!0th Nordic-Baltic Conference on Biomedical Engineering, Tampere, Finland.

Wolf, P. A., Abbott, R. D. and Kannel, W. B. (1991). "Atrial fibrillation as an independent risk factor for stroke: the Framingham Study." Stroke **22**(8): 983-8.

Wolf, P. A. and D'Agostino, R. B. (1998). "Epidemiology of stroke" in: Stroke : Pathophysiology, Diagnosis and Management. H. J. Barnett, J. P. Mohr, B. Stein and F. M. Yatsu.(editors) Philadelphia, Churchill Livingstone: 3 - 28.

Wolf, P. A., D'Agostino, R. B., Kannel, W. B., Bonita, R. and Belanger, A. J. (1988). "Cigarette smoking as a risk factor for stroke. The Framingham Study." Jama **259**(7): 1025-9.

Wolverson, M. K., Bashiti, H. M. and Peterson, G. J. (1983). "Ultrasonic tissue characterization of atheromatous plaques using a high resolution real time scanner." Ultrasound Med Biol **9**(6): 599-609.

Woo, D., Gebel, J., Miller, R., Kothari, R., Brott, T., et al. (1999). "Incidence rates of first-ever ischemic stroke subtypes among blacks: a population-based study." Stroke **30**(12): 2517-22.

Wright, I. A., Gough, N. A., Rakebrandt, F., Wahab, M. and Woodcock, J. P. (1997). "Neural network analysis of Doppler ultrasound blood flow signals: a pilot study." Ultrasound Med Biol **23**(5): 683-90.

Wu, C. M. and Chen, Y. C. (1992). "Texture features for classification of ultrasonic liver images." IEEE transactions in medical imaging **11**(2): 141-152.

Yamamoto, T. and Yamashita, T. (1998). "Low-density lipoprotein apheresis using the Liposorber system: features of the system and clinical benefits." Ther Apher **2**(1): 25-30.

Yaman, C., Sommergruber, M., Ebner, T., Polz, W., Moser, M., et al. (1999). "Reproducibility of transvaginal three-dimensional endometrial volume measurements during ovarian stimulation." Hum Reprod **14**(10): 2604-8.

Zhao, X. Q., Yuan, C., Hatsukami, T. S., Frechette, E. H., Kang, X. J., et al. (2001). "Effects of prolonged intensive lipid-lowering therapy on the characteristics of carotid atherosclerotic plaques in vivo by MRI: a case-control study." Arterioscler Thromb Vasc Biol **21**(10): 1623-9.

Zwiebel, W. J. and Knighton, R. (1990). "Duplex examination of the carotid arteries." Semin Ultrasound CT MR **11**(2): 97-135.

Appendices – Chapter 1

Appendix 1.1 First order statistics

First order statistics are computed from a histogram that measures the probability of a certain pixel occurring in an image. Consider an image with N pixels and X_i is the number of pixels of gray scale, i in the image.

1. Mean

$$\mu = \frac{1}{N}\sum_{i=1}^{N} X_i$$

2. Standard Deviation

$$\sigma = \sqrt{\frac{1}{N}\sum_{i=1}^{N}(X_i - \mu)^2}$$

3. Signal to Noise Ratio (SNR)

$$SNR = \mu / \sigma$$

4. Skewness

$$s = \frac{\sum_{i=1}^{N}(X_i - \mu)^3}{(N-1)\times\sigma^3}$$

5. Kurtosis

$$k = \frac{\sum_{i=1}^{N}(X_i - \mu)^4}{(N-1)\times\sigma^4} - 3$$

Appendix 1.2 Co-occurence matrices

Consider a rectangular matrix of N_y x N_x cells.

Where Lx = {0,1,2..... N_x}: horizontal spatial domain

And Ly = {0,1,2..... N_y} : vertical spatial domain

G = {1,2,3..... N_g} : N_g is the no. of grey tones.

L_x x L_y is the set of cells of the image ordered by their row column designation.

The image, I, can be represented as a function which assigns some grey tone in G to each cell or pair of co-ordinates in

L_x x L_y; I: L_y x L_x → G

The main component of this idea is that texture is derived from four closely related measures. These measures are arrays termed angular nearest neighbour grey tone spatial dependence matrices. To describe these matrices, consider a cell – not at the periphery of an image- to have eight nearest neighbour cells.

135° 90° 45°

4	3	2
5	•	1
6	7	8

→ 0°

Cells 1 and 5 are 0° horizontal neighbours to cell •

Cells 2 and 6 are 45° diagonal neighbours to cell •

Cells 3 and 7 are 90° vertical neighbours to cell •

Cells 4 and 8 are 135° diagonal neighbours to cell •

Assume that the texture information in an image, I, is contained in the overall or "average" spatial relationship which the grey tones in image, I, have with one another.

The relative frequencies with which two neighbouring cells separated by a distance d, one with grey tone i, the other with grey tone j is given by

$P(I,j,d,0°) = \#\{((k,l),(m,n)) \in (L_x \times L_y) \times (L_y \times L_x) \mid k-m = 0, \mid l-n \mid = d$

Where $I(k,l) = i$ and $I(m,n) = j$

This is similar for 45°, 90° and 135° and # denotes the number of elements in the set.

These matrices are symmetric. The distance can be explicitly defined by

$D((k,l),(m,n)) = \max \{ \mid k-m \mid, \mid l-n \mid \}$

EXAMPLE of a 4 x 4 matrix

0	0	1	1
0	0	1	1
0	2	2	2
2	2	3	3

The grey tone matrix would be

Grey tone

↓ →	0	1	2	3
0	(0,0)	(0,1)	(0,2)	(0,3)
1	(1,0)	(1,1)	(1,2)	(1,3)
2	(2,0)	(2,1)	(2,2)	(2,3)
3	(3,0)	(3,1)	(3,2)	(3,3)

This leads to the four grey tone spatial dependence matrices

$0°= \begin{matrix} 4 & 2 & 1 & 0 \\ 2 & 4 & 0 & 0 \\ 1 & 0 & 6 & 1 \\ 0 & 0 & 1 & 2 \end{matrix}$ $90°= \begin{matrix} 6 & 0 & 2 & 0 \\ 0 & 4 & 2 & 0 \\ 2 & 2 & 2 & 2 \\ 0 & 0 & 2 & 0 \end{matrix}$ $135° \begin{matrix} 2 & 1 & 3 & 0 \\ 1 & 2 & 1 & 0 \\ 3 & 1 & 0 & 2 \\ 0 & 0 & 2 & 0 \end{matrix}$ $45° \begin{matrix} 4 & 1 & 0 & 0 \\ 1 & 2 & 2 & 0 \\ 0 & 2 & 4 & 1 \\ 0 & 0 & 1 & 0 \end{matrix}$

To determine the number, say in (2,1) count the number of cells that the first cell has grey tone 2 and second has grey tone 1.

Appendix 1.3 Second order statistics

14 Textural Features derived from grey tone co-occurrence matrices

(1) Angular second moment

$$f_1 = \sum_i \sum_j \{p(i,j)\}^2$$

(2) Contrast

$$f_2 = \sum_{n=0}^{N_{g-1}} n^2 \left\{ \sum_{i=1}^{N_g} \sum_{j=1 \atop |i-j|=n}^{N_g} p(i,j) \right\}$$

(3) Correlation

$$f_3 = \frac{\sum_i \sum_j (ij) p(i,j) - \mu_x \mu_y}{\sigma_x \sigma_y}$$

where μ_x, μ_y, σ_x and σ_y are the means and standard deviations of p_x and p_y.

(4) Sum of squares: variance

$$f_4 = \sum_i \sum_j (i-\mu)^2 p(i,j)$$

(5) Inverse difference moment:

$$f_5 = \sum_i \sum_j \frac{1}{1+(i-j)^2} p(i,j)$$

(6) Sum average:

$$f_6 = \sum_{i=2}^{2N_g} i p_{x+y}(i)$$

(7) Sum variance

$$f_7 = \sum_{i=2}^{2N_g} (i-f_8)^2 \; p_{x+y}(i)$$

(8) Sum entropy:

$$f_8 = -\sum_{i=2}^{2N_g} p_{x+y}(i) \log(p(i,j))$$

(9) Entropy

$$f_9 = -\sum_i \sum_j p(i;j)\log(p(i,j))$$

(10)Difference variance:

$$f_{10} = \text{var}iance\ of\ p_{x-y}$$

(11)Difference entropy:

$$f_{11} = \sum_{i=o}^{N_{g-1}} p_{x-y}(i)\log\{p_{x-y}(i)\}$$

(12) & (13) Information measures of correlation

$$f_{12} = \frac{HXY - HXY1}{\max\{HX, HY\}}$$

$$f_{13} = (1 - \exp[-2.0(HXY2 - HXY)])^{1/2}$$

$$HXY = -\sum_i \sum_j p(i,j)\log(p(i,j))$$

where HX and Hy are entropies of p_x and p_y and

$$HXY1 = -\sum_i \sum_j P(i,j)\log\{p_x(i)p_y(j)\}$$

$$HXY2 = -\sum_i \sum_j p_x(i)p_{y(j)}\log\{p_x(i)p_y(j)\}$$

(14) Maximal correlation coefficient:

$$f_{14} = (\text{sec}ond\ l\text{arg}est\ eigenvalue\ of\ Q)^{1/2}$$

where $Q(i,j) = \sum_k \frac{p(i,k)p(j,k)}{p_x(i)p_y(k)}$

Appendices – Chapter 2

Appendix 2.1 3D Acquisition Protocol

1. Select Test preset group from the scanner main menu. Do not adjust the gain or any preset values. Ensure STC gains are all centralised.
2. Select "*WS*"

   Enter patient ID, study reason, patient name and date of birth.

   Select "*Start study*"
3. Select "3D" on top toolbar (3rd from right). Then select "3D without sensor" Select linear acquisition symbol (3rd from left) from the bottom left toolbar. Then select acquisition settings symbol (2nd from right).

   Change capture speed to equal to frame rate (13 fps).

   Set scan translation to 70 mm. set scan time to 12 seconds.

   Change scan direction from "+" to "-".

   Select "OK"
4. Set colour parameters as follow, if colour is not required skip to step 5. Select power on scanner. Ensure that the power box is similar in size to 3D box. Select toolbar in bottom left corner. Then select acquisition settings symbol (2nd from right).Change capture speed to equal to frame rate (13 fps).
5. Position patient supine on the bed with the head extending back and tilting slightly to the contra lateral side ensuring the device fits comfortably.
6. Prescan to ensure that the scan box size is sufficient and is correctly positioned. If not, adjust by clicking on a corner and dragging the corner to increase the size. To reposition click on the middle of the box and drag to the required position.

7. Ask patient to hold their breath and start scan by selecting "cine" while simultaneously starting probe motor
8. Check image then save by selecting "acquire new image" on top toolbar.
9. Repeat scan on carotid setting and on test setting (x2)

Appendix 2.2 Class type information for training set

Class 1	Z score (vari)	Z score (max)	Z score (imc1_iv)	Z score (SVAR_IC)	Z score (CORR_Sd)	Z score (Mean)
Mean	3.785	3.629	2.534	5.460	-6.306	4.239
Std Dev	1.783	0.630	0.320	2.104	2.679	0.694
min	0.860	2.645	1.748	2.041	-15.164	2.901
Max	8.211	5.116	3.230	11.848	-2.448	6.483

Class 2	Z score (vari)	Z score (max)	Z score (imc1_iv)	Z score (SVAR_IC)	Z score (CORR_Sd)	Z score (Mean)
Mean	3.014	2.604	2.232	2.178	-2.007	2.429
Std Dev	1.661	0.401	0.358	1.124	1.118	0.620
min	0.471	1.640	1.353	0.349	-5.164	1.014
Max	9.006	3.422	2.928	5.111	-0.045	3.948

Class 3	Z score (vari)	Z score (max)	Z score (imc1_iv)	Z score (SVAR_IC)	Z score (CORR_Sd)	Z score (Mean)
Mean	1.256	1.474	1.556	0.734	-0.321	1.210
Std Dev	0.760	0.394	0.370	0.601	0.490	0.619
min	0.185	0.636	0.575	-0.093	-1.698	-0.034
Max	4.937	2.482	2.508	2.272	0.515	2.719

Class 4	Z score (vari)	Z score (max)	Z score (imc1_iv)	Z score (SVAR_IC)	Z score (CORR_Sd)	Z score (Mean)
Mean	-0.137	0.043	0.277	-0.213	0.232	-0.009
Std Dev	0.221	0.310	0.348	0.133	0.055	0.312
min	-0.405	-0.423	-0.392	-0.386	-0.016	-0.034
Max	0.621	1.151	1.209	0.207	0.304	2.719

Class 5	Z score (vari)	Z score (max)	Z score (imc1_iv)	Z score (SVAR_IC)	Z score (CORR_Sd)	Z score (Mean)
Mean	-0.475	-0.627	-0.698	-0.366	0.277	-0.546
Std Dev	-0.088	0.239	0.365	0.044	0.009	0.231
min	-0.623	-1.184	-1.562	-0.401	0.248	-0.907
Max	-0.258	-0.179	-0.063	-0.188	0.302	0.015

Appendix 2.3 ImageJ Scale calibration results

Calibration	*Actual(cm)*	*Meas (cm)*	*Meas (cm)*	*Meas (cm)*	*Meas (cm)*	*Meas (cm)*
Side	0.5	0.5	0.51	0.51	0.51	0.5
	1	1	1	0.98	0.98	1
	1.5	1.51	1.5	1.49	1.5	1.51
	2	1.98	2.02	1.98	2	2
	2.5	2.53	2.52	2.51	2.51	2.51
Top	0.5	0.51	0.5	0.49	0.5	0.51
	1	1.01	1.01	1.01	0.99	1
	1.5	1.51	1.51	1.51	1.5	1.52
	2	2.02	2.01	2.01	2.01	2.01
	2.5	2.52	2.49	2.51	2.5	2.51
Calipers	1	1.02	1	1	0.99	1
	2	2.02	2.01	1.99	1.98	2
Phantom	0.5	0.52	0.49	0.49	0.49	0.51
	1	1.01	0.99	1	1.01	1
	2	2.02	2	1.99	2.02	2.02

Std uncertainty = Std Dev /Sqrt (n)

*% Error = ((mean-actual length)/actual) *100*

Calibration	*Actual(cm)*	*Mean (cm)*	*St Dev (cm)*	*Std uncertainty*	*% error*
Side	0.5	0.51	0.01	0.00	1.20
	1	0.99	0.01	0.00	-0.80
	1.5	1.50	0.01	0.00	0.13
	2	2.00	0.02	0.01	-0.20
	2.5	2.52	0.01	0.00	0.64
Top	0.5	0.50	0.01	0.00	0.40
	1	1.00	0.01	0.00	0.40
	1.5	1.51	0.01	0.00	0.67
	2	2.01	0.00	0.00	0.60
	2.5	2.51	0.01	0.01	0.24
Calipers	1	1.00	0.01	0.00	0.20
	2	2.00	0.02	0.01	0.00
Phantom	0.5	0.50	0.01	0.01	0.00
	1	1.00	0.01	0.00	0.20
	2	2.01	0.01	0.01	0.50
			Mean	0.00	0.28

Appendices – Chapter 4

Appendix 4.1 Plaque 1

Appendix 4.1.1 Volume measurement of plaque 1 *in vitro*

MATLAB no	Area 1 (mm^2)	Area 2 (mm^2)	Area 3 (mm^2)	Area 4 (mm^2)	Area 5 (mm^2)
53	3.7	4.4	4.0	3.5	3.7
55	9.7	10.7	9.8	9.2	10.4
57	12.5	11.4	11.0	12.4	12.3
59	16.2	14.8	14.6	16.5	16.1
61	13.6	14.5	15.5	15.5	17.0
63	23.9	23.8	24.6	26.8	27.5
65	23.3	19.8	20.4	19.6	23.8
67	21.5	22.9	24.8	20.6	25.2
69	21.2	22.6	22.9	25.6	24.8
71	28.9	28.8	26.9	28.5	24.8
73	33.1	32.5	31.3	30.6	29.1
75	33.9	35.5	34.9	33.9	32.1
77	39.4	35.8	35.8	35.0	37.4
79	42.6	42.2	41.1	42.0	41.3
81	49.1	45.8	48.6	42.9	44.8
83	51.2	51.7	51.7	50.9	50.6
85	49.4	52.3	48.7	45.5	45.9
87	46.0	47.1	46.4	41.7	42.3
89	38.5	34.7	34.6	36.2	35.6
91	28.5	31.0	46.9	28.8	23.8
93	24.9	27.4	27.5	25.0	26.3
95	28.5	29.0	26.0	27.0	28.4
97	28.2	31.0	22.9	27.5	24.4
99	29.0	26.8	26.0	26.2	27.3
101	20.4	23.5	22.1	24.2	23.9
103	21.2	19.4	19.5	21.0	22.5
105	16.4	17.3	14.3	16.8	14.0
107	15.0	13.2	12.8	12.6	13.5
109	13.2	13.2	11.7	15.8	13.3
111	7.7	5.7	6.9	7.2	7.1
Volume (mm^3)	714.0	712.2	708.1	694.2	694.4
Mean Volume (mm^3)	704.6				
St Dev (mm^3)	9.6				

Appendix 4.1.2 **Histology estimations of the five tissue types for plaque 1 using imageJ method.**

Plaque section	Haemorrhage (mm^2)	Lipid (mm^2)	Fibrous (mm^2)	Calcium (mm^2)	Elastic (mm^2)
a	1.4	0.0	2.3	0.7	0.7
b	2.1	0.5	4.8	0.2	1.3
c	1.1	0.4	6.9	0.3	1.8
d	1.9	0.5	12.9	0.8	1.8
e	4.4	1.2	11.6	0.9	2.7
f	3.2	1.5	12.5	1.2	4.1
g	3.3	0.3	9.2	0.2	1.6
h	5.3	0.0	9.8	0.0	2.1
i	10.8	0.0	8.8	1.2	2.7
j	14.8	0.0	12.5	0.6	3.5
k	19.0	0.5	12.4	0.2	2.4
l	19.7	0.7	12.3	0.7	2.5
m	15.2	1.2	11.3	0.3	2.1
n	1.2	3.3	14.6	0.3	1.6
o	0.4	1.9	10.8	0.2	2.1
p	0.5	0.6	9.4	0.0	1.7
q	0.5	0.6	9.0	0.0	2.3
r	0.0	0.0	8.4	0.0	3.4
s	0.6	0.0	9.9	0.0	2.1
t	0.8	0.0	9.7	0.0	2.7
Total area (mm^2)	106.1	13.2	199.1	7.8	45.2

Total percentage (%)	28.57	3.55	53.62	2.10	12.16

Total plaque volume (mm^3)	501.2

Key: The total plaque volume was calculated by multiplying the total area of the five tissue types by the distance between histology sections. Assuming 1.35mm between histology sections

Appendix 4.1.3 MATLAB *in vivo* analysis of plaque 1.

Image no.	Class 1 (%)	Class 2 (%)	Class 3 (%)	Class 4 (%)	Class 5 (%)
77	0.00	0.00	0.00	83.05	16.95
79	0.00	0.00	11.58	15.79	72.63
81	0.00	0.00	0.00	68.42	31.58
83	0.00	0.00	0.00	86.96	13.04
85	0.00	0.00	53.50	46.50	0.00
87	0.00	0.00	74.31	21.10	4.59
89	0.00	0.00	0.00	29.87	70.13
91	0.00	0.00	2.29	24.51	73.20
93	0.00	0.73	0.37	63.74	35.16
95	0.00	0.00	31.44	60.26	8.30
97	0.00	0.00	29.41	47.40	23.18
99	0.00	0.00	18.54	61.65	19.82
101	0.00	0.00	16.22	36.76	47.03
103	0.00	0.00	0.09	26.84	73.06
105	0.00	0.00	1.98	32.10	65.92
107	0.00	0.00	2.16	26.15	71.69
109	0.00	0.20	3.60	24.59	71.61
111	0.00	0.00	5.84	19.39	74.76
113	0.00	0.00	16.77	27.72	55.51
115	0.00	0.30	7.71	14.82	77.17
117	0.00	0.21	12.98	8.80	78.01
119	0.00	0.43	17.17	18.71	63.69
121	0.40	7.13	9.59	14.93	67.96
123	0.00	2.02	7.05	18.71	72.22
125	0.00	2.26	8.43	22.85	66.46
127	0.00	4.72	52.24	34.87	8.17
129	0.00	18.18	28.31	44.42	9.09
131	1.18	20.32	28.74	41.89	7.86
133	2.26	37.22	48.12	12.41	0.00
135	1.62	80.26	17.48	0.65	0.00
All	0.14	3.93	12.01	25.40	58.52

Appendix 4.1.4 Volume measurement of plaque 1 *in vivo*

MATLAB no.	Area 1 (mm^2)	Area 2 (mm^2)	Area 3 (mm^2)	Area 4 (mm^2)	Area 5 (mm^2)
77	5.4	5.4	6.3	5.9	4.6
79	10.3	11.4	13.0	10.8	9.5
81	6.8	6.6	4.8	6.9	6.9
83	9.4	9.5	8.8	7.9	10.1
85	15.2	16.3	17.3	16.7	16.3
87	11.4	11.2	12.0	12.5	11.4
89	15.1	15.6	14.1	14.0	15.0
91	20.2	19.1	19.0	20.1	19.3
93	15.4	14.9	14.6	15.4	15.3
95	17.1	19.7	18.3	18.4	18.4
97	23.3	22.7	24.0	23.2	24.9
99	28.7	30.2	29.3	28.4	28.8
101	23.3	25.6	24.7	23.5	23.5
103	27.4	25.8	27.4	28.2	27.9
105	27.3	27.9	26.9	27.3	28.7
107	45.6	48.0	46.7	45.3	47.0
109	41.5	42.8	43.4	42.9	44.4
111	44.8	45.2	43.5	44.6	47.2
113	42.4	44.2	44.1	43.1	44.6
115	40.4	40.1	41.2	43.3	41.3
117	44.3	42.2	45.5	45.1	44.5
119	42.4	45.3	43.5	44.2	43.0
121	59.5	58.3	59.0	56.4	59.8
123	60.9	58.4	59.1	58.5	58.5
125	46.1	47.1	45.4	45.0	46.7
127	17.0	17.9	17.3	19.5	20.6
129	20.6	18.7	19.3	19.2	21.7
131	25.8	25.1	28.6	27.9	29.4
133	24.2	21.8	17.9	16.3	17.8
135	19.1	17.1	14.4	16.7	13.5
Volume (mm^3)	750.0	753.3	748.9	746.8	759.0
Mean Volume (mm^3)	751.6				
St Dev (mm^3)	4.8				

Appendix 4.1.5 **Comparison of *in vitro* and *in vivo* images with histology for plaque 1**

Histology	In vitro image no.	In vitro match with histology	In vivo image no.	In vivo match with histology
A1	111/109/107	Match	135/133/131	No match
B1	108/106/104	Match	132/130/128	No match
C1	105/103/101	Match	129/127/125	No match
D1	102/100/98	Partial match	126/124/122	No match
E1	99/97/95	Partial match	123/121/119	No match
F1	96/94/92	Partial match	120/118/116	No match
G1	93/91/89	Partial match	117/115/113	No match
H1	90/88/86	Match	114/112/110	No match
I1	87/85/83	Partial match	111/109/107	No match
J1	84/82/80	Partial match	108/106/104	No match
K1	81/79/77	No match	105/103/101	No match
L1	78/76/74	Partial match	102/100/98	No match
M1	75/73/71	Match	99/97/95	No match
N1	72/70/68	Partial match	96/94/92	No match
O1	69/67/65	No match	93/91/89	No match
P1	66/64/62	Partial match	90/88/86	No match
Q1	63/61/59	No match	87/85/83	No match
R1	60/58/56	No match	84/82/80	No match
S1	57/55/53	No match	81/79/77	No match
T1	54/52	No match	78/76	No match

Key: The histology section was matched with the corresponding 2D images from the 3D in vitro and in vivo data sets, commenting on whether the images match, partially match or have no match for the factors of shape, size and orientation. A match would have all matching and a partial match would have some.

Appendix 4.2 Plaque 2

Appendix 4.2.1 Volume measurement of plaque 2 *in vitro*

MATLAB no	Area 1 (mm^2)	Area 2 (mm^2)	Area 3 (mm^2)	Area 4 (mm^2)	Area 5 (mm^2)
43	0.9	1.2	0.8	0.7	0.9
45	6.1	5.8	6.6	6.3	6.1
47	6.6	8.1	9.5	10.5	6.6
49	9.1	11.3	11.4	12.4	9.1
51	12.8	13.1	13.8	14.1	12.8
53	13.9	17.0	15.2	21.9	13.9
55	23.4	23.4	22.8	21.3	23.4
57	21.1	24.1	21.3	22.9	21.1
59	24.6	23.7	23.4	27.7	24.6
61	25.9	25.3	21.0	22.5	25.9
63	35.5	35.0	33.0	32.1	35.5
65	33.7	33.3	37.0	34.4	33.7
67	33.8	32.6	33.6	33.7	33.8
69	33.8	34.8	34.2	34.0	33.8
71	36.0	35.0	32.2	34.7	36.0
73	32.6	30.7	32.8	30.9	32.6
75	32.5	29.5	30.2	29.5	32.5
77	29.1	29.1	28.3	27.3	29.1
79	25.0	24.4	25.1	25.3	25.0
81	21.5	25.9	24.0	22.5	21.5
83	24.2	25.8	22.3	23.5	24.2
85	20.1	24.5	23.2	23.4	20.1
87	22.1	21.9	20.7	21.5	22.1
89	17.9	22.6	21.6	21.0	17.9
91	16.0	18.9	19.1	18.8	16.0
93	12.6	15.8	13.9	14.2	12.6
95	9.0	9.0	8.6	9.1	9.0
97	6.5	6.7	6.4	6.7	6.5
99	0.7	0.7	0.9	0.7	0.7
Volume (mm^3)	529.0	549.0	534.7	544.5	548.5
Mean Volume (mm^3)	541.2				
St Dev (mm^3)	8.9				

Appendix 4.2.2 **Histology estimations of the five tissue types for plaque 2 using imageJ method.**

Plaque section	Haemorrhage (mm^2)	Lipid (mm^2)	Fibrous (mm^2)	Calcium (mm^2)	Elastic (mm^2)
a	0.0	0.0	4.7	0.0	2.2
b	0.0	0.0	4.2	0.0	3.9
c	0.0	1.0	5.5	0.0	3.0
d	0.0	1.1	5.3	0.0	1.8
e	0.2	1.3	5.9	0.0	3.2
f	0.0	1.2	8.3	0.0	5.7
g	1.8	1.8	10.4	0.2	6.7
h	6.5	1.2	10.3	0.0	6.7
i	9.8	1.0	10.3	0.0	4.3
j	13.0	0.8	9.1	0.0	5.2
k	6.0	2.7	17.4	0.0	7.1
l	2.7	4.8	23.4	0.0	5.9
m	11.3	1.4	9.6	0.0	4.6
n	5.9	0.9	14.7	0.0	3.3
o	3.6	0.5	10.8	0.0	6.2
p	3.3	1.1	10.9	0.0	4.8
q	1.5	1.7	12.0	0.0	7.1
r	1.8	0.7	9.2	0.0	3.8
s	1.4	1.6	6.4	0.0	4.4
t	0.7	0.4	3.5	0.0	2.2
Total area (mm2)	69.5	25.4	191.9	0.2	92
Total percentage (%)	18.35	6.67	50.65	0.06	24.27

Total plaque volume (mm^3)	496.3

Key: The total plaque volume was calculated by multiplying the total area of the five tissue types by the distance between histology sections.

Assuming 1.31mm between the histology sections.

Appendix 4.2.3 MATLAB *in vivo* analysis of plaque 2

Image No.	Class 1 (%)	Class 2 (%)	Class 3 (%)	Class 4 (%)	Class 5 (%)
31	0.00	0.00	100.00	0.00	0.00
33	0.00	0.00	84.62	15.38	0.00
35	0.00	0.00	0.00	0.00	0.00
37	0.00	0.00	48.33	51.67	0.00
39	0.00	0.68	30.48	68.15	0.68
41	0.00	0.00	0.00	100.00	0.00
43	0.00	0.00	7.56	89.78	2.67
45	0.00	8.07	17.41	60.13	14.40
47	0.00	1.24	14.44	70.03	14.29
49	0.00	0.00	11.37	80.78	7.85
51	0.00	4.17	9.72	82.58	3.54
53	0.00	5.16	14.65	78.70	1.49
55	0.00	0.26	28.83	68.73	2.19
57	0.00	0.00	13.98	78.80	7.22
59	0.00	1.04	15.29	69.79	13.88
61	0.00	5.95	22.15	62.27	9.64
63	0.00	3.37	55.83	40.80	0.00
65	0.00	32.80	55.31	11.58	0.32
67	0.49	17.05	40.66	37.38	4.43
69	2.57	27.64	41.73	24.66	3.39
71	2.19	19.12	29.61	27.42	21.66
73	0.24	31.90	45.00	22.62	0.24
75	0.00	26.67	42.86	28.57	1.90
77	0.00	12.90	41.94	45.16	0.00
79	0.00	11.22	24.44	42.14	22.19
81	0.00	7.23	14.47	48.64	29.66
83	0.00	3.16	34.81	25.95	36.08
85	0.00	0.00	75.00	25.00	0.00
87	0.00	0.00	56.52	42.61	0.87
All	0.28	7.35	23.09	59.68	9.6

Appendix 4.2.4 Volume measurement of plaque 2 *in vivo*

Matlab no	Area 1 (mm^2)	Area 2 (mm^2)	Area 3 (mm^2)	Area 4 (mm^2)	Area 5 (mm^2)
31	3.9	2.5	3.7	2.8	2.9
33	4.4	4.5	4.4	4.2	4.6
35	6.3	3.6	5.6	4.5	5.7
37	8.7	9.1	8.3	8.8	9.0
39	13.6	13.3	14.2	13.0	14.1
41	13.7	14.5	16.3	14.5	14.9
43	12.4	12.6	11.9	12.8	14.0
45	21.1	22.0	23.3	22.2	22.6
47	27.7	25.8	27.3	27.0	28.1
49	24.3	23.0	22.9	23.5	23.5
51	23.8	24.8	25.8	23.2	23.4
53	25.5	27.3	28.2	26.6	27.0
55	26.7	27.6	27.4	25.9	27.1
57	31.0	31.0	33.1	30.1	33.1
59	41.0	39.6	39.8	38.9	40.7
61	39.0	37.1	37.4	37.7	39.1
63	26.1	27.2	27.6	26.4	26.8
65	26.3	25.8	26.2	25.6	24.1
67	25.9	25.7	27.4	26.0	26.8
69	31.5	33.4	31.0	32.8	31.9
71	33.4	35.2	35.3	35.5	37.1
73	24.6	22.1	24.5	22.9	22.8
75	19.8	19.7	19.1	19.5	19.0
77	26.6	24.1	25.6	24.2	24.6
79	26.0	25.9	25.8	26.2	25.5
81	26.5	23.2	24.7	24.9	24.5
83	21.5	21.5	21.6	21.6	21.9
85	11.2	10.5	10.8	12.2	11.6
87	14.6	13.9	13.8	13.8	14.1
Volume (mm^3)	575.6	565.6	580.6	566.4	578.2
Mean Volume (mm^3)	573.3				
St Dev (mm^3)	6.9				

Appendix 4.2.5 **Comparison of *in vitro* and *in vivo* images with histology for plaque 2**

Histology	*In vitro* image no.	*In vitro* match with histology	*In vivo* image no.	*In vivo* match with histology
A2	43/45	No match	31/33	No match
B2	44/46/48	Partial match	32/34/36	No match
C2	47/49/51	No match	35/37/39	No match
D2	50/52/54	Match	38/40/42	No match
E2	53/55/57	Partial match	41/43/45	No match
F2	56/58/60	Match	44/46/48	No match
G2	59/61/63	Partial match	47/49/51	No match
H2	62/64/66	Match	50/52/54	No match
I2	65/67/69	Partial match	53/55/57	No match
J2	68/70/72	No match	56/58/60	No match
K2	71/73/75	Partial match	59/61/63	No match
L2	74/76/78	Partial match	62/64/66	No match
M2	77/79/81	Match	65/67/69	No match
N2	80/82/84	Match	68/70/72	No match
O2	83/85/87	Match	71/73/75	No match
P2	86/88/90	Partial match	74/76/78	No match
Q2	89/91/93	Match	77/79/81	No match
R2	92/94/96	No match	80/82/84	No match
S2	95/97/99	No match	83/85/87	No match
T2	98/100	No match	86/88	No match

Key: The histology section was matched with the corresponding 2D images from the 3D in vitro and in vivo data sets, commenting on whether the images match, partially match or have no match for the factors of shape, size and orientation. A match would have all matching and a partial match would have some.

Appendix 4.3 Plaque 3

Appendix 4.3.1 Volume measurement of plaque 3 *in vitro*

MATLAB no	Area 1 (mm^2)	Area 2 (mm^2)	Area 3 (mm^2)	Area 4 (mm^2)	Area 5 (mm^2)
71	2.7	2.4	3.1	3.2	3.3
73	4.6	4.3	3.8	5.4	4.4
75	9.4	10.7	10.0	10.2	10.4
77	16.0	17.4	15.7	15.8	15.5
79	22.0	21.0	23.6	24.2	24.0
81	22.4	23.2	24.6	24.8	23.7
83	23.9	24.0	23.5	21.6	22.8
85	20.1	20.9	19.4	20.1	21.2
87	18.1	18.1	16.8	18.0	18.6
89	14.1	13.9	13.1	14.9	14.6
91	12.1	12.8	13.4	12.7	13.8
93	11.2	12.6	11.2	11.5	11.1
95	13.2	14.0	12.9	12.3	11.7
97	10.6	11.5	10.9	11.5	11.6
99	7.2	7.5	6.1	7.3	7.1
Volume (mm^3)	187.4	193.4	187.9	192.7	193.0
Mean Volume (mm^3)	190.9				
St Dev (mm^3)	3.0				

Appendix 4.3.2 **Histology estimations of the five tissue types for plaque 3 using imageJ method.**

Plaque section	Haemorrhage (mm^2)	Lipid (mm^2)	Fibrous (mm^2)	Calcium (mm^2)	Elastic (mm^2)
a	0.0	0.0	3.2	0.0	1.2
b	0.0	0.5	4.9	0.0	2.3
c	0.0	0.4	4.7	0.0	3.5
d	0.0	0.2	5.1	0.0	3.6
e	0.0	0.0	6.5	0.0	3.6
f	0.6	1.3	12.4	0.0	3.7
g	4.7	0.6	12.2	0.0	3.9
h	2.4	0.0	13.7	0.0	3.4
i	2.1	0.0	12.6	0.0	4.3
j	1.8	0.0	6.9	0.0	2.4
Total area (mm^2)	11.7	3.0	82.1	0.0	31.9

Total percentage (%)	9.07	2.31	63.84	0.00	24.79

Total plaque volume (mm^3)	173.6

Assuming 1.35mm between histology sections

Appendix 4.3.3 MATLAB *in vivo* analysis of plaque 3.

Image no.	Class 1 (%)	Class 2 (%)	Class 3 (%)	Class 4 (%)	Class 5 (%)
43	0.00	0.00	0.00	91.67	8.33
45	0.00	0.00	0.00	94.55	5.45
47	0.00	0.00	0.00	78.95	21.05
49	0.00	0.00	0.45	99.55	0.00
51	0.00	0.00	0.00	87.73	12.27
53	0.00	0.00	0.00	58.55	41.45
55	0.00	0.00	0.00	38.16	61.84
57	0.00	0.00	0.00	44.56	55.44
59	0.00	0.00	0.00	37.05	62.95
61	0.00	0.00	0.00	20.53	79.47
63	0.00	0.00	0.00	27.73	72.27
65	0.00	0.00	2.35	42.68	54.97
67	0.00	0.00	0.00	80.16	19.84
69	0.00	0.00	0.00	28.75	71.25
71	0.00	0.00	0.00	95.24	4.76
All	0.00	0.00	0.23	47.59	52.18

Appendix 4.3.4 Volume measurement of plaque 3 *in vivo*

MATLAB no.	Area 1 (mm^2)	Area 2 (mm^2)	Area 3 (mm^2)	Area 4 (mm^2)	Area 5 (mm^2)
43	6.7	6.7	6.3	6.4	6.2
45	7.3	7.6	7.0	7.5	7.4
47	11.4	9.7	11.9	12.1	11.3
49	15.1	13.6	15.1	11.9	11.8
51	13.1	13.8	12.9	12.8	14.7
53	17.1	19.6	20.6	19.0	20.0
55	17.4	18.8	17.7	18.9	18.1
57	19.7	17.8	17.4	18.7	18.1
59	19.6	18.7	21.6	22.0	19.5
61	16.7	18.5	18.5	17.8	16.5
63	18.2	18.8	18.8	19.7	19.1
65	19.5	17.1	15.9	15.4	17.9
67	16.6	15.0	17.1	18.7	14.8
69	11.5	11.0	10.9	11.7	14.2
71	11.9	11.7	14.1	10.7	13.5
Volume (mm^3)	200.3	197.0	203.9	201.6	201.3
Mean Volume (mm^3)	200.8				
St Dev (mm^3)	2.5				

Appendix 4.3.5 **Comparison of *in vitro* and *in vivo* images versus histology for plaque 3.**

Histology	*In vitro* image no.	*In vitro* match with histology	*In vivo* image no.	*In vivo* match with histology
A3	99/101	Partial match	43/45	No match
B3	96/98/100	No match	44/46/48	No match
C3	93/95/97	No match	47/49/51	No match
D3	90/92/94	No match	50/52/54	No match
E3	88/90/92	No match	53/55/57	No match
F3	85/87/89	Match	56/58/60	No match
G3	82/84/86	Match	59/61/63	No match
H3	79/81/83	Partial match	62/64/66	No match
I3	76/78/80	Partial match	67/69/71	No match
J3	73/75	No match	70/72	No match

Key: The histology section was matched with the corresponding 2D images from the 3D in vitro and in vivo data sets, commenting on whether the images match, partially match or have no match for the factors of shape, size and orientation. A match would have all matching and a partial match would have some.

.

.

Appendix 4.4 **Plaque 4**

Appendix 4.4.1 **Volume measurement of plaque 4 *in vitro***

MATLAB no	Area 1 (mm^2)	Area 2 (mm^2)	Area 3 (mm^2)	Area 4 (mm^2)	Area 5 (mm^2)
43	0.4	0.5	0.7	0.8	1.2
45	14.0	15.4	15.1	13.7	13.8
47	20.4	19.3	17.1	17.0	18.2
49	25.8	27.8	24.2	24.9	25.3
51	30.1	31.6	32.5	32.4	33.9
53	38.6	34.1	33.0	30.3	33.9
55	36.1	35.4	35.5	34.8	43.5
57	50.0	50.7	50.6	49.1	52.3
59	53.5	52.2	56.4	52.2	51.3
61	57.3	59.4	58.5	57.3	57.8
63	66.7	66.5	63.2	60.0	62.8
65	66.1	65.8	65.7	66.8	68.7
67	56.7	55.1	56.4	60.7	58.8
69	58.8	57.5	60.2	60.8	60.8
71	64.1	64.8	65.0	65.5	63.0
73	58.4	60.5	60.4	63.7	61.0
75	44.8	44.9	45.4	44.7	44.1
77	32.9	35.5	33.3	38.7	37.9
79	33.8	32.4	34.4	36.7	32.1
81	25.6	24.3	23.6	26.3	25.3
83	17.9	18.4	20.2	20.9	16.1
85	19.5	18.2	15.9	18.8	15.7
87	14.5	12.9	12.2	13.6	13.2
89	3.5	2.9	3.1	3.0	2.9
91	1.0	0.9	0.9	1.1	0.6
Volume (mm^3)	722.3	715.5	716.8	726.8	723.8
Mean Volume (mm^3)	721.0				
St Dev (mm^3)	4.8				

Appendix 4.4.2 **Histology estimations of the five tissue types for plaque 4 using imageJ method.**

Plaque section	Haemorrhage (mm^2)	Lipid (mm^2)	Fibrous (mm^2)	Calcium (mm^2)	Elastic (mm^2)
a	0.1	0.0	3.7	0.0	1.5
b	0.8	0.0	3.6	0.0	1.2
c	1.7	0.0	2.9	0.0	2.0
d	2.1	0.1	4.7	0.2	0.9
e	2.1	0.1	5.2	0.2	1.2
f	10.3	0.0	6.2	0.0	2.1
g	13.2	0.0	15.6	0.0	1.2
h	11.1	0.0	16.3	0.0	3.0
i	20.0	0.0	11.4	0.0	2.1
j	24.3	0.7	14.5	0.0	3.5
k	18.4	2.4	20.4	0.0	7.1
l	17.9	1.7	20.3	0.0	6.2
m	15.4	3.4	15.9	0.0	6.6
n	16.2	2.5	14.5	0.0	5.9
o	13.7	2.9	14.0	0.0	6.2
p	11.2	1.8	12.5	0.8	6.7
q	5.0	0.0	9.8	1.2	5.5
r	1.6	0.8	14.3	0.8	
s	1.7	1.6	8.5	0.5	1.0
t	2.5	1.1	8.2	0.2	0.8
Total area (mm^2)	189.3	19	222.5	3.7	64. 5
Total percentage (%)	37.94	3.80	44.60	0.75	12.92

Total plaque volume (mm^3)	563.8

Assuming 1.13 mm between sections

Appendix 4.4.3 MATLAB *in vivo* analysis of plaque 4.

Image no.	Class 1 (%)	Class 2 (%)	Class 3 (%)	Class 4 (%)	Class 5 (%)
47	0.00	0.00	0.00	100.00	0.00
49	0.00	0.00	0.00	13.04	86.96
51	0.00	0.00	5.62	42.70	51.69
53	0.00	0.00	0.00	36.65	63.35
55	0.00	0.00	0.00	1.01	98.99
57	0.00	0.00	3.86	50.45	45.70
59	0.00	1.70	10.71	49.36	38.22
61	0.00	2.21	11.75	39.46	46.58
63	0.00	0.00	0.00	32.72	67.28
65	0.00	0.00	2.52	28.31	69.17
67	0.00	0.00	0.00	1.09	98.91
69	0.00	0.00	0.00	6.57	93.43
71	0.00	0.00	1.19	21.42	77.39
73	0.00	0.00	0.11	22.22	77.67
75	0.06	3.60	12.09	42.87	41.38
77	0.00	1.60	14.58	48.23	35.59
79	0.00	0.00	12.47	53.15	34.37
81	0.00	0.15	13.75	32.87	53.23
83	0.00	0.82	15.18	58.14	25.86
85	0.00	0.79	5.68	46.76	46.76
87	0.00	0.45	5.07	55.05	39.43
89	0.00	0.00	2.06	53.48	44.46
91	0.00	0.00	3.40	47.45	49.15
93	0.00	0.00	3.07	65.73	31.20
95	0.00	0.00	8.77	63.39	27.84
All	0.00	0.67	7.16	39.54	52.63

Appendix 4.4.4 Volume measurement of plaque 4 *in vivo*

MATLAB no	Area 1 (mm^2)	Area 2 (mm^2)	Area 3 (mm^2)	Area 4 (mm^2)	Area 5 (mm^2)
47	3.5	3.5	3.2	3.3	3.6
49	7.2	7.9	7.6	7.2	7.5
51	7.3	7.6	7.1	7.9	8.1
53	10.4	9.7	10.0	10.3	11.0
55	15.5	15.7	14.8	14.3	15.5
57	18.1	18.2	17.9	18.6	20.9
59	33.3	35.7	31.6	33.0	34.8
61	29.5	28.9	27.0	28.9	30.0
63	35.3	34.9	33.5	34.6	36.9
65	49.7	44.8	51.2	50.0	49.3
67	41.3	41.1	39.9	40.2	41.6
69	35.2	44.0	41.2	41.4	40.5
71	36.8	41.3	42.1	38.9	39.6
73	40.7	38.4	40.9	40.4	37.3
75	57.7	56.0	63.6	55.3	54.4
77	52.8	51.0	51.5	53.0	53.1
79	58.6	59.7	58.2	60.9	60.6
81	49.2	41.9	50.3	51.3	47.8
83	41.3	35.3	38.3	36.8	41.4
85	41.3	41.3	38.2	41.0	42.3
87	44.4	39.5	36.4	46.8	44.2
89	39.7	37.5	34.1	41.5	33.1
91	34.6	32.6	30.1	31.2	33.2
93	30.2	31.0	32.6	30.6	33.1
95	21.7	21.8	29.0	25.0	21.9
Volume (mm^3)	754.0	739.9	749.7	760.8	759.9
Mean Volume (mm^3)	752.9				
St Dev (mm^3)	8.6				

Appendix 4.4.5 Comparison of *in vitro* images with histology for plaque 4

Histology	*In vitro* image no.	*In vitro* match with histology	*In vivo* image no.	*In vivo* match with histology
A4	95/96	No match	46/48	No match
B4	93/95/96	No match	47/49/51	No match
C4	90/92/94	No match	50/52/54	No match
D4	87/89/91	No match	52/54/56	No match
E4	85/87/89	No match	55/57/59	No match
F4	82/84/86	Partial match	58/60/62	No match
G4	79/81/83	No match	60/62/64	No match
H4	77/79/81	No match	63/65/67	No match
I4	74/76/78	Partial match	66/68/70	No match
J4	71/73/75	Partial match	68/70/72	No match
K4	68/70/72	Partial match	71/73/75	No match
L4	66/68/70	Partial match	74/76/78	No match
M4	63/65/67	Partial match	77/79/81	No match
N4	60/62/64	No match	79/81/83	No match
O4	58/60/62	No match	82/84/86	No match
P4	55/57/59	No match	85/87/89	No match
Q4	52/54/56	No match	87/89/91	No match
R4	50/52/54	No match	90/92/94	No match
S4	47/49/51	No match	93/95/96	No match
T4	46/48	No match	95/96	No match

Key: The histology section was matched with the corresponding 2D images from the 3D in vitro and in vivo data sets, commenting on whether the images match, partially match or have no match for the factors of shape, size and orientation. A match would have all matching and a partial match would have some.

.

Appendices – Chapter 5

Statistical analysis of serial volume measurements

5.1 Apheresis patients

Patient 1_R_A

Dependent Variable: Patient_1_R_A
Tukey HSD

(I) Visit	(J) Visit	Mean Difference (I-J)	Std. Error	Sig.	95% Confidence Interval	
					Lower Bound	Upper Bound
1	2	37.24000(*)	2.03382	.000	31.4212	43.0588
	3	57.17600(*)	2.03382	.000	51.3572	62.9948
	4	69.69800(*)	2.03382	.000	63.8792	75.5168
2	1	-37.24000(*)	2.03382	.000	-43.0588	-31.4212
	3	19.93600(*)	2.03382	.000	14.1172	25.7548
	4	32.45800(*)	2.03382	.000	26.6392	38.2768
3	1	-57.17600(*)	2.03382	.000	-62.9948	-51.3572
	2	-19.93600(*)	2.03382	.000	-25.7548	-14.1172
	4	12.52200(*)	2.03382	.000	6.7032	18.3408
4	1	-69.69800(*)	2.03382	.000	-75.5168	-63.8792
	2	-32.45800(*)	2.03382	.000	-38.2768	-26.6392
	3	-12.52200(*)	2.03382	.000	-18.3408	-6.7032

* The mean difference is significant at the .05 level.

Patient 1_L_A

Dependent Variable: Patient_1_L_A
Tukey HSD

(I) Visit	(J) Visit	Mean Difference (I-J)	Std. Error	Sig.	95% Confidence Interval	
					Lower Bound	Upper Bound
1	2	1.28400	1.65577	.864	-3.4532	6.0212
	3	16.47400(*)	1.65577	.000	11.7368	21.2112
	4	27.13460(*)	1.65577	.000	22.3974	31.8718
2	1	-1.28400	1.65577	.864	-6.0212	3.4532
	3	15.19000(*)	1.65577	.000	10.4528	19.9272
	4	25.85060(*)	1.65577	.000	21.1134	30.5878
3	1	-16.47400(*)	1.65577	.000	-21.2112	-11.7368
	2	-15.19000(*)	1.65577	.000	-19.9272	-10.4528
	4	10.66060(*)	1.65577	.000	5.9234	15.3978
4	1	-27.13460(*)	1.65577	.000	-31.8718	-22.3974
	2	-25.85060(*)	1.65577	.000	-30.5878	-21.1134
	3	-10.66060(*)	1.65577	.000	-15.3978	-5.9234

* The mean difference is significant at the .05 level.

Patient 2_R_A

Dependent Variable: Patient_2_R_A
Tukey HSD

(I) Visit	(J) Visit	Mean Difference (I-J)	Std. Error	Sig.	95% Confidence Interval	
					Lower Bound	Upper Bound
1	2	30.53000(*)	2.72532	.000	22.7328	38.3272
	3	33.67200(*)	2.72532	.000	25.8748	41.4692
	4	37.72600(*)	2.72532	.000	29.9288	45.5232
2	1	-30.53000(*)	2.72532	.000	-38.3272	-22.7328
	3	3.14200	2.72532	.664	-4.6552	10.9392
	4	7.19600	2.72532	.076	-.6012	14.9932
3	1	-33.67200(*)	2.72532	.000	-41.4692	-25.8748
	2	-3.14200	2.72532	.664	-10.9392	4.6552
	4	4.05400	2.72532	.467	-3.7432	11.8512
4	1	-37.72600(*)	2.72532	.000	-45.5232	-29.9288
	2	-7.19600	2.72532	.076	-14.9932	.6012
	3	-4.05400	2.72532	.467	-11.8512	3.7432

* The mean difference is significant at the .05 level.

Patient 2_L_A

Dependent Variable: Patient_2_L_A
Tukey HSD

(I) Visit	(J) Visit	Mean Difference (I-J)	Std. Error	Sig.	95% Confidence Interval	
					Lower Bound	Upper Bound
1	2	12.76800(*)	2.73793	.001	4.9347	20.6013
	3	13.82000(*)	2.73793	.001	5.9867	21.6533
	4	27.50200(*)	2.73793	.000	19.6687	35.3353
2	1	-12.76800(*)	2.73793	.001	-20.6013	-4.9347
	3	1.05200	2.73793	.980	-6.7813	8.8853
	4	14.73400(*)	2.73793	.000	6.9007	22.5673
3	1	-13.82000(*)	2.73793	.001	-21.6533	-5.9867
	2	-1.05200	2.73793	.980	-8.8853	6.7813
	4	13.68200(*)	2.73793	.001	5.8487	21.5153
4	1	-27.50200(*)	2.73793	.000	-35.3353	-19.6687
	2	-14.73400(*)	2.73793	.000	-22.5673	-6.9007
	3	-13.68200(*)	2.73793	.001	-21.5153	-5.8487

* The mean difference is significant at the .05 level.

5.2 Statin patients

Patient 1_R_S

Dependent Variable: Patient_1_R_S
Tukey HSD

(I) Visit	(J) Visit	Mean Difference (I-J)	Std. Error	Sig.	95% Confidence Interval	
					Lower Bound	Upper Bound
2	3	.55200	1.07514	.866	-2.3163	3.4203
	4	1.09000	1.07514	.583	-1.7783	3.9583
3	2	-.55200	1.07514	.866	-3.4203	2.3163
	4	.53800	1.07514	.872	-2.3303	3.4063
4	2	-1.09000	1.07514	.583	-3.9583	1.7783
	3	-.53800	1.07514	.872	-3.4063	2.3303

Patient 2_R_S

Dependent Variable: Patient_2_R_S
Tukey HSD

(I) Visit	(J) Visit	Mean Difference (I-J)	Std. Error	Sig.	95% Confidence Interval	
					Lower Bound	Upper Bound
1	2	-8.58600(*)	1.09325	.000	-11.7138	-5.4582
	3	4.57200(*)	1.09325	.004	1.4442	7.6998
	4	-4.04160(*)	1.09325	.009	-7.1694	-.9138
2	1	8.58600(*)	1.09325	.000	5.4582	11.7138
	3	13.15800(*)	1.09325	.000	10.0302	16.2858
	4	4.54440(*)	1.09325	.004	1.4166	7.6722
3	1	-4.57200(*)	1.09325	.004	-7.6998	-1.4442
	2	-13.15800(*)	1.09325	.000	-16.2858	-10.0302
	4	-8.61360(*)	1.09325	.000	-11.7414	-5.4858
4	1	4.04160(*)	1.09325	.009	.9138	7.1694
	2	-4.54440(*)	1.09325	.004	-7.6722	-1.4166
	3	8.61360(*)	1.09325	.000	5.4858	11.7414

* The mean difference is significant at the .05 level.

Patient 3_R_S

Dependent Variable: Patient_3_R_S
Tukey HSD

(I) Visit	(J) Visit	Mean Difference (I-J)	Std. Error	Sig.	95% Confidence Interval	
					Lower Bound	Upper Bound
1	2	15.03600(*)	1.57587	.000	10.5274	19.5446
	3	29.28800(*)	1.57587	.000	24.7794	33.7966
	4	24.17200(*)	1.57587	.000	19.6634	28.6806
2	1	-15.03600(*)	1.57587	.000	-19.5446	-10.5274
	3	14.25200(*)	1.57587	.000	9.7434	18.7606
	4	9.13600(*)	1.57587	.000	4.6274	13.6446
3	1	-29.28800(*)	1.57587	.000	-33.7966	-24.7794
	2	-14.25200(*)	1.57587	.000	-18.7606	-9.7434
	4	-5.11600(*)	1.57587	.024	-9.6246	-.6074
4	1	-24.17200(*)	1.57587	.000	-28.6806	-19.6634
	2	-9.13600(*)	1.57587	.000	-13.6446	-4.6274
	3	5.11600(*)	1.57587	.024	.6074	9.6246

* The mean difference is significant at the .05 level.

Patient 3_L_S

Dependent Variable: Patient_3_L_S
Tukey HSD

(I) Visit	(J) Visit	Mean Difference (I-J)	Std. Error	Sig.	95% Confidence Interval	
					Lower Bound	Upper Bound
1	2	.50000	.63227	.858	-1.3089	2.3089
	3	2.99200(*)	.63227	.001	1.1831	4.8009
	4	1.69400	.63227	.071	-.1149	3.5029
2	1	-.50000	.63227	.858	-2.3089	1.3089
	3	2.49200(*)	.63227	.006	.6831	4.3009
	4	1.19400	.63227	.272	-.6149	3.0029
3	1	-2.99200(*)	.63227	.001	-4.8009	-1.1831
	2	-2.49200(*)	.63227	.006	-4.3009	-.6831
	4	-1.29800	.63227	.210	-3.1069	.5109
4	1	-1.69400	.63227	.071	-3.5029	.1149
	2	-1.19400	.63227	.272	-3.0029	.6149
	3	1.29800	.63227	.210	-.5109	3.1069

* The mean difference is significant at the .05 level.

Patient 4_L_S

Dependent Variable: Patient_4_L_S
Tukey HSD

(I) Visit	(J) Visit	Mean Difference (I-J)	Std. Error	Sig.	95% Confidence Interval	
					Lower Bound	Upper Bound
1	2	-2.41240	2.74861	.816	-10.2762	5.4514
	3	3.45000	2.74861	.603	-4.4138	11.3138
	4	-.29620	2.74861	1.000	-8.1600	7.5676
2	1	2.41240	2.74861	.816	-5.4514	10.2762
	3	5.86240	2.74861	.185	-2.0014	13.7262
	4	2.11620	2.74861	.867	-5.7476	9.9800
3	1	-3.45000	2.74861	.603	-11.3138	4.4138
	2	-5.86240	2.74861	.185	-13.7262	2.0014
	4	-3.74620	2.74861	.539	-11.6100	4.1176
4	1	.29620	2.74861	1.000	-7.5676	8.1600
	2	-2.11620	2.74861	.867	-9.9800	5.7476
	3	3.74620	2.74861	.539	-4.1176	11.6100

Patient 5_R_S

Dependent Variable: Patient_5_R_S
Tukey HSD

(I) Visit	(J) Visit	Mean Difference (I-J)	Std. Error	Sig.	95% Confidence Interval	
					Lower Bound	Upper Bound
1	2	5.11600(*)	1.24448	.004	1.5555	8.6765
	3	-3.43600	1.24448	.060	-6.9965	.1245
	4	-7.12200(*)	1.24448	.000	-10.6825	-3.5615
2	1	-5.11600(*)	1.24448	.004	-8.6765	-1.5555
	3	-8.55200(*)	1.24448	.000	-12.1125	-4.9915
	4	-12.23800(*)	1.24448	.000	-15.7985	-8.6775
3	1	3.43600	1.24448	.060	-.1245	6.9965
	2	8.55200(*)	1.24448	.000	4.9915	12.1125
	4	-3.68600(*)	1.24448	.041	-7.2465	-.1255
4	1	7.12200(*)	1.24448	.000	3.5615	10.6825
	2	12.23800(*)	1.24448	.000	8.6775	15.7985
	3	3.68600(*)	1.24448	.041	.1255	7.2465

* The mean difference is significant at the .05 level.

Patient 6_R_S

Dependent Variable: Patient_6_R_S
Tukey HSD

(I) Visit	(J) Visit	Mean Difference (I-J)	Std. Error	Sig.	95% Confidence Interval	
					Lower Bound	Upper Bound
1	2	.25400	.50018	.956	-1.1770	1.6850
	3	-.54000	.50018	.706	-1.9710	.8910
	4	-.15200	.50018	.990	-1.5830	1.2790
2	1	-.25400	.50018	.956	-1.6850	1.1770
	3	-.79400	.50018	.413	-2.2250	.6370
	4	-.40600	.50018	.848	-1.8370	1.0250
3	1	.54000	.50018	.706	-.8910	1.9710
	2	.79400	.50018	.413	-.6370	2.2250
	4	.38800	.50018	.864	-1.0430	1.8190
4	1	.15200	.50018	.990	-1.2790	1.5830
	2	.40600	.50018	.848	-1.0250	1.8370
	3	-.38800	.50018	.864	-1.8190	1.0430

Patient 7_R_S

Dependent Variable: ptient_7_R_S
Tukey HSD

(I) Visit	(J) Visit	Mean Difference (I-J)	Std. Error	Sig.	95% Confidence Interval	
					Lower Bound	Upper Bound
1	2	3.77000(*)	.76648	.001	1.5771	5.9629
	3	2.85600(*)	.76648	.009	.6631	5.0489
	4	-.18200	.76648	.995	-2.3749	2.0109
2	1	-3.77000(*)	.76648	.001	-5.9629	-1.5771
	3	-.91400	.76648	.640	-3.1069	1.2789
	4	-3.95200(*)	.76648	.001	-6.1449	-1.7591
3	1	-2.85600(*)	.76648	.009	-5.0489	-.6631
	2	.91400	.76648	.640	-1.2789	3.1069
	4	-3.03800(*)	.76648	.006	-5.2309	-.8451
4	1	.18200	.76648	.995	-2.0109	2.3749
	2	3.95200(*)	.76648	.001	1.7591	6.1449
	3	3.03800(*)	.76648	.006	.8451	5.2309

* The mean difference is significant at the .05 level.

Patient 7_L_S

Dependent Variable: Patient_7_L_S
Tukey HSD

(I) Visit	(J) Visit	Mean Difference (I-J)	Std. Error	Sig.	95% Confidence Interval	
					Lower Bound	Upper Bound
1	2	-1.09200	1.09385	.753	-4.2215	2.0375
	3	-1.33400	1.09385	.624	-4.4635	1.7955
	4	-1.01400	1.09385	.791	-4.1435	2.1155
2	1	1.09200	1.09385	.753	-2.0375	4.2215
	3	-.24200	1.09385	.996	-3.3715	2.8875
	4	.07800	1.09385	1.000	-3.0515	3.2075
3	1	1.33400	1.09385	.624	-1.7955	4.4635
	2	.24200	1.09385	.996	-2.8875	3.3715
	4	.32000	1.09385	.991	-2.8095	3.4495
4	1	1.01400	1.09385	.791	-2.1155	4.1435
	2	-.07800	1.09385	1.000	-3.2075	3.0515
	3	-.32000	1.09385	.991	-3.4495	2.8095

Patient 8_R_S

Dependent Variable: Patient_8_R_S
Tukey HSD

(I) Visit	(J) Visit	Mean Difference (I-J)	Std. Error	Sig.	95% Confidence Interval	
					Lower Bound	Upper Bound
1	2	.86800	.85513	.743	-1.5785	3.3145
	3	-.43000	.85513	.957	-2.8765	2.0165
	4	-.86800	.85513	.743	-3.3145	1.5785
2	1	-.86800	.85513	.743	-3.3145	1.5785
	3	-1.29800	.85513	.450	-3.7445	1.1485
	4	-1.73600	.85513	.218	-4.1825	.7105
3	1	.43000	.85513	.957	-2.0165	2.8765
	2	1.29800	.85513	.450	-1.1485	3.7445
	4	-.43800	.85513	.955	-2.8845	2.0085
4	1	.86800	.85513	.743	-1.5785	3.3145
	2	1.73600	.85513	.218	-.7105	4.1825
	3	.43800	.85513	.955	-2.0085	2.8845

Patient 9_L_S

Dependent Variable: Patient_9_L_S
Tukey HSD

(I) Visit	(J) Visit	Mean Difference (I-J)	Std. Error	Sig.	95% Confidence Interval	
					Lower Bound	Upper Bound
1	2	-2.75600	2.95695	.788	-11.2159	5.7039
	3	-4.87800	2.95695	.381	-13.3379	3.5819
	4	1.22200	2.95695	.975	-7.2379	9.6819
2	1	2.75600	2.95695	.788	-5.7039	11.2159
	3	-2.12200	2.95695	.889	-10.5819	6.3379
	4	3.97800	2.95695	.549	-4.4819	12.4379
3	1	4.87800	2.95695	.381	-3.5819	13.3379
	2	2.12200	2.95695	.889	-6.3379	10.5819
	4	6.10000	2.95695	.207	-2.3599	14.5599
4	1	-1.22200	2.95695	.975	-9.6819	7.2379
	2	-3.97800	2.95695	.549	-12.4379	4.4819
	3	-6.10000	2.95695	.207	-14.5599	2.3599